

# Jordan Journal of Mechanical and Industrial Engineering (JJMIE)

JJMIE is a high-quality scientific journal devoted to fields of Mechanical and Industrial Engineering. It is published by The Jordanian Ministry of Higher Education and Scientific Research in corporation with the Hashemite University.

## EDITORIAL BOARD

---

### Editor-in-Chief

Prof. Mousa S. Mohsen

### Editorial board

Prof. Bilal A. Akash  
Hashemite University

Prof. Adnan Z. Al-Kilany  
University of Jordan

Prof. Ayman A. Al-Maaitah  
Mutah University

Prof. Moh'd A. Al-Nimr  
Jordan University of Science and Technology

Prof. Ali A. Badran  
University of Jordan

Prof. Naseem M. Sawaqed  
Mutah University

### Assistant Editor

Dr. Ahmed Al-Ghandoor  
Hashemite University

## THE INTERNATIONAL ADVISORY BOARD

---

Abu-Qudais, Mohammad  
Jordan University of Science & Technology, Jordan

Abu-Mulaweh, Hosni  
Purdue University at Fort Wayne, USA

Afaneh Abdul-Hafiz  
Robert Bosch Corporation, USA

Afonso, Maria Dina  
Institute Superior Tecnico, Portugal

Badiru, Adedji B.  
The University of Tennessee, USA

Bejan, Adrian  
Duke University, USA

Chalhoub, Nabil G.  
Wayne State University, USA

Cho, Kyu-Kab  
Pusan National University, South Korea

Dincer, Ibrahim  
University of Ontario Institute of Technology, Canada

Douglas, Roy  
Queen's University, U. K

El Bassam, Nasir  
International Research Center for Renewable Energy,  
Germany

Haik, Yousef  
United Arab Emirates University, UAE

Jaber, Jamal  
Al- Balqa Applied University, Jordan

Jubran, Bassam  
Ryerson University, Canada

Kakac, Sadik  
University of Miami, USA

Khalil, Essam-Eddin  
Cairo University, Egypt

Mutoh, Yoshiharu  
Nagaoka University of Technology, Japan

Pant, Durbin  
Iowa State University, USA

Riffat, Saffa  
The University of Nottingham, U. K

Saghir, Ziad  
Ryerson University, Canada

Sarkar, MD. Abdur Rashid  
Bangladesh University of  
Engineering & Technology, Bangladesh

Siginer, Dennis  
Wichita State University, USA

Sopian, Kamaruzzaman  
University Kebangsaan Malaysia, Malaysia

Tzou, Gow-Yi  
Yung-Ta Institute of Technology and  
Commerce, Taiwan

## EDITORIAL BOARD SUPPORT TEAM

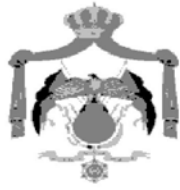
---

<b>Language Editor</b> Dr. Abdullah Jaradat	<b>Publishing Layout</b> MCPD. Osama AlShareet
--	---

### SUBMISSION ADDRESS:

---

Prof. Mousa S. Mohsen, Editor-in-Chief  
Jordan Journal of Mechanical & Industrial Engineering,  
Hashemite University, PO Box 330127, Zarqa, 13133, Jordan  
E-mail: jjmie@hu.edu.jo



Hashemite Kingdom of Jordan



Hashemite University

Jordan Journal of  
Mechanical and Industrial Engineering

JJMIIE

*An International Peer-Reviewed Scientific Journal*

<http://jjmie.hu.edu.jo/>

ISSN 1995-6665

# Jordan Journal of Mechanical and Industrial Engineering (JJMIE)

JJMIE is a high-quality scientific journal devoted to fields of Mechanical and Industrial Engineering. It is published by The Jordanian Ministry of Higher Education and Scientific Research in corporation with the Hashemite University.

**Introduction:** The Editorial Board is very committed to build the Journal as one of the leading international journals in mechanical and industrial engineering sciences in the next few years. With the support of the Ministry of Higher Education and Scientific Research and Jordanian Universities, it is expected that a heavy resource to be channeled into the Journal to establish its international reputation. The Journal's reputation will be enhanced from arrangements with several organizers of international conferences in publishing selected best papers of the conference proceedings.

**Aims and Scope:** Jordan Journal of Mechanical and Industrial Engineering (JJMIE) is a refereed international journal to be of interest and use to all those concerned with research in various fields of, or closely related to, mechanical and industrial engineering disciplines. Jordan Journal of Mechanical and Industrial Engineering aims to provide a highly readable and valuable addition to the literature which will serve as an indispensable reference tool for years to come. The coverage of the journal includes all new theoretical and experimental findings in the fields of mechanical and industrial engineering or any closely related fields. The journal also encourages the submission of critical review articles covering advances in recent research of such fields as well as technical notes.

## Guide for Authors

### Manuscript Submission

High-quality submissions to this new journal are welcome now and manuscripts may be either submitted online or mail.

**Online:** For online submission upload one copy of the full paper including graphics and all figures at the online submission site, accessed via E-mail: [jjmie@hu.edu.jo](mailto:jjmie@hu.edu.jo). The manuscript must be written in MS Word Format. All correspondence, including notification of the Editor's decision and requests for revision, takes place by e-mail and via the Author's homepage, removing the need for a hard-copy paper trail.

**By Mail:** Manuscripts (1 original and 3 copies) accompanied by a covering letter may be sent to the Editor-in-Chief. However, a copy of the original manuscript, including original figures, and the electronic files should be sent to the Editor-in-Chief. Authors should also submit electronic files on disk (one disk for text material and a separate disk for graphics), retaining a backup copy for reference and safety.

Note that contributions may be either submitted online or sent by mail. Please do NOT submit via both routes. This will cause confusion and may lead to delay in article publication. Online submission is preferred.

### Submission address and contact:

Prof. **Mousa S. Mohsen**, Editor-in-Chief  
Jordan Journal of Mechanical & Industrial Engineering,  
Hashemite University,  
PO Box 330127, Zarqa, 13133, Jordan  
E-mail: [jjmie@hu.edu.jo](mailto:jjmie@hu.edu.jo)

**Types of contributions:** Original research papers

**Corresponding author:** Clearly indicate who is responsible for correspondence at all stages of refereeing and publication, including post-publication. Ensure that telephone and fax numbers (with country and area code) are provided in addition to the e-mail address and the complete postal address. Full postal addresses must be given for all co-authors.

**Original material:** Submission of an article implies that the work described has not been published previously (except in the form of an abstract or as part of a published lecture or academic thesis), that it is not under consideration for publication elsewhere, that its publication is approved by all authors and that, if accepted, it will not be published elsewhere in the same form, in English or in any other language, without the written consent of the Publisher. Authors found to be deliberately contravening the submission guidelines on originality and exclusivity shall not be considered for future publication in this journal.

**Supplying Final Accepted Text on Disk:** If online submission is not possible: Once the paper has been accepted by the editor, an electronic version of the text should be submitted together with the final hardcopy of the manuscript. The electronic version must match the hardcopy exactly. We accept MS Word format only. Always keep a backup copy of the electronic file for reference and safety. Label the disk with your name. Electronic files can be stored on CD.

**Notification:** Authors will be notified of the acceptance of their paper by the editor. The Publisher will also send a notification of receipt of the paper in production.

**Copyright:** All authors must sign the Transfer of Copyright agreement before the article can be published. This transfer agreement enables Jordan Journal of Mechanical and Industrial Engineering to protect the copyrighted material for the authors, but does not relinquish the authors' proprietary rights. The copyright transfer covers the exclusive rights to reproduce and distribute the article, including reprints, photographic reproductions, microfilm or any other reproductions of similar nature and translations.

**PDF Proofs:** One set of page proofs in PDF format will be sent by e-mail to the corresponding author, to be checked for typesetting/editing. The corrections should be returned within 48 hours. No changes in, or additions to, the accepted (and subsequently edited) manuscript will be allowed at this stage. Proofreading is solely the author's responsibility. Any queries should be answered in full. Please correct factual errors only, or errors introduced by typesetting. Please note that once your paper has been proofed we publish the identical paper online as in print.

### **Author Benefits**

**Page charge:** Publication in this journal is free of charge.

**Free off-prints:** Three journal issues of which the article appears in along with twenty-five off-prints will be supplied free of charge to the corresponding author. Corresponding authors will be given the choice to buy extra off-prints before printing of the article.

### **Manuscript Preparation:**

**General:** Editors reserve the right to adjust style to certain standards of uniformity. Original manuscripts are discarded after publication unless the Publisher is asked to return original material after use. If online submission is not possible, an electronic copy of the manuscript on disk should accompany the final accepted hardcopy version. Please use MS Word for the text of your manuscript.

**Structure:** Follow this order when typing manuscripts: Title, Authors, Affiliations, Abstract, Keywords, Introduction, Main text, Conclusions, Acknowledgements, Appendix, References, Figure Captions, Figures and then Tables. For submission in hardcopy, do not import figures into the text - see Illustrations. For online submission, please supply figures imported into the text AND also separately as original graphics files. Collate acknowledgements in a separate section at the end of the article and do not include them on the title page, as a footnote to the title or otherwise.

**Text Layout:** Use double spacing and wide (3 cm) margins. Ensure that each new paragraph is clearly indicated. Present tables and figure legends on separate pages at the end of the manuscript. If possible, consult a recent issue of the journal to become familiar with layout and conventions. All footnotes (except for table and corresponding author footnotes) should be identified with superscript Arabic numbers. To conserve space, authors are requested to mark the less important parts of the paper (such as records of experimental results) for printing in smaller type. For long papers (more than 4000 words) sections which could be deleted without destroying either the sense or the continuity of the paper should be indicated as a guide for the editor. Nomenclature should conform to that most frequently used in the scientific field concerned. Number all pages consecutively; use 12 or 10 pt font size and standard fonts. If submitting in hardcopy, print the entire manuscript on one side of the paper only.

**Corresponding author:** Clearly indicate who is responsible for correspondence at all stages of refereeing and publication, including post-publication. The corresponding author should be identified with an asterisk and footnote. Ensure that telephone and fax numbers (with country and area code) are provided in addition to the e-mail address and the complete postal address. Full postal addresses must be given for all co-authors. Please consult a recent journal paper for style if possible.

**Abstract:** A self-contained abstract outlining in a single paragraph the aims, scope and conclusions of the paper must be supplied.

**Keywords:** Immediately after the abstract, provide a maximum of six keywords (avoid, for example, 'and', 'of'). Be sparing with abbreviations: only abbreviations firmly established in the field may be eligible.

**Symbols:** All Greek letters and unusual symbols should be identified by name in the margin, the first time they are used.

**Units:** Follow internationally accepted rules and conventions: use the international system of units (SI). If other quantities are mentioned, give their equivalent in SI.

**Maths:** Number consecutively any equations that have to be displayed separately from the text (if referred to explicitly in the text).

**References:** All publications cited in the text should be presented in a list of references following the text of the manuscript.

Text: Indicate references by number(s) in square brackets in line with the text. The actual authors can be referred to, but the reference number(s) must always be given.

List: Number the references (numbers in square brackets) in the list in the order in which they appear in the text.

### **Examples:**

Reference to a journal publication:

- [1] M.S. Mohsen, B.A. Akash, "Evaluation of domestic solar water heating system in Jordan using analytic hierarchy process". Energy Conversion & Management, Vol. 38, No. 9, 1997, 1815-1822.

Reference to a book:

- [2] Strunk Jr W, White EB. The elements of style. 3rd ed. New York: Macmillan; 1979.

Reference to a conference proceeding:

- [3] B. Akash, S. Odeh, S. Nijmeh, "Modeling of solar-assisted double-tube evaporator heat pump system under local climate conditions". 5th Jordanian International Mechanical Engineering Conference, Amman, Jordan, 2004.

Reference to a chapter in an edited book:

- [4] Mettam GR, Adams LB. How to prepare an electronic version of your article. In: Jones BS, Smith RZ, editors. Introduction to the electronic age, New York: E-Publishing Inc; 1999, p. 281-304

**Free Online Color:** If, together with your accepted article, you submit usable color and black/white figures then the journal will ensure that these figures will appear in color on the journal website electronic version.

**Tables:** Tables should be numbered consecutively and given suitable captions and each table should begin on a new page. No vertical rules should be used. Tables should not unnecessarily duplicate results presented elsewhere in the manuscript (for example, in graphs). Footnotes to tables should be typed below the table and should be referred to by superscript lowercase letters.



---

<b>PAGES</b>	<b>PAPERS</b>
425 – 432	Dynamic Control Card in a Production System Controlled by Conwip Approach <i>Paolo Renna</i>
433 – 442	Conceptual Understanding of Mass and Stiffness Fixed Points of Discrete Vibrational Systems <i>M. Abu-Hilal, A.R. Touqan</i>
443 – 450	Experimental Investigations of the Effect of Some Insulating Materials on The Compressive Strength, Water Absorption and Thermal Conductivity of Building Bricks. <i>Ali M. Othman</i>
451 – 466	Novel Method of Productivity Improvement and Waste Reduction through Recycling of Submerged Arc Welding Slag <i>Dalgobind Mahto, Anjani Kumar</i>
467 -476	Design and Manufacturng of Self Actuating Traction Drives with Solid and Hollow Rollers <i>Wisam M. Abu-Jadayil, Mousa S. Mohsen</i>
477 – 486	Cylindrical Solar Cooker with Automatic Two Axes Sun Tracking System <i>Essam Abdallah, Mohammed Al_Soud, Ali Akayleh, Salah Abdallah</i>
487 – 494	Mathematical Modeling and Performance Optimization for the Paper Making System of a Paper Plant <i>Rajiv Khanduja, P. C. Tewari, R.S. Chauhan, Dinesh Kumar</i>
495 – 502	Reduction of Vibration of Industrial Equipments <i>M. A. Nawafleh, N.Al-Kloub, M. Tarawneh, R. M. Younes</i>
502 - 506	Property Estimation with Automated Ball Indentation Using Artificial Neural Network and Finite Element Simulation <i>Kamal Sharma, Vivek Bhasin, A. K. Ghosh</i>
507 - 516	Exergoeconomic Analysis for Unit Gt14 of South Tripoli Gas Turbine Power Plant <i>Giuma M. Fellah, Fathi A. Mgherbi, Saleh M. Aboghres</i>
517 - 522	Total Productive Maintenance Review and Overall Equipment Effectiveness Measurement <i>Osama Taisir R.Almeanazel</i>
523 – 530	Effect of EGR on Performance and Emission Characteristics of Natural Gas Fueled Diesel Engine <i>S.K. Mahla, L.M. Das, M.K.G. Babu</i>

---



# Dynamic Control Card in a Production System Controlled by Conwip Approach

Paolo Renna \*

*University of Basilicata, Dipartimento di Ingegneria e Fisica dell'Ambiente (DIFA)*

*Via dell'Ateneo Lcuano,10, 85100, Potenza , Italy*

---

## Abstract

In this paper, the focus is on the dynamic control card in a conwip system. An approach to set the number of cards in order to adapt to the change of the production systems both in terms of external change as the demand and internal change as the work time of the machine, failures and so on. A Multi Agent Architecture is proposed to implement a flexible and extensible approach that can be implemented in a supply chain and not only in a single manufacturing system. Then, a set of rules is proposed to change the number of cards in the system. A dynamic simulation environment has been developed to test the control approach under different dynamic states. The performance measures evaluated are the average utilization of the manufacturing system, the throughput time, throughput, work in process and average available cards. The proposed approach is compared with a kanban control.

© 2010 Jordan Journal of Mechanical and Industrial Engineering. All rights reserved

Keywords: Conwip; kanban; Multi Agent Systems; Dynamic Environment; Simulation.

---

## 1. Introduction

The pull production control approach leads to reduce inventory and hence the associated cost of inventory reduction, where the manufacturing scenarios allow applying this control approach. The implementation of a pull production control systems can be achieved by kanban or conwip.

In kanban systems [1], a production authorization cards, called Kanban, are used to control and limit the releases of parts into each production stage. Conwip system [2] uses a single card type to control the total amount of Work In Process (WIP) permitted in the entire production system. When a job order arrives to a CONWIP system, a card is attached to the job, provided cards are available at the beginning of the production system. Otherwise, the job must wait in a backlog. When a job is processed at the final station, the card is removed and sent back to the beginning of the production system, where it might be attached to the next job waiting in the backlog. In these control approaches, the number of cards involves significantly the performance of the production systems. In case of kanban systems, it has to design the number of cards for each production stage and there are *n-variables*; in case of conwip systems only one parameter has been

designed: the number of cards of the entire production systems.

The design of the number of cards in pull systems can be obtained by two approaches [3]:

- Card setting; it sets the number of cards given a manufacturing condition in order to obtain an adequate level of performance. In this case the number of card is fixed and can be re-designed when the manufacturing conditions change significantly.
- Card control; it identifies a set of rules that change or maintain the number of cards in the production systems. Then, the number of cards is variable in order to optimize the performance of the production system.

In this paper, the focus is the formulation of a set of rules to card control in a conwip system where the manufacturing conditions are changing dynamically. The approach is tested by developing a dynamic simulation environment and it is compared with a kanban system. In section 2 is discussed the literature on card controlling approaches. In section 3 is explained the proposed approach and in section 4 the simulation environment developed has been illustrated. In section 5 the simulation results are discussed. Finally, the conclusions and future development are showed in section 6.

---

\* Corresponding author. paolo.renna@unibas.it

## 2. Literature Review

There are few researches in developing approaches of dynamic card controlling and for specific purposes. Gupta and Alturki [4] developed an approach in a kanban system with two types of cards. The variables to set are: the initial number of kanban, the instant to re-planning the number of cards and an acceptable probability of backlog. The objective is to reduce the backordered demand and the WIP by the knowledge of the demand on the next period.

Hoop and Roof [5] proposed a procedure that dynamically increase or decrease the number of cards by a statistical throughput control in a make to order environment. Then, a throughput rate level is set and the throughput of the system is monitored; if the throughput is over or under the limits, then cards are added or subtracted to the system.

Takahashi and Nakamura [6] explained an approach for make to stock environments. In the proposed approach by the simulation it is analyzed the average waiting time of the customers for different demand rates and for different number of cards. Then, it is defined a target value for the average customers waiting time and if a change of the demand rate is detected, the number of cards is changed by the results of the simulation runs.

Christelle et al. [7] analyzed a CONWIP system which consists of three stations in series. They proposed an analytical method to evaluate performance of conwip systems with inspection for the two following cases: saturated systems and system with external demands.

Yang [8] investigated the performance of Single-kanban, Dual-kanban, and Conwip for the production of different parts on a single flow line.

Tardif and Maaseidvaag [9] proposed an approach in a make to stock environments controlled by a conwip system. The objective of the approach is the trade off between the inventory level of finished goods and the backordered demand. The procedure is the following: if the inventory level is under a defined lower control limit an extra card is added, if the inventory level is over a defined upper control limit the card is subtracted. In this approach, a maxim number of extra card is available.

Framinan et al. [10] described an approach on card controlling in a conwip system. The objective of the procedure is to obtain a given throughput rate for make to order environments. It is fixed a time interval of monitoring the throughput rate level; if the throughput is over a defined upper control limit the card is subtracted. In this approach, a maxim number of extra card is available.

Kumar and Panneerselvam [11] discussed the literature concerning the kanban system. The authors point out the importance of the dynamic set of the minimum number of kanbans.

From the analysis of the literature the following issue can be drawn:

- In some approaches proposed, the number of parameters to set is numerous; then a proper procedure to set these parameters to adapt at changing of the manufacturing environments is needed.
- Many approaches assume that some data are known, like demand, or can be estimated by simulation.

- Some approaches proposed concerning make to order environments, while other are developed for make to stock environments.

The proposed approach is based on a set of rules in order to increment or decrease the number of cards available in manufacturing system. The approach concerns both make to order and make to stock environment and it works on few parameters to set; no data about demand or lead time are known in this approach. A proper simulation environment has been developed to test the proposed approach in a conwip system and the variability of the performance changing the parameters to set. Moreover, the performance is estimated in a very dynamic environment in order to study the adaptability of the proposed approach.

Finally, the proposed approach is developed by a Multi Agent System paradigm in order to obtain a distributed control system.

## 3. The proposed approach

The proposed approach concerns the decision to increase or decrease the number of cards by observing the manufacturing conditions. The changing of the manufacturing conditions can be classified in:

- external; in this case, the changing is caused by external events such as the demand (volume or distributions).
- internal; in this case the changing is caused by elements of the production system, such as the manufacturing times, failures of the resources, and so on.

The objective of the approach is to adapt the number of the cards to the manufacturing conditions in order to obtain an opportune level of performance in terms of: throughput, lead time, WIP and utilization of the production system.

The control approach is based on monitoring the average utilization of the manufacturing resources and the average utilization of the cards. From the point of view of the cards utilization:

- a low utilization of the cards can be caused by high number of cards or the reduction of the demand;
- low number of cards or increase of demand lead to a high utilization of the cards.

From the point of view of the average manufacturing resources utilization:

- a low system utilization can be caused by the decrease of the demand or a low number of cards that limits the number of parts in the production systems;
- a high system utilization can be caused by the increase of the demand or a high number of cards that leads to increment the number of parts in the production system.

In order to obtain a decision control approach by limited computational time four rules has been proposed as showed in table 1.

Table 1. Card number control rules

Rule no.	
1	if average system utilization is high and average cards utilization is high then increment number of cards
2	if average system utilization is high and average cards utilization is low then reduce number of cards
3	if average system utilization is low and average cards utilization is high then increment number of cards
4	if average system utilization is low and average cards utilization is low then reduce number of cards

The rules in Table 1 are computed in a periodic review approach; the disadvantage is the introducing of a new parameter to set like the interval between the reviews.

A Multi Agent Systems (MAS) paradigm [12, 13] can be adopted to implement the control approach. In particular, two agents have been proposed: a control agent and manufacturing agent.

The development of a distributed architecture leads to obtain the following advantage:

- distributed and open, lacking central control and standardized communication;
- heterogeneous: compatibility and interfacing problems;
- rapid change: new subsystems appear, existing ones disappear
- rapid growth: huge amount of unstructured information;

The Manufacturing agent provides the information about the manufacturing conditions to the control agent in order to implement the policy control.

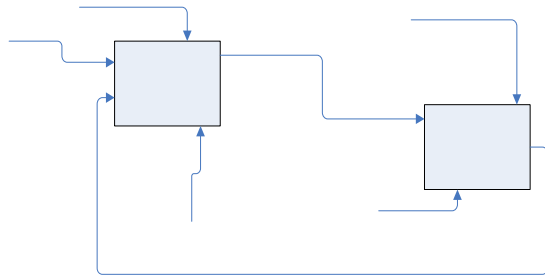


Figure 1. IDEF0 Diagram.

Figure 1 shows the basic representation of the agent's interaction during the control process. As the reader can notice in the IDEF0 diagram of Figure 1, it is possible to locate two independent processes: the control process that is performed by the control agent and the manufacturing system process, which is performed by the manufacturing agent. The control process is triggered by the periodic review time and it is constrained by the Strategy constraints of the control approach. The output of this process is the request of information about the manufacturing systems. In order to process such outputs the control process uses a proper control strategy.

The manufacturing system process is triggered by the control agent request information and it is constrained by objectives of the manufacturing system. The manufacturing system process elaborates the information

about the manufacturing conditions to submit to the control process. Such process is undertaken by using proper manufacturing system information.

The control agent implements the above rule on the manufacturing conditions information provided by the manufacturing agent and decides about the number of cards. The processes showed in Figure 1 are a general framework that can be specialized to particular enterprise architecture.

Figure 2 shows the activity diagram of the control approach proposed in this paper, in particular the following action can be located:

- The Manufacturing System Agent sets initial cards number like the number of the kanban control approach and waits for the periodic review date;
- After the review time, the Manufacturing System Agent collects the performance about the average utilization of the manufacturing system and the cards and sends it to the Control Agent;
- The Control Agent applies the four rules (see table 1) and sends to the Manufacturing System Agent whether the number of cards has to be increased, decreased or nothing action is to be performed.
- The manufacturing System Agent applies the policy of the Control Agent and waits for the subsequent period of review.

The initial number of cards is the same as in the kanban approach. As benchmark is developed a kanban control system with fixed number of cards computed by the following expression:

$$n \geq \frac{DL(1 + \alpha)}{Cap} \quad (1)$$

where,

$n$  is the number of kanban;

$D$  is the average demand;

$L$  is the lead time;

$Cap$  is the capacity of the containers.

#### 4. Simulation Environment

In order to test the proposed control approach the Arena® discrete event simulation platform by Rockwell Software, Inc. is selected for building up the simulation model.

#### Discrete event simulation

- in many commercial tools and simulation packages, nowadays the simulation model is automatically created from high level modeling languages and notations
- allows to validate and optimize dynamic and discrete systems such as production systems. These models facilitate evaluating different scenarios and maximizing their potential output and benefits. Arena®
- based on the known SIMAN simulation language - is well suited for modeling shop floors of production systems in which each entity (part) follows a manufacturing route through production resources (servers, material handling systems, buffers, and so forth) [14]. The production system simulated consists

of three manufacturing cells, in order to test the control policy, the manufacturing times are equal for each manufacturing cell and in particular 5 unit of time. The production system manufactures a single type of product that visits the three manufacturing cells. The initial number of cards is the same of the kanban policy control in the same conditions (equation 1). The length of the simulation is 1500 unit of unit time. Table 2 reports the simulation experiments conducted (scenarios).

Table 2. Simulation Experiments.

Scenario	Interarrival	Manufacturing times
1	Constant – negexpo(0.1)	constant – equal for each manufacturing cell: 5 unit time
2	Constant – negexpo (0.2)	constant – equal for each manufacturing cell: 5 unit time
3	Impulsive interarrival: negexpo(0.1) for 500 unit time negexpo(0.3) for 500 unit time negexpo(0.1) for 500 unit time	constant – equal for each manufacturing cell: 5 unit time
4	Impulsive interarrival negexpo(0.1) for 650 unit time negexpo(0.5) for 200 unit time negexpo(0.1) for 650 unit time	constant – equal for each manufacturing cell: 5 unit time
5	constant – negexpo (0.2)	constant – equal for each manufacturing cell: 5 unit time cell 2: 10 unit time for a 500 unit time
6	constant – negexpo (0.2)	constant – equal for each manufacturing cell: 5 unit time cell 2: 15 unit time for a 500 unit time

The scenarios concern the inter-arrival of the parts:

- constant during the simulation experiment with two levels of congestion of the manufacturing system (scenarios 1 and 2);
- constant with impulse that simulate an exception of the customer demand (scenarios 3 and 4);

From the point of view of the manufacturing system:

- working time constant end equal for each manufacturing cell (scenarios from 1 to 4);
- working time constant end equal for each manufacturing cell and for a single manufacturing cell, a temporal variation of the working time (scenarios 5 and 6).

The performance measures computed for each simulation scenario are: throughput, manufacturing lead time, utilization of the manufacturing resources, WIP, number of cards and the utilization of the cards.

Furthermore, because of the random input and in order to guarantee a statistical validity of the results, for each run, the number of executed replications guarantees, for the output performance measures, that the length of confidence intervals (95% level) of the mean among replications is lower than 10 % of the mean itself.

Several scenarios have been considered to test the control policy as showed in table 2.

The simulations have been conducted for a kanban system used as a benchmark and in a manufacturing system with the proposed dynamic control card.

## 5. Simulation Results

The results of the simulation are showed in table 3. Table 3 shows the percentage difference of the proposed approach compared with the fixed number of cards (benchmark – kanban).

The results of scenarios 1 and 2 with constant demand lead to the following issues:

- the average utilization of the manufacturing systems decrease when the demand is increased;
- the throughput time is reduced when the congestion of the manufacturing system is low;
- the throughput is affected by low variation;
- The dynamic control leads to better performance about the work in process and reduce the number of available cards when the congestion is high.

The dynamic conwip approach proposed adapts the number of cards to the dynamic conditions of the manufacturing system obtaining better performance than kanban approach. The improvements are better when the congestion level is low.

The results of scenarios 3 and 4 with impulsive variation of the demand lead to the following issues:

- the average utilization of the manufacturing systems and the throughput are affected by low variation;
- a low reduction of the throughput time;
- the average available cards increasing, while the work in process decrease; the cards is available only in the periods when is necessary to increment it.

These results show how the performance of the proposed approach improve when external exceptions as demand changes occur.

The results of scenarios 5 and 6 with one working time different form the others machines in a limited period:

- the significantly variations are both the reduction of working in process and the available cards.

When the working times are very different among the manufacturing cells, the improvements of the proposed approach is reduced.

In summary, the main benefits of the proposed approach, compared with a kanban system are: the reduction of the Work In Progress and the reduction of the lead time. The benefits are evaluated in the last column of table 3 that reports the average value of the performance over the all scenarios.

Finally, several simulations are conducted compared the time of the periodic review. The results reported in figure 3 are match up with the periodic review of 500 unit times.

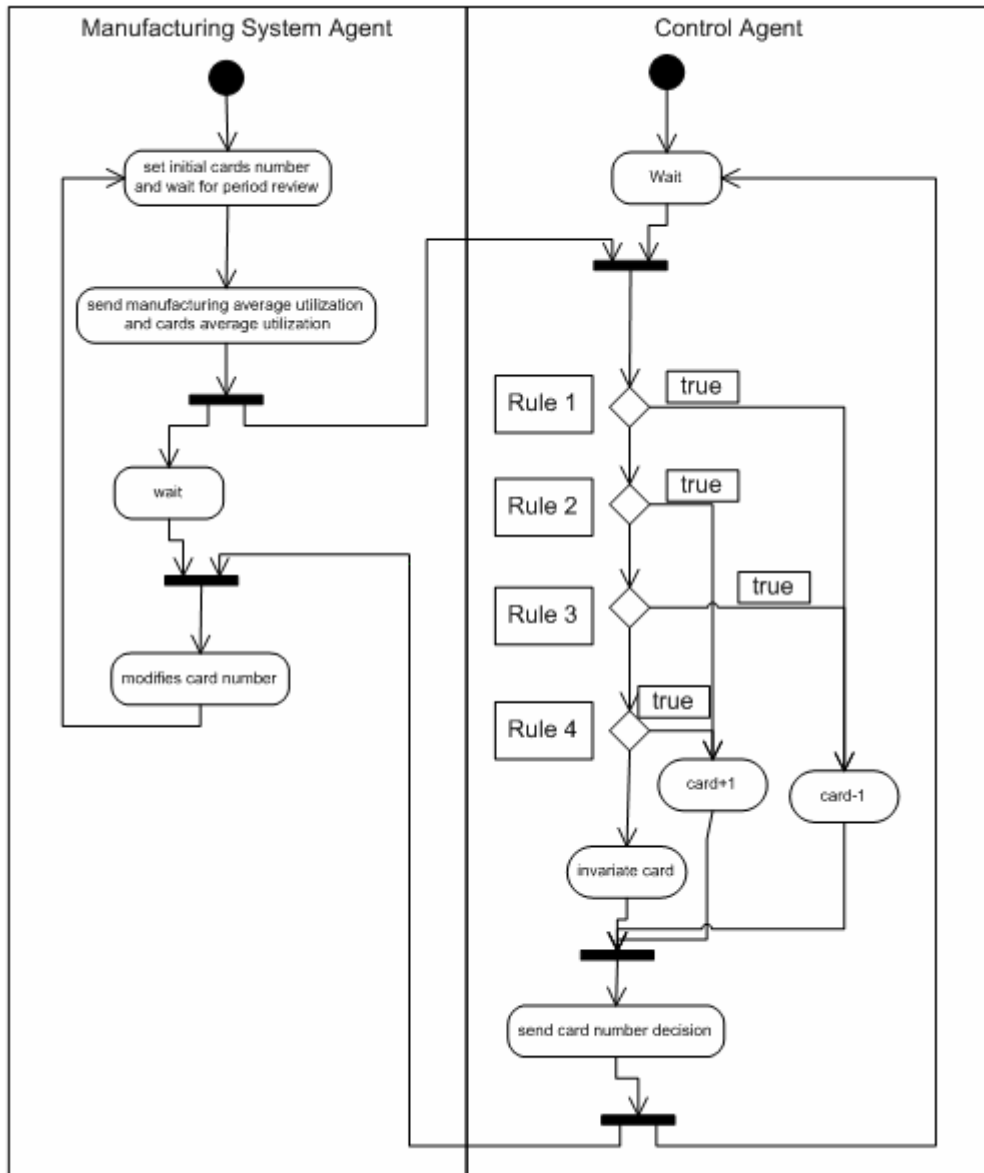


Figure 2. UML activity diagram.

Table 3. Simulation Results.

	Scen. 1	Scen. 2	Scen. 3	Scen. 4	Scen. 5	Scen. 6	Average
<b>Average system utilization</b>	-0.37%	-2.78%	-0.46 %	-0.33%	-0.88%	-0.95%	-0.96%
<b>Throughput time</b>	-33%	3.75%	-7.90%	-6.13%	-1.83%	-1.50%	-7.77%
<b>Throughput</b>	0%	-1.64%	0.41%	0.33%	-0.10%	-0.11%	-0.19%
<b>Wip</b>	-3%	-37.38%	-23.73%	-19.44%	-11.79%	-10.74%	-17.68%
<b>Available card</b>	29.67%	-37.33%	10%	14.33%	-30.50%	-30.33%	-7.36%

The values reported in the graphs of figure 3 are the following:

- 1 -> 400 unit times;
- 2 -> 300 unit times;
- 3 -> 200 unit times;
- 4 -> 100 unit times;
- 5 -> 50 unit times;
- 6 -> 15 unit times.

As the reader can notice, the approach is robust against the different values of periodic review. In particular, only

for very low period (about 15 unit times) the performance is more variable because the control approach is instable and it leads to modify the number of cards more times.

## 6. Conclusions and Future Development

In this paper an approach to dynamic control the number of cards in a conwip system has been developed. A Multi Agent System is proposed to implement a set of rules to control the number of card. The MAS leads to

develop a distributed approach that can be integrate in a wide manufacturing system with different control systems. Moreover, the MAS architecture can be integrated in the upper level of production planning and control of the enterprise. The proposed approach is compared with a kanban system and a dynamic simulation environment has been developed for validation. The simulation results show that the proposed approach leads to reduce significantly

the WIP in a dynamic environment both for the demand and for working time. The others performance are more close between the proposed approach and kanban system. Another issue is that the approach proposed is robust to the interval time of periodic review; the dynamic control approach is unstable when the periodic review time is comparable to working time of the manufacturing resources.

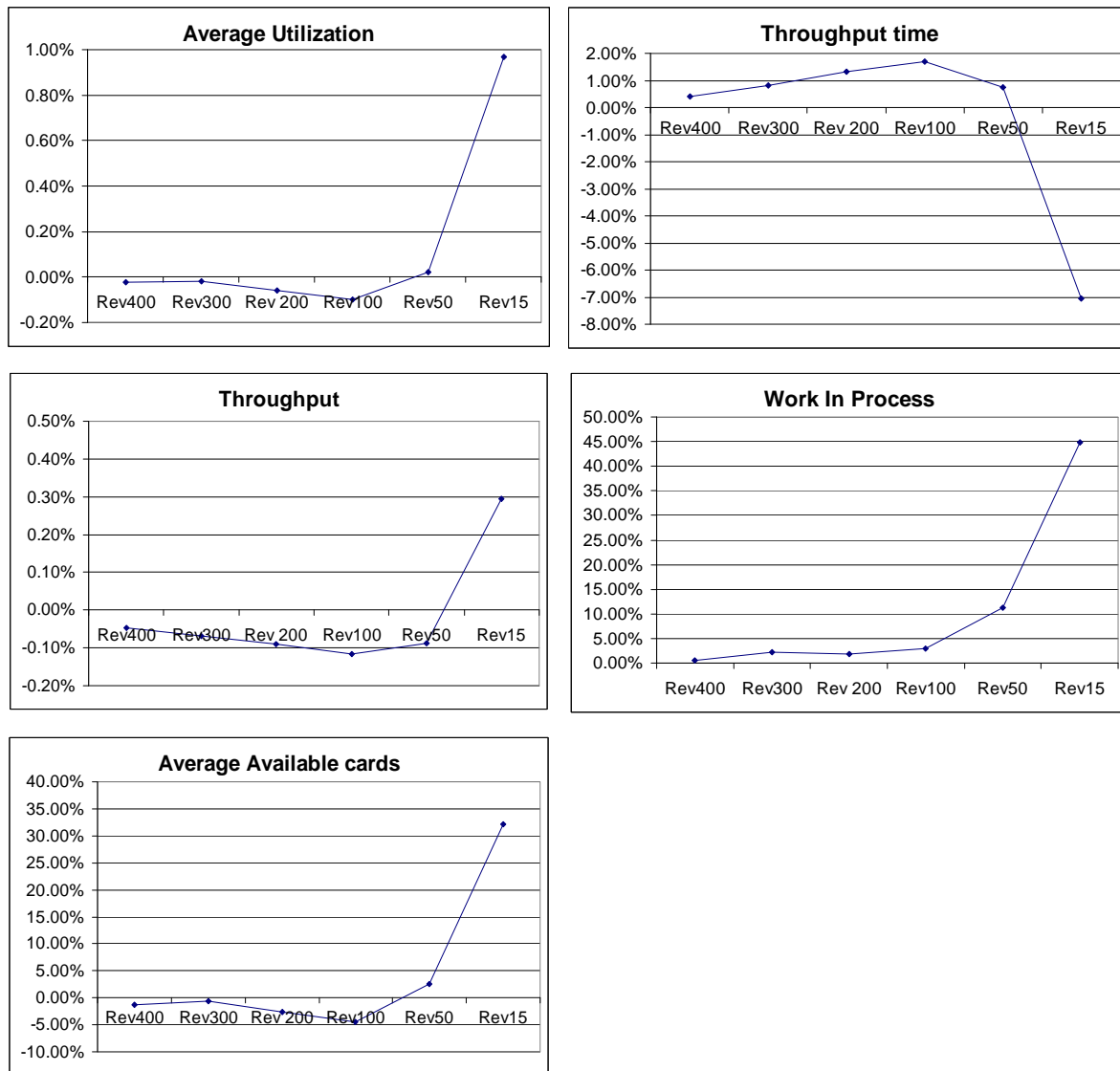


Figure 3. Simulation performance comparison average scenarios.

The main results achieved by the research are:

The dynamic control is implemented by Multi Agent Architecture. This allows to obtain the advantages of: computational efficiency, reliability, extensibility, robustness, maintainability, responsiveness, flexibility, and reuse.

- The dynamic control card proposed allows to reduce Work In Process and lead time of the parts. The improvements are tested in several dynamic conditions by a simulation environment. The different scenarios tested allow to quantify the benefits for each scenario characteristics.

- The proposed approach leads to significantly improvements where external exceptions occur as the demand variability.

Future researches concern the extending the approach to multi-product environment and the implementation of a fuzzy inference engine in order to reduce the number of adding or subtracting of cards.

## Acknowledgement

Author wish to thank the anonymous referees whose suggestions and comments contribute to improve the value of this paper.

## References

- [1] Y. Monden, "Toyota Production System" Industrial Engineering and Management Press, 1983, Atlanta.
- [2] M.L. Spearman, D.L. Woodruff, W.J. Hoop, "Conwip: A pull alternative to Kanban". International Journal of Production Research, Vol. 28, No. 5, 1990, 879-894.
- [3] J.M. Framinan, P.L. Gonzales, R. Ruiz-Usano, "The Conwip production control system: Review and research issues". Production Planning & Control, Vol. 14, No.3, 2003, 255-265.
- [4] S. M. Gupta, A. Y. Al-Turki, "An algorithm to dynamically adjust the number of kanbans in stochastic processing times and variable demand environment". Production Planning & Control, Vol. 8, No. 2, 1997, 133-141.
- [5] W.J. Hoop, M.L. Roof, "Setting WIP levels with statistical throughput control (STC) in CONWIP production lines". International Journal of Production Research, Vol. 36, No. 4, 1998, 867-882.
- [6] K. Takashi, N. Nakamura, "Reacting JIT ordering systems to unstable changes in demand". International Journal of Production Research, Vol. 37, No. 10, 1999, 2293-2313.
- [7] D. Christelle, F. Yannick, H.S. Lee, "Performance evaluation and design of CONWIP system with inspection". International Journal of Production Economics, Vol. 64, No. 1-3, 2000, 219-229.
- [8] K. K. Yang, 2000. "Managing flow line with single-kanban, dual – Kanban or Conwip". Production and Operational Management, Vol. 9, No. 4, 2000, 349 – 365.
- [9] V. Tardif, L. Maaseidvaag, "An adaptive approach to controlling Kanban systems". European Journal of Operational Research, Vol. 132, No. 2, 2001, 411-424.
- [10] J.M. Framinan, P.L. Gonzales, R. Ruiz-Usano, "Dynamic card controlling in a Conwip system". International Journal of Production Economics", Vol. 99, No. 1-2, 2006, 102-116.
- [11] C.S. Kumar, R. Panneerselvam, "Literature review of JIT-KANBAN system". International Journal of Advanced Manufacturing Technology, Vol. 32, No. 3-4, 2007, 393-408.
- [12] W. Shen, D.H. Norrie, "Agent-based systems for intelligent manufacturing: a state-of-the-art survey". Knowledge and Information Systems, an International Journal Vol. 1, No. 2, 1999, 129-156.
- [13] Reaidy, Y.J. Liu, D. Diep, P. Massotte, J. Intelligent agents for production systems. In: d'Amours, S., Guinet, A. editors. Intelligent Agent-based Operations Management, London, Kogan Page Science, 2003, p. 147-164.
- [14] W. D. Kelton, R. P. Sadowsky, D. A. Sadowsky, "Simulation with Arena". Avenue of Americas, New York: Mc Graw Hill, 1998.



# Conceptual Understanding of Mass and Stiffness Fixed Points of Discrete Vibrational Systems

M. Abu-Hilal <sup>a,\*</sup>, A. R. Touqan <sup>b</sup>

<sup>a</sup>Department of Mechanical Engineering, An Najah National University, Nablus P.O.Box 7, Tel.00970-9-2345113, Palestine

<sup>b</sup>Department of Civil Engineering, An Najah National University, Nablus P.O.Box 7, Tel.00970-9-2345113, Palestine

## Abstract

The presence of mass and stiffness fixed points in the frequency responses of vibrational systems may greatly affect the design of these systems. In this paper, the physical reason for the occurrence of mass and stiffness fixed points and the relationship between them and the phenomenon of internal absorber are investigated. It is found that the frequencies at which mass and stiffness fixed points occur, represent eigenfrequencies of subsystems of the whole vibrational system. Furthermore, it is found that the mass and stiffness fixed points are strongly related with the phenomenon of internal absorbers.

© 2010 Jordan Journal of Mechanical and Industrial Engineering. All rights reserved

Keywords: Mass Fixed Points, Stiffness Fixed Points, Vibration Control, Internal Absorber.

## 1. Introduction

The presence of damping, mass, and stiffness fixed points in the frequency responses of vibrating systems may complicate their vibration control since these fixed points can only be recognized if the parameters of the system are varied. A mass fixed point is an intersection of the frequency responses of a dynamic system for different values of the mass. Damping and stiffness fixed points are similarly defined. At a fixed point frequency, the vibration amplitude remains constant, independent of the values of the varied parameters. There to, when the operating frequency lie close to a mass (stiffness) fixed point frequency, then the amplitude of vibration cannot be effectively controlled by varying the values of masses (stiffnesses).

In addition to their dependence on the masses and stiffnesses of the dynamic system, the mass and stiffness fixed points are dependent on the location of the force application. That is because the location of the force application affects the phenomenon of the internal absorber, which is related with the force balance on different masses of the system.

Mass and stiffness fixed points may be used to design vibrational systems with zero or constant amplitudes for some masses of a system which can even include variable masses or stiffnesses.

Damping fixed points of systems with one and two degrees of freedom were treated in connection with

vibration absorption and vibration isolation by many authors, including Den Hartog [1] and Klotter [2]. Bogy and Paslay [3] used the damping fixed points to obtain optimal damping for the purpose of minimizing the maximum steady state response of a particular linear damped two-degree-of-freedom vibratory system. Henney and Raney [4] used the damping fixed points to find approximate analytical expressions for optimum damping for a uniform beam forced and damped in four different configurations. Dayou [5] examined the fixed points theory for global vibration control of a continuous structure using vibration neutralizer.

Mass, stiffness, and damping fixed points of a system with two degrees of freedom were considered by Abu-Hilal [6], where the frequencies at which damping, mass, and/or stiffness fixed points occur and their amplitudes were determined analytically. Also Abu-Hilal [7] presented a procedure for determining the mass and stiffness fixed point frequencies of vibratory discrete linear system with  $n$  degrees of freedom. To verify the given procedure, all mass and stiffness fixed point frequencies of a system with three degrees of freedom were determined in closed forms.

In this paper the nature of the mass and stiffness fixed points of vibratory discrete linear dynamic systems and their physical meaning are investigated. Furthermore, the relationship between mass and stiffness fixed points and the phenomenon of internal absorber are studied. The vibration amplitudes at fixed points frequencies of an undamped system with three degrees of freedom as shown in Fig. 1 are determined and discussed. Although a three degrees of freedom system is studied in this contribution, the obtained results are general and applicable to systems

\* Corresponding author. hilal122@yahoo.com

with  $n$  degrees of freedom. A three degrees of freedom system is used in this study in order to obtain the fixed points frequencies and their amplitudes in closed forms.

**2. Mathematical Formulation and Implementation**

The equation of motion of an undamped linear system with  $n$  degrees of freedom is given as

$$\mathbf{M}\ddot{\mathbf{x}} + \mathbf{K}\mathbf{x} = \mathbf{F} \tag{1}$$

where  $\mathbf{M}$ ,  $\mathbf{K}$ , and  $\mathbf{x}$ , are the mass matrix, the stiffness matrix, and the displacement vector of the system, respectively, and  $\mathbf{F}$  is the excitation force vector. If a harmonic force  $\mathbf{F} = \mathbf{P}\cos\omega t$  is assumed, where

$\mathbf{P} = [P_1, \dots, P_n]^T$  is the vector of the force amplitudes and  $\omega$  is the circular excitation frequency, then the steady-state displacement vector of the system is obtained by using the solution

$$\mathbf{x} = \mathbf{X}\cos\omega t \tag{2}$$

Substituting Eq. (2) into Eq. (1) and simplifying yields

$$(\mathbf{K} - \omega^2\mathbf{M})\mathbf{X} = \mathbf{P} \tag{3}$$

where  $\mathbf{X} = [X_1, \dots, X_n]^T$  is the vector of the displacement amplitudes,  $X_j = X_{j1} + \dots + X_{jn}$  is the vibration amplitude of mass  $j$ , and  $X_{jg}$  ( $j, g = 1, 2, \dots, n$ ) is the frequency response of mass  $j$  due to a force  $P_g$  applied at position  $g$ , with all other forces equal to zero (i.e.,

$$P_{j1} = \dots = P_{j(g-1)} = P_{j(g+1)} = \dots = P_{jn} = 0).$$

In this contribution we set  $P_g = P_0$ .

The frequency response  $X_{jg}$  can be obtained from Eq. (3) and written in a bilinear form as given in [7] as:

$$X_{jg} = P_g \frac{a_1 e_i + a_2}{a_3 e_i + a_4} \tag{4}$$

where  $e_i$  represents a stiffness  $k_i$  or a mass  $m_i$  and  $a_1, a_2, a_3,$  and  $a_4$  are polynomials in the variable  $\omega^2$ .

The frequency response  $X_{jg}$  has a mass or a stiffness fixed point if [7]

$$\frac{a_1}{a_3} = \frac{a_2}{a_4} \tag{5}$$

The frequencies of these fixed points are determined by equating  $X_{jg}$  to two different values of  $e_i$ .

Using Eq. (5) or the procedure presented in [7], we obtain the frequencies of the mass and stiffness fixed points of the three mass system shown in Fig. 1. These frequencies are given in third row of Table 1, where

$$\omega_1 = 0 \tag{6}$$

$$\omega_2 = \sqrt{k_1/m_1} \tag{7}$$

$$\omega_3 = \sqrt{k_3/m_3} \tag{8}$$

$$\omega_4 = \sqrt{(k_1 + k_2)/m_1} \tag{9}$$

$$\omega_5 = \sqrt{k_3(m_2 + m_3)/m_2 m_3} \tag{10}$$

$$\omega_{6,7} = \sqrt{\frac{1}{2m_1 m_2} [b_1 \mp \sqrt{b_1^2 - b_2}]} \tag{11}$$

$$\omega_{8,9} = \sqrt{\frac{1}{2m_1 m_2} [b_3 \mp \sqrt{b_3^2 - b_4}]} \tag{12}$$

$$\omega_{10,11} = \sqrt{\frac{1}{2m_2 m_3} [b_5 \mp \sqrt{b_5^2 - b_6}]} \tag{13}$$

$$b_1 = k_1 m_2 + k_2 (m_1 + m_2) \tag{14}$$

$$b_2 = 4k_1 k_2 m_1 m_2 \tag{15}$$

$$b_3 = k_1 m_2 + k_2 (m_1 + m_2) + k_3 m_1 \tag{16}$$

$$b_4 = 4(k_1 k_2 + k_1 k_3 + k_2 k_3) m_1 m_2 \tag{17}$$

$$b_5 = k_2 m_3 + k_3 (m_2 + m_3) \tag{18}$$

$$b_6 = 4k_2 k_3 m_2 m_3 \tag{19}$$

Examining these frequencies yields that these frequencies are the natural frequencies of the systems shown in Fig. 2 which represent subsystems of the original system shown in Fig.1.

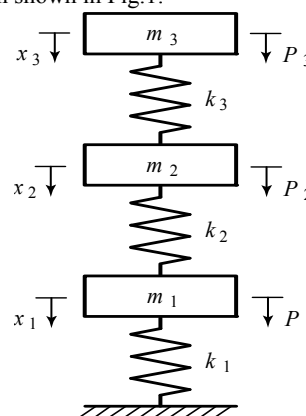


Fig. 1. Three-degree-of-freedom system.

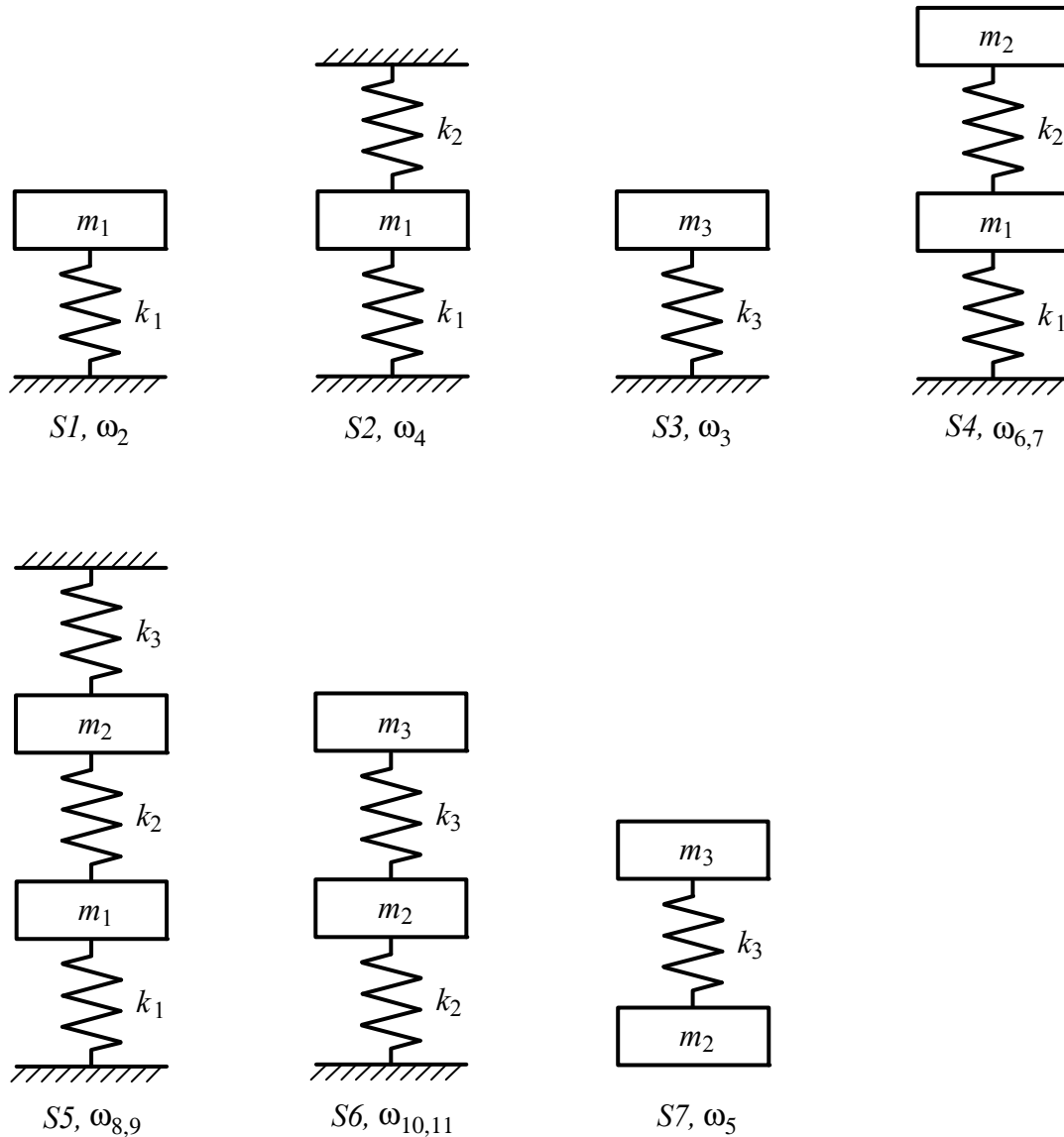


Fig. 2. Subsystems of a three-degree-of-freedom system.

In general, we can conclude, that the frequencies of mass and stiffness fixed points of vibrational linear discrete systems are natural frequencies of subsystems of the whole system.

The vibrational amplitudes  $A_{ij}$  at the fixed points frequencies of the system considered are listed in Table 1. Empty cells mean that the dynamic responses  $X_{ij}$  have no fixed points by varying the corresponding parameters  $k_i$  or  $m_i$ . For instance, from the fourth row of the table we can read that the dynamic response  $X_{11}$  has no stiffness fixed points by force application on mass  $m_1$  with the frequency  $\omega_3$  and varying the stiffnesses  $k_1$  or  $k_2$ . Other cells provide values of amplitudes  $A_{ij}$  as provided in the appendix.

### 3. Conceptual Analysis of Results

The following is conceptual discussion of the results given in Table 1.

#### 3.1. Fixed points at the frequencies $\omega_{10}$ and $\omega_{11}$

By a force application on mass  $m_1$  in Fig.1 with an excitation frequency  $\omega$  equal to one of the two natural frequencies  $\omega_{10}, \omega_{11}$  of the subsystem  $S6$  shown in Fig. 2, the subsystem  $S6$  serves in this case as an internal absorber to the subsystem  $S1$  shown in Fig.2. That is because at these frequencies the force transmitted from the spring  $k_2$  to the mass  $m_1$  is equal but opposite to the force acting there, so that  $m_1$  remains at rest ( $x_1=0$ ). The subsystem  $S6$  vibrates at  $\omega_{10}$  in its first mode and at  $\omega_{11}$  in its second mode with proportional amplitudes. In both cases, the amplitude  $A_{21}$  of mass  $m_2$  is equal to  $P_0/k_2$ , because of the force balance at  $m_1$  ( $k_2 A_{21} \cos(\omega_i t) = P_0 \cos(\omega_i t)$ ,  $i=10,11$ ). The amplitudes of mass  $m_3$  are then obtained from the eigenvectors of system  $S6$  and are given as

$$A_{31} = \frac{k_3}{k_3 - m_3 \omega_i^2} A_{21}, \quad i=10,11 \quad (20)$$

Table 1. Mass and stiffness point frequencies  $\omega_i$  and their amplitudes  $A_{ij}$  for the three-degree-of-freedom-system shown in Fig.1

	Varying parameter																					
	$k_1$			$k_2$				$k_3$				$m_1$				$m_2$			$m_3$			
	$\omega_3$	$\omega_{10}$	$\omega_{11}$	$\omega_1$	$\omega_2$	$\omega_3$	$\omega_5$	$\omega_1$	$\omega_4$	$\omega_6$	$\omega_7$	$\omega_1$	$\omega_3$	$\omega_{10}$	$\omega_{11}$	$\omega_1$	$\omega_3$	$\omega_4$	$\omega_1$	$\omega_4$	$\omega_8$	$\omega_9$
$A_{11}$		0	0	$C_1$			$C_{10}$	$C_1$				$C_1$		0	0	$C_1$	$C_8$		$C_1$			
$A_{21}$	0	$C_4$	$C_4$	$C_1$	$C_{12}$	0	$C_{10}$	$C_1$	$C_4$			$C_1$	0	$C_4$	$C_4$	$C_1$	0	$C_4$	$C_1$	$C_4$		
$A_{31}$		$C_{15}$	$C_{16}$	$C_1$	$C_{14}$		$C_{11}$	$C_1$		$C_{19}$	$C_{20}$	$C_1$		$C_{15}$	$C_{16}$	$C_1$	$C_9$	$C_7$	$C_1$		$C_{17}$	$C_{18}$
$A_{12}$	0	$C_4$	$C_4$	$C_1$	$C_{12}$	0	$C_{10}$	$C_1$	$C_4$			$C_1$	0	$C_4$	$C_4$	$C_1$	0	$C_4$	$C_1$	$C_4$		
$A_{22}$	0				$C_{12}$	0		$C_2$	0			$C_2$	0			$C_2$	0	0	$C_2$	0		
$A_{32}$	$C_5$				$C_{14}$	$C_5$		$C_2$	0	$C_{21}$	$C_{22}$	$C_2$	$C_5$			$C_2$	$C_5$	0	$C_2$	0	$C_5$	$C_5$
$A_{13}$		$C_{15}$	$C_{16}$	$C_1$	$C_{14}$		$C_{11}$	$C_1$		$C_{19}$	$C_{20}$	$C_1$		$C_{15}$	$C_{16}$	$C_1$	$C_9$	$C_7$	$C_1$		$C_{17}$	$C_{18}$
$A_{23}$	$C_5$				$C_{14}$	$C_5$		$C_2$	0	$C_{21}$	$C_{22}$	$C_2$	$C_5$			$C_2$	$C_5$	0	$C_2$	0	$C_5$	$C_5$
$A_{33}$					$C_{13}$					$C_{21}$	$C_{22}$	$C_3$				$C_3$		$C_6$	$C_3$		0	0

All three frequency responses  $X_{i1}$  have mass and stiffness fixed points at the frequencies  $\omega_{10}$  and  $\omega_{11}$  since their amplitudes  $A_{i1}$  are independent of  $k_1$  and  $m_1$  at these frequencies. These frequency responses are shown in Fig. 3, first column for different values of  $m_1$ .

Also if the force  $P$  acts on the masses  $m_2$  or  $m_3$ , then the frequency responses  $X_{i, i=2,3}$  stay having mass and stiffness fixed points at  $\omega_{10}$  and  $\omega_{11}$  (but with nonzero amplitudes), that is because of the symmetry of the system matrices  $\mathbf{M}$  and  $\mathbf{K}$  of the whole system shown in Fig. 1. On the other hand, the fixed points at  $\omega_{10}$  and  $\omega_{11}$  in the frequency responses of masses  $m_2$  and  $m_3$  vanish in this case. Figure 3, second column shows dynamic responses for different values of  $m_1$  by force application on mass  $m_2$ .

3.2. Fixed points at the frequencies  $\omega_8$  and  $\omega_9$

By force application on mass  $m_3$  in Fig.1 with an excitation frequency  $\omega$  equal to one of the two natural frequencies  $\omega_8$  and  $\omega_9$  of the subsystem  $S5$  given in Fig. 2, this system serves as an internal absorber to the mass  $m_3$ . That is because at these frequencies the force transmitted from the spring  $k_3$  to the mass  $m_3$  is equal but opposite to the excitation force acting there, so that  $m_3$  remains at rest ( $x_3 = 0$ ). The subsystem  $S5$  vibrates at  $\omega_8$  in its first mode and at  $\omega_9$  in its second mode with proportional amplitudes. In both cases, the amplitude of mass  $m_2$  is equal to  $P_0/k_3$ , because of the force balance at  $m_3$  ( $k_3x_2 = P$ ). The amplitude of mass  $m_1$  is then obtained from the eigenvectors of system  $S5$  and given as

$$A_{i3} = \frac{k_2}{k_1 + k_2 - m_1\omega_i^2} A_{23} \quad i=8,9 \quad (21)$$

The frequency responses  $X_{i3, i=1,2,3}$  have mass fixed points at the frequencies  $\omega_8$  and  $\omega_9$  since their amplitudes  $A_{i3}$  are independent of the values of  $m_3$  at these frequencies.

Also if the force  $P$  acts on the masses  $m_1$  or  $m_2$ , then mass  $m_3$  stays keeping its fixed points at the frequencies  $\omega_8$  and  $\omega_9$ , because of the symmetry of the mass and stiffness matrices of the whole system which leads to  $X_{ij}=X_{ji, i,j=1,2,3}$ . The frequency responses of masses  $m_1$  and  $m_2$  possess in this case no fixed points more.

3.3. Fixed points at the frequencies  $\omega_6$  and  $\omega_7$

By force application on mass  $m_3$  in Fig. 1, the amplitudes of all three masses  $A_{i3}$  remain constant at the frequencies  $\omega_6$  and  $\omega_7$  independent of the values of  $k_3$ . This means that at these frequencies, the spring  $k_3$  remains undeformed, so that at these frequencies  $x_3 = x_2$ , i.e. there is no relative motion between the masses  $m_2$  and  $m_3$ . Hence by varying the values of  $k_3$ , the frequency responses  $X_{i3}$  get stiffness fixed points at  $\omega_6$  and  $\omega_7$  as shown in Fig.4.

By force application on the masses  $m_1$  or  $m_2$  at the frequencies  $\omega_6$  or  $\omega_7$  and varying the values of  $k_3$ , the stiffness fixed points of the dynamic responses  $X_{11}, X_{12}, X_{21},$  and  $X_{22}$  vanish, where  $X_{31}$  and  $X_{32}$  stay having fixed points at  $\omega_6$  and  $\omega_7$  because of the symmetry of the mass and stiffness matrices of the whole system.

3.4. Fixed points at the frequencies  $\omega_2$  and  $\omega_5$

Varying the values of  $k_2$  yields stiffness fixed points at the frequencies  $\omega_2$  and  $\omega_5$ . At the frequency  $\omega_2$ , all the frequency responses  $X_{ij}$ , except  $X_{11}$  have stiffness fixed points since their amplitudes  $A_{ij}$  at this frequency are independent of the stiffness  $k_2$ . At the frequency  $\omega_5$ , the frequency responses  $X_{11}, X_{21}, X_{31}, X_{12},$  and  $X_{13}$  have stiffness fixed points.

By force application on mass  $m_2$  or  $m_3$  at the frequency

$$\omega_2 = \sqrt{\frac{k_1}{m_1}},$$

the natural frequency of the system  $S1$ ,

the system  $S7$  vibrates in its own way unaffected from the spring  $k_2$ , as if this spring does not exist.

In order to maintain the whole system connected by the force application on the masses  $m_2$  or  $m_3$  at the frequency  $\omega_2$ , and at the same time the spring  $k_2$  remains undeformed, the amplitude of mass  $m_1$  must equal to the amplitude of the neighborhood mass  $m_2$  in this case as shown in Table 1, 6<sup>th</sup> column; i.e.  $X_{12}=X_{22}$ , and  $X_{13}=X_{23}$ .

By force application on  $m_2$ , the vibration amplitudes of masses  $m_2$  and  $m_3$ , respectively, become: respectively, become:

$$A_{22} = \frac{m_1(k_3 m_1 - k_1 m_3) P_0}{k_1 [k_1 m_2 m_3 - k_3 m_1 (m_2 + m_3)]} \quad (22)$$

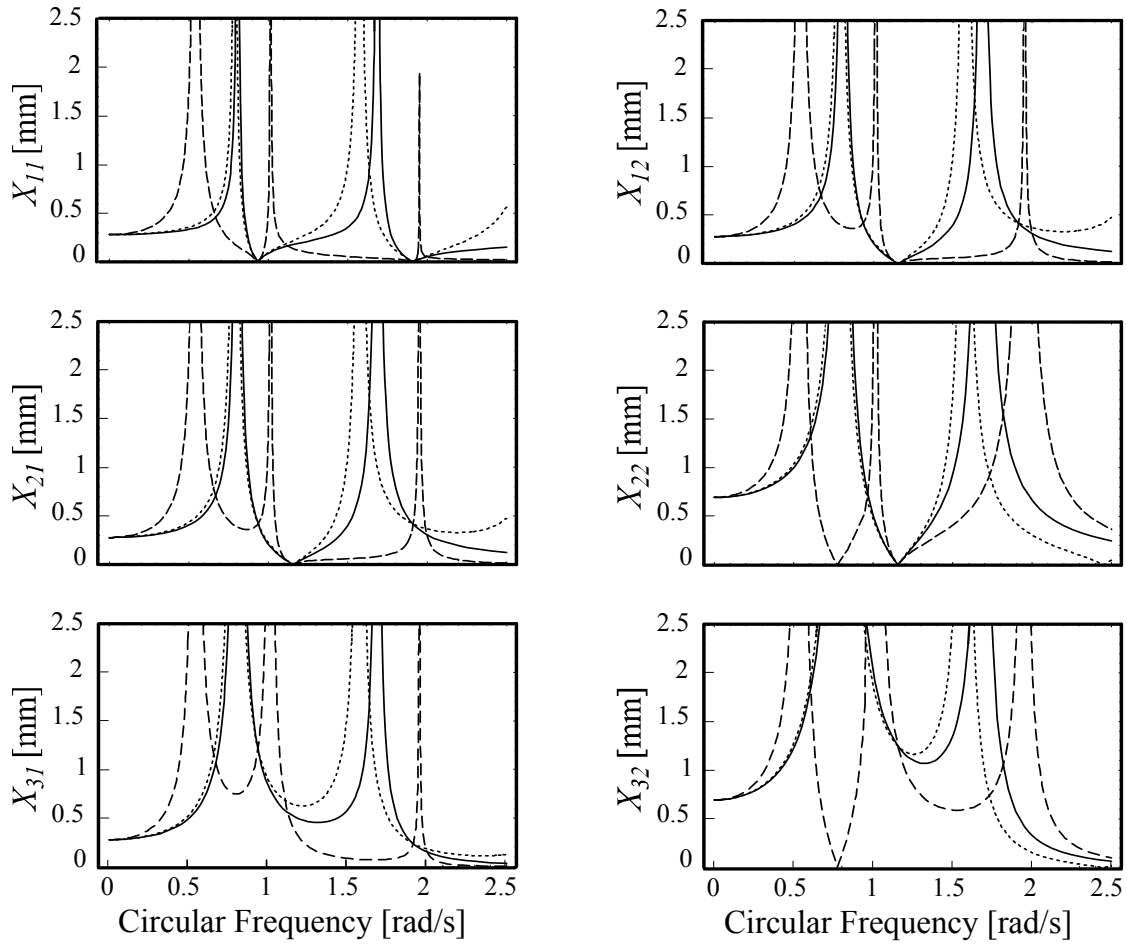


Fig. 3. Frequency responses  $X_{ij}$  for the system shown in Fig. 1 for the arbitrary selected parameters:  $k_1 = 36$  N/m,  $k_2 = 24$  N/m,  $k_3 = 8$  N/m,  $m_2 = 10$  kg,  $m_3 = 6$  kg,  $P_0 = 0.01$  N and different values of  $m_1$ . (—)  $m_1 = 2$  kg, (····)  $m_1 = 10$  kg, (-----)  $m_1 = 100$  kg.  $\omega_{10} = 0.935$  rad/s,  $\omega_{11} = 1.913$  rad/s.

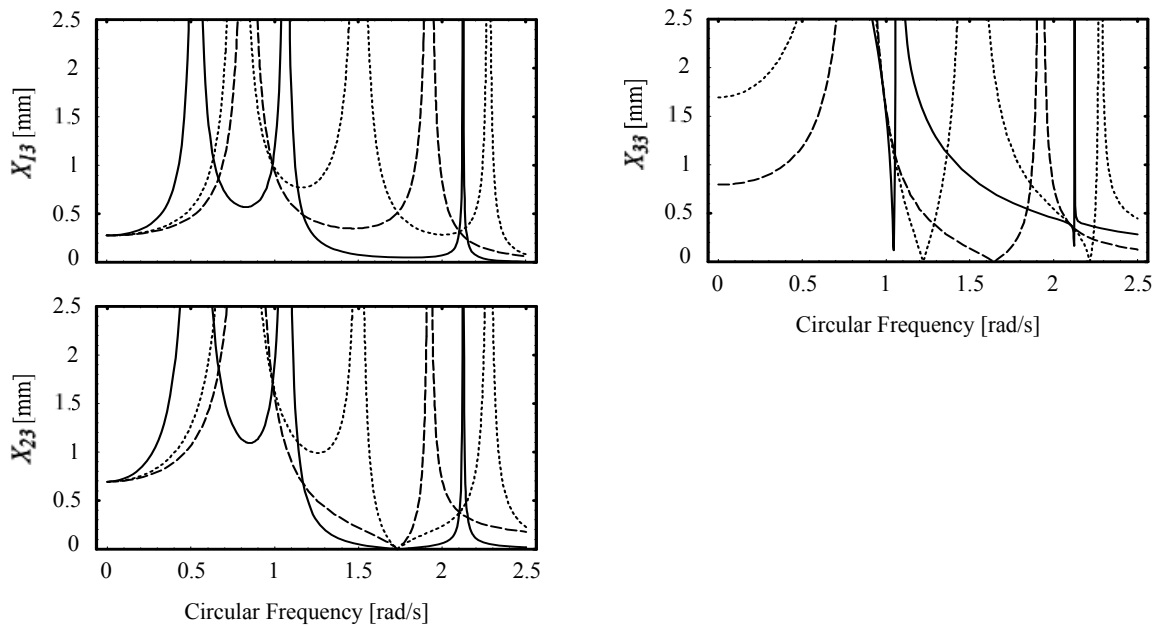


Fig. 4. Frequency responses  $X_{i3}$  for the system shown in Fig. 1 for the arbitrary selected parameters:  $k_1 = 36$  N/m,  $k_2 = 24$  N/m,  $m_1 = 20$  kg,  $m_2 = 10$  kg,  $m_3 = 6$  kg,  $P_0 = 0.01$  N and different values of  $k_3$ . (—)  $k_3 = 2$  N m<sup>-1</sup>, (····)  $k_3 = 10$  N m<sup>-1</sup>, (-----)  $k_3 = 100$  N/m.  $\omega_6 = 0.988$  rad/s,  $\omega_7 = 2.103$  rad/s.

$$A_{32} = \frac{m_1^2 k_3 P_0}{k_1 [k_1 m_2 m_3 - k_3 m_1 (m_2 + m_3)]} \quad (23)$$

By the force application on  $m_2$ , the amplitude of  $m_2$  becomes  $A_{22} = A_{32}$  because of the symmetry of the system matrices. The amplitude of mass  $m_3$  is then

$$A_{33} = \frac{m_1 (k_3 m_1 - k_1 m_2) P_0}{k_1 [k_1 m_2 m_3 - k_3 m_1 (m_2 + m_3)]} \quad (24)$$

By the force application on mass  $m_1$  at the frequency  $\omega_2$ , the fixed point of  $X_{11}$  vanishes whereas  $X_{21}$  and  $X_{31}$  stay keeping their fixed points at  $\omega_2$  because of the symmetry of the mass and stiffness matrices of the whole system. The amplitudes of masses  $m_2$  and  $m_3$  are then  $A_{21} = A_{12}$  and  $A_{31} = A_{13}$ , respectively.

By force application on mass  $m_1$  at the frequency  $\omega_5$ , the natural frequency of the subsystem  $S7$ , the subsystem  $S7$  vibrate in its second mode shape with an amplitude ratio  $A_{31}/A_{21} = m_2/m_3$ . The system  $S1$  vibrates at this frequency with the amplitude

$$A_{11} = \frac{P_0}{k_1 - m_1 \omega_5^2} \quad (25)$$

In order to remain the spring  $k_2$  undeformed, the mass  $m_2$  vibrates with the same amplitude and in the same direction as  $m_1$  as shown in Table 1, 8<sup>th</sup> column, that is

$$A_{21} = \frac{P_0}{k_1 - m_1 \omega_5^2} \quad (26)$$

For the amplitude of mass  $m_3$  we get

$$A_{31} = \frac{m_2}{m_3} A_{21} = \frac{m_2}{m_3} \frac{P_0}{k_1 - m_1 \omega_5^2} \quad (27)$$

Also because of the symmetry of the system matrices  $\mathbf{M}$  and  $\mathbf{K}$ , the amplitudes of mass  $m_1$  by the application of the force on  $m_2$  or  $m_3$  become  $A_{12} = A_{31}$ , and  $A_{13} = A_{21}$ , respectively, and its frequency responses  $X_{13}$  and  $X_{12}$  have stiffness fixed points at  $\omega_5$ .

### 3.5. Fixed points at the frequencies $\omega_3$ and $\omega_4$

#### 3.5.1. Force application on $m_2$

If the force  $P$  acts on mass  $m_2$  in Fig.1 with an excitation frequency equal to one of the eigenfrequencies  $\omega_4$  and  $\omega_3$ , of subsystems  $S2$  and  $S3$ , respectively, shown in Fig. 2, then these subsystems act as internal absorbers for mass  $m_2$  as shown in Fig. 5.

*Absorber S2 at the frequency  $\omega_4$*

This case occurs when the mass  $m_2$  is acted upon a force with the natural frequency  $\omega_4$  of the subsystem  $S2$ . At this frequency, the subsystem  $(m_2, k_3, m_3)$  remains at rest ( $x_2 = x_3 = 0$ ), where the internal absorber  $S2$  vibrates at its natural frequency with the constant amplitude  $A_{12} = P_0/k_2$ , which is obtained from the force balance at  $m_2$ ; that is, from  $k_2 A_{12} \cos \omega_4 t = P_0 \cos \omega_4 t$ , follows:  $A_{12} = P_0/k_2$ . Also the frequency responses  $X_{i2}$ ,  $i=1,2,3$  have mass and stiffness fixed points at the frequency  $\omega_4$  since the

amplitudes  $A_{i2}$  are independent of  $m_2$ ,  $m_3$ , and  $k_3$  at this frequency as shown in Table 1.

*Absorber S3 at the frequency  $\omega_3$*

If the excitation frequency of the applied load becomes equal to  $\omega_3$ , the natural frequency of the subsystem  $S3$ , then this subsystem vibrates with a constant amplitude  $A_{32}$  at its natural frequency, where the subsystem  $(k_1, k_2, m_1, m_2)$  remains at rest ( $x_1 = x_2 = 0$ ). Therefore at the frequency  $\omega_3$  all three frequency responses  $X_{i2}$  have mass and stiffness fixed points by varying the values of  $k_1, k_2, m_1$ , or  $m_2$ . The vibration amplitude  $A_{32}$  of mass  $m_3$  follows from the force balance at  $m_2$ . (from  $k_3 A_{32} \cos \omega_3 t = P_0 \cos \omega_3 t$  follows:  $A_{32} = P_0/k_3$ ).

Also the frequency responses  $X_{2i}$ ,  $i=1,2,3$  have always fixed points at the absorber frequencies  $\omega_3$  and  $\omega_4$  independent of which mass, the force acts, because of the symmetry of the system matrices. However, the amplitude of  $m_2$  may become nonzero when the force is applied on the other masses.

#### 3.5.2. Force applied on mass $m_1$

When the force  $P$  acts on mass  $m_1$  at the frequency  $\omega_3$ , the natural frequency of the top subsystem  $S3$  ( $k_3$ - $m_3$ -system), then the forces acting on mass  $m_2$  will be balanced ( $k_3 x_3 = k_2 x_1$ ), since  $S3$  serves at this frequency as an absorber for mass  $m_2$ . Therefore, at the frequency  $\omega_3$  mass  $m_2$  remains at rest independent of the values of  $k_1, k_2, m_1$ , and  $m_2$ , whereas the masses  $m_1$  and  $m_3$  vibrate out of phase with different but proportional amplitudes.

Using the theory of vibration of single degree of freedom systems [8], we obtain for the amplitude of mass  $m_1$

$$A_{11} = \frac{P_0}{k_1 + k_2 - m_1 \omega_3^2} = \frac{m_3 P_0}{k_3 m_1 - (k_1 + k_2) m_3} \quad (28)$$

From the force balance at mass  $m_2$  where  $k_3 x_3 = k_2 x_1$ , we obtain for the vibration amplitude of mass  $m_3$

$$A_{31} = \frac{k_2}{k_3} A_{11} = \frac{k_2}{k_3} \frac{m_3 P_0}{k_3 m_1 - (k_1 + k_2) m_3} \quad (29)$$

From Eqs. (28) and (29) it is observable that the amplitudes of the masses  $m_1$  and  $m_3$  are independent of  $m_2$  at the frequency  $\omega_3$ . Therefore their frequency responses  $X_{11}$  and  $X_{31}$  possess mass fixed point at  $\omega_3$  by varying the values of  $m_2$ .

Also if the force acts on mass  $m_1$  at the frequency  $\omega_4$ , then the amplitude of  $m_2$  becomes  $A_{21} = A_{12} = P_0/k_2$  because of symmetry of the mass and stiffness matrices of the entire system. The amplitude of  $m_3$  becomes in this case

$$A_{32} = \frac{k_3}{k_2} \frac{P_0}{k_3 - m_3 \omega_4^2} = \frac{k_3}{k_2} \frac{m_1 P_0}{k_3 m_1 - (k_1 + k_2) m_3} \quad (30)$$

which is independent of mass  $m_2$ . Hence the frequency response  $X_{31}$  has a mass fixed point at  $\omega_4$  by varying the values of  $m_2$ . However, the mass fixed point of the frequency response  $X_{11}$  vanishes in this case.

#### 3.5.3. Force applied on mass $m_3$

When the force  $P$  acts on the mass  $m_3$  at the frequency  $\omega_4$ , the natural frequency of the bottom subsystem  $S2$  ( $k_1$ -

$k_2$ - $m_1$ -system), then the forces acting on mass  $m_2$  will be balanced ( $k_3x_3 = k_2x_1$ ), since  $S2$  serves in this case as an

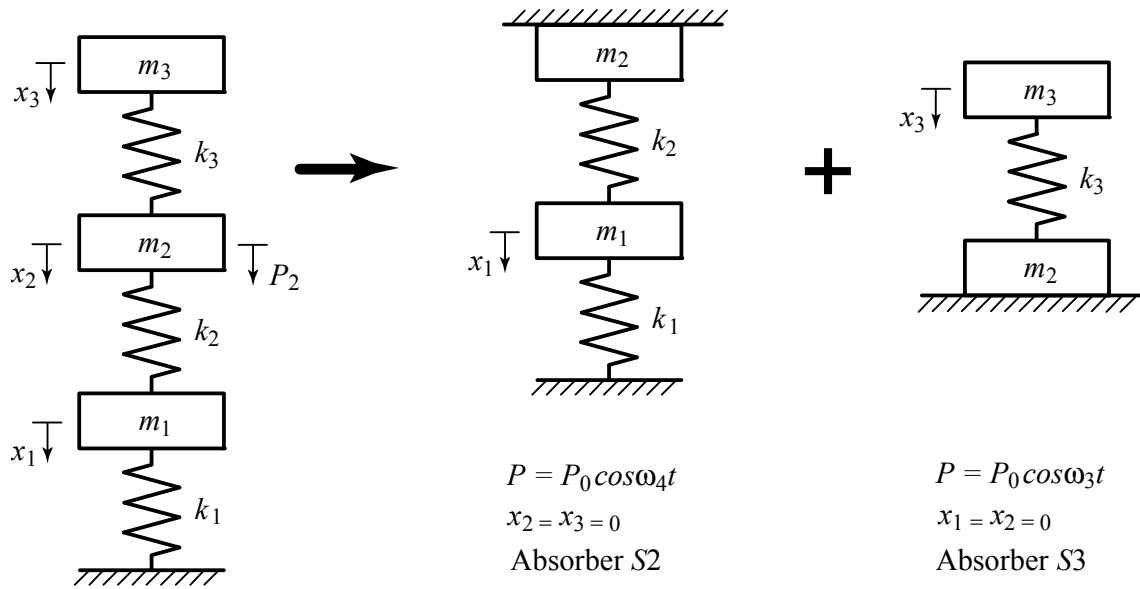


Fig. 5. Entire and subsystems (as absorbers).

internal absorber for mass  $m_2$ . Therefore at this frequency,  $m_2$  remains at rest independent of the values of  $k_3$ ,  $m_2$ , and  $m_3$ , whereas the masses  $m_1$  and  $m_3$  vibrate out of phase with different but proportional amplitudes. The vibration amplitude of mass  $m_3$  may be obtained from the subsystem  $S3$  as

$$A_{33} = \frac{P_0}{k_3 - m_3 \omega_4^2} = \frac{m_1 P_0}{k_3 m_1 - (k_1 + k_2) m_3} \quad (31)$$

From the force balance on mass  $m_2$  where  $k_3x_3 = k_2x_1$  we get for the vibration amplitude of mass  $m_1$ :

$$A_{13} = \frac{k_3}{k_2} A_{33} = \frac{k_3}{k_2} \frac{m_1 P_0}{k_3 m_1 - (k_1 + k_2) m_3} \quad (32)$$

From Eqs. (31) and (32) it is obvious that the amplitudes of the masses  $m_1$  and  $m_3$  are independent of mass  $m_2$  at the frequency  $\omega_4$ . Therefore their frequency responses  $X_{13}$  and  $X_{33}$  have mass fixed points at  $\omega_4$  by varying the values of  $m_2$ . Also at the frequency  $\omega_3$ , the amplitude of mass  $m_1$  becomes

$$A_{13} = \frac{k_2}{k_3} \frac{P_0}{[k_1 + k_2 - m_1 \omega_3^2]} = \frac{k_2}{k_3} \frac{m_3 P_0}{k_3 [k_3 m_1 - (k_1 + k_2) m_3]} \quad (33)$$

which is independent of mass  $m_2$ . Hence the frequency response  $X_{13}$  has a mass fixed point at  $\omega_3$  by varying the values of  $m_2$ . On the other hand, the mass fixed point of the frequency response  $X_{33}$  vanishes in this case.

### 3.6. Fixed points at the frequency $\omega_1$ (static case)

The static deflections  $A_{s,i}$  of the masses  $m_1$ ,  $m_2$ , and  $m_3$  due to the force amplitude  $P_0$  are defined as follows:

The force acts on mass  $m_1$

$$A_{s,1} = A_{s,2} = A_{s,3} = \frac{P_0}{k_1} \quad (34)$$

The force acts on mass  $m_2$

$$A_{s,1} = \frac{P_0}{k_1} \quad (35)$$

$$A_{s,2} = A_{s,3} = \frac{(k_1 + k_2) P_0}{k_1 k_2} \quad (36)$$

The force acts on mass  $m_3$

$$A_{s,1} = \frac{P_0}{k_1} \quad (37)$$

$$A_{s,2} = \frac{(k_1 + k_2) P_0}{k_1 k_2} \quad (38)$$

$$A_{s,3} = \frac{(k_1 k_2 + k_1 k_3 + k_2 k_3) P_0}{k_1 k_2 k_3} \quad (39)$$

From Eqs. (34) through (39) it is obvious that the static deflections  $A_{s,i}$  are independent of the masses  $m_i$ ,  $i=1,2,3$ . Therefore all frequency responses  $X_{ij}$ ,  $i,j=1,2,3$  have mass fixed points at the frequency  $\omega_1 = 0$ . Since all static deflections are dependent on the stiffness  $k_1$ , varying the values of this stiffness will not lead to stiffness fixed points in all frequency responses  $X_{ij}$ .

By force application on mass  $m_1$ , all frequency responses  $X_{i1}$  have stiffness fixed points by varying the values of  $k_2$  or  $k_3$ .

By force application on mass  $m_2$ , all frequency responses  $X_{i2}$  have stiffness fixed points at  $\omega_1$  when the values of  $k_3$  are varied. Also only  $X_{12}$  possesses a stiffness fixed point by varying the values of  $k_2$ .

Acts the force on the mass  $m_3$ , then the frequency response  $X_{i3}$  has stiffness fixed points at  $\omega_1$  by varying the values of  $k_2$  or  $k_3$  and  $X_{23}$  has a stiffness fixed point by varying  $k_3$ . The response  $X_{33}$  has no fixed points at  $\omega_1$  in this case.

#### 4. Conclusions

In this paper, the physical nature of mass and stiffness fixed points of undamped linear discrete vibrational systems is explored. It is found that the mass and stiffness fixed points frequencies of these systems represent natural frequencies of subsystems of the entire system. Furthermore, it is found that these fixed points are strongly related with the phenomenon of internal absorber and can be used to design vibratory systems with zero or constant amplitudes for some masses of the system. Also the mass and stiffness fixed points frequencies and their amplitudes of a system with three degree of freedom were determined and discussed in detail.

#### References

- [1] Den Hartog J.P. Mechanical Vibrations. New York: McGraw-Hill; 1956.
- [2] Klotter K. Technische Schwingungslehre, Zweiter Band, Schwinger von mehreren Freiheitsgraden. Berlin/New York: Springer-Verlag; 1981.
- [3] D.B. Bogy, P.R. Paslay, "An evaluation of the fixed point method of vibration analysis for a particular system with initial damping". Transactions of American Society of Mechanical Engineers, Journal of Engineering for Industry, Vol. 85B, 1963, 233-236.
- [4] A. Henney, J.P. Raney, "The optimization of damping of four configuration of vibrating uniform beam". Transactions of American Society of Mechanical Engineers, Journal of Engineering for Industry, Vol. 85B, 1963, 259-264.
- [5] J. Dayou, "Fixed-points theory for global vibration control using vibration neutralizer". Journal of Sound and Vibration, Vol. 292, No. 3-5, 2006, 765-776.
- [6] M. Abu-Hilal, "Fixed points of two-degree of freedom systems". Shock and Vibration, Vol. 5, No. 3, 1998, 199-205.
- [7] M. Abu-Hilal, "Mass and Stiffness fixed points of vibrational discrete systems". Journal of Sound and Vibration, Vol. 254, No. 5, 2002, 997-1004.
- [8] Rao S.S. Mechanical Vibration, 3rd ed., New York: Addison-Wesley Publishing Company; 1995.

Appendix

$$C_1 = \frac{P_0}{k_1} \quad (40)$$

$$C_2 = \frac{(k_1 + k_2)P_0}{k_1 k_2} \quad (41)$$

$$C_3 = \frac{(k_1 k_2 + k_1 k_3 + k_2 k_3)P_0}{k_1 k_2 k_3} \quad (42)$$

$$C_4 = \frac{P_0}{k_2} \quad (43)$$

$$C_5 = \frac{P_0}{k_3} \quad (44)$$

$$C_6 = \frac{m_1 P_0}{k_3 m_1 - (k_1 + k_2) m_3} \quad (45)$$

$$C_7 = \frac{k_3}{k_2} \frac{m_1 P_0}{[k_3 m_1 - (k_1 + k_2) m_3]} \quad (46)$$

$$C_8 = \frac{m_3 P_0}{k_3 m_1 - (k_1 + k_2) m_3} \quad (47)$$

$$C_9 = \frac{k_2}{k_3} \frac{m_3 P_0}{[k_3 m_1 - (k_1 + k_2) m_3]} \quad (48)$$

$$C_{10} = \frac{m_2 m_3 P_0}{k_1 m_2 m_3 - k_3 m_1 (m_2 + m_3)} \quad (49)$$

$$C_{11} = \frac{m_2^2 P_0}{k_1 m_2 m_3 - k_3 m_1 (m_2 + m_3)} \quad (50)$$

$$C_{12} = \frac{m_1 (m_1 k_3 - k_1 m_3) P_0}{k_1 [k_1 m_2 m_3 - k_3 m_1 (m_2 + m_3)]} \quad (51)$$

$$C_{13} = \frac{m_1 (m_1 k_3 - k_1 m_2) P_0}{k_1 [k_1 m_2 m_3 - k_3 m_1 (m_2 + m_3)]} \quad (52)$$

$$C_{14} = \frac{k_3 m_1^2 P_0}{k_1 [k_1 m_2 m_3 - k_3 m_1 (m_2 + m_3)]} \quad (53)$$

$$C_{15} = \frac{k_3}{k_2} \frac{P_0}{[k_3 - m_3 \omega_{10}^2]} \quad (54)$$

$$C_{16} = \frac{k_3}{k_2} \frac{P_0}{[k_3 - m_3 \omega_{11}^2]} \quad (55)$$

$$C_{17} = \frac{k_2}{k_3} \frac{P_0}{[k_1 + k_2 - m_1 \omega_8^2]} \quad (56)$$

$$C_{18} = \frac{k_2}{k_3} \frac{P_0}{[k_1 + k_2 - m_1 \omega_9^2]} \quad (57)$$

$$C_{19} = \frac{2m_2^2}{m_3} \frac{P_0}{[m_2 (k_1 - k_2) - k_2 m_1 + C]} \quad (58)$$

$$C_{20} = \frac{2m_2^2}{m_3} \frac{P_0}{[m_2 (k_2 - k_1) + k_2 m_1 + C]} \quad (59)$$

$$C_{21} = \frac{m_2}{k_2 m_3} \frac{[m_2 (k_2 + k_1) - k_2 m_1 + C] P_0}{[m_2 (k_2 - k_1) + k_2 m_1 - C]} \quad (60)$$

$$C_{22} = \frac{m_2}{k_2 m_3} \frac{[m_2 (k_2 + k_1) - k_2 m_1 - C] P_0}{[m_2 (k_2 - k_1) + k_2 m_1 + C]} \quad (61)$$

$$C = \sqrt{[k_1 m_2 + k_2 (m_1 + m_2)]^2 - 4k_1 k_2 m_1 m_2} \quad (62)$$



# Experimental Investigations of the Effect of Some Insulating Materials on the Compressive Strength, Water Absorption and Thermal Conductivity of Building Bricks.

Ali M. Othman \*

Mechanical Engineering Department, Philadelphia University, 19392, P.O. Box 1, Jordan

## Abstract

An experimental investigation was carried out to study the possibility of decreasing the consumed energy in buildings in Jordan by decreasing the thermal conductivity of building bricks. Insulation materials with different weight percentages are mixed with the traditional materials of the building bricks used in Jordan. The used materials were polystyrene, polycarbonate, polyethylene of (2.5, 5, 10 & 15wt %), wood dust and natural cork of (1, 2, 3, & 4 wt %), glass wool and rock wool layer of ( 24, 36, 48 and 60 gm). The water absorption, compressive strength and thermal conductivity, of the prepared bricks were determined and the obtained results are discussed and compared. The results showed that addition of the insulating materials resulted in reduction of water absorption in the entire materials examined (a minimum of -4.14% for glass wool addition) except natural cork and wood dust (a maximum of +207.62% of natural cork addition). The results also indicated a decrease in the compressive strength as much as (90.71 %) for both glass wool and natural cork additions. A pronounced decrease in thermal conductivity was also noticed of about 70 % of its value for the case of glass wool and natural cork additions, at addition rate of 4% weight.

© 2010 Jordan Journal of Mechanical and Industrial Engineering. All rights reserved

Keywords: Thermal Conductivity, Building Materials, Insulating Materials, Water Content, Compressive Strength.

$\lambda$	:Thermal conductivity	J/kg.K
$\Delta$	:Difference	

## Nomenclature

### Alphabetic Symbols

A	:Area	$m^2$
$C_s$	:Specific heat	J/kg.K
dT	:Temperature difference	$^{\circ}C$
HFM	:Heat flow meter output	mV
k1-k6	:Calibration constants	----
Ls	:Sample thickness	m
$q_x$	:Heat rate	W
R	:Thermal resistance	$m^2.k/W$
$R_{tot}$	:Thermal resistance	k/W
$T_C$	:Cold plate temperature	$^{\circ}C$
$T_H$	:Hot plate temperature	$^{\circ}C$
$\bar{T}$	:Mean temperature	$^{\circ}C$
$t_s$	:Sampling interval	s
U	:Overall heat transfer coefficient	W/K.m <sup>2</sup>

### Greek Symbols

$\rho$	:Density	(kg/m <sup>3</sup> )
--------	----------	----------------------

## 1. Introduction

Jordan is a Middle Eastern developing and non-oil producing country. In the long future the country will continue to be dependent on imported oil, since 94% of the total energy requirements are imported and only 6% are covered from local sources. The locally produced crude oil and natural gas covers only 3.7% of the overall consumed energy. In the last three years an unexpected large increase of oil prices occurred and badly influenced the Jordan economy, which raised the cost of consumed energy to 23 % of the Gross National Product of the country as reported in MEMR annual report [1]. Yahia, et al. [2] showed that in the years (2003-2007) the total energy consumption in the domestic (household) sector reached (21-23) % from the total energy consumption, from which the energy consumption due to heating, ventilation and air-conditioning in buildings represents the important part of total energy consumption in Jordan. Also Yahia, et al. [2] showed that one of the main problems facing hotels in Jordan is the high consumption of energy caused by heating, ventilation, and air conditioning systems (HVAC) and lighting, as well as other equipments in different

\* Corresponding author. drothman@philadelphia.edu.jo

departments; this is mainly due to the lack of insulation techniques in most hotels, so Jordan's government and people are compelled to take all measures for more efficient energy consumption. An important measure for energy saving is to lower building energy requirements to a minimum. Papadopoulos and Giama [3] reported that the energy consumption in the building sector constitutes a major part (40%) of the annual EU final energy use (European Commission, 2001). The most significant part of this amount of energy is consumed in space heating while the cooling demands, are still relatively small. Various measures that may be applied to lower building energy consumption are natural and controlled ventilation, solar shading, various types of glazing, orientation, shape of buildings, and thermal mass. Jaber [4] reported that more efficient energy consumption can be achieved by improving the buildings energy behavior by reducing the energy consumed by heating, ventilation and air-conditioning. In Jordan energy improvements can be also achieved by minimizing the energy consumption by using thermal insulating materials with low conductivity values (less than 0.04 W/m.K) and with a proper thickness. Papadopoulos [5] showed that an increase of thermal insulation thickness from 5 cm in 1975 to the current valid minimum of 20 cm resulted in drop of the average specific annual consumption from 300 kWh/m<sup>2</sup> to 50 kWh/m<sup>2</sup>.

Al-Sanea [6] found that the inclusion of a 5-cm thick molded polystyrene layer reduced the roof heat transfer load to one-third of its value in an identical roof section without insulation. Hernandez-Olivares et al. [7] studied mechanical and thermal properties of a composite material that is made of cork and gypsum; they found that cork-gypsum composite is characterized by both low thermal conductivity and low density. On the other hand, the mechanical properties of cork-gypsum composite are poor, and such a composite material was suggested for use in building applications as partitions.

Mohsen and Akash [8] showed that large energy savings about (76.8%) can be achieved when polystyrene is used for both wall and roof insulations. Those results were concluded in the light of the fact that only 5.7% of dwelling in Jordan's urban areas have been provided with wall insulation and none of the roofs. They also reported that concrete blocks forms 63 % of construction materials in Jordan. Jubran et al. [9] investigated the use of Jordan Valley clay with addition of straw, chicken feather, human hair, cement and polystyrene as insulating materials. The percentage of insulating materials in the brick ranged from 2 to 20 %. They also found that the combined additives consisting of 10 % rock wool, 5% human hair and 5% cement gave the best thermal and mechanical properties. Jaber and Hammad [10] showed that adding thermal insulation system proved to be effective nearly 82% of the estimated required heating energy was saved by using thermal insulation of 0.057 m and about 7.2 m<sup>2</sup> of Trombe wall system where added and the payback period was less than 2 year. Awni Al-Otoom et al [11] presented a new technology based on crystallization of the salt solution of sodium acetate, which can be produced via the reaction of acetic acid and sodium carbonate. It is believed that the crystals of this salt grow relatively fast and, hence, minimize the pore volumes inside the concrete and increase the service life of the concrete. An optimum

concentration of the solution was reported as 20 wt %. Bulent et al. [12] showed that using waste polyethylene and rubber pieces, which exist in environment and can be obtained with almost no cost remarkably, lower thermal conductivity of ordinary concrete. It is found that the insulation performance is improved for polyethylene bottle pieces between 10.27% and 18.16%, depending on the geometries of added pieces. The reuse of these materials in concretes seems to be good choice for contributing to cleaner environment and lower insulation cost.

The major construction materials of walls in Jordan are stone, reinforced concrete; cement blocks, mud and others. The cement blocks are the most widely used construction materials in Jordan, which forms about 63%; therefore decreasing their thermal conductivity will comprehend wide type of buildings and lead to significant savings in the consumed energy by heating and air-conditioning.

The main objective of this work is to investigate the effect of the addition of some insulation materials with different weight percentages on the water absorption, compressive strength and the thermal conductivity of the bricks used in building houses in Jordan. The objective of this arrangement besides lowering the thermal conductivity is to encourage the bricks factories locally and regionally to use some improved insulation materials in building bricks.

## 2. Theoretical Considerations

The inside door temperature of building is affected by the three modes of heat transfer: convection, conduction and radiation. The major portion of heat is transmitted into the building by conduction mode through the walls in addition to heat losses by air leakage. The thermal conductivity for steady state condition of a single wall can be calculated from the following Fourier's law [13]:

$$q_x = -\lambda A \frac{dT}{dx} \quad (1)$$

Where,  $q_x$  is the heat rate in (W),  $A$  is the area of the wall normal to the direction of heat transfer in (m<sup>2</sup>),  $dx = x_2 - x_1 = L$  represents the wall thickness in (m),  $dT = (T_{s, o} - T_{s, i})$  is the temperatures of the inside and outside surfaces of the wall in (K) and  $\lambda$  is the thermal conductivity of the wall material (W/m.K).

The composite walls involve several layers of different materials with different thermal conductivities. In the composite systems it is often convenient to work with Newton's law of cooling using the following equation:

$$q_x = UA\Delta T \quad (2)$$

Where  $U$  is the overall heat transfer coefficient (W/K.m<sup>2</sup>) and defined as  $U = \frac{1}{R_{tot}A}$ , where  $R_{tot}$  is the total thermal resistance (k/W) and represents the sum of all parallel and series thermal resistances and  $\Delta T$  is the overall temperature difference. In this research work the thermal conductivity of bricks containing different weight percentages of insulating materials are experimentally determined and compared with thermal conductivity of the bricks which do not contain any insulating materials.

### 3. Materials, Equipment and Experimental Procedures

#### 3.1. Materials

The materials used throughout this work are the typical ones used in manufacturing the ordinary bricks used in building houses in Jordan. These are cement, soft sand cobble stones and white soft sand. Other insulating materials were used and added in different weight percentages to the bricks. These are: polystyrene, polycarbonate, polyethylene, natural cork, wood dust, glass wool and rock wool.

The insulation materials were chosen because of their ease of handling, low water absorption values, low cost and low thermal conductivity [14, 15]

#### 3.2. Equipment

The Hilton B480 Thermal Conductivity of Buildings & Insulating Materials Unit shown in Figure. 1 was used to measure the thermal conductivity of the different manufactured specimens. The apparatus consists mainly of an insulated fiberglass hinged enclosure. The base section of the closure contains the heat flow meter and the cold plate assembly and mounted on four springs. The plate is cooled with water to maintain it at constant temperature. The enclosure lid houses the electrically heated hot plate, which is electronically controlled for setting the required temperature. A computerized system is used to determine and display the measured values of thermal conductivity.

The faces of the enclosure are insulated to ensure adiabatic boundary condition and to ensure that all faces of the specimen are not in direct contact with the hot and the cold plates. This thermal conductivity measuring method is a heat flow meter method which complies with the International Standard for steady-state measurement, ISO8301, [16].

The compressive strength of the different specimens was determined using the universal testing machine.

#### 3.3. Experimental Procedures

The experimental procedure started with preparation of the dry concrete bricks following the same procedure used in preparation of the bricks used in buildings in Jordan, which is in accordance with the International Standards. The bricks were of the dimensions 300x300x30 mm. In this research work thirty three specimens were prepared for water absorption, compressive strength and the thermal conductivity tests. The insulating materials were added in different weight percentages during the preparation of the specimens. Summary of the data regarding the tested bricks is shown in Table 1. Each sample has been left to dry for 60 days at ambient temperature of 25 °C. All insulating materials were added in the form of small solid pieces except the rock and glass wool, in which insulation layer is inserted in the middle of the block, this arrangement is done due to difficulties of obtaining these materials in solid pieces.

Table 1. Specimens' Specifications.

Insulation Material (IM)	Specimen code	Cement, coarse, sand and water(w/c) content (%)	(IM) Content in specimen (%) or (gm)	IM Density ( $\rho$ )(kg/m <sup>3</sup> )	Thermal Conductivity ( $\lambda$ ) (W/m.K)	Specimen Mass (gm)	Specimen Number
Standard	S	1:3.33:1.66:0.81	0	----	----	2168	1
Polystyrene 330	PS1,2,3,4	1:3.33:1.66:0.81	2.5,5,10 & 15%	1050	0.08-0.1	2110,2081, 1985, 1919	4
Polycarbonate	PC1,2,3,4	1:3.33:1.66:0.81	2.5,5,10 & 15%	1200-1220	0.19-0.22	2134,2110, 2036, 1985	4
Polyethylene 218	P1,2,3,4	1:3.33:1.66:0.81	2.5,5,10 & 15%	910-925	0.305-0.37	2080,1970 1980,1879	4
Polyethylene 952	PE1,2,3,4	1:3.33:1.66:0.81	2.5,5,10 & 15%	945-964	0.42-0.51	2124,2088 1977,1900	4
Wood dust	WS1,2,3,4	1:3.33:1.66:0.81	1,2,3, & 4%	550-650	0.13-0.16	2125,2087 1991, 1835	4
Natural Cork	NC1,2,3,4	1:3.33:1.66:0.81	1,2,3 & 4%	100-150	0.04 - 0.05	2005,1890, 1752,1595	4
Glass wool	GW1,2,3,4	1:3.33:1.66:0.81	24,36,48 & 60 gm	10-75	0.03 – 0.04	2150,2113, 2098,2040	4
Rock wool	RW1,2,3,4	1:3.33:1.66:0.81	24,36,48 & 60 gm	23-200	0.042–0.052	2170,2141, 2127,2100	4

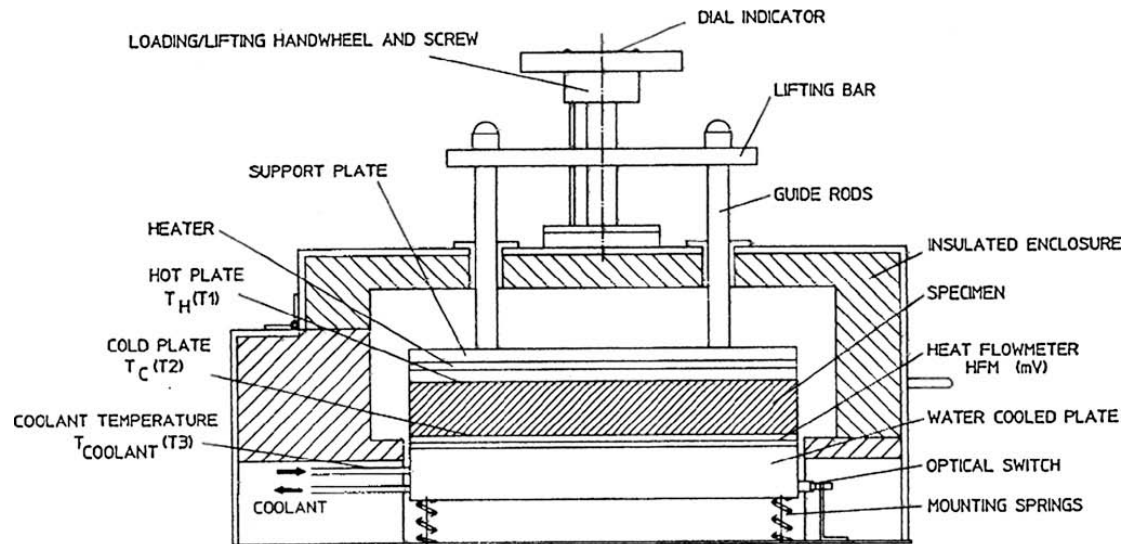


Figure 1. Cross-sectional diagram of the B480 heat flow meter apparatus (P.A. Hilton Ltd.).

### 3.3.1. Water Absorption Test

This test was performed in accordance with ASTM D-570-81 standard. Tap water was used in this test. The specimen was placed in a container of water at room temperature. At the end of 24 h the sample was removed from water and the process was repeated until it reached the saturation (equilibrium) condition. During this period, the specimens' weight difference was recorded at different times. The uncertainty average was ( $\pm 0.1$ gm). The percentage of water retention (WR %) was calculated using the following formula:

$$WR\% = \frac{\text{weight of wet sample} - \text{weight of dry sample}}{\text{weight of dry sample}} \times 100\% \quad (4)$$

### 3.3.2. Determination of the Compressive Strength

The mechanical strength of each specimen was determined using the universal testing machine, where the specimen was compressed between the upper and lower platens of the machine until fracture of the specimen had occurred. The uncertainty average of the used machine was ( $\pm 0.1\%$ ).

### 3.3.3. Determination of Thermal Conductivity

For determination the thermal conductivity the specimen is positioned between the hot and the cold plates and adjusted until the test position lamp illuminates to denote that the correct pressure has been applied. The determination of the thermal conductivity of the specimen requires the measurement of the following four parameters:

- The hot plate temperature  $T_H$ , with a suitable range from (0 to 70°C)
- The cold plate temperature  $T_C$  in °C
- The coolant fluid temperature  $T_{\text{coolant}}$  with a suitable range from (0 to 40°C)
- The heat flow meter (HFM) output in (mV)

The values of  $T_H$ ,  $T_C$  and the heat flow meter output are taken after the steady state condition has been reached. This state is reached when the difference in five consecutive readings at sampling interval give values of

thermal resistance to within (1%) without changing monotonically in one direction. The sampling interval is stated in, ISO8301, as  $t_s = \rho \cdot C_s \cdot L_s \cdot R$  or 300 s, whichever is the greatest, where  $\rho$  is the density in ( $\text{kg}/\text{m}^3$ ),  $C_s$  specific heat in ( $\text{J}/\text{kg}\cdot\text{K}$ ),  $L_s$  the thickness in (m) and  $R$  is thermal resistance in ( $\text{m}^2\cdot\text{k}/\text{W}$ ) of the specimen. At each sample interval, the measured values of ( $T_H$ ,  $T_C$  and output of the heat flow meter) are passed to the computer through a serial communications board which is an integrated part of the instrument, for data logging purposes. The thermal conductivity is then automatically determined by a computer program using the following equation:

$$\lambda = \frac{L_s \left( (k_1 + (k_2 \cdot \bar{T})) + ((k_3 + (k_4 \cdot \bar{T})) \cdot \text{HFM}) + ((k_5 + (k_6 \cdot \bar{T})) \cdot \text{HFM}2) \right)}{dT} \quad (3)$$

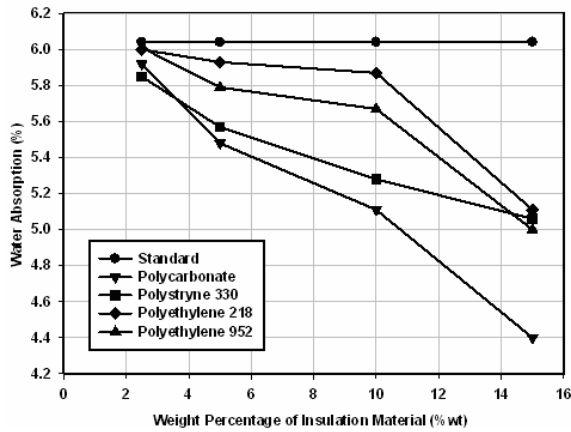
Where  $k_1$  to  $k_6$  are calibration constants supplied with the instrument, HFM is the heat flow meter reading,  $L_s$  is the specimen thickness in m,  $\bar{T} = (T_H + T_C)/2$  is the average temperature and  $dT = (T_H - T_C)$  is the temperature difference. The humidity of the room was controlled and maintained lower than 50%, and the thickness ( $L_s$ ) of each slab specimen was measured by the device. It is worth pointing out that in all the experiments the standard error of measurement on average was less than 5% of the measured value.

## 4. Results and Discussion

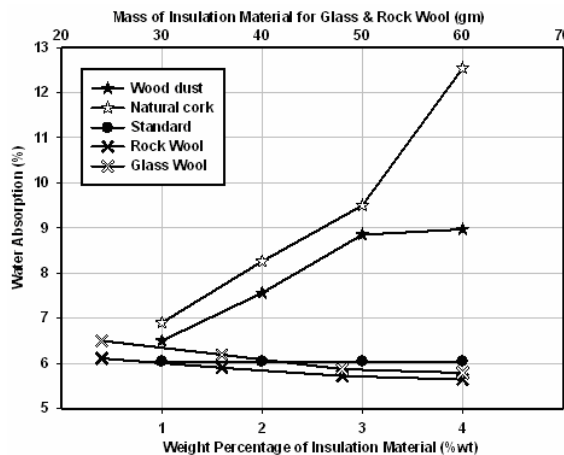
### 4.1. Effect of the Insulating Material Addition on Water Absorption

Effect of insulation material on water absorption is shown in Figures (2a and 2b). Also the figures include the standard specimen, which does not include insulation materials.

It can be seen from Figure (2a) that increasing the weight percentage of the insulating materials results in reduction of the water absorption for the following insulating materials: polycarbonate, polystyrene 330, polyethylene 952 and polyethylene 218, arranged in



(a)



(b)

Figure 2, (a)Weight percentage of insulation material viz. water absorption percentage, (b) Weight percentage of insulation material viz. water absorption percentage.

sequence starting with the minimum water absorption percent, (polycarbonate).

However, this was not the case for the other insulating materials namely natural cork and wood dust, where the water retention percentage i.e. absorption percentage was found to increase with the increase of their weight percentage as indicated by Figure (2b). This can be explained in terms of porosity in the main structure of these materials, as the number of bores is much higher than the case of the previously four mentioned insulating materials in Figure (2a). This increase is also due to the increase in the material mass diffusivity (due to the addition of insulation) and to the ability of insulation material to absorb water.

Furthermore it can also be seen from Figure (2b) that in the case of glass wool and rock wool there is little or no difference in the water absorption percentage of the reference standard specimen, being maximum in the case of rock wool (6.62%).

The different values of water absorption percent for the different insulating materials are explicitly shown in Table (2).

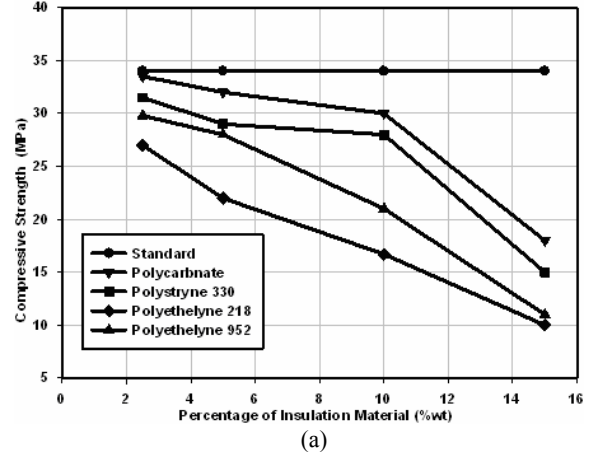
It can be seen from this table the maximum absorption percent is in case of natural cork addition being (+207.62%) followed by wood dust (+148.51%) whereas the minimum absorption percent is in the case of glass

wool addition (-4.14%) followed by rock wool addition (-6.62%).

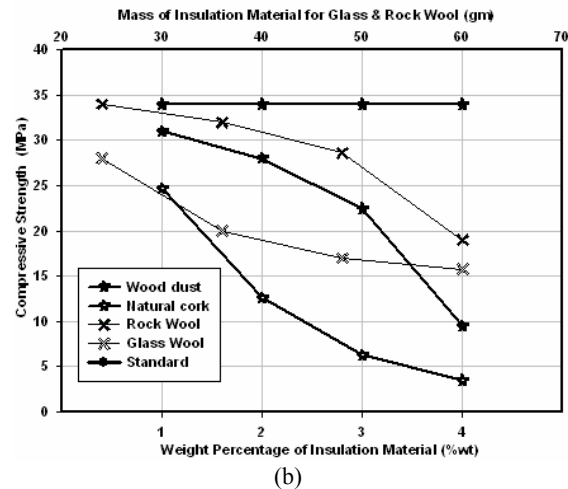
This is confirmed by the weight of the blocks shown in Table (1); where the higher the porosity percent the higher will be the number of pores resulting in less weight

#### 4.2. Effect of the Insulating Materials on Compressive Strength

The effect of the weight addition of insulating materials on the compressive strength of the building bricks is shown in Figures (3a & 3b) for polycarbonate, polystyrene 330, polyethylene 952 and polyethylene 218, also included is the standard specimen (without addition of insulating material) for comparison purposes.



(a)



(b)

Figure 3. (a)Weight percentage of insulation material against its compressive strength, (b) Weight percentage of insulation material against its compressive strength.

It can be seen from Figure (3a) that for all the above mentioned insulating materials the compressive strength decreases as the weight percentage of the insulating material increases. The highest decrease is in the case of polyethylene 218 addition and the minimum decrease is in the case of polycarbonate addition. Furthermore it can be seen from this figure that the decrease in compressive strength occurs gradually by the increase of the weight percentage (up to 10%) in the case polycarbonate and polystyrene 330 additions and up to 5% in the case of polyethylene 952 addition.

The same trend was observed in the case of rock wool, wood dust, glass wool and natural cork, as indicated by the curves of Figure (3b). The minimum decrease in

compressive strength is in the case of rock wool followed by wood dust then glass wool. The maximum reduction in compressive strength is in the case of natural cork, being 90.71 %, Table (2). The effect of mass of insulation materials and the compressive strength is shown in Figures (4a &4b). It can be observed in these figures that the

denser is the specimen, the higher is the compressive strength. This result is also concluded by Khedari et al. [17]

The values of the effect of addition of different insulating material on their compressive strength are explicitly shown in Table 2.

Table 2. Comparison among the effect of different insulating materials at their maximum addition rate on weight, water absorption compressive strength and thermal conductivity.

Insulation Material (IM)	Specimens Code	Content of ( IM)	Compressive strength	Absorption	Thermal Conductivity	Weight
		(%)or(gm)	(%)	(%)	(%)	(%)
Standard	S	0	100.00	100	100	100
Polystyrene 330	PS4	15	44.10	83.77	53.58	88.50
Polycarbonate	PC4	15	52.30	72.84	61.12	91.56
Polyethylene 218	P04	15	29.40	84.60	56.88	86.67
Polyethylene 952	PE4	15	32.35	82.78	55.43	87.63
Wood dust	WS4	4	27.94	148.51	52.48	84.64
Natural Cork	NC4	4	10.29	207.62	33.91	73.57
Glass wool	GW4	60(gm)	46.47	95.86	33.71	94.10
Rock wool	RW4	60(gm)	55.88	93.38	69.46	96.86

#### 4.3. Effect of the Insulating Material Addition on Thermal Conductivity

The effect of the weight addition of insulating material on thermal conductivity of the building bricks is shown in Figures (5a and 5b).

It can be seen from these figures that, for all the eight tested insulating materials, as the weight percentages increases the thermal conductivity decreases. However, the decreasing rate is more pronounced for the insulating materials in Figure (5b) namely the wood dust, rock wool, natural cork and glass wool. The addition of any these materials becomes effective after 1.5 weight percentage addition for ( wood dust & cork) and 36 gm for (rock & glass wool), and reduces the thermal conductivity of the brick to less than half its value in the case of wood dust, natural cork and glass wool. The most effective insulating material among this group is glass wool and natural cork, where the thermal conductivity dropped to above 70 % of its value, at addition rate of 4% weight.

Compared to the other group presented in Figure (5a), which includes polycarbonate, polyethylene 218, polystyrene 330 and polyethylene 952, it can be seen that those presented in Figure (5a) are less effective in reducing the thermal conductivity, and their addition becomes effective after 5% weight addition and they did not reduce the thermal conductivity more than 37% in the case of polyethylene 952, which is the most effective insulating material in this group. Even at addition rate of 15% weight, none of the insulating materials of this group resulted in 50% reduction. It is worth noting that at addition rate more than 10% weight, their effectiveness in reducing the thermal conductivity becomes comparable as

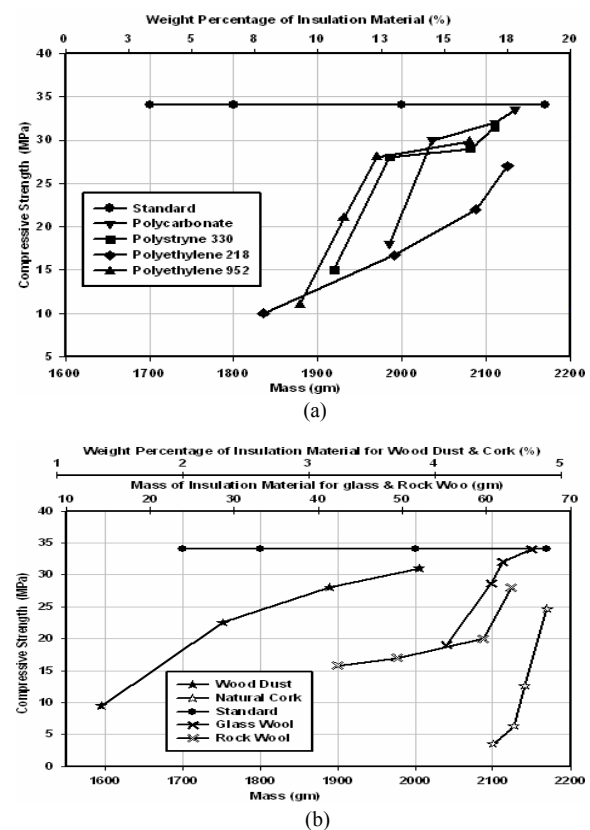


Figure 4. (a) Mass of specimen viz. its compressive strength, (b) Mass of specimen viz. its compressive strength.

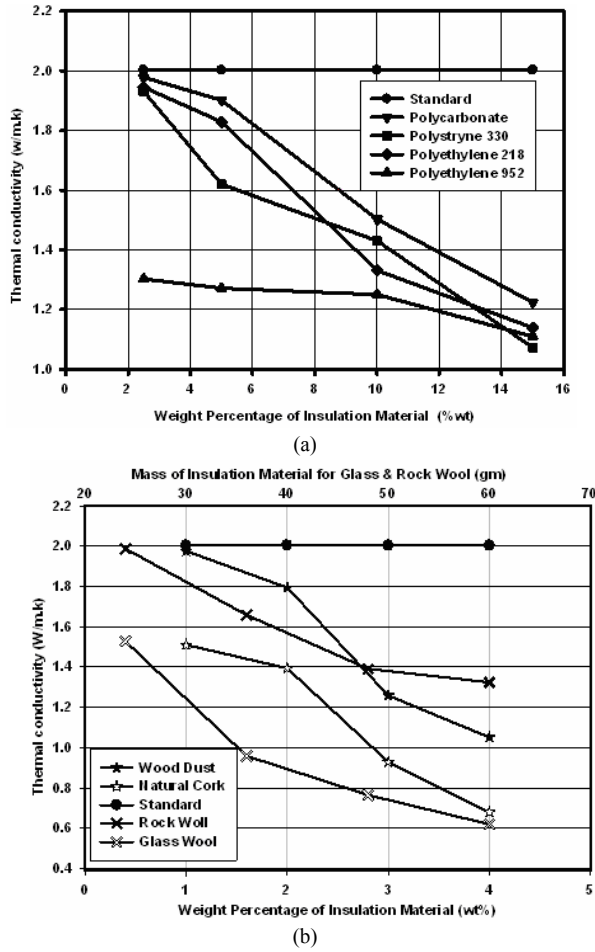


Figure 5. (a) Weight percentage of insulation material viz. thermal conductivity, (b) Weight percentage of insulation material viz. thermal conductivity.

implicated in Figure (5a). This is in general agreement with the findings reported in references 7 and 18. The effect of addition of any of the insulating materials on mass and thermal conductivity is shown in Figures (6a and 6b) from which it can be seen that for any of the added insulating materials as mass increases the thermal conductivity increases which is in general agreement with the findings reported in references [19 , 20].

#### 4.4. Comparison among the Eight Different Added Insulating Materials

Figure (7) summarizes the effect of the addition of different added insulating materials on weight, water absorption, compressive strength and thermal conductivity, as compared to the standard specimen without addition of any of the added insulating materials.

### 5. Conclusions

The following points may be concluded from the results obtained in this research work:

- Addition of any of the insulating materials, except natural cork and wood dust, at any rate to the building bricks used in Jordan resulted in reduction of water absorption, decrease in the compressive strength and pronounced decrease in thermal conductivity.

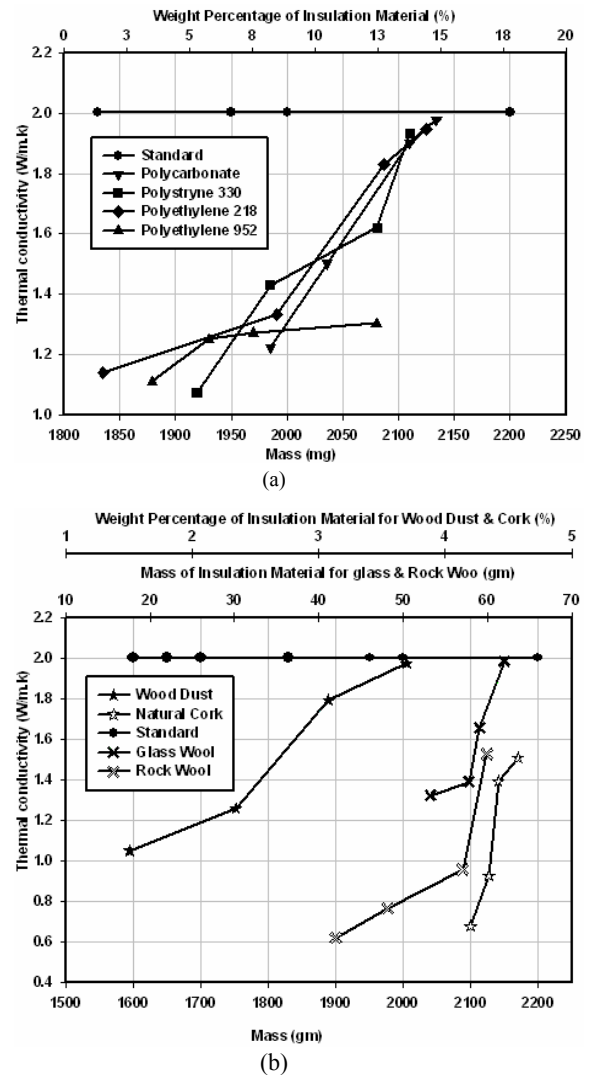


Figure 6. (a) Mass of specimen viz. its compressive strength, (b) Mass of specimen viz. its compressive strength.

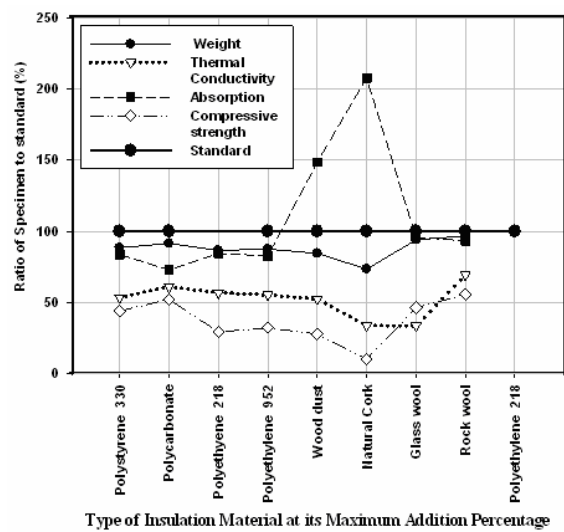


Figure 7. Comparison among the effect of the different insulating materials at their maximum addition rate on weight, water absorption compressive strength and thermal conductivity.

- The most effective material among the tested insulating materials in reducing thermal conductivity is found to be glass wool and natural cork, followed by wood dust and polystyrene 330, then polyethylene 952 and polyethylene 218. The least effective insulating materials in reducing the thermal conductivity of the building bricks are polycarbonate and rock wool.
- Addition of any of the insulating material resulted in decrease of the compressive strength of the building bricks. The minimum reduction in mechanical strength is caused by addition of rock wool and polycarbonate. However these insulating materials are the least effective ones in the reducing the thermal conductivity of the building bricks.
- The maximum absorption percent is in case of natural cork addition being (+207.62%) and the minimum absorption percent is in the case of glass wool addition (-4.14%).
- The minimum decrease in compressive strength is in the case of rock wool and the maximum reduction in compressive strength is in the case of natural cork, being (90.71 %).
- The most effective insulating material is glass wool and natural cork, where the thermal conductivity dropped to above (70 %) of its value, at addition rate of 4% weight.
- Finally, it is concluded that the addition of glass wool is the most effective insulating material, with moderate decrease in the mechanical strength and water absorption.

## References

- [1] MEMR annual reports, Ministry of Energy and Mineral Resources. Amman, Jordan: MEMR; 1995–2001.
- [2] A.Yahia , M. Mustafa, S. Al-Mashaqbah , K. Mashal , M.Mohsen , "Potential of energy savings in the hotel sector in Jordan", Energy Conversion and Management, Vol. 49 , 2008, 3391–3397.
- [3] A.M. Papadopoulos, E. Giama, "Environmental performance evaluation of thermal insulation materials and its impact on the building", Building and Environment Vol.42 ,2007, 2178–2187
- [4] J.O .Jaber. "Future energy consumption and greenhouse gas emissions in Jordanian industries". Applied Energy, Vol.71, 2002; 15–30.
- [5] A.M .Papadopoulos, M.A .Papadopoulos. "Insulation materials for buildings design". First national conference for the building and the environment, Athens, Greece, 2001.
- [6] S.A.Al-Sanea. "Thermal performance of building roof elements. Building and Environment" .Vol.37, 2002, 665–675.
- [7] Hernandez-Olivares, F., M.R.Bollati, M. del Rio, M., B.Parga-Landa, "Development of cork–gypsum composites for building applications". Construction and Building Materials, Vol.13, 1999, 179–186.
- [8] M. Mohsen, B. A.Akash, Some prospects of energy saving in Jordan, Energy conservation and Management, Vol.42 ,2001,1307-1315
- [9] B.A. Jubran, S.M.Habali, M.A.S.Hamdan, Adnan I.O.Zeid, "Some mechanical and thermal properties of clay bricks for Jordan valley region Materials and Structure", Vol.21, September 1988, No.125, 364-369
- [10] S.Jaber,M. Hamdan, "The Thermal and economical analysis of renewable energy buildings", Towards low energy house in Jordan, Proceeding of GCREEDER conference, Amman – Jordan, 2009
- [11] Al-Otoom, A. Al-Khlaifa and A.Shawaqfeh, "Crystallization Technology for Reducing Water Permeability into Concrete", Industrial & Engineering Chemistry Research Vol.46,2007, 5463-5467
- [12] Bulent Yesilata , Yusuf Isiker , Paki Turgut "Thermal insulation enhancement in concretes by adding waste PET and rubber pieces", Construction and Building Materials Vol.23,2009, 1878–1882
- [13] F.P.Incropera,D.P. Dewitt, L.Bergman andA.S Lavine," Fundamentals of Heat and Mass Transfer", Six edition , John Wiley & Sons, 2007,USA(Ch. 1 & 3),
- [14] J.A.Wordingham, P.Reboul, "Dictionary of Plastics, third edition". Newnes Middlesex, England. 1968.
- [15] F.W. Billmeyer "Textbook of Polymer Science", Second edition. John Wiley, New York. 1984.
- [16] ISO 8301:1991 Thermal insulation - Determination of steady-state thermal resistance and related properties - Heat flow meter apparatus International Standard Organization; 2006
- [17] J .Khedari, B .Suttisonk., N .Paratinthong., J.Hirunlabh., "New lightweight construction materials with low thermal conductivity", Cement & Concrete Composites,Vol.23,2002, 65-70
- [18] M .Luai. Al-Hadhrami and A. Ahmad, "Assessment of thermal performance of different types of masonry bricks used in Saudi Arabia", Applied Thermal Engineering Vol.29 ,2009, 1123–1130
- [19] A. Benazzouk , O. Douzane, K. Mezreb, B. Laidoudi, M. Que'neudec," Thermal conductivity of cement composites containing rubber waste particles: Experimental study and modeling", Construction and Building Materials ,Vol.22 ,2008,573–579
- [20] M. Bederina , L. Marmoret , K. Mezreb , M.M. Khenfer , A. Bali , M. Que'neudec "Effect of the addition of wood shavings on thermal conductivity of sand concretes: Experimental study and modeling", Construction and Building Materials Vol.21 ,2007,662–668

# Novel Method of Productivity Improvement and Waste Reduction Through Recycling of Submerged Arc Welding Slag

Dalgobind Mahto<sup>\*</sup>, Anjani Kumar

*Department of Production and Industrial Engineering, National Institute of Technology, Jamshedpur: 831014, India*

## Abstract

The traditional welding flux is costly and the flux used in Submerged Arc Welding (SAW) generates wastages known as Slag. It is generally thrown away as a waste after use. This poses the problem of storage, disposal, and environmental pollution and needs landfill space apart from exhaust of non-renewable resources. If by recycling the used flux can be reused in product yielding same quality parameter as the new flux, then the cost of the input will go down significantly. However, this requires extensive trial and error experimentation because it is often difficult to know how the slag ingredients interact after recycling to determine the operational characteristics of the recycled flux and the final performance of the welded structure. Keeping this in mind an experiment has been conducted in a manufacturing unit with small investment. As far as possible weld qualification tests were performed using recycled flux to get it to be qualified in a National Accreditation Board of Laboratories in the final products made from recycled slag. While comparing, it was indeed revealed that the product has better chemical analysis, dye penetration test, radiography, mechanical tests and metallurgical investigations than the product from new flux. Cost analysis of recycled slag per 100 kg was calculated and compared with the equivalent fresh flux available in the market according to the principle of market value method or reversal cost method. It is similar to the technique of by product revenue deducted from production cost. The cost analysis has revealed in terms of % of saving that it could be to the extent of 70.73%.

© 2010 Jordan Journal of Mechanical and Industrial Engineering. All rights reserved

Keywords: Submerged Arc Welding, Flux; Recycling, Reuse; Waste Reduction.

## 1. Introduction

Welding is a complex multi-disciplinary technology requiring permanent modernization of manufacture with new machines, permanent education of workers, and introduction of most recent manufacturing processes. Productivity in fusion arc welding processes can be increased in several ways. Application of numerous welding technologies in fabrication and maintenance processes covers wide range of industrial cases from steam generator to aircraft to high precision equipment of almost every industrial sector.

Among the different Arc welding processes, Submerged Arc Welding (SAW) process finds wide industrial application due to its easy applicability; high current density and ability to deposit a large amount of weld metal using more than one wire at the same time. It is highly emphasized in manufacturing because of its natural qualities such as easiness in controlling process variables, high quality, deep penetration, smooth finish, capability to weld thicker sections and prevention of atmospheric contamination of the weld pool.

The flux used in SAW after use generates wastages of Flux i.e., which is known as Slag. It is generally thrown

away as a waste after use. This poses the problem of storage, disposal, and environmental pollution and needs landfill space apart from exhaust of non-renewable resources. The flux is very costly and, if the used flux i.e. slags can be reused in product yielding same quality parameter as the new flux then the cost of the input of SAW will go down significantly.

Considering this view, an experiment has been conducted in a manufacturing unit with small investment on the additional arrangements for recollection of generated slag. The slag was collected and mixed with additives and subsequently used in the sample.

Weld qualification tests were carried out using recycled slag to get it qualified in a National Accreditation Board of Laboratories in the sample of final products made from recycled slag. Comparison discovered that the product has better chemical analysis, dye penetration test, radiography, mechanical tests and metallurgical examinations than the product from new flux.

Submerged Arc Welding is basically an arc-welding process in which the arc is concealed by a blanket of granular and fusible flux. The physical properties of flux are important considerations in SAW for improving welding properties. SAW is an economical method for producing tools and machine parts with required surface properties, particularly resistance to wear and corrosion.

The source of heat for SAW is obtained from the arc generated between a bare solid metal in the form of a

<sup>\*</sup> Corresponding author. mahto123@rediffmail.com

consumable wire or strip electrode and the work piece. The arc is maintained in a cavity of molten flux or slag that refines the weld metal and protects it from atmospheric contamination. Alloy ingredients in flux attempt to enhance the mechanical properties and crack resistance of the weld deposit. Therefore, as Flux is one of the essential ingredients of SAW, it is of utmost importance to select SAW Flux properly in order to improve weld quality.

Since, the development of the SAW process, there has been attempts by technologists and researchers to increase its productivity and to decrease the welding cost. The cost of the flux is a major part of the total welding cost for the SAW process[1]. It has been estimated that, in general, one kg of flux is consumed for every kg of weld metal deposited. Flux consumption increases with an increase in arc voltage. About 2500 tonnes of flux are being used every year in India alone. After welding, such a large quantity of flux becomes slag and that is treated as waste. The slag is then disposed-of. The basic question is whether the slag can be recycled or not. If, Cost-effective recycling of slag is possible, it will not only overcome the problems of storage and disposal, but also save non-renewable resources.

## 2. Objective of this Study

Adityapur Industrial Area is the industrial hub of Jharkhand state in India. There are many small and medium industries in which SAW facilities are available. They cater to the needs of many original equipment manufacturers by supplying qualitative products. But on the cost parameters most of the ventures are unable to compete with the competitors. On the other hand, there is always a pressure from the customer to reduce some percentage of cost as an effort of continual improvement. This study has been conducted in a small industry, where SAW facilities are available and with the support of top management of the organization. The monthly output of slag is approximately 700 – 1000 kg at present and with the commissioning of 2<sup>nd</sup> phase the quantity will be approximately doubled.

In order to fulfill the major objective, slag was recycled and the characteristics of recycled slag were evaluated by performing weld qualification tests, chemical composition, mechanical properties and metallurgical investigations. At the same time, the evaluation of weld metal were carried out to justify other aspects like:

1. To find out means and ways about possibility of recycling SAW slag.
2. To compare the weld metal chemistry achieved with recycled slag against laid down requirements of available AWS and ASME specifications.
3. To find out Mechanical as well as Chemical parameters either they match with available international specifications range or not
4. To witness and observe aesthetic appeal of beads possible without any visual defects or not.
5. To study the stability and slag detachability with the recycled slag.
6. To reduce the wastages of Slag
7. To protect the environment from pollution.
8. To contribute to the improvement of global quality of life through use and innovation in welding and joining technologies

## 3. Literature Review

SAW process was developed by the E O Paton Electric Welding Institute[1] in Russia, during the second world war, and it was used for many different applications during that time, most notable for its use on the T34 tank. Submerged Arc Welding is just what its name says. Desire for the mankind to improve the quality of life, conserve the natural resources, protect the environment etc. has been the major driving force for innovations in the field of materials and their application. In this regard, a major advance in systematizing the study of welding flux was begun by Christensen and Chipman[2] who investigated acidic coatings on shielded metal arc electrodes. Others following[3-5] have made similar studies on SAW fluxes. Since, the development of the SAW process, there has been attempts by technologists and researchers to increase its productivity and to decrease the welding cost. The cost of the flux is a major part of the total welding cost for the SAW process. It has been estimated that, in general, one kg of flux is consumed for every kg of weld metal deposited. Flux consumption increases with an increase in arc voltage. About 2500 tonnes of flux are being used every year in India alone[6].

Waste reduction is an important issue in today's context. The main objective of the waste reduction is to minimize waste while the resource management aims to maximize the utilization of resources. According to Mitra and Eagar [7] the alloying elements lost in slag on welding by flux are Mn upto -0.30 Pct, Si upto -0.31 Pct and Cr - 4.83 Pct Hence, the basic question is whether the slag can be recycled or not. If, cost-effective recycling of slag is possible, it will not only overcome the problems of storage and disposal, but also save non-renewable resources because. But, very few efforts have been done to study and validate the use of slag after recycling.

Generally the industrial firms are reluctant to provide information on quantity and composition of waste for fear of show cause from regulating authorities. The quantum of waste generated reflects the inefficiency of the organization. The Government of India through national committee of science and technology works on the projects of recycling and gives solutions. The director general of supplies and disposal regulates on supplies and disposals. Similarly, Metal Scrap Trade Corporation and Minerals and Metal Trading Corporation have suggested some procedures for the manner of disposal and market analysis. Organization for the economic co-operation and development has advocated to consider safety, efficiency, cost effectiveness, waste minimization and feasibility to industries ,while selecting a specific technique for system and /or component recycling[8].

### 3.1. Recycling of SAW Slag

SAW fluxes are granular, fusible mineral compounds of various proportions and quantities, manufactured by several different methods. In addition, some fluxes may contain intimately mixed metallic ingredients to deoxidize the weld pool. Any flux is likely to produce weld metal of somewhat different composition from that of the electrode used with it due to chemical reactions in the arc and sometimes to the presence of metallic ingredients in the flux. A change in arc voltage during welding will change

the quantity of flux interacting with a given quantity of electrode and may, therefore, change the composition of the weld metal. This latter change provides a means of describing fluxes as "neutral," "active," or "alloy."

From the review of Specification No AWS 5.17[9] for carbon steel electrodes and fluxes for submerged arc welding A99, the types of fluxes are neutral fluxes, active fluxes, alloy fluxes, crushed slags and closed-loop, crushed slags

Neutral fluxes are those, which will not produce any significant change in the weld metal chemical analysis as a result of a large change in the arc voltage, and thus, the arc length. The primary use for neutral fluxes is in multi pass welding, especially when the base metal exceeds 25 mm in thickness. The considerations as suggested by AWS 5.17[9] that neutral fluxes contain little or no deoxidizers. They rely on the electrode to provide deoxidation. Single-pass welds with insufficient deoxidation on heavily oxidized base metal may be prone to porosity, centerline cracking, or both. It maintains the chemical composition of the weld metal even when the voltage is changed; it is not always true that the chemical composition of the weld metal is the same as the chemical composition of the electrode used. It is used to maintain the weld metal chemical composition through a range of welding voltages, weld properties. Strength level and impact properties can change changes in other welding parameters such as depth of fusion, heat input, and number of passes.

Active fluxes are those, which contain small amounts of manganese, silicon, or both. These deoxidizers are added to the flux to provide improved resistance to porosity and weld cracking caused by contaminants on or in the base metal. The primary use for active fluxes is to make single pass welds, especially on oxidized base metal.

The considerations as suggested by AWS 5.17[9] that Active fluxes contain some de oxidizers, the manganese, silicon, or both, in the weld metal. The active flux will vary with changes in arc voltage. An increase in manganese or silicon increases the strength and hardness of the weld metal in multi pass welds but may lower the impact properties. For this reason, the voltage may need to be more tightly controlled for multi pass welding with active fluxes than when using neutral fluxes. Some fluxes are more active than others. This means they offer more resistance to porosity due to base-metal surface oxides in single-pass welds than a flux, which is less active, but may pose more problems in multi pass welding.

Alloy fluxes are those, which can be used with a carbon steel electrode to make alloy weld metal. The alloys for the weld metal are added as ingredients in the flux. The primary use for alloy fluxes is to weld low alloy steels and for hard facing.

Christensen[10] has classified fluxes into three types namely manganese silicate, calcium silicate and basic. For each flux he characterized the amount of Mn, Si, and O transfer by two variables. The variables are the initial or nominal manganese content and an operational parameter. Kubli and Sharav[11] showed that the oxygen content of submerged arc weld metal decreases with increasing flux basicity.

Slag formed during the welding process is subsequently crushed for use as a welding flux is defined as crushed slag. This is different from a recycled flux, which was

never fused into a slag and can often be collected from a clean surface and reused without crushing.

Slag generated by a fabricator from a specific brand of flux under controlled welding conditions and crushed for subsequent reuse by the same fabricator is defined as closed-loop, crushed slag. Closed-loop, crushed slag, or blends of closed-loop, crushed slag with the original brand of unused flux ensure better control of input material by virtue of the inherent partnering of the fabricator with the crusher.

If blending of slag with unused flux is done, changes in the original brand of unused flux or in the blending ratio can affect the quality of the final product.

It is reported that TITUS Steel Company[12] has been reclaiming slag for fabricators in the USA. The Paton Electric Welding Institute of Ukraine [13] has also reported the development of a technology for recycling of slag.

However, from the available literatures it is evident that the first attempt at recycling of SAW Slag was reported by Alfred Beck and Jackson[14]. He used a closed loop recycling process and started practicing this in 1963. However, the response from industry was very poor, because of stringent AWS and ASME codes, combined with the reluctance of fabricators to use a recycled product. By 1996 AWS and ASME codes were amended to permit the use of recycled slag.

Beck and Jackson [14] further revealed their finding that if it is processed properly and according to code requirements, recycled slag could be reliably used as a substitute to fresh flux. They further emphasized a saving up to 50% of the total cost of purchased flux by recycling the slag.

Devis and Baily[15] established that fused calcium silicate flux, which has fully reacted during manufacturing, produces no change on reheating. Such a flux contains no readily oxidizable material and can be recycled.

A few researchers have also explored the possibility of using a mixture of fresh flux and slag. Research carried-out by Livshits et al[16] has shown the possibilities of using pulverized slag crust mixed with iron filings for hard facing applications. They additionally confirmed that this process is efficient and cost-effective.

Moi et al[17] and Pal et al.[18] found that of mixture containing up to 20% fused slag in fresh flux produces no change in weld metal chemistry.

Milichenko et al[19]. have proposed a new method for preparing alloying fluxes for hard facing by enriching the flux with ferro-alloys.

Their[20] has proposed empirical equations for computing the alloy content of the weld metal. In spite of the fact that from the available literature of Singh and Pandey [21], it was found that slag is being recycled by some companies but they are professional recyclers and have not disclosed the methodology, may be due to commercial reasons. Pandey et al.[22] found that an acceptable bead geometry can be achieved using recycled slag and have claimed a saving of 68.6% using recycled slag.

Many other investigators like Farias et al[23], Du Plessis et al.[24] and Kanjilal et al[25] tried to understand the role of each flux ingredients on the weld-metal properties and operational characteristics of the process by

varying only the individual flux ingredient in a given flux system observed that this approach by its very nature failed to take into account the simultaneous variation of the flux ingredients as well as their interaction effects.

The significant interactions effect of flux ingredients has been reported previously by Lau et al[26], and Kanjilal et al[27] further stress that this assessment of flux ingredient interaction has been recognised as increasingly important in welding flux design, where it may be necessary to determine the combined synergetic and antagonistic effects of many flux ingredients.

The need for the reduction of the number of experiments has been the concern of welding flux researchers and manufacturers. Although modeling tools can not completely eliminate experiments, it can drastically reduce the number of experiments. Quintana et al[28].observed that a reduction in the number of experimental welds from 30 to 5 in GMAW leads to about 80% energy savings. Obviously the benefits of the reduction in the number of experimental welds would be higher by the time the savings on materials, labour and time are considered.

According to Ademola et al[29] to arrive at an optimum flux composition and mitigate the problems of the traditional approach, an alternative approach is to develop mathematical models through effective and strategic planning, design and execution of experiments. With the availability of such models, the formulation of welding flux can be based on quantitative footing. According to them, such an approach minimizes the expenditure of time, labour and materials.

The steps/ procedures have been suggested by NIST/SEMATECH[30], Gunaraj and Murugan[31], and Allen et al[32]to follow while planning and conducting welding flux research in the subject mixture experiments typically involving the following, which could also be implemented for recycling of slag:

- Define the objectives of the experiment
- Select the flux ingredients and where necessary any other factor to be studied e.g. process variables
- Identify any constraints on the flux components or other factors in order to specify the experimental region
- Identify the response variables to be measured
- Propose an appropriate model for modeling the response data as functions of the flux ingredients and other factors selected for the experiment
  - Select an experimental design that is sufficient not only to fit the proposed model but which allows a test of model adequacy as well
  - Conduct the experiment as per the design matrix
  - Measure and record the responses
  - Develop the mathematical models
  - Calculate the coefficients of the polynomials
  - Check the adequacy of the model developed
  - Conduct the confirmatory test
- Present the main and interaction effects of the different ingredients on the responses
  - Use the model to predict the combination of flux ingredients that will give the desired response
  - Perform actual experiments with the designed flux
  - Analyze the results

The efficacy of the methodology in welding flux research has been demonstrated by Kanjilal et al[33-36] Their paper presents a brief discussion on mixture design. The procedure of mixture experiment, the analytical model forms and the sequence of model fitting are discussed but not fully developed. Areas of welding flux research where the various mixture designs may be useful are suggested.

Most recently Kaveh et al[37] have developed a methodology of recycling of slag obtained from the application of powder in submerged arc welding used in low carbon steel grade st 37. Their research highlights finding a method for recycling such wastes by making use of phases assessment systems (X-ray diffractometry XRD), chemical composition assessment systems (X-ray fluorescence XRF), phases type and form assessment system (Scanning electro microscope SEM), and carbon and sulphur value assessment system (Strolein system) and by using separation, formulation, and ceramic sintering

A quantity of information is also available in the [www.recycleflux.com](http://www.recycleflux.com)[38]in which recycling and disposing methodologies have been given.

In view of the strong support found from review of available literature for the slag recycling, one common recommendation witnessed that SAW Slag can be recycled with adding certain quantities of additives.

#### 4. Plan of Experiments

After going through the books, reference materials and reviews from journals, holding detailed discussions with the Welding Experts, Shop Personals, and Inspectors, it was formally decided to take up the study. It was decided to gather the information of SAW as far as possible. Side by side it was decided to evaluate and generate the data related to mechanical properties and chemical properties of the raw material being welded. This was decided in view of the facts that welded material property is the main issue in this case to be dealt with. If the alternate methods are able to match the mechanical as well as chemical properties, the alternate material can be used. It was decided that methodologies of reusing the slag is the best option, if possible, in least cost than the fresh flux

##### 4.1. Experimental Set up

The experiment was conducted in the company abbreviated as ABC to keep confidentiality of the company. The industry has modern SAW facility having following specification.

- Model: Auto weld 1000 I
- Input power (kva): 44
- Current range (Ampere): 60-1000
- Input supply: 380-440 v, 3 Phase, 50 Hz supply

The job is fixed at the desired position and the SAW torch moves forward or backward on the tractor, which runs through parallel rails The inbuilt features of the tractor used were 120Volts rated input Voltage, Wire diameter 1.6 to 6 mm with scratch or retract arc starting method, 100-1500 mm/min speed, 200-4500 mm/ min wire feed rate, 0-80 mm vertical adjustment,  $\pm 30$  mm horizontal adjustments with  $45^\circ$  inclination of the welding torch as well as the welding head. The flux hopper was suitably mounted along with spool holder arrangement.

#### 4.2. Process adopted to Recycle the Slag

A systematic approach is needed to recycle the total system waste. SAW process is carried out in the plant facility where more than one material is used. The slag may contain oil, mill scale, chips, dust and other consumables. Hence, the collection of slag requires much attention. Various strategies have been proposed to reduce the wastages through recycling like; moisture and oil must be removed from the compressed air used in the re-cycling system. Addition of additives must be done with the proportion as they remain in the new flux. Foreign material such as mill scale must be removed by a suitable system, such as sieving.

As a generator, one have "cradle-to-grave" responsibility for the hazardous waste produced. Below is a short outline of the adopted recycling procedures.

- Project Initiation

Assigning project specific job numbers was of critical importance in initiating a project. Job and lot numbers were utilized to track all materials as they moved through the processing.

- Temporary Storage

Depending upon the requirements of the job, the material was moved to temporary storage or drop boxes placed on site.

- Representative Sample and Document Procurement

Throughout blasting operations, spent abrasives will be accumulated in the containment facilities. When sufficient volumes of spent grit have been accumulated, representative samples of the material will be collected. Depending on actual volumes of waste generated, collection of several samples for analysis may be indicated.

- Testing and Designation

Selecting applicable chemical analysis for a waste stream was critical to waste recycling because selection of the wrong analysis could generate added costs. Hence, appropriate tests were carried out and once tested; the material is designated based on characteristic criteria.

- Disposal or Recycling Recommendation Once the material was designated an appropriate disposal or recycling facility was recommended.
- Transportation

Once the spent slag waste has been accepted for recycling or disposal the material was transported to the facility depending upon its designation.

- Decontamination

The drop boxes were used for slag materials. They were thoroughly cleaned and decontaminated prior to use. Records were also maintained on this operation.

- Chain-of-Custody Documentation

Throughout the entire handling of the material, chain-of-custody documentation has been maintained. This enabled tracking everything in the process: identification, storage, testing, designation, transportation, and disposal/recycling facilities.

The specific waste collection and recycling strategies adopted have been summarized and presented below

- Design of economic basis to facilitate separation at source
- To provide every organization with a set of four standard bins to separately collect the metallic, plastic, paper and other miscellaneous waste. The bins should be designed properly.
- Design the appropriate collection system
- Incentive to encourage segregation of waste at source
- Timely collection of waste
- Selection of representative sample and documentation
- Disposal or Recycling Recommendation
- Use appropriate technology to recycle
- Insure its ultimate use, and
- Compare the recycling cost with fresh one

Traditionally, no slag is reused in the submerged arc welding. The aim was to test whether slag can be recycled and used further in the production or not. To test this theory a plan of investigation has been made. The detail plan of investigation has been shown in Fig. 1. The various steps are;

1. Welding with fresh flux
2. Welding with pure crushed slag
3. Comparison of weld metal chemistry
4. Processing of slag
5. Weld qualification test with recycled slag
  - Chemical test for chemistry of weld metal
  - Test plates for radiography
  - Mechanical testing, and Metallurgical investigations.

#### 4.3. Welding with Fresh Flux

Three Mild steel sample weld pads were prepared and welded with fresh flux. A weld pad sample is shown in Fig.2. The original fresh flux used was F7AZ which was use in combination with EL-8 filler wire of 2 mm thickness. The welding parameters and other conditions were in accordance with AWS-SFA 5.17. Preheat is essential for heavy mild steel weldments and alloyed metals to assure good mechanical properties. Multiple pass welds require an interpass temperature equal to the preheat temperature until the weld is completed. The interpass temperature was maintained by six program control unit which controlled and memorized the current, voltage, welding speed and temperature. The ideal parameters specified in AWS-SFA 5.17, and parameters maintained are tabulated in Table 1.

#### 4.4. Welding with pure slag

Slag waste was crushed and meshed to the granular size like that of the original flux. Three weld pads similar to Fig.2 have been made with pure slag maintaining same parameters given in table 1 using crushed slag with EL-8 wire in accordance with AWS SFA 5.17 for chemical analysis of weld metal.

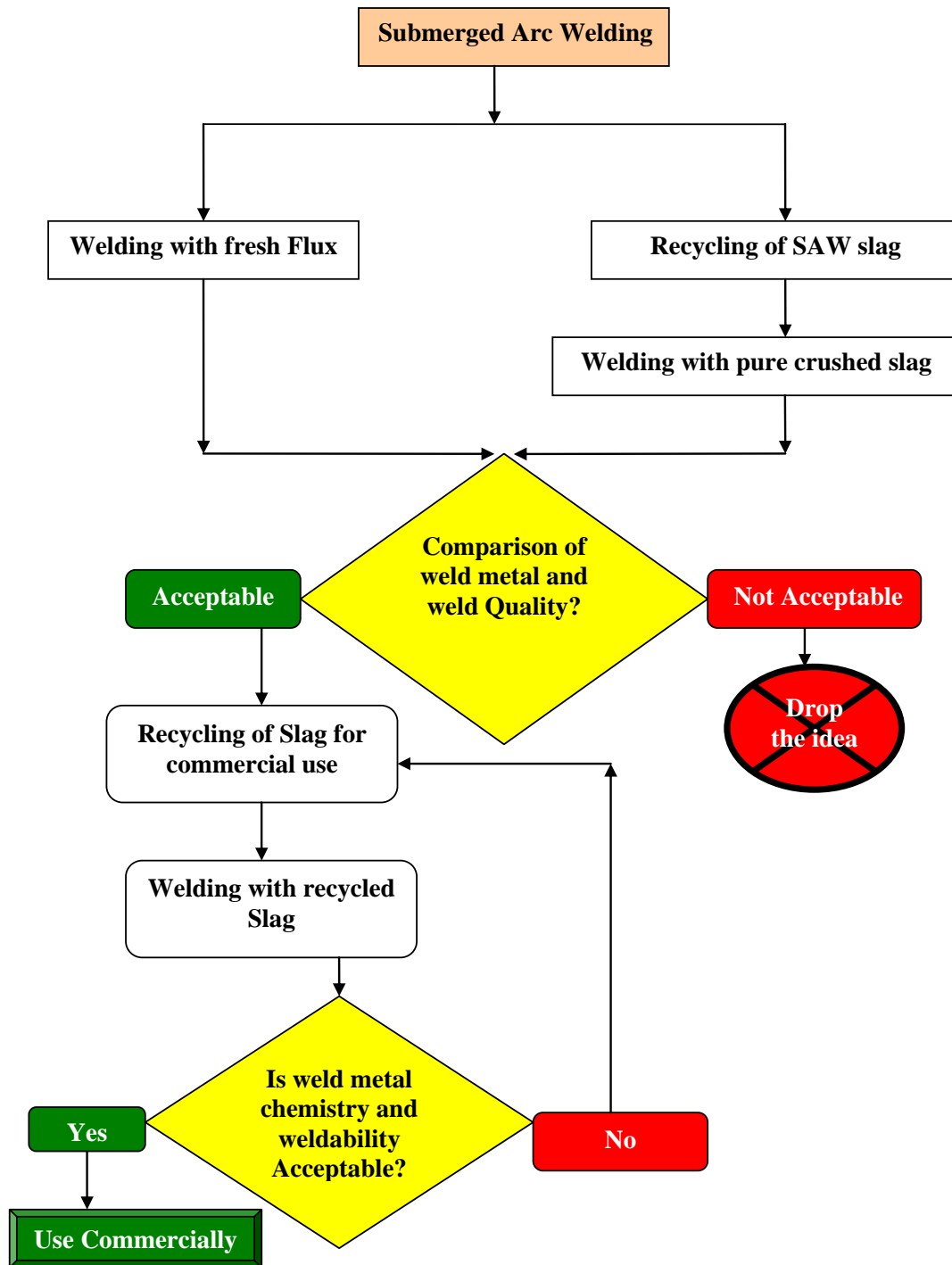


Fig.1 Process flow diagram for recycling of slag

Table1 Specified parameters and maintained parameters in sample pieces

SI No	Parameter	Unit	Specified parameter range or Chosen	Maintained parameter
1	Current	Ampere	300-400	360
2	Voltage	Volts	26 - 30	30
3	Travel speed	mm /sec	5-6	5
4	Pre heat temperature	<sup>0</sup> F ( <sup>0</sup> C)	60- 325 <sup>0</sup> F (15-165 <sup>0</sup> C)	250 <sup>0</sup> F (122 <sup>0</sup> C)
5	Inter pass temperature	<sup>0</sup> F ( <sup>0</sup> C)	275- 325 <sup>0</sup> F (135-165 <sup>0</sup> C)	300 <sup>0</sup> F (150 <sup>0</sup> C)
6	Electrode size	mm	2	2
7	Flux	Granular	F7AZ	F7AZ
8	Position of welding		Flat	Flat
9	Material		Suitable	IS 2062
10	Thickness	mm	Not specified	10

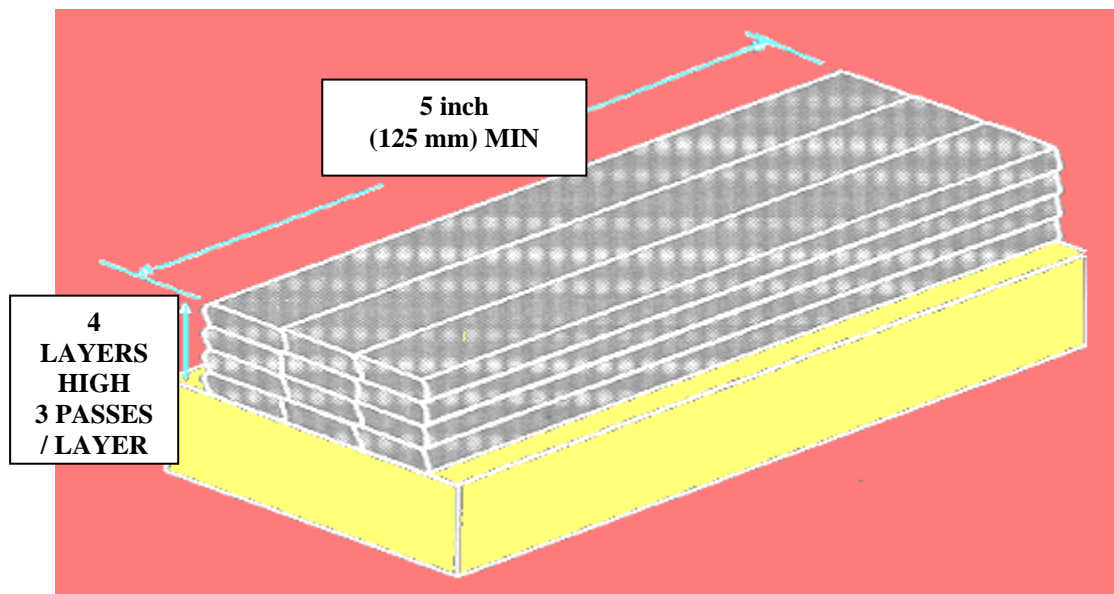


Fig.2 Weld pad for chemical analysis of weld metal [9]

### 5. Recycling / Modification of slag

Slag formed during the welding process that is subsequently crushed for use as a welding flux is defined as crushed slag. This is different from a recycled flux, which was never fused into a slag and can often be collected from a clean surface and reused without crushing. Crushed slag and blends of crushed slag with unused (virgin) flux may be classified as a welding flux under this specification, but shall not be considered to be the same as virgin flux. Although it is possible to crush and reuse submerged arc slag as a welding flux, the crushed slag, regardless of any addition of virgin flux to it, is a new and chemically different flux. This is because the

slag formed during submerged arc welding does not have the same chemical composition or welding characteristics as the virgin flux. Its composition is affected by the composition of the original flux, chemical reactions which occur due to the welding arc, the base metal and electrode compositions, and the welding parameters.

Based on the information (loss or gain of elements) provided by above experiments, slag was modified. Under these modifications slag was crushed and subsequently milled in ball mill to convert into powder form. Alloying elements / deoxidizers were added and mixed mechanically in a ball mill for 30 minutes so that the ingredients could form a homogeneous mixture. 20% solution of potassium silicate binder was added to wet the

dry mixed powder, wet mixed for 15 minutes and passed through a 10 mm mesh screen to form small pellets.

These pellets were mixed and dried separately in air for 24 hours and then were sintered at 850 °C for two hours in a muffle furnace. Sintered mass was then crushed and separated to the required grain size and termed as recycled slag.

## 6. Welding with Recycled Slag

For welding with recycled slag El-8 filler wire was chosen and recycled slag in combination with EL-8 filler wire was used for preparation of chemical pad. Chemical composition of weld pad was checked with a spectrometer and compared with AWS requirements. The modifications were used in different combination of additives and each

time 3 samples weld pads were made. Five possible combinations of weld pads were made. As such total 15 numbers of weld pads were made using recycled slag. The modifications were repeated until acceptable chemistry of weld metal was achieved.

The weld pads were similar to 2 and maintained same parameters given in Table 1.

Chemical composition of weld metal deposited with fresh flux, pure crushed slag and with recycled slag was critically analyzed and compared with AWS requirements for deciding further course of action. The chemical composition analysis of weld metal was carried out in a national accreditation board of laboratories with a spectrometer. The reported findings have been presented and are recoded in Table 2.

Table 2. Comparison of chemical composition of weld metal

	C	Mn	Si	S	P
AWS requirement	0.05 – 0.15	0.80 – 1.25	0.1 – 0.35	0.03 Max	0.03 Max
With pure slag	0.025	0.541	0.128	.023	0.028
With fresh flux	0.053	0.646	0.216	.028	0.0327
With recycled slag	0.072	0.812	0.178	.026	0.029

Trial runs along with corresponding chemical composition of weld metal have been shown in Table 3.

Table 3. Chemical composition of trial weld pads in different combination of recycled slag.

Trial No	Additives in % of Slag	C	Mn	Si	S	P
1.	CaCO <sub>3</sub> +SiO <sub>2</sub> = 7.1% F-Mn + F-Ti = 5.2 %	0.054	1.74	0.277	.025	0.042
2.	CaCO <sub>3</sub> +SiO <sub>2</sub> =10.1% F-Mn + F-Ti =2.6%	0.087	0.428	0.142	.029	.0276
3.	CaCO <sub>3</sub> +SiO <sub>2</sub> =10% F-Mn + F-Ti =4.2%	0.070	0.557	0.140	0.025	.0237
4.	CaCO <sub>3</sub> +SiO <sub>2</sub> =10% F-Mn + F-Ti =5.8% F-Si = 1%	0.061	0.683	0.136	0.026	.0271
5.	CaCO <sub>3</sub> +SiO <sub>2</sub> =10.3% F-Mn + F-Ti =7.26% F-Si = 2%	0.075	0.832	0.199	0.025	.030

## 7. Weld Qualification Tests and Results

To determine the performance of recycled slag different weld qualification tests have been carried out. Once acceptable chemical composition of weld metal was achieved with recycled slag, following tests were performed to ascertain its performance.

### 7.1. Preparation of Sample For Different Tests

Three test assemblies each with fresh flux, pure slag; and recycled slag were prepared considering the

specification of AWS SFA 5.17. The dimensions of test assemblies are maintained as shown in Fig. 3(a), Fig. 3(b) and Fig. 3(c) and Table 5.

### 7.2. Testing of Assembly

Test assemblies were subjected to visual inspection, dye-penetration test and radiography before cutting for specimens meant for mechanical testing. Tensile and impact specimens were machined and tested in accordance with AWS SFA 5.17. Results of mechanical test are shown in Table 4.

Table 4 Results of mechanical properties testing

Heading	YS N/ mm <sup>2</sup>	UTS N/ mm <sup>2</sup>	% Elongation	Charpy Impact J (at 0° C)	Radiography
AWS Requirement	360	420	24	90	Must Pass
Pure slag	320	370	32.7	72.9	Failed
Fresh flux	381.6	455.6	30.5	116.7	Passed
Recycled slag	423.7	525.95	34.5	109.1	Passed

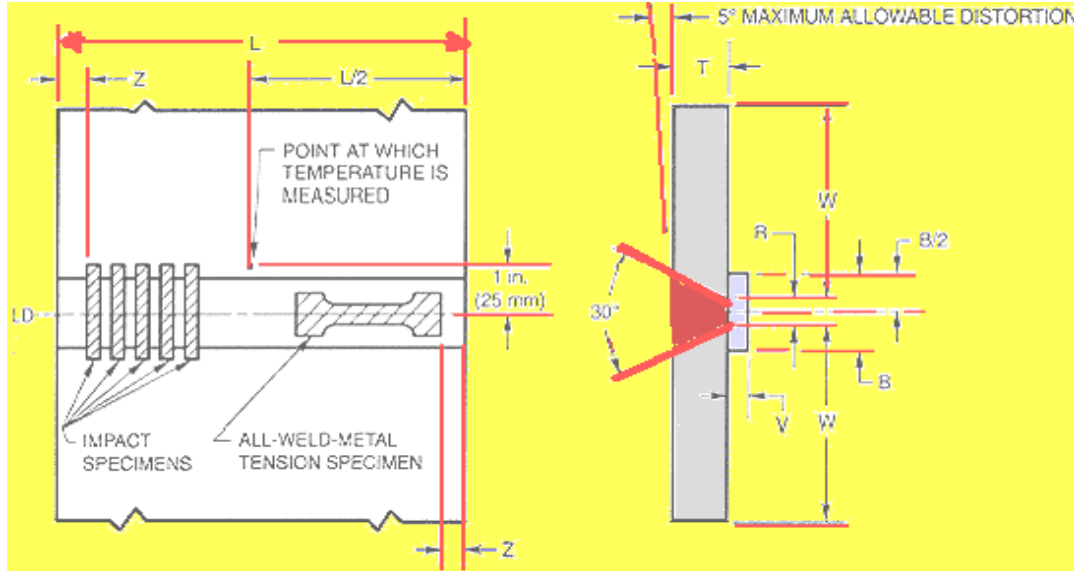


Fig 3(a) Joint configuration and location of test specimen

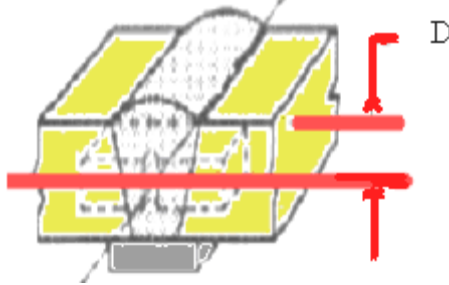


Fig 3(b) Location of impact test specimen.

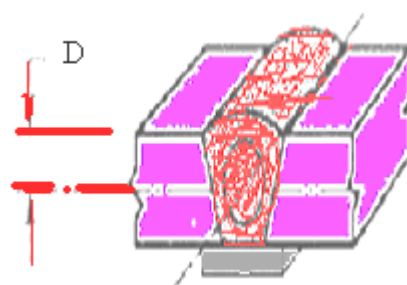


Fig 3(c) Location of all weld metal tension test specimen.

Table 5. Symbols and dimensions in inch and mm for samples as per fig 3(a), 3(b) and 3(c).

Letter Symbol	Dimensions	Inch	mm
L	Length(min)	12	305
T	Thickness	1±1/16	25±1.5
W	Width(min)	5	127
V	Backup Thickness	1/2±1/16	13±1.5
D	Specimen Centre	3/8±1/32	9.5±1.0
B	Backup Width(min)	2	50
R	Root Opening	1/2±1/16	13±1.5

7.2.1. Visual Examination

All three types of test specimens (assemblies) were visually inspected during and after welding. During welding with pure slag, it was observed that undercuts have occurred along the sidewall of groove, which, were later removed by grinding. Slag detachability was poor.

No such problems were experienced during welding with recycled and fresh available flux. Stable arc was

observed from the voltmeter. No under cut, surface porosity, and pockmarks were observed on the welded test assemblies. The bead was smooth and its appearance was good.

7.2.2. Dye-penetration Test

After removal of the reinforcement with the help of a grinding machine and dressing it, dye-penetration test was carried out on all the test assemblies to detect porosity and

surface cracks. First with the cleaner the weld surface was cleaned, dried and then die penetrant was applied over the surface. 15 minutes time was allowed to enter the penetrant. The excess penetrant was then removed by soft and clean cotton .A developer was then applied to the surface. The developer acted as a blotter and drew out a portion of the penetrant from the flaws and the flaws were immediately detected. Scattered porosity was observed on the test sample deposited with pure slag. No surface defect was observed on the test assemblies prepared with fresh flux and recycled slag.

7.2.3. Radiographic Test

X-ray radiography was used to detect defects in the samples. It was observed that test assembly prepared with pure slag was unsatisfactory in radiography. Porosity, slag inclusion and lack of fusion were observed. Porosity may be due carbon dioxide gas formed in molten pool by oxidation of carbon, as deoxidizers have already been exhausted. Slag inclusion may be due entrapment of slag in under-cuts as slag detachability was poor. Slag entrapped in sidewall under-cut may lead to porosity. Test plates deposited with recycled and fresh flux cleared the radiographic test. Evaluations of weld radiographs were as per 9.25.2 of AWS D1.1-88.

7.2.4. Tensile Test

The results of all weld tensile and impact tests of all the test assemblies as well as AWS requirements are shown in Table 2. Recycled slag with EL-08 wire combination confirms to AWS SFA A5.17; F7A0-EL8 classification, which is equivalent to Mergearc<sup>1</sup> SAF-6 flux. As per this classification, for this flux (Recycled slag)-wire combination minimum yield strength, ultimate tensile strength and % elongation required are 360 N/mm<sup>2</sup>, 420 N/mm<sup>2</sup> and 20% respectively, which was achieved with

the recycled slag. Fresh flux also fulfilled above criteria. In case of pure slag with EL-08 wire combination, yield and ultimate tensile strength achieved was 320 and 370 N/mm<sup>2</sup> respectively which is below the acceptable range. This may be due to lesser amount of alloying elements (C, Mn and Si) content in the weld metal. These results are in good agreement with the chemical composition.

7.2.5. Impact Test

In evaluating the test results, the highest and the lowest values obtained have been discarded as dictated by AWS codes. According to this code, two of the remaining three values should be equal, or exceed, the specified (90 J) energy level and the average of the three should not be less than the required (90 J) energy level at 0°C. This condition was satisfied in case of recycled slag, where as in case of pure slag the average and minimum impact values were 72.9 J and 52.2 J at 0 °C, which are un- acceptable. The presence of slag inclusion, porosity and lack of fusion may be the reason for the low impact value. Addition of alloying elements / deoxidizers reduces the level of oxygen as a result decreased amount of non-metallic inclusions. This resulted in improved toughness as in case of recycled slag.

7.2.6. Micro Hardness

Change in microstructure, grain growth, hardness and residual stress in a weldment are very much dependent on the temperature distribution, peak temperature and cooling rate. Fig.4 compares the micro-hardness survey carried on the cross section of weld bead deposited with pure slag, fresh flux and recycled slag respectively. It has signified that the hardness achieved with recycled slag was more than achieved with pure slag and similar with fresh flux. Increased amount of C, Mn and Si through recycled slag resulted in higher hardness.

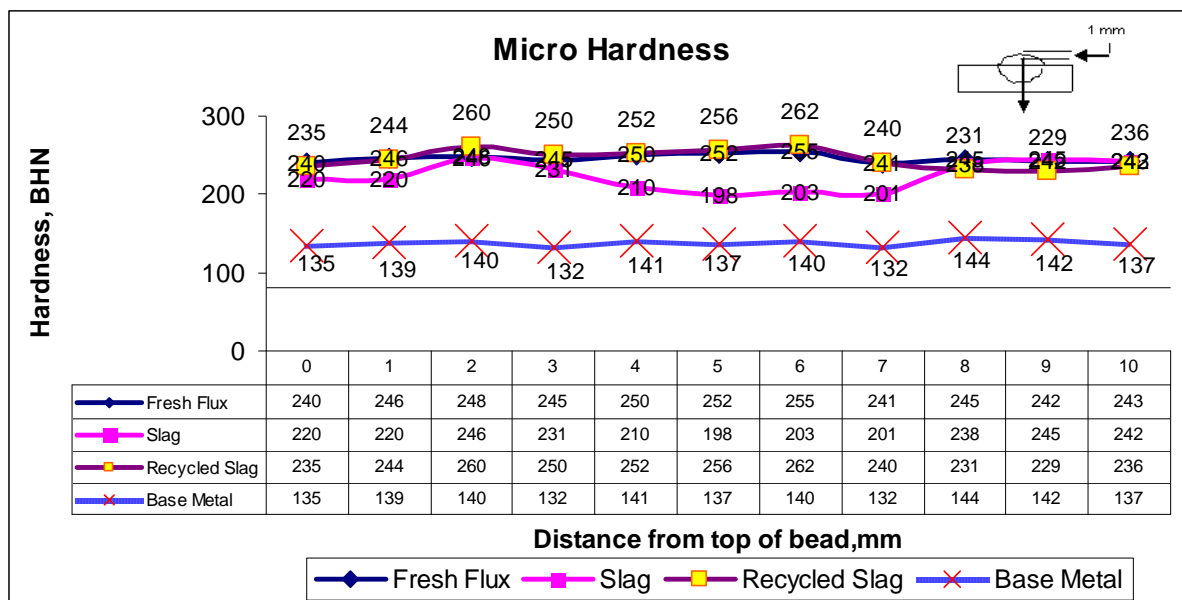


Fig. 4 Micro-hardness survey across the beads

### 7.2.7. Fractography

Scanned electron micrographs of the fractured tensile test specimens could be seen from Fig 5 and 6 belonging to the weld metal deposited with pure slag and recycled slag respectively. Both the micrographs illustrated ductile mode of failure. However, Fig.6 pointed toward larger dimple size and consequently indicated higher energy

absorption before fracture, which, further supported the results of tensile and impact tests. The theoretical relation is that larger the dimple size, higher the energy absorption. It can be attributed to the increased amount of carbon, manganese and silicon in the weld metal deposited with recycled slag.

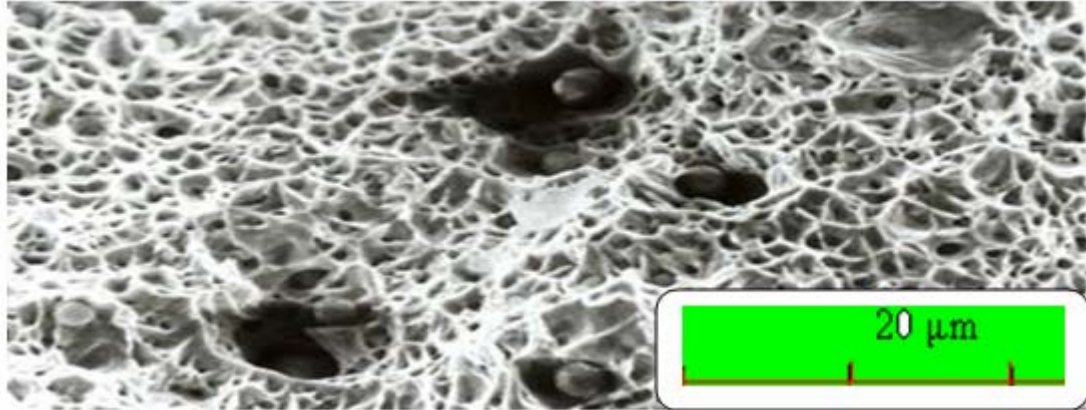


Fig 5. Scanning electron micrograph of the fractured tensile sample of weld metal deposited with pure slag.

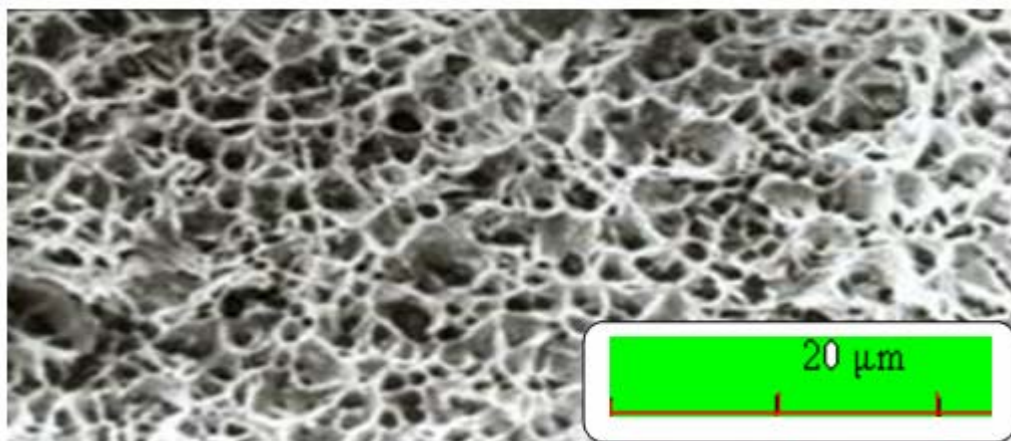


Fig. 6 Scanning electron micrograph of fractured tensile sample of weld metal deposited with recycled Slag.

### 7.2.8. Metallurgical examinations

For metallurgical analysis and micro-hardness survey beads on plates were deposited at 0.8 kJ / mm heat input. Microstructure of weld metal deposited with pure slag, fresh flux and recycled slag has been shown in Fig.7, Fig 8 and Fig.9.

The presence of columnar grains with grain boundary ferrite and islands of polygonal ferrite could be seen from the microstructure of weld metal deposited with pure crushed slag. Ferrite side plates were also observed. The

presence of significant volume fractions of grain boundary ferrite and polygonal ferrite can be attributed to the very low percentage of carbon (0.025%) in the weld metal deposited with pure slag.

The microstructure of weld metal obtained with recycled slag (Fig.9) indicated that the average width of columnar grains is smaller. In addition, the amount of grain boundary ferrite has reduced, the crystallite size within the columnar grains was smaller, and there was more acicular ferrite. This decrease in primary ferrite could be attributed to the increased percentage of carbon (0.08%).

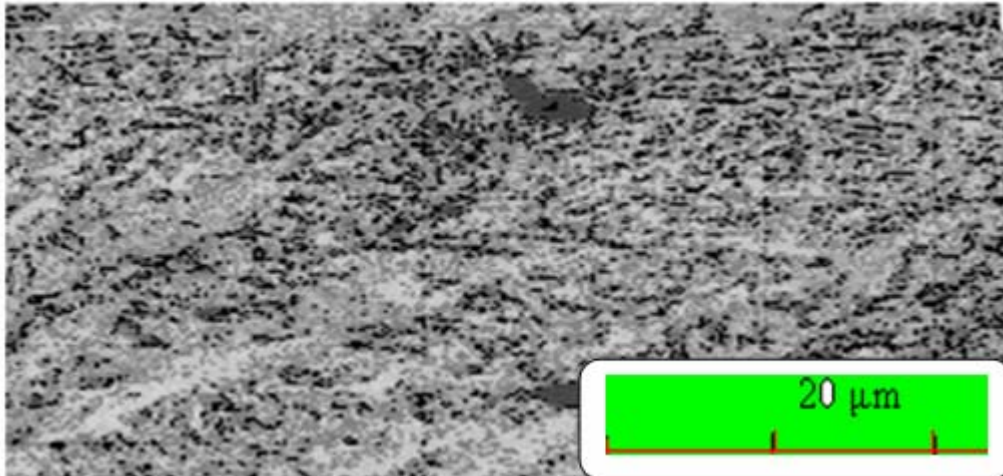


Fig.7 Microstructure of weld metal deposited with pure flux

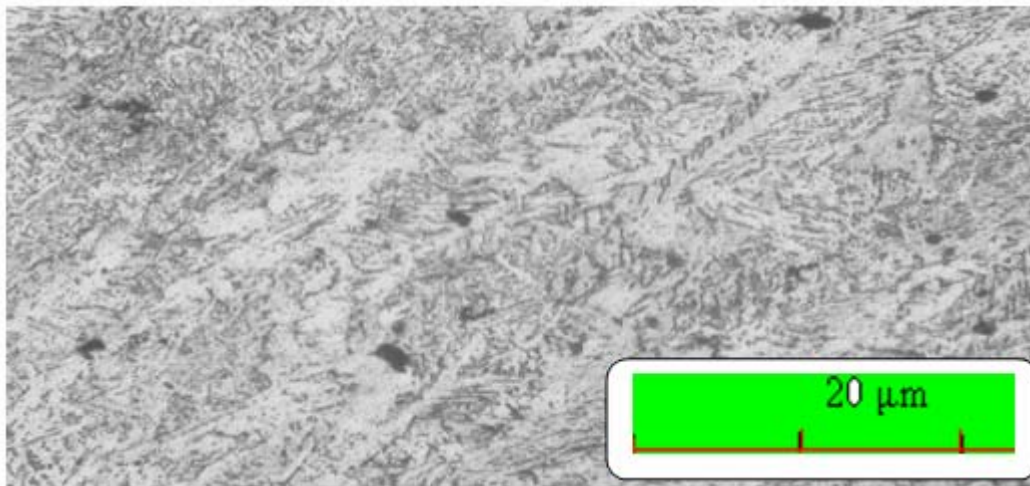


Fig. 8 Microstructure of weld metal deposited with pure slag

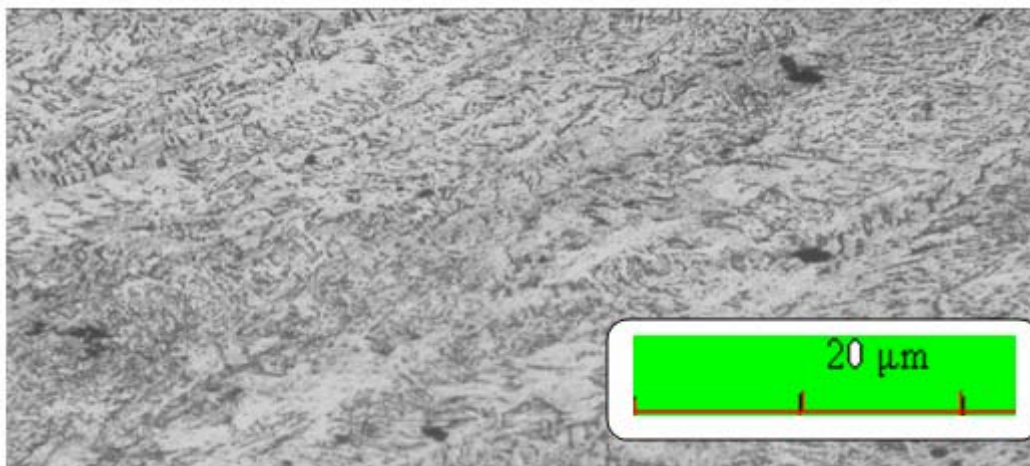


Fig. 9 Microstructure of weld metal deposited with recycled Slag

## 8. Cost Analysis

By products are difficult to cost because a true cost is indivisible. But, Cost analyses can provide estimates of what a program's costs and benefits are likely to be, before it is implemented. It also helps improve understanding of program operation, and tell what levels of intervention are most cost-effective. Considering these view, Cost analysis of recycled slag per 100 kg was calculated and compared with the equivalent fresh flux available in the market according to the principle of market value method or reversal cost method. It is similar to the technique of by product revenue deducted from production cost. These certainly enable the company to decide a certain level of services to a specific number of clients at specified costs.

Simple mathematical calculations have been carried out gathering market value of the raw materials and additives which are coupled with the manufacturing cost. Labour costs are considered according to the current rates set by the local governing authorities. As per the standard norm being followed by the company overhead and profit are considered at 10% and 12 % respectively. The detail conversion cost per 100 kg was thus obtained which was compared with the fresh flux available at a price from the local market. Approximately, 71 % saving has been reported. Although, no relative significance of the environmental impact cost have been considered and calculated. This recycling will save lots of environmental hazards and pollution, which have adverse effect on the quality of life. The detail analysis has been done and presented in Table 6.

Table 6. Cost breakup of recycled slag and fresh flux per 100 kg

SI No	Cost Head	Material Specification	Process description	Cost	% of Cost
				US Dollar	
1	Raw Material Slag	Slag	Cost of Slag used inclusive of Transportation charges	1.10	2.63
2	Additive	Ferro Manganese	Cost of additive used	8.80	21.03
3	Additive	Ferro Silicon	Cost of additive used	6.05	14.46
4	Additive	Ferro Titanium	Cost of additive used	6.60	15.77
5	Additive	Calcium Carbonate	Cost of additive used	0.47	1.13
6	Additive	Silicon Oxide	Cost of additive used	0.39	0.92
7	Binder	Potassium Silicate	Cost of binder used	3.30	7.89
8	Processing		Sintering Cost	3.30	7.89
9	Crushing and Milling Cost		Crushing and Milling of Slag with additives	2.97	7.10
10	Labour Cost		Cost of Labour employed in the job	45.00	107.53
11	Sub Total			33.97	
12	Over Head @ 10 %	On 1 to 11		3.40	
13	Profit @ 12%	On 1 to 12		4.48	
14	Conversion cost per 100 kg Recycled slag			41.85	
15	Actual Market Price of fresh flux			143.00	
16	Saving			101.15	
17	% Saving			70.73	

## 9. Discussion.

Slag can be re-cycled successfully and the following guidelines should be adopted for slag re-cycling and its subsequent use. A locally applicable slag purification and recycling arrangement has been developed.

The following recommendations have been done for obtaining better results from the use of recycled slag.

1. During continuous welding operations unused slag can be recycled and returned to the flux hopper for re-use.
2. Slag and metallic particles should be removed from the recycled slag and discarded prior to using recycled slag.

3. Fines should be removed from recycled slag. Excessive levels of fines will impair the welding performance and degrade the weld bead appearance.
4. Slag should be used mixed with additives and binder re-crushed and processed as flux for welding operations.
5. Following a break in welding operations any unused recycled slag should be removed from the welding machine hopper and stored in a heated hopper (250-300°F, 120-150°C) for a maximum period of 24 hours.
6. This slag should then be mixed with twice its volume of new flux prior to reuse.
7. Care should be taken when using forced air recycling systems to ensure that such systems use only dry air and that the slag particles are not damaged or degraded by using high air flow rates (which can result in the formation of large quantities of dust). Only dry air must be used in forced air recycling systems to prevent moisture pick up by the slag. Compressed air systems used for operating power tools should not be used for flux recovery as they may contain oil lubricant.
8. During the manufacturing process SAW Wires are baked at a high temperature and following manufacture the flux coating has low moisture content. Prior to use with recycled slag proper care has to be taken. SAW Wires should be left in their unopened original moisture proof hermetically sealed containers and stored in a dry area. Once the container is opened, the deep sealing lid should be replaced as the lid provides an effective barrier to moisture ingress. Once the container is opened, the electrodes should be stored in a cabinet equipped with either a desiccant or heated to 10-15°F (6-8°C) above the highest expected ambient temperature or both.

## 10. Conclusions

The weld metal properties in this research are determined either in the as-welded condition or after a post weld heat treatment [one hour at 1150°F (620°C)], or both. Most of the weld metals are suitable for service in either condition, but the research does not cover all of the conditions that such weld metals may encounter in fabrication and service. Procedures employed in practice may require voltage, amperage, type of current, and travel speeds that are considerably different from those specified in the submerged arc welding standards. It has been observed a fluctuation of  $\pm 8\%$  from specified ranges.

In addition, differences encountered in electrode size, electrode composition, electrode extension, joint configuration, preheat temperature, interpass temperature, and post weld heat treatment can have a significant effect on the properties of the joint. Within a given electrode classification, the electrode composition can vary sufficiently to produce variations in the mechanical properties of the weld deposit in both the as-welded and post weld heat-treated conditions. Post welds heat-treatment times in excess of the 1-hour used for classification purposes in this specification.

From the research of the nontraditional approach in reducing cost through scientific involvements in recycling saw slag, the following conclusions can be drawn.

1. SAW slag can be recycled.
2. SAW slag recovery program should not be carried out without testing to prove the recycled product will have no detrimental effect on the weld deposit.
3. Weld metal chemistry achieved with recycled slag was within the acceptable range of AWS SFA 5.17-89 / A5.17M-97.
4. The mechanical properties of weld metal were acceptable as per AWS SFA 5.17-89.
5. Good appearance of beads without any visual defects was observed.
6. Arc stability and slag detachability both were good with the recycled slag.
7. The recycling of SAW slag is a feasible alternative to buying new flux for saw process users. It provides economic benefit to companies and allows them to environmentally responsible.
8. The use of recycled slag is economical by 70.73% in the present rate of consumables.

## References

- [1] <http://www.paton.kiev.ua>, Browsed on 26 December 2007.
- [2] Christensen N., and J. Chipman, "Welding Resources Council Bulletin" January 1953, Vol. 15
- [3] Kubli R.A., and W.B. Sharav, "Categorizing the effect of flux in submerged arc welding", *Welding Journal*, Vol. 40, No. 11 1961, 497s.
- [4] Eagar T.W., "Weldments: Physical Metallurgy and Failure Phenomena", General Electric Company, Schenectady, New York, 1979.
- [5] Chai C.S. and Eagar T.W., "The Effect of SAW Parameters on Weld metal Chemistry", *Ibid.* Vol. 59(3), 1980, 93s-98s
- [6] International Institute of Welding, "A World of Joining Experience" Paris, FRANCE, IIW White paper, Version of January 2008
- [7] Mitra U. and Eagar T.W., "Slag Metal Reaction during Welding; part I. Evaluation and Reassessment of Existing Theories", *Metallurgical Transactions*, American Society for Metals, Vol. 22B, 1991, 65-79.
- [8] U.S. Geological Survey, Reston, "Flow Studies For Recycling Metal Commodities In The United States", Version 1.0, Virginia, USA., 2003.
- [9] Specification No SFA5.17, "(Identical with AWS SFA5.17 / A5.17M-97) for Carbon Steel Electrodes and Fluxes for Submerged Arc Welding" A99, 1998, 353-370.
- [10] Christensen N., "Report No 602138 NTIS", Arlington, V.A., November 1965.
- [11] Their H., April, "Proceedings of the conference on Weld Pool Chemistry and Metallurgy", The Welding Institute, London, 1980.
- [12] <http://www.titussteel.com> Browsed on 26 December 2007
- [13] Chai C.S. and Eagar T.W., "Slag Metal Equilibrium during Submerged Arc Welding", *Metallurgical Transactions*, American Society for Metals, Vol. 12B, 1981, 539-547
- [14] Beck, H.P. and Jackson, R.A., June "Recycling SAW Slag Proves Reliable and Repeatable" *Welding Journal*, 1996, 51-54.
- [15] Davis, M.L.E. and Bailey, N., "Properties of Submerged Arc Welding Fluxes.-A Fundamental Study" *Metal Construction*, Vol. 14, No. 4, 1982. 202 - 209.

- [16] Livshits, L.G. and Shiryaev, A.I., "A New Ceramic Flux for Hard Facing," *Welding Production*, Jan.1960, 28-29
- [17] Moi, S.C., Bandyopadhyay, A and Pal, P.K., "Submerged Arc Welding With a Mixture of Fresh Flux and Fused Slag," National Seminar on Advances in Materials and Processing, IIT, Roorkee 2001.
- [18] Pal, P.K., Bandyopadhyay, A. and Bala, A.K., "Some Aspects of Submerged Arc Welding with Mixture of Fresh Flux and Fused Slag," International Conference, Dhaka, Bangladesh, 2001.,
- [19] Milichenko, S.L. and Zuravlev, I.V., "A Method Whereby Fused Welding Fluxes Can be Enriched with Ferro Alloys" *Welding Production*, 1960,74-75.
- [20] Their H., April "IIW Documents XII 802-03", The Welding Institute, London, 1983.,
- [21] Pandey S, Singh K and Mani A., "Effect of Recycled Slag on Weld Bead Geometry in Submerged Arc Welding" 14<sup>th</sup> ISME International Conference on mechanical Engineering in Knowledge Age, DCE, New Delhi, Dec. 2005.
- [22] Singh K, Pandey S and Mani A., "Recycling of Submerged Arc Welding Slag," *Australasian Welding Journal*, Vol.51, 2006,34-38
- [23] Farias, J.P., Scotti, A., Balsamo, P.S.S. and Surian, E., "The Effect of Wollastonite on Operational Characteristics of AWS E6013 Electrodes", *Journal of the Brazilian Society of Mechanical Science and Engineering*, Vol. XXVI, No. 3, 2004, 317-322.
- [24] Du Plessis, J., Du Toit, M., and Pistorious, P.C., "Reducing the Diffusible Hydrogen Content of Shielded Metal Arc Welds by Means of Fluoride and Calcite Flux Additions", *IIW Doc II-1590-06*, 2006.
- [25] Kanjilal, P., Majumder, S.K., and Pal, T.K., "Prediction of Submerged Arc Weld-Metal Composition from Flux Ingredients with the Help of Statistical Design of Mixture Experiment", *Scandinavian Journal of Metallurgy*, Vol. 33, 2004, 146-159.
- [26] Lau, T., Weatherly, G.S., and McLean, A., "Gas/Metal/Slag Reactions in Submerged Arc Welding Using CaO-Al<sub>2</sub>O<sub>3</sub> based Fluxes", *Welding Journal*, Vol. 65, No. 2, 1986, 343-347.
- [27] Kanjilal, P., Majumder, S.K., and Pal, T.K., "Prediction of Submerged Arc Weld-Metal Composition from Flux Ingredients with the Help of Statistical Design of Mixture Experiment", *Scandinavian Journal of Metallurgy*, Vol. 33, 2004, 146-159.
- [28] Quintana, M.A., DebRoy, T., Vitek, J.M. and Babu, S.S., "Novel Optimization Methodology for Welding Process/Consumable Integration", Technical Report Submitted To The United States Department of Energy, Repot No DOE-ID14204-F1; Award No. DE-FC36-011D14204, 2006.
- [29] Ademola D.A.; F.A.OyawaleII, "Mixture experiments and their applications in welding flux design", *Journal of the Brazilian Society of Mechanical Science and Engineering*, Vol. XXX, No. 4,2008.,
- [30] NIST/SEMATECH, "e-Handbook of Statistical Methods", Downloaded from <http://www.itl.nist.gov/div898/handbook>, 10/09/06 2006.
- [31] Gunaraj, V. and Murugan N., "Prediction of Heat-Affected Zone Characteristics in Submerged Arc Welding of structural steel Pipes", *Welding Journal*, Vol. 81, No. 1, 2002, 95s-98s.
- [32] Allen, T.T., Richard, R.W., Tagliabue, D.P. and Maul, G.P., "Statistical Process Design for Robotic GMA Welding of Sheet Metal", *Welding Journal*, Volume 81, Number 5, 2002, 45s-51s.
- [33] Kanjilal, P., Majumdar, S.K. and Pal, T.K., "Prediction of Acicular Ferrite from Flux Ingredients in Submerged Arc Weld Metal of C-Mn Steel" *ISIJ International*, Vol.4, No. 6, 2005a, 876-885.
- [34] Kanjilal, P., Pal, T.K. and Majumdar, S.K., "Prediction of Mechanical Properties in Submerged Arc Weld Metal of C-Mn Steel" *Materials and Manufacturing Processes*, Vol. 22, 2005b, 114-127
- [35] Kanjilal, P., Pal, T.K. and Majumdar, S.K., "Combined Effect Of Flux And Welding Parameters On Chemical Composition And Mechanical Properties Of Submerged Arc Weld Metal", *Journal Of Materials Processing Technology*, Vol. 171, Issue 2, 2006, 223-231.
- [36] Kanjilal, P., Pal, T.K. and Majumdar, S.K., "Prediction of Element Transfer in Submerged Arc Welding", *Welding Journal*, Vol.86, No. 5, 2007, 135s-148s.
- [37] Kaveh, A., Haghghati, A.H., and Mirzahassemi A.R., "Recycling the slag obtained from the Application of Powder in Submerged Arc Welding", *Journal of Environmental Science and Technology*, Vol.38, Autumn, 2008,
- [38] <http://www.recycleflux.com> Browsed on 26 December 2007.
- [39] ESAB AB, "Technical Handbook Reg No XA 001 36020 05 2008", USA, 2008.



# Design and Manufacturing of Self Actuating Traction Drives with Solid and Hollow Rollers

Wisam M. Abu-Jadayil<sup>a,\*</sup>, Mousa S. Mohsen

<sup>a</sup> Department of Mechanical Engineering, The Hashemite University, Zarqa, 13135, Jordan

<sup>b</sup> Department of Industrial Engineering, The Hashemite University, Zarqa, 13135, Jordan

## Abstract

The friction drive speed reducer proposed by Flugrad and Qamhiyah in 2005 was mainly investigated in this paper. That self actuating traction drive uses six intermediate cylindrical rollers to transmit motion. Those rollers fail by fatigue. So, this research built a numerical simulation model to find the optimum size of those rollers which give the least contact stresses and so the longest fatigue life. Then those rollers were replaced by hollow ones. The numerical simulation results showed that the contact stresses values decreased in case of having the rollers hollow, which means longer fatigue lives of those rollers. The hollow rollers were found to live more than 30 times the solid ones under same loading conditions. To validate the simulation results and practical application of the proposed model by Flugrad and Qamhiyah, two traction drives were manufactured from aluminum with the optimum dimensions found numerically. The hollow rollers were manufactured with 60% percentage of hollowness, that the ratio of the internal diameter to the external diameter was 60%. The hollowness was filled with rubber which has very low modulus of elasticity, which is very close to represent the hollow space. The two friction drive models were experimentally tested and could successfully transmit motion and reduce speed.

© 2010 Jordan Journal of Mechanical and Industrial Engineering. All rights reserved

Keywords: Fatigue Life; Hollow Rollers; Traction Drive Speed Reducer.

## 1. Introduction

Traction drives with cylindrical rollers have high radial load capacity. They contain rollers that are cylindrical in shape. Machine elements in concentrated rolling motion (rolling element bearings) may fail for a variety of causes, like wear, what is known as galling failure, localized plastic deformation, over loading and overheating. Most or all of these causes may be avoided or reduced by careful system design and manufacture. Even so, the system may then fail eventually by fatigue. In rolling element bearings, the fatigue occurs where there are rolling contacts that suffer from repeated loading. To date, there is no proper examination of the damage in the rolling contacts. It is just known that repeated stressing of the machine elements causes irreversible changes in them, which results in the formation of cracks. These cracks occur after a random number of load cycles based on the stress distribution inside the machine element. The sign of the crack propagation is formation of some damage in the contact surface known as pitting or spalling [2]. Since the stress distribution within the machine element is a main factor of determining fatigue life, some design changes should be

made to redistribute the contact stresses of the rolling elements. Making rollers hollow might be a good technique to redistribute those contact stresses.

Using hollow rollers in the roller bearings had the interest of some designers because of their advantages over solid rollers. These include reducing the material used in making the rollers, less weight for the roller bearing, and the ability to preload the hollow roller element, giving it more stability with less noise and vibration. Hollow roller bearings are single or double row radial bearings with an inner ring, outer ring and hollow or thin wall rollers. In traction drives, two or more sets of rollers are used in contact between the inner race and the outer ring. They utilize traction or friction to transmit torque and power. Ai [3,4] indicated that traction drives have unique characteristics which are not present in gears. Like the high mechanical efficiency, little or no backlash, low noise and vibration. In friction drives, the power is transmitted between the contacted surfaces using Coulomb friction. No lubricant is used in friction drives. A good example of traction drives using cylindrical roller bearings is the self actuating traction drive designed by Flugrad and Qamhiyah [4]. This friction drive is used as a basis for this work for testing the fatigue life of hollow rollers in traction drives. Even so, the results can be generalized for

\* Corresponding author. wisam@hu.edu.jo

cylindrical rollers used in roller bearings and other traction drives.

Ai [3, 4] developed planetary traction drive transmission with zero spin. Traction drives with their two types; the fixed ration transmission (FRT) and the continuous variable speed (CVT) have the problem of the spin motion that causes rotational sliding between the contacted surfaces about an axis normal to the surfaces and thus must be oil-lubricated [3]. The spin motion causes power loss and component wear. The zero spin design of Ai [3,4] improved the mechanical efficiency of the traction drives when operated with lubricant and running dry. He found that lubricant churning-loss is an important power sink. So, traction drives running dry might have higher mechanical efficiency than running with lubricant.

Using traction drives has many advantages over gears, such as less noise, easier to manufacture, and easier and cheaper to maintain. On the other hand, one of the main disadvantages of using the traction drives over gears is its weight. For the same load application, the required traction drive is heavier than the required gear system. So, this paper interest is to find a solution for the two problems of the cylindrical rollers; their fatigue life and their heavy weight. A solution for both these problems can be found by using hollow rollers instead of solid rollers in the traction drives. Using the hollow rollers means less weight. And so the problems are partially solved. This works investigating the fatigue life of the traction drive compared to traction drive with solid rollers.

In Abu Jadayil [5], numerical simulations of two rollers under pure rolling contact with normal and tangential loads, have been made to study the fatigue life of hollow rollers, and to compare it to solid rollers. The results of that work showed that hollow rollers have longer fatigue life than solid ones. The optimum percentage of hollowness with the longest fatigue life was found to be around 50% in case of combined normal and tangential loading.

This paper is trying to theoretically and experimentally verify the results achieved by Abu Jadayil [5] by building a numerical simulation models for the self actuation traction drive proposed by Flugrad and Qamhiyah [1], a model with solid rollers and another with hollow rollers. Then the manufactured traction drives with optimum dimensions were tested experimentally to investigate their rollers' fatigue lives.

## 2. Literature Review

The distribution of the tangential loading in the area of contact was studied by Mindlin in 1949 [6]. He assumed one elastic body sliding over the other, and he assumed the tangential loading value at the point of contact did not exceed the product of the coefficient of friction between the two bodies and the normal loading value. The value of the coefficient of friction he used in his analysis was 0.33. He found that the tangential loads generate infinite stress at the boundaries of the contact area. In the same year, Poritsky [7] obtained a solution using two different methods for the same problem, but with coefficient of friction of 0.3.

Smith and Liu [8] extended the solution obtained by Poritsky [7] to consider the effects of these stresses in causing failure by inelastic yielding and fatigue. They assumed the Hertzian distribution of the normal and tangential loads over the area of contact. The resulting stresses of applying the normal and tangential loads were represented in a closed form. A coefficient of friction of 0.33 as a proportionality factor between the tangential and normal loads was used.

The interest in using hollow rollers in bearings started in the 19<sup>th</sup> century. Many patents were issued for different designs of hollow roller bearings. In 1897 Miller [9] received a patent for a hollow roller bearing in which the rollers were formed of spirally wound strips of metal. Eight years later Fownes [10] patented a thin walled hollow roller bearing. In his invention he tried to provide more flexibility and soften the shocks the vehicle was subjected to on rough roads. In the next year a more flexible roller bearing was invented by Canre [11]. He used slots in the walls of his thin walled tabular rollers. After that many designers received many patents for new hollow roller designs, like Lockwood [12], Steenstrup [13] and Lockwood [14]. One of the best deigns for hollow roller bearings was made by Steffenini [15] in 1947. He discussed the use of preloaded hollow rollers, including cylindrical, tapered, wrapped and layered rollers with complete and partial hollowness.

Many researchers started to discuss the advantages and disadvantages of hollow rollers. Hanau [16] described the advantages of roller bearings with over 50 percent hollowness in high speed applications. Given [17] pointed out the advantages of hollow roller bearings in driving turbine shafts at the required speed. Harris and Aaronson [18] utilized this advantage in his patent with 60 to 80 percent hollowness. In his design, he increased the hollowness to be able to increase the preloading and so reduce the roller skidding.

Zaretsky [19] reported many experimental tests made between 1967 and 1978 to investigate the fatigue life of hollow balls, hollow rollers and cylindrical hollow balls. He indicated that calculations made by Harris in 1968 [20] showed that using hollow balls in the bearings causes the reduction of the centrifugal loading as a result of reducing the mass of the rolling element. He believes that to have significant effect on the bearing fatigue life, the mass should be reduced at least 50% by using hollow rolling elements.

Bowen utilized the advantages of preloading the hollow rollers and their superior characteristics in his patents in 1976 [21] and 1977 [22]. Many unique characteristics of the hollow roller were discussed by Bowen and Bhateja [23]. They noted that in low speed hollow rollers, the limiting factor of the fatigue life is the contact stresses. These stresses can be reduced by increasing the number of the preloaded hollow rollers sharing the load. At high speeds, Bowen and Bhateja thought the lighter weight of the rollers and the complete preloading and roller's compliant nature, all tend to increase the contact surface fatigue life. So the bending stresses, especially those happening at the bore surface would be the fatigue life limiting factor. Bowen and Bhateja [23] experimentally investigated the 50 to 80 percent hollowness. They found

that rollers with a hollowness range from 60 to 70 percent are the best to use for most applications.

The fatigue life of the hollow roller bearings compared to solid roller bearings has been studied by many researchers. The general trend has been to agree that the fatigue life is improved in the case of hollow roller bearings. However, they used different methods to prove that.

The contact problem of hollow cylinders was analyzed by Hong and Jianjun [24]. They used three hollowness percentages in their analysis; 50%, 60% and 70%. As defined earlier for the hollow rollers, the hollowness percentage is the ratio of the diameter of the hole to the outer diameter of the cylinder. In their experimental results, they found that the contact stresses of 50% hollow cylinders are 33%-35% less than contact stresses of solid cylinders. That was related to the increase of the contact area of hollow cylinders. In their theoretical analysis they found that in rollers with 50% hollowness, most of the deformation occurs at the contact region, and the amount of bending deformation is very small. This shows why they behave like solid cylinders. Hong and Jianjun [24] concluded that when hollowness is less than 70%, fatigue life of contacting bearings can be improved. That is not related to the change in the contact width, but to the decrease of the contact stresses.

Since running rollers without lubricant increases the mechanical efficiency as indicated by Ai [2,3], numerical simulation in this work assumes no lubricant present between the two rollers in contact. Moreover, running the rollers dry increases the fatigue life as demonstrated by Way [25].

### 3. Traction Drive Selection

Most speed reducer in use today utilizes gears to produce an output speed different than the input speed. There are, however, other types of speed reducers in use, including traction drive speed reducer. These depend on friction between rolling elements to transmit torque from the input member to the output member. The rolling elements are held together with a prescribed normal force to generate the required friction force based on the power to be transmitted by the device. However, these devices are not self-actuating. Further, these devices often require a separate clutch to allow the output to be disengaged from the input. It is therefore a principal object of this invention proposed by Flugrad and Qamhiyah [1] is to provide a traction drive speed reducer which is self-actuating. A further object of this invention is to provide a self-actuating traction drive speed reducer wherein the normal force on the roller members is only present when needed to permit the rolling elements to be operationally disengaged. A still further object of this invention is to provide a self-actuating traction drive speed reducer which can be easily engaged and disengaged in response to changing speed requirements.

The speed reducer proposed here is designed so that the configuration of the rolling elements creates the needed normal force in response to the torque exerted back on the system by the downstream loading. Thus the device is self-actuating. Since the normal force is only present when needed, the rolling elements of the device can readily be

disengaged, thus eliminating the need for a separate clutch in the drive system. This feature can be exploited to design a transmission with several distinct speed ratios which can be engaged and disengaged in response to changing speed requirements.

Many traction drives were developed by researchers. A cone roller toroidal traction drive was developed by Tanaka in 1988 [26]. In that work the a traction drive CVT of toroidal rolling elements changes its speed ratio by the control of the attitude angle of the power roller of which control force is induced from a little side slip. Design scheme for multidisk Beier traction variators was produced by Younes in 1992 [27]. The unique design feature of the Beier traction variator is that it can provide a higher power capacity per unit volume by using multiple thin disk pairs in a planetary system. Compared to these traction drive designs, the self actuating traction drive of Flugrad and Qamhiyah [4] has unique characteristics; mainly being self actuating, that rollers do not need to be in contact all the time. That would result in significant increase in the fatigue life of the rollers. The list of products in which this new self-actuating traction drive speed reducer might be used is seemingly endless. Currently, gear-driven units are used for many of these applications. Since this new traction drive design consists of cylindrical-shaped rollers rather than complex shaped gear teeth, it will be simpler to manufacture, easier to assemble, and will run quieter.

## 4. Problem Statement and Solution Technique

### 4.1. Problem Statement.

Much of the research has been centered on the use of hollow rollers in roller bearings. Research in this area has shown hollow rollers to have advantages in accuracy of rotation and stiffness, even at high speeds. A related area of interest is the use of hollow rollers in pure rolling contact with another roller. One main advantage of using hollow rollers in a roller bearing is the additional sharing of load between rollers as the rollers deflect more than solid rollers do under the same load, the reduction in stress is seen when the area of contact between the rollers expands under load.

One of the main disadvantages of friction drive systems compared to gear drive systems is the size required. The size of a friction drive system must be larger to account for the stress induced due to the normal force required to prevent slip. Using hollow rollers in a friction drive system can decrease the stresses in the rollers, thereby allowing smaller rollers to be used. Since the need for all inherent advantages in traction drive speed reducer instead of geared one, the configuration must be studied very well, installed and assembled in such away that all these benefits and improvements in the design can be implemented and provided.

The study here will discuss every improvement in the traction drive, how can we implement it and the needed design and configuration in order to be exploited. Figure 1 shows most of the parts in this embodiment.

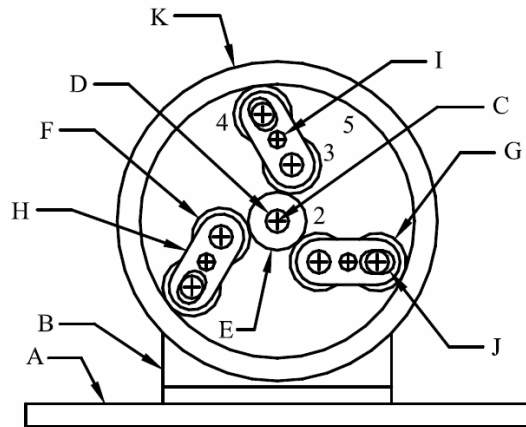


Figure 1. Speed Reducer Embodiment [1].

Part **A** is the mounting plate on which the assembly is mounted. Part **B** is the back plate, which is securely fastened to part **A**. The back plate holds a bearing which defines the axis of rotation for the input and output members. This axis is identified as **C** in the figure. The input shaft is marked as **D** and the input member, part **E** is rigidly attached to **D** and rotates with it. There are three pairs of intermediate rollers shown in the figure, but there could be more or less than three sets. A typical inner roller is labeled **F**, and **G** is an outer roller.

Inner and outer rollers are held in proximity to one another by the roller plate, **H**. The outer hole, **J**, through which the outer roller shaft protrudes, is slightly elongated. This allows the inner and outer rollers to press firmly against one another, generating sufficient friction to transmit torque through the unit. The roller plate, along with the inner and outer rollers, is free to rotate about pin, **I**. The mid plate, in which the three pins are mounted, is shown in Figure 2. The slots are elongated to allow the roller plates and inner and outer rollers to seek a configuration with the inner roller pressed firmly against the input member, and the output roller pressed firmly against the output member, part **K**.

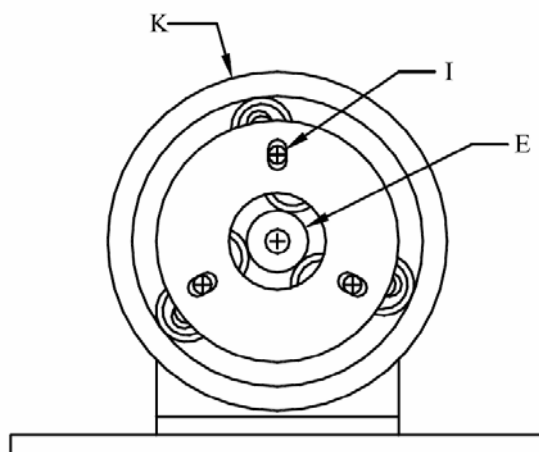


Figure 2. Speed Reducer Embodiment; Including the Mid Plate [1]

By using hollow rollers in the friction drive system have the advantages in accuracy of rotation and stiffness, even at high speeds, which leads to:

- Decrease the stresses in the rollers, thereby allowing smaller rollers to be used, due to the additional sharing of load between rollers as the rollers deflect more than solid rollers do under the same load, the reduction in stress is seen when the area of contact between the rollers expands under load.
- Decrease the device weight (some of the material is being removed).
- Since the contact stresses between the cylindrical rollers are decreased, the fatigue lives of those rollers are expected to increase, which is the main concern of using hollow rollers in that traction drive instead of solid rollers.

#### 4.2. Solution Technique.

The work of this research passes through three main stages. The first stage is the design stage of the traction drive. The second stage is the fabrication of the traction drive, one with hollow rollers and another friction drive with solid rollers. The last stage is the testing of the speed reducers to make sure they are working well in transmitting the motion with speed reduction and to investigate their fatigue lives.

##### 4.2.1. The Design Stage.

Using the ProEngineering software, a CAD model was constructed for the traction drive proposed by Flugrad and Qamhiyah [1]. Initial values were chosen for the traction drive parts' dimensions. The ProEngineering contains a Pro-Mechanica package that enabled us to assign forces and reactions to the model parts. The main objective of the design stage was to get the optimum dimensions for the parts with the least values of the contact stresses.

One of the main disadvantages of friction drive systems compared to gear drive systems is the weight of the embodiment, hence, using a lightweight material will overcome the weight issue, such as using aluminum (AL), as it is suggested in this study. Aluminum has a density of  $2.71\text{g/cm}^3$ , modulus of elasticity of  $73.08\text{ GPa}$ , and Poisson's ration of  $0.33$ . Since aluminum is a ductile material, it will allow the rollers and the whole embodiment surfaces to get more flattened, which means distributing the forces applied on the surfaces normally on a larger area, so that the pressure on the parts will be decreased, allowing more fatigue life cycles for the rollers. While in hollow rollers the rubber was used to fill the hollowness since the axels and the pins need a rigid body to be fixed with, selecting the rubber was based on it's low density and modulus of elasticity ( $\rho=0.92\text{ g/cm}^3$ ,  $E=0.05\text{ GPa}$ ,  $\nu=0.5$ ). Based on initial load of  $100\text{ N.m}$ , initial dimensions were suggested for the rollers as follows:  $r_2 = 55\text{ mm}$ ,  $r_3 = r_4 = 40\text{ mm}$  and  $r_5 = 183\text{ mm}$ . Based on those dimensions, it was found that:  $\Phi = 70.69^\circ$ ,  $\alpha_1 = 19.23^\circ$ ,  $\alpha_2 = 12.64^\circ$ ,  $\psi = 38.83^\circ$ , and  $R = 114.62\text{ mm}$ .

By trial and error strategy, the dimension values were varied until the minimum contact stresses on the solid rollers were obtained.

Those minimum contact stresses resulted in optimum dimensions of:  $r_2 = 31.25$  mm,  $r_3 = r_4 = 33$  mm and  $r_5 = 157.5$  mm. Based on those dimensions, it was found that:  $\Phi = 34.18^\circ$ ,  $\alpha_1 = 11.45^\circ$ ,  $\alpha_2 = 5.88^\circ$ ,  $\psi = 16.85^\circ$ , and  $R = 93.4$  mm.

Where:

$r_2$ : the radius of the input rod

$r_3$  and  $r_4$ : the radii of the cylindrical rollers

$r_5$ : the radius of the outer ring.

The angles are shown in Figure 3.

Based on these geometrical values, the coefficient of friction ( $\mu$ ) was estimated using equation 1 to be at least 0.30.

$$\mu \geq \frac{\sin(\alpha_1 + \alpha_2)}{\left(\frac{r_3 - r_2}{R}\right) \cos \alpha_2 + \cos(\alpha_1 + \alpha_2)} - 1 \quad (1)$$

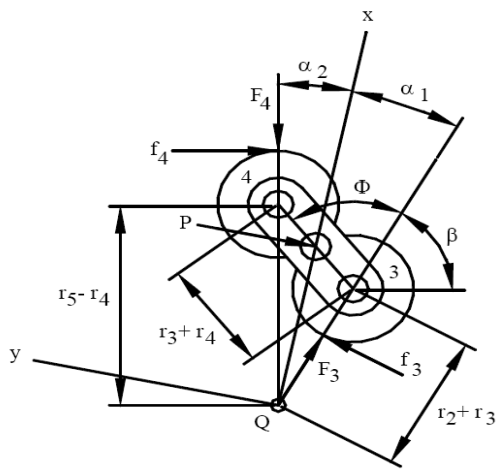


Figure 3. Dimensioned Intermediate Rollers [1]

All of parts which were designed as shown in the following figures:

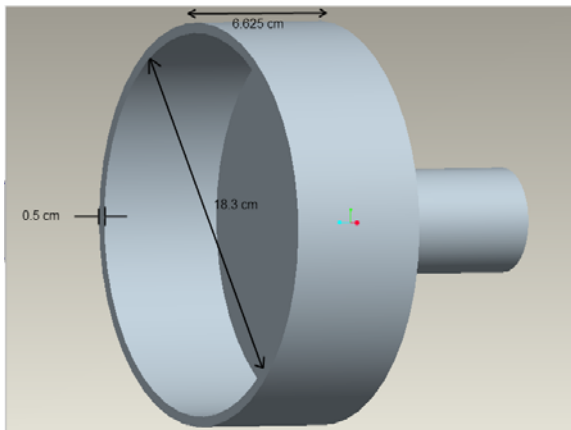


Figure 4. Output ring.

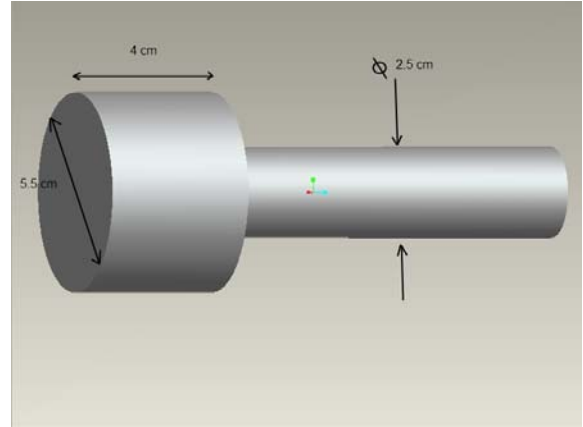


Figure 5. Input rod.

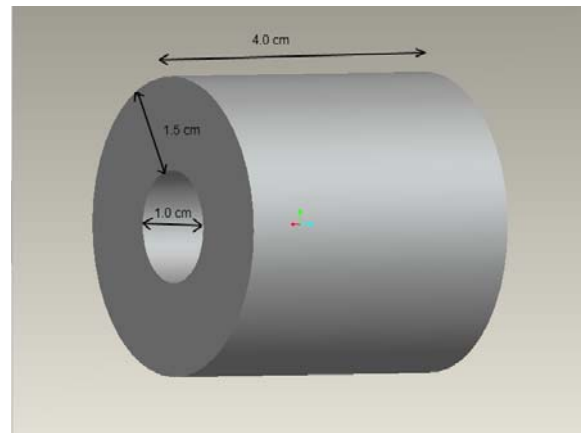


Figure 6. Solid roller

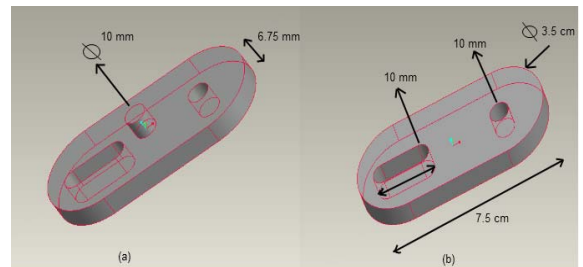


Figure 7 a. Outer roller plate b. Inner roller plate

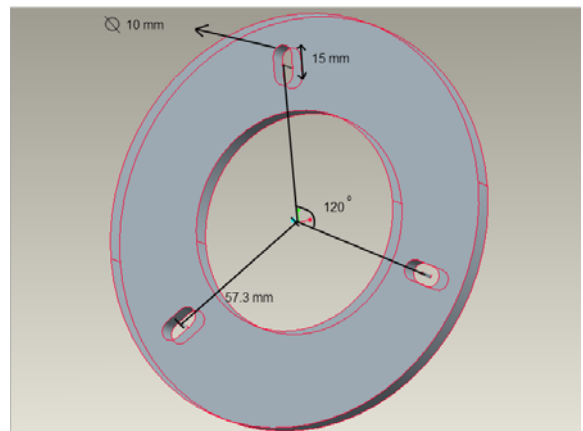


Figure 8. Mid plate.

### Design Analysis.

In most manufacturing operations the material is generally subjected to triaxial stresses which will lead to a more complex state of stress, relationship between the stresses will predict yielding. These relationships are known as yield criteria. The most common yield criteria are the maximum-shear-stress criterion and the distortion - energy criterion using the Von Mises stresses.

In this study those criterions have been used to determine and illustrate where would the elements of the speed reducer get plastically deformed or any stresses that remain within the parts after they have been deformed and all external forces have been removed.

Pro-Engineer software uses these two criteria to analyze the forces applied on the parts and illustrate the stress distribution on each element of the model, in order to find the areas with high stress concentration.

After the forces on each element are being analyzed the software will obtain the stress distribution as a multicolored figure, each color represent a range of stress values, as shown in Figure 9.

Same optimum dimensions obtained for the solid rollers were chosen for the hollow rollers. The traction drive with hollow rollers was subjected to the same loading conditions of the traction drive with solid rollers. The percentage of hollowness used was 60%.

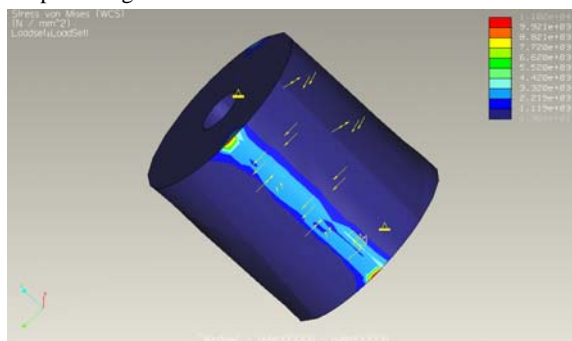


Figure 9. Distributed Stresses in Colors.

#### 4.2.2. Manufacturing Stage.

The parts of the traction drives were fabricated based on the optimum dimensions obtained from the simulation models in the design stage. The output member of the traction drive that is shown in Figure 10 was fabricated by sand casting process. Casting is most often used for making complex shapes that would be otherwise difficult or uneconomical to make by other methods. Moreover casting is the easiest way to manufacture parts. In manufacturing the traction drive it is required to have the outer ring and output shaft as one piece to avoid any slippage and stress concentration there. The easiest and most economical way to do it is by casting. Midplate shown in Figure 11 was fabricated by casting process because of its complex shape. To separate the motion of input member from the fixed midplate, a bearing was used. The cylindrical rollers were fabricated from extruded rods of Aluminum.

The extruded rod was cut to the specified dimension of the rollers and using the lathe machine the solid rollers were drilled for the center pin, and the hollow rollers were drilled up to 60% percentage of hollowness. The hollow rollers were filled by rubber as shown in Figure 12. Figure 13 shows the manufactured roller plate with the optimum design dimensions using lathe machine.

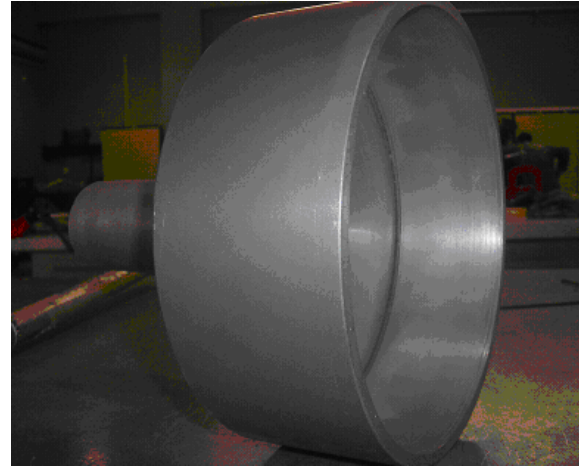


Figure 10. Casted Output Member.

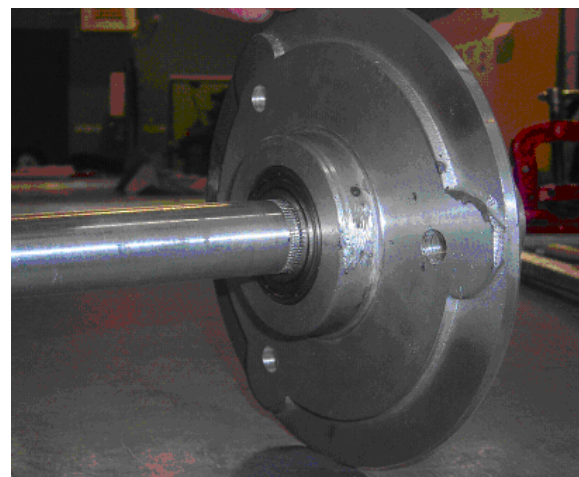


Figure 11. Casted midplate and input member

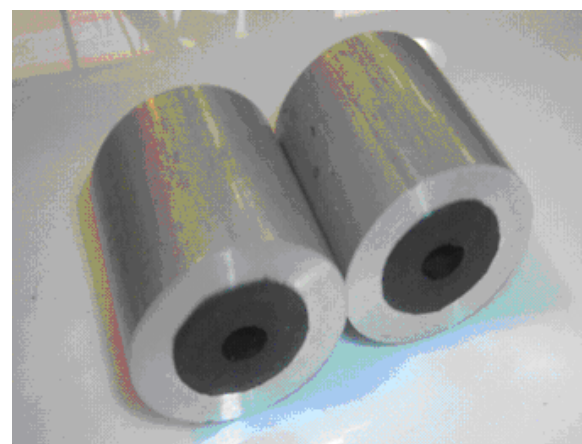


Figure 12. Hollow rollers reshaped at lathe machine.

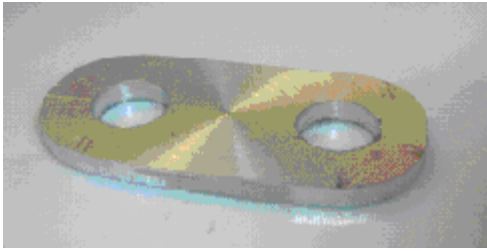


Figure 13. Roller plate after being drilled and refinished

#### Assemblage Stage.

After the fabrication of all parts of both friction drives, the one with solid rollers and the one with hollow rollers, parts were assembled together as shown in Figure 14.

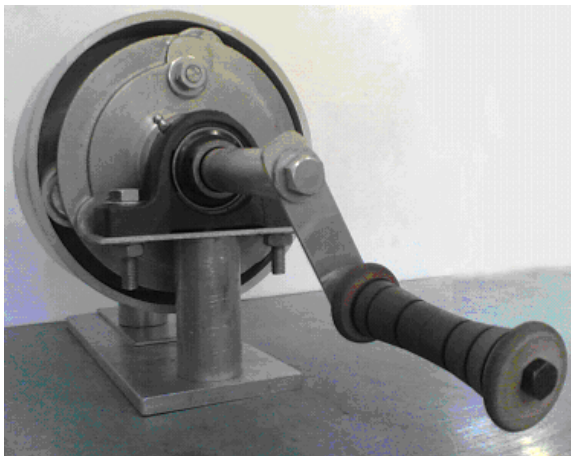


Figure 14. The speed reducer after assembled

#### Testing Stage.

Manually the manufactured friction drives passed the test and could transfer motion to the output member successfully. Then they were tested using input motor to generate input rotational motion, and output brake acting as output load on the outer member. Speed and torque transducers were fixed on the input and output shafts. The output load were fixed at a constant value of 100 N.m in both testing cases, the testing of the friction drive with solid rollers and the testing of the friction drive with hollow rollers. The two friction drives with hollow rollers and with solid rollers could successfully transmit motion from input shaft to the output shaft with reducing the speed at fixed ratio. No problems appeared during their operation. The friction drives with hollow rollers could work in parallel and in series with the solid rollers friction drive.

### 5. Discussion of The Results

As mentioned before, Pro-Engineer software offers a practical way to preview the results of applying load on each part of the two models of the traction drives. Each part of the two models –solid rollers model, and hollow rollers model- was subjected to different values of load, in order to make a clear comparison between the two models. Figure 15 shows a comparison between the solid roller used in the solid rollers traction drive and the hollow roller used in the hollow roller traction drive when subjected to same loading conditions. It can be clearly seen that stresses are distributed more in the body of the hollow roller, which resulted in lowering the maximum value of the

stress. In case of the solid roller the stresses are more concentrated in the contact region of the roller with the other parts, and so the values of these stresses are very high. The red color indicated the areas of the highest stress value. The value of the red color is much higher in case of the solid roller as the figure shows. It is 54.51 MPa for the solid roller and it is 44.03 MPa in case of the hollow roller when both subjected to a load of 100 N.m. The flexibility of the hollow rollers resulted in expanding the contact patch of the roller with the other parts in contact and so distributing the contact stresses on larger area. That is why the maximum stress is lower in case of hollow roller.

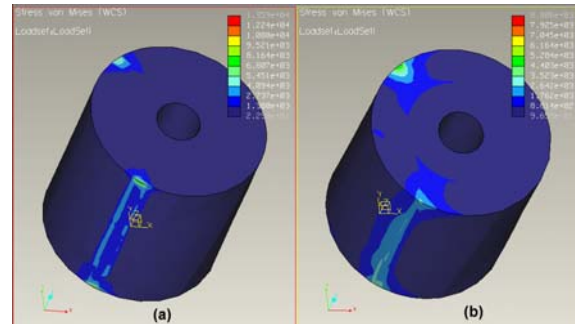


Figure 15. Distribution of stresses on: (a) A Solid roller (b) A Hollow roller

The effects of having the cylindrical rollers hollow on the other parts of the traction drive were also studied. Figure 16 shows the outer ring of traction drive with solid rollers and the traction drive with hollow rollers. The outer ring of the hollow rollers traction drive was subjected to less contact stresses in very limited areas and the values of those stresses were much lower than the contact stresses on the outer ring of the solid rollers traction drive. The maximum stress value on the outer ring of the solid roller traction drive was 14.51 MPa compared to 2.494 MPa maximum stress value on outer ring of the hollow rollers traction drive. So, the flexibility of the hollow rollers made its contact patch with the outer ring larger and so less contact stress value was detected. That makes the fatigue life of the outer ring used in the hollow rollers traction drive much higher.

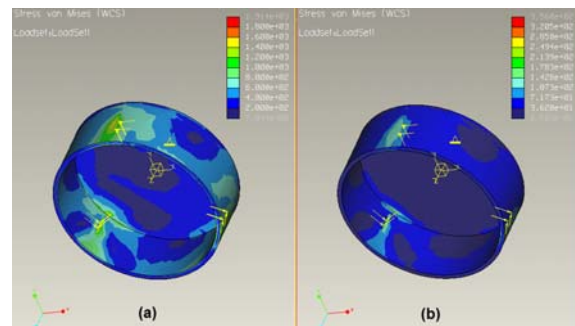


Figure 16. Distribution of stresses on output member, when using: (a) Solid rollers, (b) Hollow rollers

When investigating all parts of the traction drives, it was found that the maximum stress values were found on the roller plates. As Figure 17 shows, the maximum stresses on the roller plates of the hollow rollers traction drive was 75.54 MPa, but the values of the maximum stress values increased to 120 MPa in the roller plates of the solid rollers traction drive. These high values of the

stress make the roller plates the weakest part in the traction drive for constant loading. But since these plates are not subjected to fatigue loading, they are not going to fail in fatigue and they can survive with a factor of safety of 2.67 in case of solid rollers and 4.21 in case of hollow rollers based on a yield stress value of 320 MPa for aluminum.

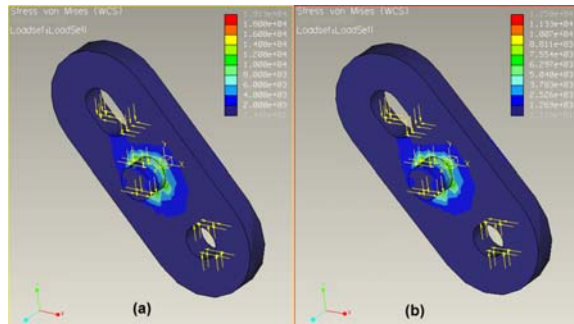


Figure 17. Distribution of stresses on the roller plate, when using: (a) Solid rollers, (b) Hollow rollers

Table 1 compares the maximum Von Mises stress values of solid rollers traction drive parts and the hollow rollers traction drive parts. Based on the S-N curve of Aluminum, the number of cycles each part can survive before fatigue failure is presented in the table. So, the hollow rollers when used in the traction drive, they can theoretically survive around 30 times the solid rollers. The outer rotating ring in contact with hollow roller is going to have much longer fatigue life than the ring in contact with solid roller. As Table 1 shows the outer ring of the hollow traction drive has a fatigue life of 2 million times the fatigue life of the outer ring of the solid rollers traction drive. These results completely agree with the findings of Abu Jadayil [5]. Also other stationary parts in contact with those cylindrical rollers are going to survive longer when they are in contact with hollow rollers rather than being in contact with solid rollers.

Table 1. The maximum Stresses and the number of cycles of traction drive parts

Part Name	Maximum Von Mises Stress (MPa)	No. of Cycles (N)
Solid Cylindrical Roller	54.51	$3 * 10^9$
Hollow Cylindrical Roller	44.03	$9 * 10^{10}$
Output Ring with Solid Cylindrical Roller	14.51	$5 * 10^{15}$
Output Ring with Hollow Cylindrical Roller	2.494	$1 * 10^{22}$

## 6. Conclusions and Recommendations

Based on the research results, the main conclusions can be summarized in the following points:

- The self actuating traction drive proposed by Flugrad and Qamhiyah [1] can be easily fabricated and

assembled. Practically it is very successful in transmitting motion and reducing speed by a fixed ratio. It can be used with solid cylindrical rollers or with hollow cylindrical rollers.

- When comparing the stress distribution on both hollow and solid rollers when subjected to combined normal and tangential loading, it was found that better stress distribution was resulted for hollow rollers with lower peak stress values. So, it is expected that hollow rollers, with 60% percentage of hollowness, have longer fatigue life than identical solid rollers.
- Replacing solid rollers by hollow ones filled with rubber in traction drives, reduces their weights and increases their fatigue lives. That means time and money savings.
- Using hollow rollers instead of solid cylindrical rollers in the self actuating traction drive proposed by Flugrad and Qamhiyah [1] increases the fatigue lives of other parts in contact with the cylindrical rollers which subjected to fatigue loading, and factor of safety for stationary parts in contact with the cylindrical rollers.

## References

- [1] D. Flugrad, A. Qamhiyah, "A Self-Actuating Traction-Drive Speed Reducer". Journal of Mechanical Design, Vol. 127, No. 4, 2005, 631-636.
- [2] R. Gohar, "Elastohydrodynamic". Imperial College Press, 2001.
- [3] X. Ai, "Development of Zero-Spin Planetary Traction Drive Transmission: Part 1-Design and principles of Performance calculation". Journal of Tribology, Vol. 124, 2002, 386-391.
- [4] X. Ai, "Development of Zero-Spin Planetary Traction Drive Transmission: Part 1-Performance Testing and Evaluation". Journal of Tribology, Vol. 124, 2002, 392-397.
- [5] W. Abu Jadayil, "Relative fatigue life estimation of cylindrical hollow rollers in general pure rolling contact". Journal of Tribotest, Vol. 14, 2008, 27-45.
- [6] R. D. Mindlin, "Compliance of Elastic Bodies in Contact". Journal of Applied Mechanics, Vol. 71, 1949, 259-268.
- [7] H. Poritsky, "Stresses and Deflections of Cylindrical Bodies in Contact With Application to Contact of Gears and Locomotive Wheels". Journal of Applied Mechanics, Vol. 72, 1950, 191-201.
- [8] J. O. Smith, C. K. Liu, "Stresses Due to Tangential and Normal Loads on an Elastic Solid With Application to Some Contact Stress Problems". Journal of Applied Mechanics, Vol. 20, 1953, 157-166.
- [9] W. L. Miller, "Roller Bearing". U.S. Patent # 595, 328, 1897.
- [10] W. C. Fownes, "Roller Bearing". U.S. Patent # 785, 944, 1905.
- [11] T. S. Crane, "Flexible Roll for Roller Bearings". U.S. Patent # 828, 387, 1906.
- [12] C. S. Lockwood, "Cage for Rolls in Roller Bearing". U.S. Patent # 868, 105, 1906.

- [13] P. S. Steenstrup, "Roll Mounting for Roller Bearings". U.S. Patent # 859, 347, 1907.
- [14] C. S. Lockwood, "Wearing Piece for Ends of Spirally Wound Rolls". U.S. Patent # 964, 287, 1910.
- [15] M. F. Steffenini, "Roller Bearing with Preloaded Hollow Rollers". French Patent # 946, 559, 1947.
- [16] H. Hanau, "New Concepts in Bearing Designs and Applications". Industrial Tectonics Inc.; 1965, p. 20-22.
- [17] P. S. Given, "Main-shaft Preloaded Roller Bearings". ASME Paper, 1965.
- [18] T. A. Harris, S. F. Aaronson, "Anti-Skid Bearing". U.S. Patent # 3, 410, 618, 1968.
- [19] E. V. Zaretsky, "Tribology for Aerospace Applications". STLE SP-37, Society of Tribologist and Lubrication Engineers, 1997, 409-424.
- [20] T. A. Harris, "On the Effectiveness of Hollow Balls in High-speed Thrust Bearings". ASLE Transactions, Vol. 11, 1968, 290-294.
- [21] W. L. Bowen, "Full Complement Bearing Having Preloaded Hollow Rollers". U.S. Patent # 3, 930, 693, 1976.
- [22] W. L. Bowen, "Roller Bearing of Superior Run-Out Characteristics". U.S. Patent # 4, 002, 380, 1977.
- [23] W. L. Bowen, C. P. Bhateja, "The Hollow Roller Bearing". ASME Transactions, Vol. 102, 1980, 222-228.
- [24] L. Hong, L. Jianjun, "Analysis of Contact Problems on Hollow Cylindrical Rollers". Journal of Tribology, Vol. 17, No. 3, 1997, 253-259.
- [25] S. Way, "Pitting Due to Rolling Contact". Journal of Applied Mechanics, Vol. 57, 1935, A49-58.
- [26] H. Tanaka, "Power transmission of a cone roller toroidal traction drive". Nippon Kikai Gakkai Ronbunshu, C Hen/Transactions of the Japan Society of Mechanical Engineers, Part C, Vol. 54, No. 503, 1988, 1577-1583.
- [27] Y. K. Younes, "Design scheme for multidisk Beier traction variators". Journal of Mechanical Design, Vol. 114, No. 1, 1992, 17-22.



# Cylindrical Solar Cooker with Automatic Two Axes Sun Tracking System

Essam Abdallah<sup>a</sup>, Mohammed Al\_Soud<sup>b</sup>, Ali Akayleh<sup>b</sup>, and Salah Abdallah<sup>c</sup>

<sup>a</sup>Department of Mechanical Engineering, Al – Balqa Applied University, Jordan,

<sup>b</sup>Department of Electrical Engineering, Tafila Technical University, Jordan

<sup>c</sup>Department of Mechanical and Industrial Engineering, Applied Science University, Jordan

## Abstract

All concentrating solar cookers were found to provide adequate temperature needed for cooking. But the common problem of these systems is the need for frequent tracking, and standing in the sun while cooking. This problem could be tackled if one goes in for automatic sun tracking. In this work a cylindrical solar cooker with two axes sun tracking system was designed, constructed and operated. Mechanical system; which consists of two parts, one for altitude tracking and another for rotating around vertical axes was designed and constructed. The hardware and software components of the two axis sun tracking system were designed. The programming method of control with open loop system was employed. The programmable logic controller (PLC) was used to control the motion of surface on which the solar cooker was mounted. A continuous test during different days in the year 2008 from 8:30 am to 4:30 pm was performed. The test showed that the using of cylindrical solar cooker system with two axes tracking can increase water temperature up to 90 °C.

© 2010 Jordan Journal of Mechanical and Industrial Engineering. All rights reserved

Keywords: Cylindrical Solar Cooker, Automatic Control, Tracking System, PLC

## 1. Introduction

The energy section in Jordan depends heavily on the imported oil and gas products. This energy policy put the country in tough economic situations and slowed down the economical growth in the last years. This situation is worsening by the dramatic increase in the crude oil prices worldwide and in the increased demand on energy consumption. Jordan lies in high solar insulation band, where the average insulation intensity on horizontal surface is approximately 5 – 7 KWh/m<sup>2</sup>/d, which is one of the highest in the world [1].

Solar cooking is often considered a solution looking for a problem. Solar cookers have long been presented as an interesting solution to the world's problem of dwindling fuel wood sources and other environmental problems associated with fuel demand for cooking. The use of solar cookers resulted in appreciable fuel and time savings as well as increased energy security for households using commercial fuels [2].

In [3], a one year comparative field test of seven different types of solar cookers involving 66 families in 3 study areas in South Africa has been conducted. Overall, families use solar cookers on 38% of all days and for 35%

of all cooked meals; they express clear preferences for certain cooker types. Solar cookers, together with wood (stoves and open fires, used on 42% of all days), are the cooking appliances most used. Fuel consumption measurements show overall fuel savings of 38% resulting in estimated pay – back periods (through monetary fuel savings) from 8 months onwards, depending on the type and region.

Solar cooking in boarding schools and communal centers in isolated areas demands the heating of large quantities of food. In [4], 3 different kinds of absorbers were presented. They were optimized to fulfill different functions in a concentrator of an area of 2 m<sup>2</sup>. These alternatives allow the possibility of satisfying the needs of a communal dining center, cooking for up to 30 children, once each concentrator has been installed.

In [5] and [6], the policy formulation for cooking energy substitution by renewable energy is addressed in multi – criteria context. A survey is conducted to know the perceptions of different decision making groups on present dissemination of various cooking energy alternatives in India. Nine cooking energy alternatives are evaluated on 30 different criteria comprising of technical, economic, environmental, social, behavioral and commercial issues. It is found that liquefied petroleum gas stove is the most preferred device, followed by kerosene stove, solar box cooker (SBC) and parabolic solar cooker (PSC).

In [7], the simply designed the low cost parabolic type solar cooker was made and tested. The energy and exergy

\* Corresponding author. akayleh\_em@yahoo.com

efficiencies of the cooker were experimentally evaluated. The energy output of the SPC varied between 20.9 and 78.1 W, whereas its exergy output was in the range 2.9 – 6.6 W. It is found that the energy and exergy efficiencies of the SPC were in the range of 2.8 – 15.7 and 0.4 – 1.25 respectively.

In [8], for the first time, the SPC of the cylindrical trough shape is analyzed from the exergy viewpoint. Equations for heat transfer between the three surfaces: cooking pot, reflector and imagined surface making up the system, were derived. The exergy efficiency of the SPC was found to be relatively very low (~1%), and to be about 10 times smaller than the respective energy efficiency which is in agreement with experimental data.

In [9], a fresnel type domestic concentrating cooker was designed. The cooker has an aperture area of 1.5 m<sup>2</sup> and a focal length of 0.75 m. It was found to provide an adequate temperature needed for cooking, frying and preparation of chapattis.

The majority of researchers used box type cooker in their works [10-22]. In [10], a transient mathematical model is presented for a box – type solar cooker with one step outer reflector hinged at the top of the cooker. To validate the model, the temperature distribution obtained by computer simulation is compared with experimental results. Good agreement between experimental and theoretical results is observed.

In [11], the performance of a box – type solar cooker with auxiliary heating was studied and analyzed. This is done with the help of a built – in heating coil inside the cooker or a retrofit electric bulb in a black painted cylinder. It is found that the use of auxiliary sources allows cooking on most cloudy days.

In [12], a simple mathematical model is presented for a box – type solar cooker with outer – inner reflectors. The cooker performance is investigated by computer simulation in terms of the cooker efficiency as well as characteristics and specific boiling items. The overall utilization efficiency of the cooker is 31%.

In [13], the thermal analysis of a hot box solar cooker which is manufactured in Istanbul Technical University has been done using the fourth order Ronge – Kutta method. The results obtained have been given comparatively with the experimental results measured from the cooker.

In [14] a model to predict the cooking power of a solar cooker based on three controlled parameters (solar intercept area, overall heat loss coefficient and absorber plate thermal conductivity) and three uncontrolled variables (insulation, temperature difference and load distribution) is presented. The model was validated for commercially available solar cookers of both the box and concentrating types.

In [15], a simple wooden hot box with one reflector solar cooker was designed, fabricated and tested. Maximum inner temperature reached 160°C under field conditions of Giza, Egypt.

In [16], a series of tests were carried out during nine days to make comparison of the Sudanese box – type solar cooker against the other Indian designs. Sudanese solar box cooker showed better thermal performance. Using internal, external reflectors and sloping of the top cover added significantly to the thermal performance indicated

by the amount of heat absorbed and hence the achieved plate temperature.

In [17], a method is outlined to find out a reflector performance factor and an orientation factor that depend upon the elevation angle of the sun, the solar surface azimuth angle and the reflector tilt. The analysis is applied to a cooker placed at Aden in Yemen. The results indicate that with proper cooker orientation. The improvement in the performance of the cooker due to the reflector reached during winter is more than 100% at lower elevation angles and is more than 60% at higher elevation angles.

In [18], the influences that govern solar box cookers: HS7534, HS7033 and the newest design HS5521 were described. Its volume is only 35% of the volume of HS7033 and cheaper. The performance comparison of the last two solar cookers is described based on the data collected during testing with and without load.

In [19], the design philosophy, construction and measured performances of a plane – reflector augmented box – type solar energy cooker are presented. The experimental solar cooker consists of an aluminum plate absorber painted with black matt and a double glazed lid. Predicted water boiling times using the two figures of merit compared favorably with the measured values. The performance of the cooker with the plane reflector in place was improved tremendously compared to that without the reflector in place.

In [20], a hot box solar cooker with used engine oil as a storage material has been designed, fabricated and tested so that cooking can be performed even in the late evening. The performance and testing of a storage solar cooker was investigated by measuring stagnation temperatures and conducting cooking trials. The efficiency of the hot box storage solar cooker was found to be 27.5%.

In [21], the top heat losses that constitute the major losses from the box type solar cooker have a strong influence on the thermal performance. To predict or evaluate the thermal performance of a cooker, the top heat loss coefficient  $U_{tw}$  for a water loaded cooker should be known. The conducted investigations reveal that the pot water requires less time to reach a certain temperature with an increase in solar radiation level, while, as expected, it takes longer time with higher values of load of water in the pots. However, the effect of wind speed on the time required for certain rise in pot water temperature is marginal.

In [22], the performance of conventional box type solar cookers can be improved by better designs of cooking vessels with proper understanding of the heat flow to the material to be cooked. An attempt was made to arrive at a mathematical model to understand the heat flow process to the cooking vessel and thereby to the food to be cooked. The mathematical model considers a double glazed hot box type solar cooker loaded with two different types of vessels, kept either on the floor of the cooker or on lugs. It is found from the experiments and the modeling that the cooking vessel with a central cylindrical cavity lugs results in higher temperature of the thermal fluid than that of a conventional vessel on the floor or on lugs.

In [23], a box type solar cooker with one or four cooking pots was constructed and tested in Tatna (Egypt) prevailing weather conditions. Experiments were performed during July 2002 using the cooker with or

without load. The suggested cooker is able to cook most kinds of food with an overall utilization efficiency of 26.7%.

In [24], a novel design of solar cooker is introduced in which the absorber is exposed to solar radiation from the top and bottom sides. A set of plane diffuse reflections is used to direct the radiation onto lower side of the absorber plate. The performance of the new cooker and the conventional box type solar cooker is investigated. Results under the same operating conditions show that the absorbers of the box type solar cooker and the double exposure cooker attain 140°C and 165°C respectively.

In [25], the thermal performance of a prototype solar cooker based on an evacuated tube solar collector with phase change material (PCM) storage unit is investigated. Cooking experiments with PCM storage processes were carried out simultaneously. The cooker performance under a variety of operating and climatic conditions was studied at Mie, Japan.

In [26], the concept of conical focus is revealed and the design of a solar cooker is explained. The cooker was practically tested for grilling both white and red meat in a record time. A method for obtaining real boiling of water (100°C) using a solar heater is described.

In [27], the role of the vessel inside the solar cooker was discussed. Raising the vessel by providing few lugs will make the bottom of the vessel a heat transfer surface. This change improves the performance of the system by improving the heat transfer rates in booth heating and cooling modes.

All types of concentrating solar cookers were found to provide adequate temperatures needed for cooking, frying and preparation of chapattis. But the common problem of all concentrating cookers with manual tracking, like the need for frequent tracking, and standing in the sun. This problem could be tackled if one goes in for automatic sun tracking [9, 28, 29].

In this work cylindrical solar cooker with two axes, sun tracking, PLC controlled system was designed and constructed. The system was characterized by a fairly simple electromechanical setup. This reduces cost, maintenance and the possibility of failure.

## 2. Mechanical Design of Cylindrical Solar Cooker.

The amount of power produced by a solar system depends upon the amount of sun light to which it is exposed. As suns position changes throughout the day, the solar system must be adjusted so that it is always aimed precisely at the sun, as a result, produces the maximum possible power. Single axis tracking systems are considerably cheaper and easier to construct, but their efficiency is lower than that of two axes sun tracking systems. On the other hand, some solar systems require only two axis tracking [30,31,32].

Fig.1 and fig. 2 show front view and side view of schematic diagram for a proposed solar cooker. Cylindrical solar cooker consist of half cylinder made of steel. In inner side of half cylinder small mirrors with a dimension of 6cm \* 6cm are distributed and stucked by a silicon material. A blackened steel tube with 10cm diameter was

replaced on the focus line in the half cylinder. The mirrors inside the half cylinder reflect and concentrate the sunlight on a tube.

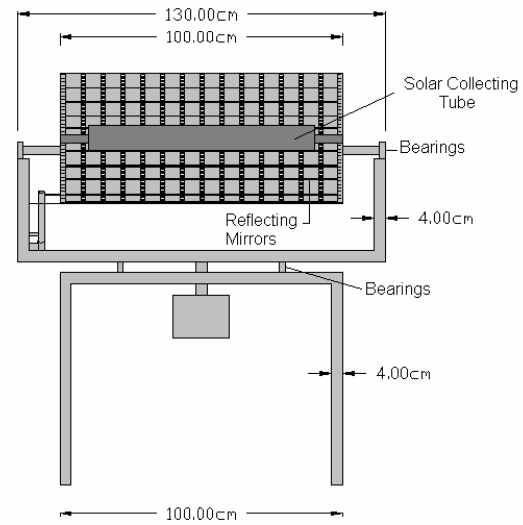


Fig.1 Cylindrical Solar Cooker Front View

This cooker works as follows: The liquid is poured through an opening into the cylindrical tube, where it is cooked there for a suitable time. When the cooking is done, the same opening is used to let the food out. When dirty, the tube can be easily removed for cleaning.

The drive motor M1 for tracking around vertical axes was designed to track the slope angle  $\beta$ , which is the angle between the plane of the surface in question and the horizontal. The drive motor M2 was designed to track the surface azimuth angle  $\gamma$ , which is the deviation of projection of normal to the collecting surface on the horizontal surface to the north south axis. The positions of tracking motors M1 and M2 are shown in fig.1 and fig.2

In this mechanical design four principles were used:

1. Concentrating sunlight into a small area
2. Converting the light to heat where a blackened tube will absorb almost all of the sunlight and turn it into heat.
3. Trapping heat by using plastic bag to cover the half cylinder with blackened tube
4. Tracking the sun disk by means of tracking motors M1 and M2.

## 3. Electromechanical System Description:

The electromechanical system consists of two drivers , the first for the joint rotating about the vertical axis to track the solar azimuth angle  $\gamma_s$  and the second one for the joint rotating about the horizontal axis to track the zenith angle  $\theta_z$  as shown in figure 3.

The system has two bridge rectifiers, the first one PS1 that converts the 220 VAC of the supply network into 24 VDC to power the PLC, and the second rectifier PS2 which converts 220 VAC of supply network into 24 VDC to provide the electrical motor M2 with 24 VDC. FI is a frequency inverter which is used to provide the electrical motor M1 with controlled voltage and frequency. The FI is used as an electrical gear to reduce the speed of M1 to the suitable value (33,34 & 35).

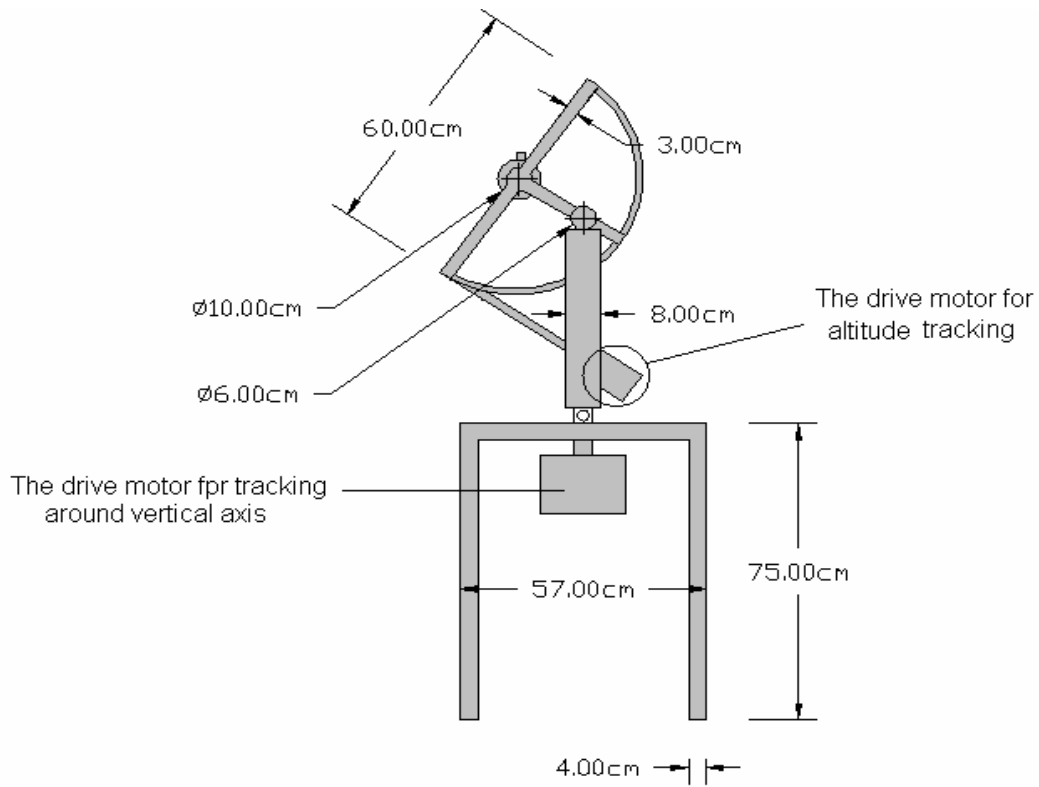


Fig.2 Cylindrical Solar Cooker Side View

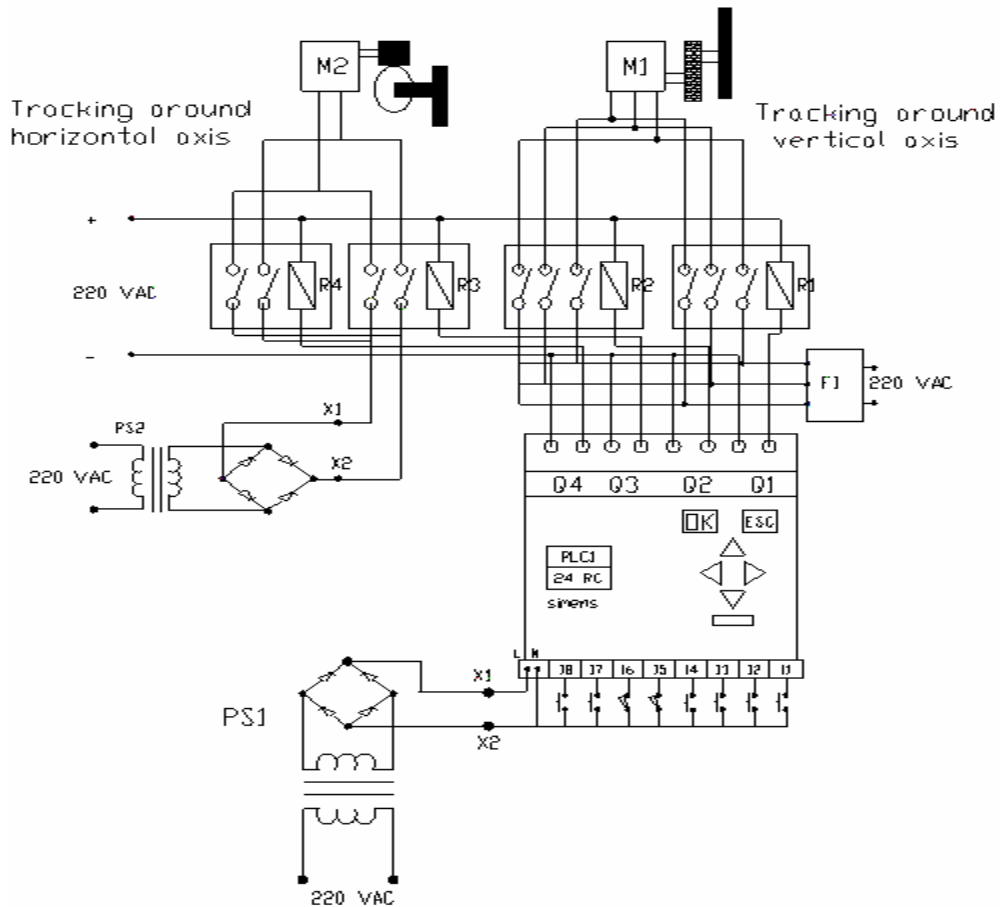


Fig3. The electromechanical circuit for driving of two motors

The PLC has eight inputs, and they are used as the following:

- I1-Push button to start automatic mode of tracking
- I2 -Push button to stop tracking
- I3-Switch for manual operation of tracking in the forward direction for vertical motor M1. It is used to adjust the system.
- I4-Switch for manual operation of tracking in the backward direction for vertical motor M1. It is used to adjust the system.
- I5-Limit switch, it is used to backward the system to start position (zero position) for vertical motor M1.
- I6-Limit switch, it is used to stop the vertical motor M1 at start position
- I7-Switch for manual operation of tracking in the forward direction for horizontal motor M2. It is used to adjust the system.
- I8-Switch for manual operation of tracking in the backward direction for horizontal motor M2. It is used to adjust the system.

Also the PLC has four outputs, and four outputs were used, these are as following:

- Q1-It represents the forward direction of motion through the relay R1 for motor M1 of tracking around vertical axis.
- Q2-It represents the backward direction of motion through the relay R2 for motor M1 of tracking around vertical axis.
- Q3-It represents the forward direction of motion through the relay R3 for motor M2 of tracking around the horizontal axis.
- Q4-It represents the backward direction of motion through the relay R4 for motor M2 of tracking around the horizontal axis.

**4. Programming of The Control System**

The optimal spherical solar cooker positions can be defined by two angles,  $\beta$  &  $\gamma$ , as shown in [36].  $\beta$  is the slope of surface, and  $\gamma$  is the surface azimuth angle. For two axes tracking, the cooker positions are determined as follows:

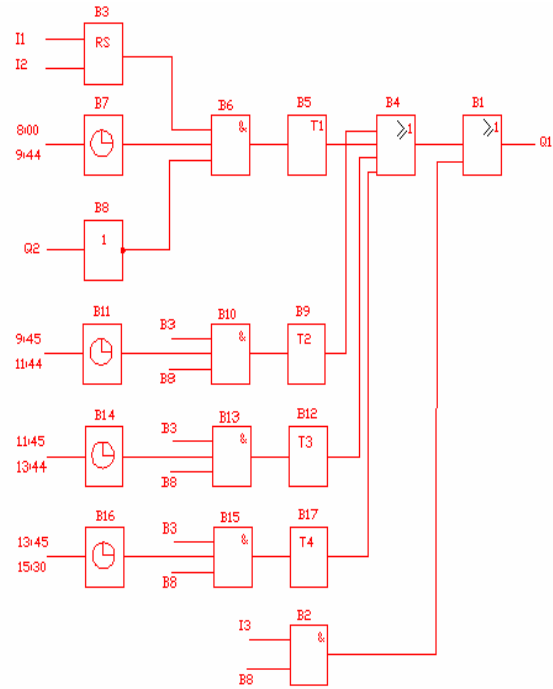
$$\beta = \theta_z \text{ and } \gamma = \gamma_s. \tag{1}$$

Calculations have been done to determine the different solar angles for Amman that are required in this work. This allowed the calculation of the optimal position of tracking surface during the daylight hours. The daylight hours were divided into 4 identical time intervals T1, T2, T3 and T4, during which the motor speeds (deg/s) were determined. Then the PLC programming was done based on the solar angles analysis and motor speed calculations. The PLC controls the intermittent position adjustments made by the motors. This means that the motor for tracking around the horizontal axis will be idle for 10-20 minutes according to the different intervals of time mentioned and works only for a few seconds, the motor for vertical tracking will be idle for 15-35 minutes and works for a few seconds. The LOGO 24 RC PLC system which uses the functional diagram language of programming is used to control the motors operation in this work [37, 38, 39].

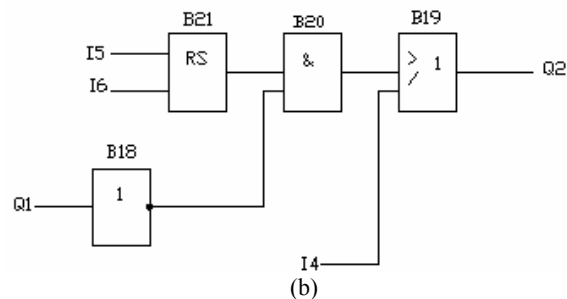
The PLC program of the system driving the vertical tracking motor is represented in fig (4). The program consists of two parts related to the two types of motion, forward and backward. From the theoretical calculated

results of the solar azimuth angle  $\gamma_s$ , it is deduced the forward motion will cover all the intervals of time T1, T2, T3 and T4. The blocks B7, B11, B14, and B16 are clocks that represent the four above mentioned intervals of time. The clocks actuate the recycles B5 B9, B12, and B17, which represent on – off timers. The clocks must be adjusted to the calculated positions function of time. The block B19 will operate the vertical tracking motor in the backward direction after sunset.

**A) Forward Direction**



(a)



(b)

Fig 4. The functional PLC program for the plane rotated about the vertical axis, (a) Forward Direction, (b) Backward Direction.

The PLC program of the system driving the slope angle tracking motor is represented in fig.5. The program consists of two parts also according to the motion, up and down direction. From the theoretical calculated angles values, it is noted that  $\beta$  (slope) decreases from its maximum at sunrise until it reaches its minimum at noon. This represents the up direction motion, which covers the intervals of time T1 and T2. The down direction motion occurs from noon till sunset where  $\beta$  is a maximum. This period of time will cover the intervals T3 and T4.

The blocks B25, B30, B34, and B39 are clocks that represent the four above mentioned intervals of time. The clocks actuate the recycles B23, B28, B32 and B37, which represents on-off timers. The clocks must be adjusted to the calculated position as a function of time.

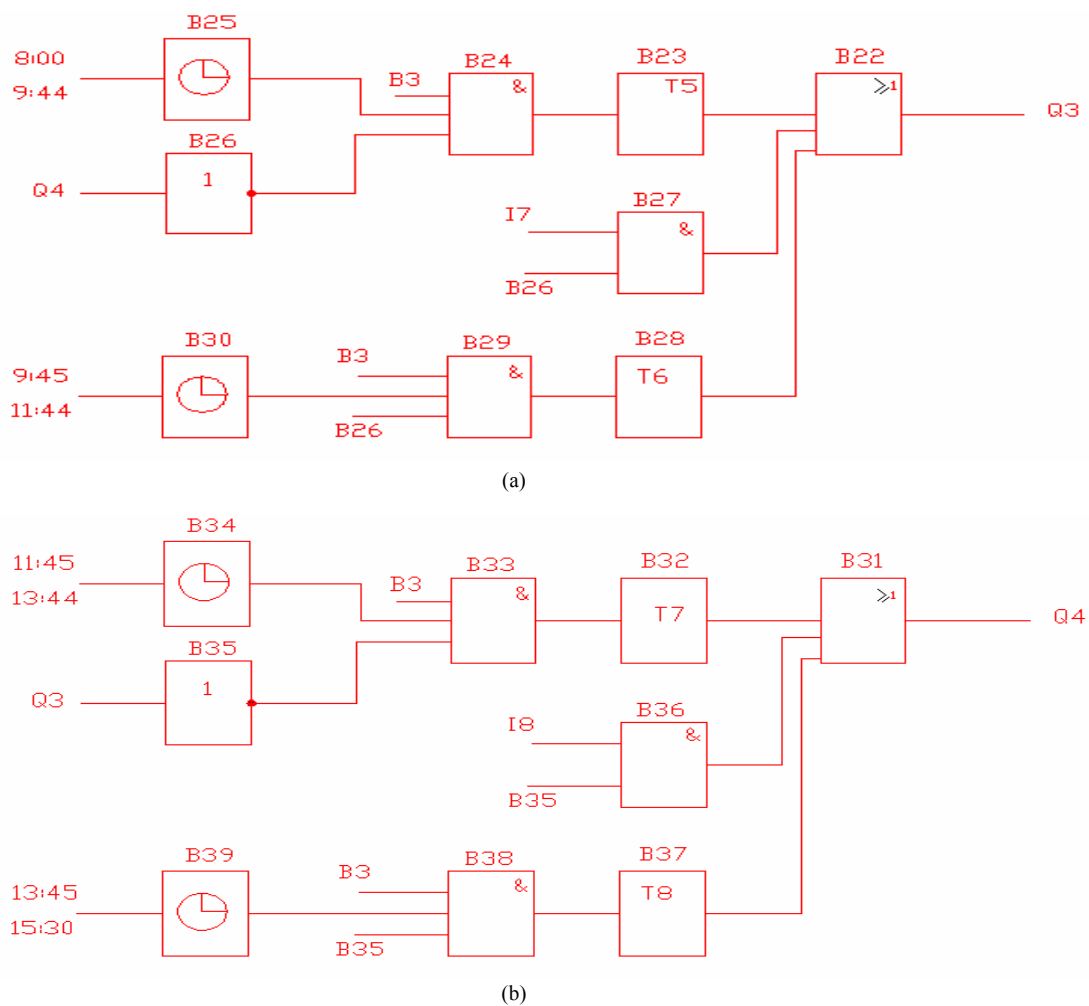


Fig5. The functional PLC program for the tracking of slope angle, (a) Up Direction , (b) Down Direction.

## 5. Experimentation and Results.

Experiments done on the cylindrical solar cooker with two axes sun tracking system were carried out on three days; 24/5/2008, 12/6/2008 and 16/8/2008. The experimental work was fully carried out in the renewable energy laboratory at the Applied Science University, in Amman- Jordan. Each experiment started from 8:30

morning to 4:30 afternoon. The measuring electronic parts were tested and calibrated before being used on the various tests. The global solar radiation on a horizontal surface was measured using Kipp and Zonen pyranometer. Calibrated thermocouples (type – K) coupled to digital thermometer are used to measure the temperature. Fig(6) shows different views of the designed and tested system.

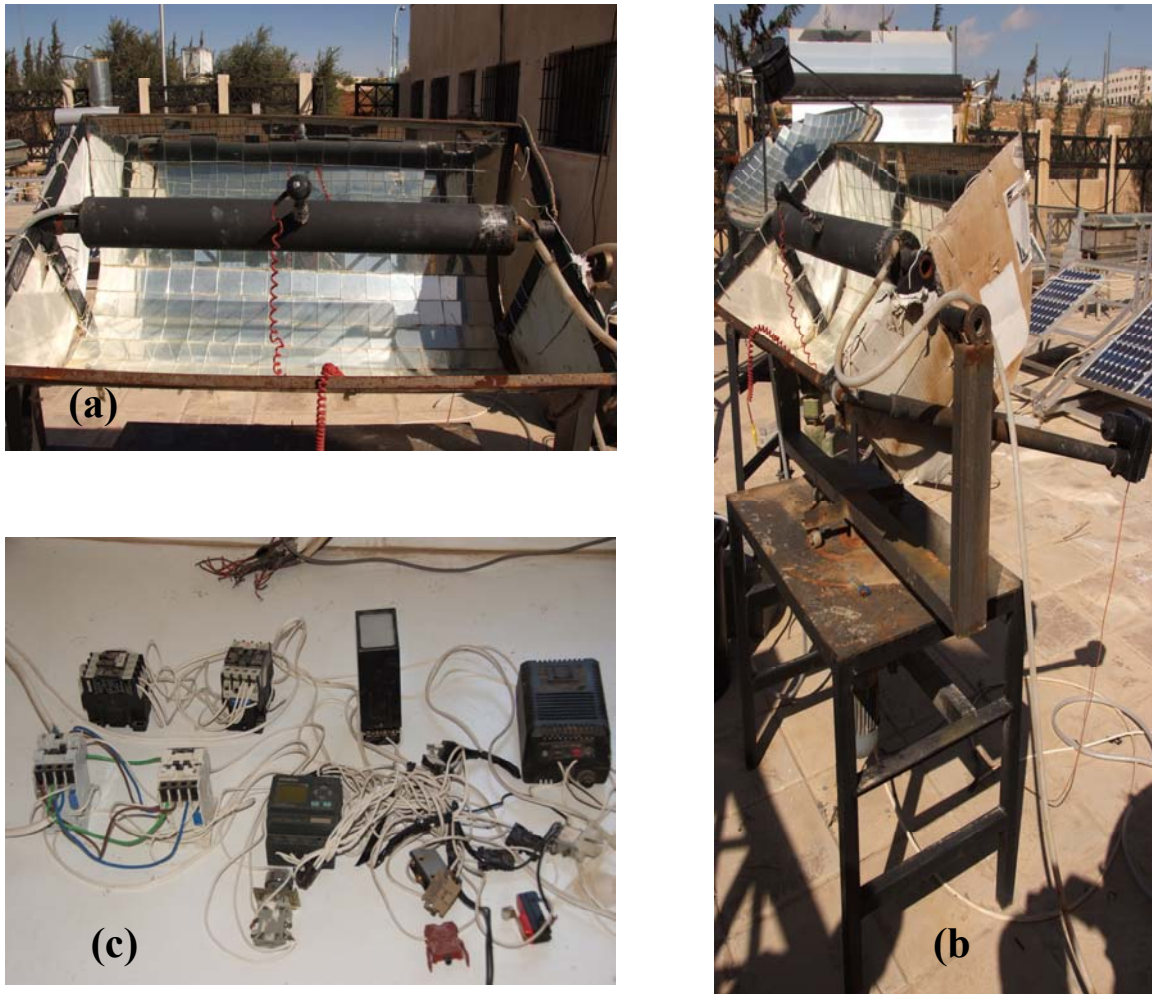


Figure 6. (a) Front view of cylindrical solar cooker .(b) Side view of cylindrical solar cooker with mechanical base and driving motors. (c) The hardware components of the control circuit.

Fig.7 and fig.8 show the variation in ambient temperature and the variation in the solar intensity through three summer days.

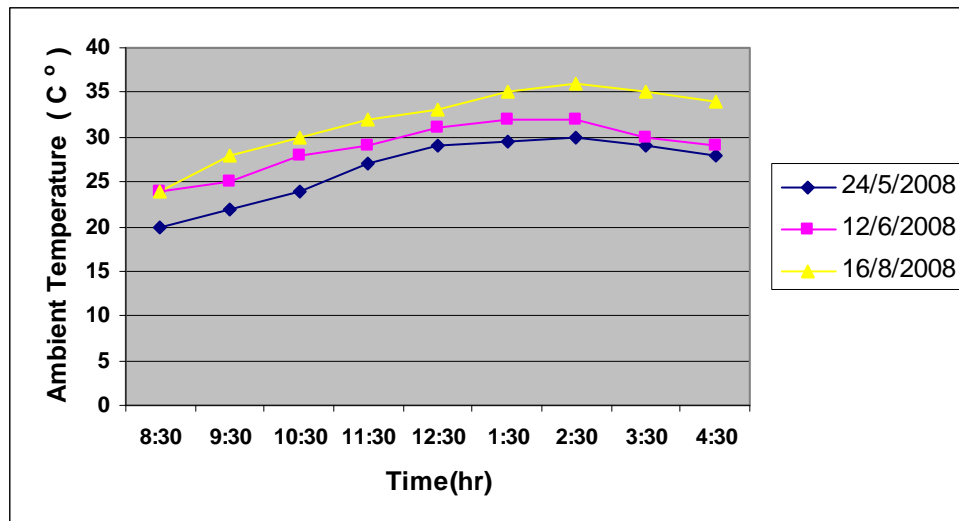


Fig.7 The Ambient Temperature variation function of time

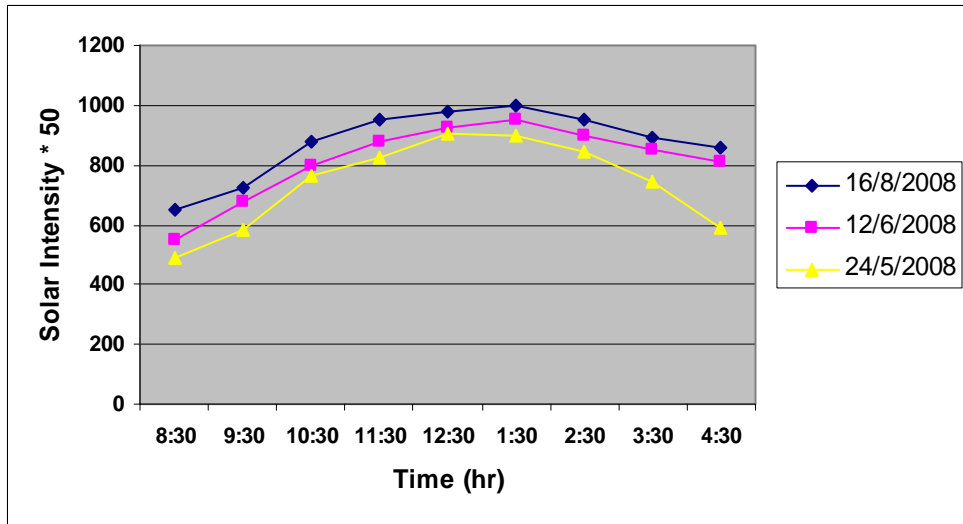


Fig.8 The Solar Intensity variation function of time

Fig.9 and fig.10 show the variation in water temperature function of time inside the collecting tube and the variation of the tube surface temperature function of time. the figures show an increase in the water temperature during early hours of the day until it reaches the maximum values around noon correspondingly to the highest solar radiation and then decreases due sunset.

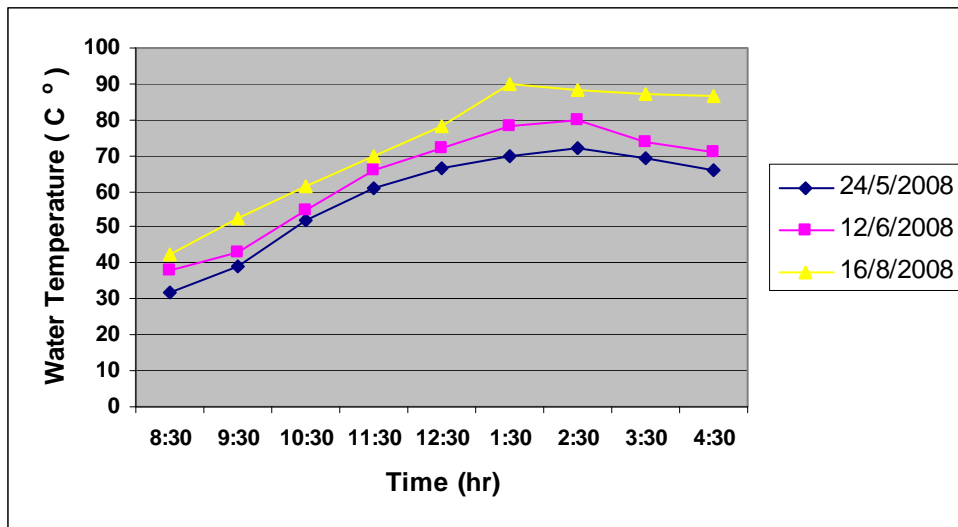


Fig.9 The Water Temperature variation function of time

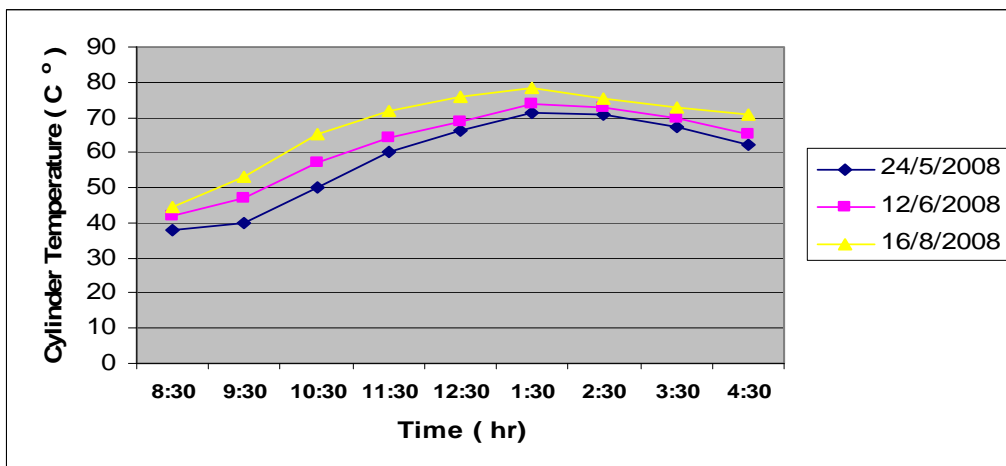


Fig.10 The Outside tube Temperature variation function of time

From the curve of water temperature variation function of time it is seen that the water temperature inside tube reached 90 °C in normally summer days, where the maximum ambient temperature registered 36 °C. This shows that water temperature inside tube could still reach further higher rates on hotter days. It is noticed after studying all the curves, that the water temperature inside tube increases when the ambient temperature is hotter or where the solar intensity is prevalent.

When using this system for cooking or simply heating water, the latitude of location, season, and wind speed and weather conditions as cloudy days or dusty days should be considered. It should be remembered that food containing moisture cannot get much hotter 100 °C in any case, so it is not necessary to cook at the high temperature indicated in standard cookbooks. Because the food does not reach too high temperature, it can be safely left in the cooker all day without burning. This type of cookers can be used to warm food, drinks and can also be used to pasteurize water or milk.

## 6. Conclusion

In this work a cylindrical solar cooker with two axes sun tracking system was designed, constructed and operated. Mechanical system; which consists of two parts, one for altitude tracking and another for rotating around vertical axes was designed and constructed. The hardware and software components of the two axis sun tracking system were designed. The programming method of control with open loop system was employed. The programmable logic controller was used to control the motion of surface on which the solar cooker was mounted. A continuous test during different days in the year 2008 from 8:30 am to 4:30 pm was performed. The test showed that the using of cylindrical solar cooker system with two axes tracking can increase water temperature up to 90 °C.

## Acknowledgments

The authors express their gratitude to Eng. Dana Salameh, The supervisor of the Automation Laboratory in the Applied Science University for writing assistance during preparing of this work.

## References

- [1] O. Badran, Study in industrial applications of solar energy and the range of its utilization in Jordan. *Renewable Energy*, 24, 2001, 485-490.
- [2] M. Wentzel and A. Pouris, The development impact of solar cookers: A review of solar cooking impact research in South Africa. *Energy Policy*, 35, 2007, 1909-1919.
- [3] E. Biermann, M. Grupp and R. Palmer, Solar cooker acceptance in South Africa: Results of a comparative field test. *Solar Energy*, 66, 1999, 401-407.
- [4] J. Franco, C. Cadena and L. Saravia, Multiple use communal solar cookers. *Solar Energy*, 77, 2004, 217-223.
- [5] S. Pohekar and M. Ramachandran, Multi criteria evaluation of cooking energy alternatives for promoting parabolic solar cooker in India. *Renewable Energy* 22, 2004, 1449-1460.
- [6] S. Pohekar and M. Ramachandran, Multi criteria evaluation of cooking devices with special reference to utility of parabolic solar cooker in India, *Energy* 31, 2006, 1215-1227.
- [7] H. Ozturk, Experimental determination of energy and exergy efficiency of the solar parabolic cooker. *Solar Energy* 77, 2004, 67-71.
- [8] R. Petela, Exergy analysis of the solar cylindrical parabolic cooker. *Solar Energy* 79, 2005, 221-233.
- [9] Sonune and S. Philip, Development of a domestic concentrating cooker. *Renewable Energy* 28, 2003, 1225-1234.
- [10] El-Sebal and S. Aboul-Enein, A box type solar cooker with one stop outer reflector. *Energy* 22, 1997, 515-524.
- [11] M. Hussain, K. Das and A. Huda, The performance of a box type solar cooker with auxiliary heating. *Renewable Energy* 12, 1997, 151-155.
- [12] El-Sebal, Thermal performance of a box type solar cooker with outer – inner reflectors. *Energy* 22, 1997, 969-978.
- [13] Binark and N. Turkmen, Modeling of a hot box solar cooker. *Energy Conversion and Management* 37, 1996, 303-310.
- [14] P. Funk and D. Larson, Parametric model of solar cooker performance, *Solar Energy* 62, 1997, 63-68.
- [15] M. Mohammad, H. El-Ghetany and A. Abdel Dayem, Design, construction and field test of hot box solar cookers for African Sahel region, *Renewable Energy* 14, 1998, 49-54.
- [16] Mohammad Ali, Design and testing of Sudanese solar box cooker. *Renewable Energy* 21, 2000, 573-581.
- [17] Algifri and H. Al-Towaie, Efficient orientation impacts of box type solar cooker on the cooker performance. *Solar Energy* 70, 2001, 165-170.
- [18] H. Suharta, A. Sayigh, K. Abdullah and K. Mathew, The comparison of three types of Indonesian solar box cookers. *Renewable Energy* 22, 2001, 379-387.
- [19] O. Ekechukwu and N. Ugwuoke, Design and measured performance of a plane reflector augmented box type solar energy cooker, *Renewable Energy* 28, 2003, 1935-1952.
- [20] N. Nahar, Performance and testing of a hot box storage solar cooker. *Energy Conversion and Management* 44, 2003, 1323-1331.
- [21] S. Kumar, Thermal performance study of box type solar cooker from heating characteristic curves. *Energy Conversion and Management* 45, 2004, 127-139.
- [22] Reddy and A. Rao, Prediction and experimental verification of performance of box type solar cooker – Part I. Cooking vessel with central cylindrical cavity, *Energy Conversion and Management* 48, 2007, 2034-2043.
- [23] El-Sebaili and A. Ibrahim, Experimental testing of a box type solar cooker using the standard procedure of cooking power, *Renewable Energy* 30, 2005, 1861-1871.
- [24] E. Amer, Theoretical and experimental assessment of a double exposure solar cooker, *Energy Conversion and Management* 44, 2003, 2651-2663.
- [25] S. Sharma, T. Iwata, H. Kitam and K. Sagara, Thermal performance of a solar cooker based on an evacuated tube solar collector with a PCM storage unit, *Solar Energy* 78, 2005, 416-426.
- [26] E. Sharaf, A new design for an economical, highly efficient, conical solar cooker, *Renewable Energy* 27, 2002, 599-619.
- [27] Narasimha Rao, S. Subramanyam, Solar cookers – Part I: cooking vessel on lugs, *Solar Energy* 75, 2003, 181-185.

- [28] S. Abdallah, O. Badran., Sun tracking system for productivity enhancement of solar still. *Desalination*, 220, 2008, 669-676.
- [29] S. Abdallah., The effect of using sun tracking systems on the voltage-current characteristics and power generation of flat plate photovoltaics. *Energy Conversion & Management*, 45, 2004, 1671-1679.
- [30] Barakat, B., Rahab H, Mohmedi B and Naiit N, Design of a tracking system to be used with photovoltaic panels. *Proceedings of the Fourth Jordanian International Mechanical Engineering Conference JIMEC* , 2001, 471-488.
- [31] Neville RC., Solar energy collector orientation and tracking mode, *Solar Energy* 20, 1978, 7-11.
- [32] Khalifa AN, Al-Mutwalli SS., Effect of two axis sun tracking on the performance of compound parabolic concentrators, *Energy Conversion and Management* 10, 1998, 1073-1079.
- [33] Hession PJ., Bonwick WJ., Experience with a sun tracker system, *Solar Energy* 32, 1984, 3-11.
- [34] Baltas P., Tortoreli M., Russel P. Evaluation of power output for fixed and step tracking photovoltaic arrays, *Solar Energy* 37, 2, , 1986, 147-163.
- [35] Brunotte M., Goetzberger A., Blieske U., Two stage concentrator permitting concentration factors up to 300X with one axis tracking, *Solar Energy* 56, 3, , 1996, 285-300.
- [36] Duffie J., Beckman W., *Solar engineering of thermal processes*, 2<sup>nd</sup> ed. USA: John Wiley & Sons; 1991.
- [37] A. Al-Mohamad., Efficiency improvement of photovoltaic panels using a sun tracking system. *Applied Energy*, 79, 2004, 345-354.
- [38] Abdallah S., Nijmeh S., Design, construction and operation of one axis sun tracking system with PLC control. *Jordan J Appl Sci Univer*, 4, 2, , 2002, 45-53.
- [39] Abdallah S., Nijmeh S., Two axes sun tracking system with PLC control. *Energy Conversion & Management*, 45, 2004, 1931-1939.

# Mathematical Modeling and Performance Optimization for the Paper Making System of a Paper Plant

Rajiv Khanduja<sup>a,\*</sup>, P.C. Tewari<sup>b</sup>, R.S.Chauhan<sup>c</sup>, Dinesh Kumar<sup>d</sup>

<sup>a</sup> Department of Mechanical Engineering, SKIET, Kurukshetra-136118, Haryana, India.

<sup>b</sup> Department of Mechanical Engineering, NIT, Kurukshetra-136119, Haryana, India.

<sup>c</sup> Department of Electronic and Communication Engineering, JMIT, Radaur, Yamuna Nagar-135133, Haryana, India.

<sup>d</sup> Department of Mechanical & Industrial Engineering, Indian Institute of Technology, Roorkee, Utranchal-247667, India.

## Abstract

This paper deals with the mathematical modeling and performance optimization for the paper making system in a paper plant using Genetic Algorithm. The paper making system of a paper plant has four main subsystems, arranged in series and parallel. Considering exponential distribution for the probable failures and repairs, the mathematical formulation of the problem is done using probabilistic approach and differential equations are developed based on Markov birth-death process. These equations are then solved using normalizing conditions to determine the steady state availability of the paper making system. The performance of each subsystem of the paper making system in a paper plant has also been optimized using Genetic Algorithm. Therefore, the findings of the present paper will be highly useful to the plant management for the timely execution of proper maintenance decisions and hence to enhance the system performance.

© 2010 Jordan Journal of Mechanical and Industrial Engineering. All rights reserved

Keywords: Performance Optimization, Paper Making System, Genetic Algorithm.

## 1. Introduction

The paper industry comprises of large complex engineering systems arranged in series, parallel or a combination of both the configurations. Some of these systems are chipping, cooking, washing, bleaching, screening, stock preparation and paper making. These systems are normally arranged in hybrid configuration. The important process of a paper industry, upon which the quality of paper depends, is the paper making process. In the process of paper formation, the chips from storage are fed in to a digester to form the pulp, which is processed through various subsystems called knotter, decker, opener and washing. Then the washed pulp is bleached to get chlorine free white pulp, which is further passed through screen and cleaner to separate out oversize and odd shape particles. After that, the stock of the pulp is prepared with the addition of chemicals and fillers to change the paper properties and is stored in the tank. The pulp from the storage tank, with the help of pump, is fed to head stock of the paper making machine to adjust the thickness of the paper. The pulp runs over a wire mat running on rollers, and water from the pulp is sucked through vacuum pumps arranged in parallel. The wet paper passes through the heated rollers together with a synthetic belt (the press

section) and is dried in drier section in two stages. The dried paper is finally rolled on a pope reel. The schematic flow diagram of paper making system is shown in figure 1

### 1.1. Literature Review

The available literature reflects that several approaches have been used to analyze the steady state behavior of various systems. Dhillon et al. [1] have frequently used the Markovian approach for the availability analysis, using exponential distribution for failure and repair times. Kumar et al. [2, 3, and 4] dealt with reliability, availability and operational behavior analysis for different systems in the paper plant. Srinath [5] has explained a Markov model to determine the availability expression for a simple system consisting of only one component Gupta et al. [6] have evaluated the reliability parameters of butter manufacturing system in a dairy plant considering exponentially distributed failure rates of various components. The reliability of the system is determined by forming the differential equations with the help of transition diagram using Markovian approach and then solving these differential equations with the help of fourth order Runge-Kutta method. They applied the recursive method for calculating long run availability and MTBF using numerical technique. Sunand et al. [7] dealt with maintenance management for ammonia synthesis system in fertilizer plant. Shooman [8] suggested different methods for the reliability computations of systems with dependent failures. Tewari et al. [9, 10] dealt with the determination of availability for the systems with elements

\* Corresponding author. rajiv\_khanduja@rediffmail.com

exhibiting independent failures and repairs or the operation with standby elements for sugar industry. They also dealt with mathematical modeling and behavioral analysis for a refining system of a sugar industry using Genetic Algorithm. Sunand et al. [11] discussed simulated availability of CO<sub>2</sub> cooling system in a fertilizer plant. Rajiv et al. [12, 13] have developed decision support system for stock preparation system of paper plant. They also dealt with availability of bleaching system of paper plant. Kalyanmoy Deb [14] has explained the optimization techniques and how they can be used in the engineering problems. Goldberg [15] made a systematic study on G.A. mechanism, and identified three basic operators: reproduction, crossover and mutation. So that the G.A. has higher opportunity for obtaining near optimal solutions. Castro and Cavalca [16] presented an availability optimization problem of an engineering system assembled in series configuration which has the redundancy of units and teams of maintenance as optimization parameters. Genetic Algorithm was used to reach the objective of availability, considering installation and maintenance costs. Chales and Kondo [17] tackled a multi objective combinatorial optimization problem. They used Genetic Algorithm to optimize the availability and cost of a series and parallel repairable system. Ying-Shen Juang et al. [18] proposed a genetic algorithm based optimization model to optimize the availability for a series parallel system. The objective is to determine the most economical policy of component's mean time between failure (MTBF) and mean time to repair (MTTR).

## 2. System Description

The paper making system comprises of four main subsystems, which are as follows:

1. Subsystem G<sub>1</sub>: This subsystem consists of a wire mat units in series used for depositing the suspended fiber on the top of wire mash (water from pulp is sucked by vacuum pumps). It also controls the width of paper sheet produced. Its failure causes complete failure of system.
2. Subsystem G<sub>2</sub>: This subsystem consists of one synthetic belt units to supports the fiber running through press and dryer sections. Its failure causes complete failure of system.
3. Subsystem G<sub>3</sub>: This subsystem consists of a number of rollers in series to help the wire mat and synthetic belt to roll on them smoothly. Failure of anyone of these will cause complete system failure.
4. Subsystem G<sub>4</sub>: This subsystem consists of six vacuum pumps in parallel used for sucking water from pulp through wire mat. Four pumps remain operating at a time, while remaining two pumps are in standby. Complete failure of the system takes place only when more than two pumps fail at a time

This system is associated with a common steam supply and failure in this supply needs emergency attention. Failure in steam supply affects the subsystems (which are in good condition otherwise), resulting in further delay in operation of the system.  $\lambda_{32}$  and  $\mu_{32}$  are the failure and repair rates for this special failure.

## 3. ASSUMPTIONS AND NOTATIONS

The transition diagram (figure-2) of paper making system shows the two states, the system can acquire i.e. full working and failed state. Based on the transition diagram, a performance-evaluating model has been developed. The following assumptions and notations are addressed in developing the probabilistic models for paper making system of the paper plant concerned:

### Assumptions

1. Failure/repair rates are constant over time and statistically independent.
2. A repaired unit is as good as new, performance wise for a specified duration.
3. Sufficient repair facilities are provided, i.e. no waiting time to start the repairs.
4. Standby units (if any) are of the same nature and capacity as the active units.
5. System failure /repair follow exponential distribution.
6. Service includes repair and /or replacement.
7. System may work at a reduced capacity / efficiency.
8. There are no simultaneous failures among system. However, simultaneous failure may occur among various subsystems in a system.

### Notations

The following notations are addressed for the purpose of mathematical analysis of the paper making system:

- G<sub>1</sub>, G<sub>2</sub>, G<sub>3</sub>, G<sub>4</sub> : Represent good working states of respective wire mat, synthetic belt, roller, vacuum pump.
- g<sub>1</sub>, g<sub>2</sub>, g<sub>3</sub>, g<sub>4</sub> : Represent failed states of respective wire mat, synthetic belt, roller, vacuum pump.
- $\lambda_{28}, \lambda_{29}, \lambda_{30}, \lambda_{31}$  : Respective mean constant failure rates of G<sub>1</sub>, G<sub>2</sub>, G<sub>3</sub>, G<sub>4</sub> .
- $\mu_{28}, \mu_{29}, \mu_{30}, \mu_{31}$  : Respective mean constant repair rates of g<sub>1</sub>, g<sub>2</sub>, g<sub>3</sub>, g<sub>4</sub>.
- $\lambda_{32}$  : Failure rate of steam supply
- $\mu_{32}$  : Repair rate of steam supply
- P<sub>0</sub>(t) : State probability that the system is working at full capacity at time t.
- P<sub>i</sub>(t) : State probability that the system is in the i<sup>th</sup> state at time t.
- P<sub>i</sub>'(t) : First-order derivative of the probabilities.

## 4. Mathematical Modeling

The mathematical modeling is carried out using simple probabilistic considerations and differential equations are developed on the basis of Markov birth-death process. These equations are further solved for determining the steady state availability of the paper making system. Various probability considerations give the following differential equations associated with the paper making system:

States 0, 4 & 8 - Full capacity working.

States 1 to 3, 5 to 7, 9 to 12 & 0SF to 12SF show that unit is in failed state due to complete failure of one or the other subsystem of the unit.

**PULP FROM STOCK  
PREPARATION UNIT**

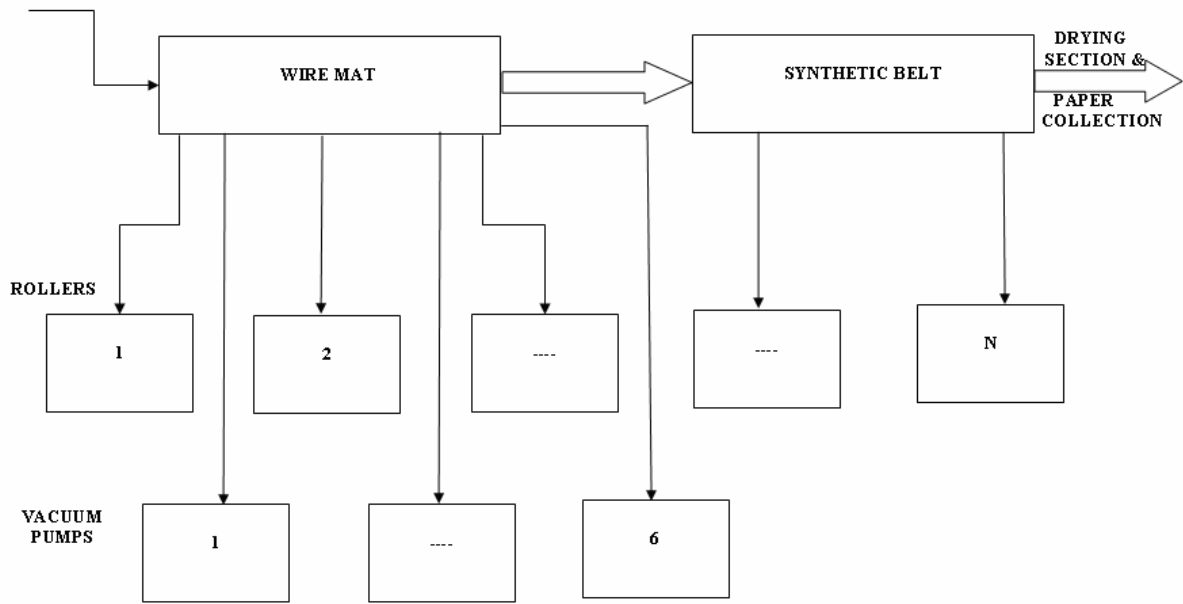


Figure 1. Schematic Flow Diagram of Paper Making System.

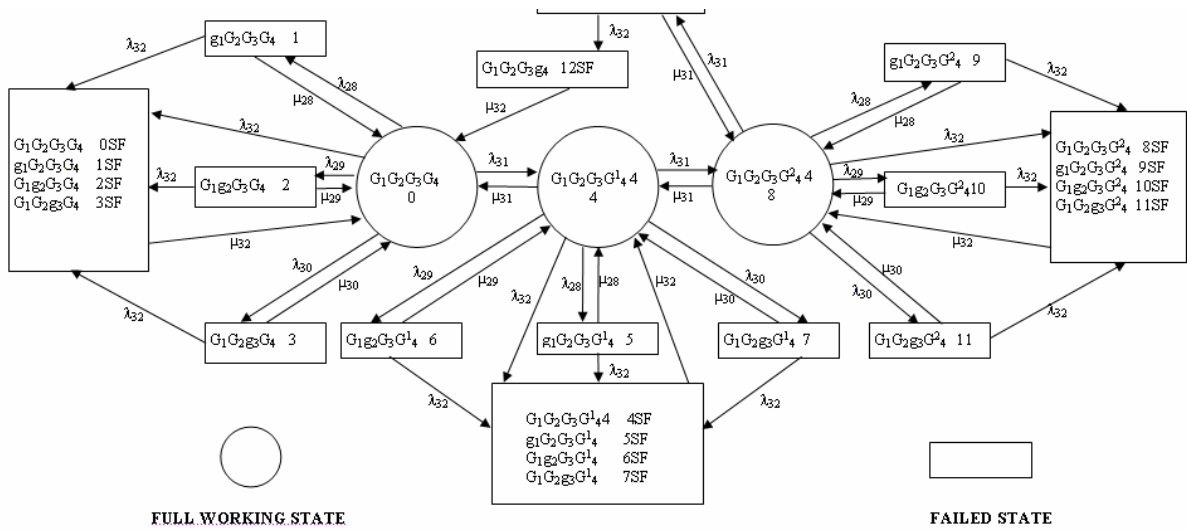


Figure 2. Transition Diagram of Paper Making System.

$$P'_0(t) + \sum_{i=28}^{32} \lambda_i P_0(t) = \sum_{i=28}^{31} \mu_i P_{i-27}(t) + \mu_{32} \sum_{j=0}^3 P_{jSF}(t) + \mu_{31} P_{12SF}(t) \tag{1}$$

$$P'_4(t) + \sum_{i=28}^{32} \lambda_i P_4(t) + \mu_{31} P_4(t) = \sum_{i=28}^{31} \mu_i P_{i-23}(t) + \lambda_{31} P_0(t) + \mu_{32} \sum_{j=4}^7 P_{jSF}(t) \tag{2}$$

$$P'_8(t) + \sum_{i=28}^{32} \lambda_i P_8(t) + \mu_{31} P_8(t) = \sum_{i=28}^{31} \mu_i P_{i-19}(t) + \lambda_{31} P_4(t) + \mu_{32} \sum_{j=8}^{11} P_{jSF}(t) \tag{3}$$

$$P'_i(t) + \lambda_{32} P_i(t) + \mu_{28} P_i(t) = \lambda_{28} P_j(t) \quad \text{where } i=1,5,9 \quad j=0,4,8 \tag{4}$$

$$P'_i(t) + \lambda_{32} P_i(t) + \mu_{29} P_i(t) = \lambda_{29} P_j(t) \quad \text{where } i=2,6,10 \quad j=0,4,8 \tag{5}$$

$$P'_i(t) + \lambda_{32} P_i(t) + \mu_{30} P_i(t) = \lambda_{30} P_j(t) \quad \text{where } i=3,7,11 \quad j=0,4,8 \tag{6}$$

$$P'_{iSF}(t) + \mu_{32} \sum_{i=0}^{12} P_{iSF}(t) = \sum_{i=0}^{12} \lambda_{32} P_j(t) \tag{7}$$

Where  $i=0,1,2,3,4,5,6,7,8,9,10,11,12$  &  $j=0,1,2,3,4,5,6,7,8,9,10,11,12$   
 With initial conditions at time  $t = 0$   
 $P_i(t) = 1$  for  $i = 0 = 0$  for  $i \neq 0$

**5. Solution of Equations**

*5.1. Steady State Behavior*

For steady state behavior, the various systems of a paper plant are expected to run failure free infinitely (for a very long period). So, the steady state availability (time independent performance behavior) of each unit/system may be obtained by setting  $d/dt = 0$  and  $t \rightarrow \infty$  into respective equations i.e. (1) to (7) and then solving these equations recursively, we get:

$$\begin{aligned} P_1 &= C_1 P_0 & P_2 &= C_2 P_0 & P_3 &= C_3 P_0 & P_4 &= LP_0 \\ P_5 &= C_1 LP_0 & & & & & & \\ P_6 &= C_2 LP_0 & P_7 &= C_3 LP_0 & P_8 &= NLP_0 & P_9 &= C_1 NLP_0 \\ P_{10} &= C_2 NLP_0 & & & & & & \\ P_{11} &= C_3 NLP_0 & P_{12} &= MNLP_0 & & & & \\ P_{0SF} &= BP_0 & P_{1SF} &= BC_1 P_0 & P_{2SF} &= BC_2 P_0 & & \\ P_{3SF} &= BC_3 P_0 & & & & & & \\ P_{4SF} &= BLP_0 & P_{5SF} &= B C_1 LP_0 & P_{6SF} &= BC_2 LP_0 & & \\ P_{7SF} &= BC_3 LP_0 & & & & & & \\ P_{8SF} &= BNLP_0 & P_{9SF} &= BC1NLP_0 & & & & \\ P_{10SF} &= BC2NLP_0 & P_{11SF} &= BC3NLP_0 & & & & \\ P_{12SF} &= BMNLP_0 & & & & & & \end{aligned}$$

Where

$$\begin{aligned} C1 &= \lambda_{28}/(\lambda_{32} + \mu_{28}) & C2 &= \lambda_{29}/(\lambda_{32} + \mu_{29}) \\ C2 &= \lambda_{29}/(\lambda_{32} + \mu_{29}) & & \\ C3 &= \lambda_{30}/(\lambda_{32} + \mu_{30}) & L &= \lambda_{31}/\{\lambda_{31} + \mu_{31} - (N * \mu_{31})\} \\ N &= \lambda_{31}/\{\lambda_{31} + \mu_{31} - (M * \mu_{31})\} & & \\ M &= \lambda_{31}/(\lambda_{32} + \mu_{31}) & B &= \lambda_{32}/\mu_{32} \end{aligned}$$

Using Normalizing condition i.e. sum of all the state probabilities is equal to one

$$\sum_{i=0}^{12} P_i + \sum_{j=0}^{12} P_{jSF} = 1, \text{ we get:}$$

$$\begin{aligned} &P_0 + C_1 P_0 + C_2 P_0 + C_3 P_0 + LP_0 + C_1 LP_0 + C_2 LP_0 + C_3 LP_0 \\ &+ NLP_0 + C_1 NLP_0 + C_2 NLP_0 + C_3 NLP_0 + MNLP_0 \\ &+ BP_0 + BC_1 P_0 + BC_2 P_0 + BC_3 P_0 + BLP_0 + BC_1 LP_0 + BC_2 LP_0 \\ &+ BC_3 LP_0 + BNLP_0 + BC_1 NLP_0 + BC_2 NLP_0 + BC_3 NLP_0 \\ &+ BMNLP_0 = 1 \\ &P_0[(1+C_1+C_2+C_3)+L(1+C_1+C_2+C_3)+NL(1+C_1+C_2+C_3 \\ &+M)+B(1+C_1+C_2+C_3)+BL(1+C_1+C_2+C_3)+BNL(1+C_1+ \\ &C_2+C_3+M)]=1 \\ &P_0(Z1+ LZ1+ NLZ2+ BZ1+ BLZ1+ BNLZ2)=1 \\ &P_0[Z1(1+L+B+BL)+ Z2(NL+BNL)]=1 \\ &P_0(Z1Y1+Z2Y2)=1 \\ &P_0=1/(Z1Y1+Z2Y2) \end{aligned} \tag{8}$$

Where

$$\begin{aligned} Z1 &= 1+C_1+C_2+C_3 \\ Z2 &= 1+ C_1+C_2+C_3+M \\ Y1 &= ((1+L+B+(B*L)) \\ Y2 &= ((N*L)+ (B*N*L)) \end{aligned}$$

Now, the steady state availability (Av.) of the paper making system is given by summation of all the full working and reduced capacity states probabilities.

$$A_v = P_0 + P_4 + P_8$$

$$A_v = P_0 + LP_0 + NLP_0$$

$$A_v = P_0(1 + L + NL)$$

$$A_v = \frac{P_0(1 + L + NL)}{((Z_1 Y_1) + (Z_2 Y_2))} \quad (9)$$

Here, system performance has been evaluated in terms of availability.

### 6. Genetic Algorithm

Genetic Algorithms are computerized search and optimization algorithms based on the mechanics of natural genetics and natural selection. Genetic Algorithms have

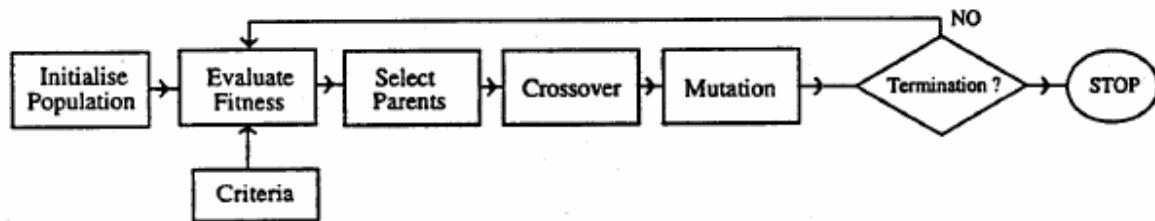


Figure 3

6. Perform the crossover of the parents to produce two off springs.
7. Mutate if required.
8. Place the child strings to new population.
9. Compute the fitness of each individual in new population.
10. Create best-fit population from the previous and new population.
11. Repeat the steps 4 to 10 until the best individuals in new population represent the optimum value of the performance function (System Availability).

### 7. Performance Optimization Using genetic Algorithm

The performance optimization of the paper making system is highly influenced by the failure and repair parameters of each subsystem. These parameters ensure high performance of the system. Genetic Algorithm is proposed to coordinate the failure and repair parameters of each subsystem for stable system performance i.e. high availability. Here, number of parameters is ten (five failure parameters and five repair parameters). The design procedure is described as follows:

To use Genetic Algorithm for solving the given problem, the chromosomes are to be coded in real structures. Unlike, unsigned fixed point integer coding parameters are mapped to a specified interval  $[X_{min}, X_{max}]$ , where  $X_{min}$  and  $X_{max}$  are the minimum and maximum values of system parameters. The maximum value of the availability function corresponds to optimum values of system parameters. These parameters are optimized according to the performance index i.e. desired availability level. To test the proposed method, failure and repair rates are determined simultaneously for optimal value of unit availability. Effect of number of generations, population and crossover probability size on the availability of the paper making system is shown in Table 1, 2 and 3. To specify the computed simulation more precisely, trial sets are also chosen for Genetic Algorithm and system

become important because they are found to be potential search and optimization techniques for complex engineering optimization problems. The action of Genetic Algorithm is shown in figure-3 for parameter optimization in the present problem can be stated as follows:

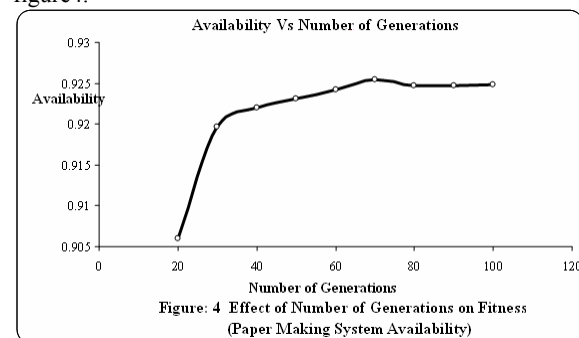
1. Initialize the parameters of the Genetic Algorithm.
2. Randomly generate the initial population and prepare the coded strings.
3. Compute the fitness of each individual in the old population.
4. Form the mating pool from the old population.
5. Select two parents from the mating pool randomly.

parameters. The performance [availability] of the paper making system is evaluated by using the designed values of the unit parameters.

Failure and Repair Rate Parameter Constraints are  $\lambda_{28}, \mu_{28}, \lambda_{29}, \mu_{29}, \lambda_{30}, \mu_{30}, \lambda_{31}, \mu_{31}, \lambda_{32}, \mu_{32}$

Parameters	$\lambda_{28}$	$\mu_{28}$	$\lambda_{29}$	$\mu_{29}$	$\lambda_{30}$	$\mu_{30}$	$\lambda_{31}$	$\mu_{31}$	$\lambda_{32}$	$\mu_{32}$
Minimum	0.001	0.10	0.001	0.10	0.002	0.10	0.02	0.10	0.02	0.10
Maximum	0.005	0.50	0.005	0.50	0.006	0.50	0.10	0.50	0.10	0.50

Here, real-coded structures are used. The simulation is done to maximum number of generations, which is varying from 20 to 100. The effect of number of generations on availability of the paper making system is shown in figure4.



The optimum value of system's performance is 92.55%, for which the best possible combination of failure and repair rates is  $\lambda_{28} = 0.0043, \mu_{28} = 0.3300, \lambda_{29} = 0.0036, \mu_{29} = 0.3497, \lambda_{30} = 0.0056, \mu_{30} = 0.2059, \lambda_{31} = 0.0918, \mu_{31} = 0.1013, \lambda_{32} = 0.0649, \mu_{32} = 0.1287$  at generation size 70 as given in table 1.

Now the simulation is done to maximum number of population size, which is varying from 20 to 100. The programme handled with the maximum value of the population size and terminated with heuristic result. The effect of population size on availability of the paper

making system is shown in figure5. The optimum value of system's performance is **92.57%**, for which the best possible combination of failure and repair rates is  $\lambda_{28} = 0.0017$ ,  $\mu_{28} = 0.4039$ ,  $\lambda_{29} = 0.0024$ ,  $\mu_{29} = 0.1573$ ,  $\lambda_{30} = 0.0042$ ,  $\mu_{30} = 0.2347$ ,  $\lambda_{31} = 0.0727$ ,  $\mu_{31} = 0.1046$ ,  $\lambda_{32} = 0.0574$ ,  $\mu_{32} = 0.1552$  at **population size 70** as given in table 2.

Again, the simulation is done for maximum number of crossover probability, which is varying from 0.10 to 0.90. Crossover and mutation function performed through their

selection with stochastic universal sampling. This function also performed through the double point crossover. The effect of crossover probability on availability of the paper making system is shown in figure 6. The optimum value of system's performance is **92.52%**, for which the best possible combination of failure and repair rates is  $\lambda_{28} = 0.0013$ ,  $\mu_{28} = 0.3004$ ,  $\lambda_{29} = 0.004$ ,  $\mu_{29} = 0.1436$ ,  $\lambda_{30} = 0.0035$ ,  $\mu_{30} = 0.2291$ ,  $\lambda_{31} = 0.0815$ ,  $\mu_{31} = 0.1051$ ,  $\lambda_{32} = 0.0996$ ,  $\mu_{32} = 0.1298$  at **crossover probability 0.60** as given in table 3.

Table 2: Effect of Population Size on Availability of the Paper Making System Using Genetic Algorithm.

Population Size	Availability	$\lambda_{28}$	$\mu_{28}$	$\lambda_{29}$	$\mu_{29}$	$\lambda_{30}$	$\mu_{30}$	$\lambda_{31}$	$\mu_{31}$	$\lambda_{32}$	$\mu_{32}$
20	0.9048	.0044	.1	.0039	.1011	.0048	.3185	.0748	.1846	.0482	.1040
30	0.9181	.0034	.1304	.0039	.3018	.0042	.4039	.0973	.1195	.0426	.1639
40	0.9182	.0047	.1274	.0049	.1567	.0022	.2257	.1	.1	.0803	.3861
50	0.9247	.0045	.2707	.005	.2882	.0038	.4149	.0963	.1	.0958	.3917
60	0.9245	.0048	.1006	.005	.4704	.0042	.3867	.1	.1059	.0519	.3062
70	0.9257	.0017	.4039	.0024	.1573	.0042	.2347	.0727	.1046	.0574	.1552
80	0.9254	.0031	.1430	.0039	.1477	.0054	.3429	.0975	.1	.0251	.1134
90	0.9253	.005	.1585	.002	.1425	.006	.2308	.1	.1	.0564	.2492
100	0.9253	.0044	.1	.0042	.1492	.006	.2	.1	.1	.0986	.1021

(Mutation Probability=0.015, Number of Generations=80, Crossover Probability=0.85)

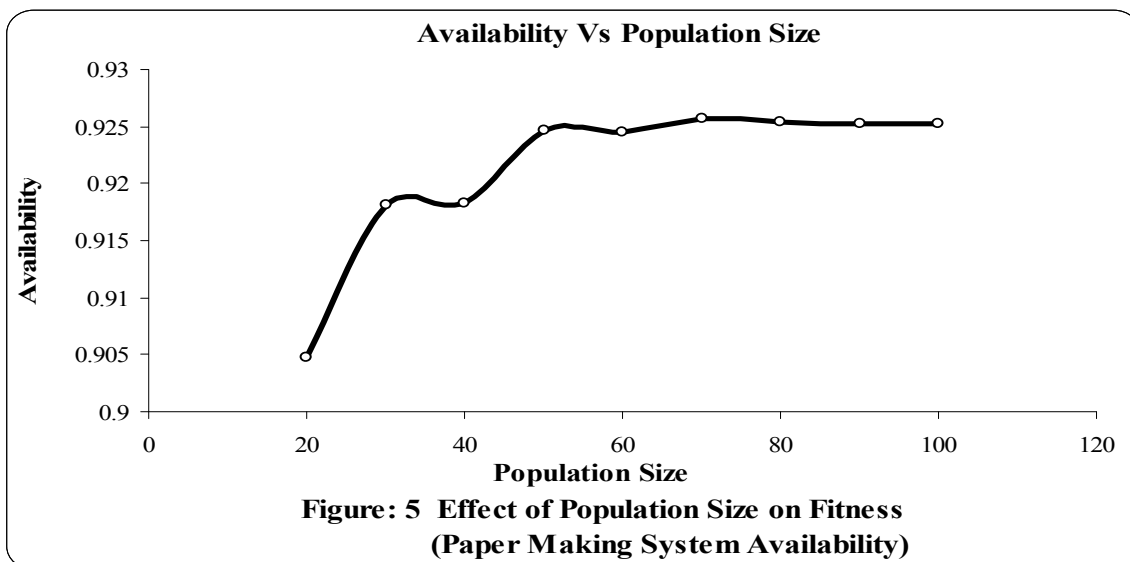
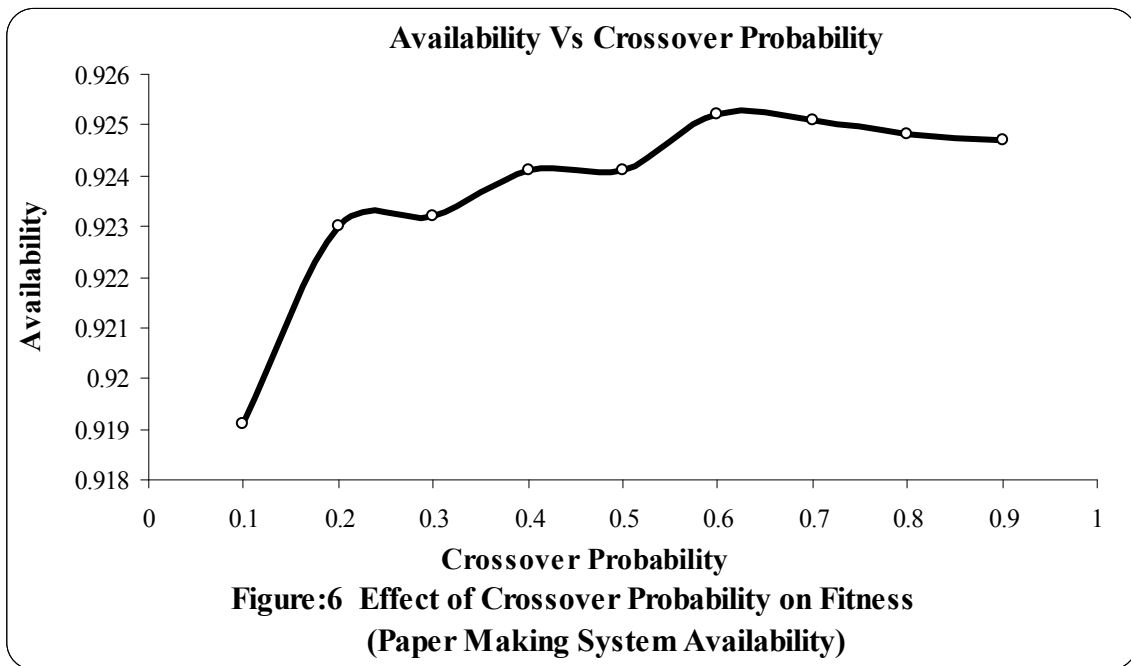


Table 3: Effect of Crossover Probability on Availability of the Paper Making System Using Genetic Algorithm.

Crossover Probability	Availability	$\lambda_{28}$	$\mu_{28}$	$\lambda_{29}$	$\mu_{29}$	$\lambda_{30}$	$\mu_{30}$	$\lambda_{31}$	$\mu_{31}$	$\lambda_{32}$	$\mu_{32}$
.10	0.9191	.0048	.1691	.0035	.2076	.0048	.3171	.0985	.1028	.02	.2576
.20	0.9230	.0044	.2133	.0047	.1807	.0052	.3152	.0741	.1715	.0817	.1867
.30	0.9232	.0048	.3238	.0027	.2407	.0032	.2037	.0985	.1153	.0728	.1896
.40	0.9241	.005	.1539	.005	.1449	.006	.2046	.0967	.1017	.0232	.1259
.50	0.9241	.005	.1694	.0034	.4951	.0052	.3103	.0929	.1637	.0242	.4532
<b>.60</b>	<b>0.9252</b>	<b>.0013</b>	<b>.3004</b>	<b>.004</b>	<b>.1436</b>	<b>.0035</b>	<b>.2291</b>	<b>.0815</b>	<b>.1051</b>	<b>.0996</b>	<b>.1298</b>
.70	0.9251	.0039	.4425	.0046	.2063	.006	.4338	.0853	.2891	.0452	.2817
.80	0.9248	.0032	.3576	.0042	.1	.006	.2202	.1	.1002	.0931	.1294
.90	0.9247	.0023	.1056	.0024	.1663	.0049	.2696	.0968	.1074	.0912	.2012

(Mutation Probability=0.015, Number of Generations=80, Population Size=80)



**8. Conclusions**

The mathematical modeling and performance optimization of the paper making system of a paper plant has been carried out in this paper. Genetic Algorithm Technique is hereby proposed to select the various feasible values of the system failure and repair parameters along with system availability levels. Finally, Genetic Algorithm Technique is successfully applied to coordinate simultaneously these parameters for determining an optimum level of system availability. Besides, the effect of Genetic Algorithm parameters such as number of generations, population size and crossover probability on

the system performance i.e. availability has also been analyzed. By varying the above mentioned parameters of Genetic Algorithm the optimum system availability achieved is about 93% with best possible combinations of the failure and repair rates of all the subsystems of the paper making system. Then, the findings of this paper are discussed with the concerned paper plant management. Such results are found highly beneficial for the purpose of performance optimization of a paper making system in the paper plant concerned.

## References

- [1] Dhillon B S, Singh C. Engineering Reliability- New techniques and applications. John Willey and sons, New York; 1981.
- [2] Kumar D, Singh I P, and Singh J, "Reliability analysis of the Feeding System in the Paper Industry". *Microelectron Reliability*, Vol. 28, No. 2, 1988, 213-215.
- [3] Kumar Dinesh, Singh Jai and Pandey PC, "Availability analysis of the washing system in the paper industry". *Microelectron Reliability*, Vol. 29, 1989, 775-778.
- [4] Kumar Dinesh, Singh Jai and Pandey PC, "Operational behavior and profit function for a bleaching and screening system in the paper industry". *Microelectron Reliability*, Vol. 33, 1993, 1101-1105.
- [5] Srinath L S, *Reliability Engineering*. 3<sup>rd</sup> edition, East-West Press Pvt. Ltd., New Delhi, India; 1994.
- [6] Gupta P, Lal A, Sharma R and Singh J, "Numerical analysis of reliability and availability of the series processes in butter oil processing plant". *International journal of quality and reliability management*, Vol. 22, No.3, 2005, 303-316.
- [7] Sunand Kumar, Dinesh Kumar, Mehta NP, "Maintenance Management for Ammonia Synthesis System in a Urea Fertilizer Plant". *International Journal of Management and System (IJOMAS)*, Vol.15, No.3, 1999, 211-214.
- [8] Shooman M L, "Reliability computation for Systems with Dependents Failures". *IEEE Annual Symposium on Reliability*, 1996.
- [9] Tewari PC, D Joshi, M Sreenivasa Rao, "Mathematical Modeling and Behavioral Analysis of a Refining System using Genetic Algorithm". *National Conference on Competitive Manufacturing Technology and management for Global Marketing*, Chennai, 2005.
- [10] Tewari PC, Dinesh Kumar, Mehta NP, "Decision Support System of Refining System of Sugar Plant". *Journal of Institution of Engineers (India)*, Vol.84, 2003, 41-44.
- [11] Sunand Kumar, Tewari PC, Sharma Rajiv, "Simulated Availability of CO<sub>2</sub> Cooling System in a Fertilizer Plant". *Industrial Engineering Journal (Indian Institution of Industrial Engineering, Mumbai)*, Vol.36, No.10, 2007, 19-23.
- [12] Rajiv Khanduja, Tewari PC, Dinesh Kumar, "Development of Performance Evaluation System for Screening Unit of Paper Plant". *International Journal of Applied Engineering Research*, Vol.3, No. 3, 2008, 451-460.
- [13] Rajiv Khanduja, Tewari PC, Dinesh Kumar, "Availability Analysis of Bleaching System of Paper Plant". *Journal of Industrial Engineering, Udyog Pragati, N.I.T.I.E. Mumbai (India)*, Vol.32, 2008, 24-29.
- [14] Kalyanmoy Deb, *Optimization for Engineering Design: Algorithms and examples*, Prentice Hall of India, New Delhi, India 1995.
- [15] Goldberg D E, *Genetic Algorithm in Search, Optimization and Machine Learning*. Pearson Edition, Asia; 2001.
- [16] Castro H F, Cavalca K, "Availability optimization with Genetic Algorithm". *International Journal of Quality and Reliability Management*, Vol.20, No.7, 2003, 847-863.
- [17] Chales C, Kondo A, "Availability allocation to repairable systems with genetic algorithms: a multi-objective formulation". *Reliability Engineering and System Safety*, Vol. 82, No. 3, 2003, 319-330.
- [18] Ying-Shen Juang, Shui-Shun Lin and Hsing-Pei Kao, "A knowledge management system for series-parallel availability optimization and design". *Journal of Expert system with application* Vol. 34, 2008, 181-193.

## Reduction of Vibration of Industrial Equipments

M. A. Nawafleh <sup>a,\*</sup>, N. Al-Kloub <sup>b</sup>, M. Tarawneh <sup>c</sup>, and R. M. Younes <sup>d</sup>

<sup>a</sup>Department of Civil Engineering, Al-Hussein Bin Talal University, Ma'an, Jordan

<sup>b</sup>Department of Mechanical Engineering, Al-Balqa' Applied University, Amman, Jordan

<sup>c</sup>Department of Mechanical Engineering, Mutah University, Karak, Jordan

<sup>d</sup>Department of Civil Engineering, Tafila Technical University, Tafila, Jordan

### Abstract

Vibration of industrial equipment is the bad factor influencing its production state, working conditions of staff, and job safety. In course of technology development the more and more potent machines are used. It is quite often accompanied by the increase of a vibration level experienced by the equipment is transmitted to the building structures and through the staffs. A model of the production machine has been installed on the vibration dampers. The system of equation has been permitted to evaluate the reduction of the machine vibrations caused by the unbalance movement of its members, thereby, transmitting it onto the floor.

© 2010 Jordan Journal of Mechanical and Industrial Engineering. All rights reserved

Keywords: Industries, Equipment, Vibration, Resonance, Insulation, Conditions, Environment.

### 1. Introduction

The more potent machines become, the more their vibration disturbs people. Vibration is not only harmfully affects an organism, but also hinders fulfillment of working operations, both mentally, and physical. A vibration with frequencies 25-40 and 60-90 Hz is degraded as visual perception. When frequency of vibration is close to the natural frequency of oscillations of the human body, equal about 5 Hz, operating of vibration becomes especially ideal. In different parts of body the natural frequencies make: in pelvic area 4-6 Hz, in abdominal area 4-8 HZ, and the Head 30 Hz. The effect of vibration to a man is shown at fig. 1 [1].

The sources of vibrations of industrial equipment are: impulse applies technological forces, impacts, unbalance of rotated parts, inertia forces of parts with periodic motion. Therefore, the problem of reducing harmful vibrations remains actually permanently; one solution to the problem is the improvement of the kinematics, balancing of the inertia forces, developing of the shock free technological processes. However these actions are not always possible. That is why the other way to reduce the harmful effect of vibration is the vibration insulation of the equipments, installed on building structures.

Vibration insulation is the reduction of the transmission of vibrations which is reached by the installation of pliable members of small stiffness between vibratory units and adjacent structures [2]. As the vibration

absorbers, the springs, rubber and elastic members, pneumatic, hydraulic, combined devices are used.

### 2. Model of a machine installed on elastic vibration absorbers

The analysis of vibrations of production equipment carried out by many researchers [2, 3, and 4]. Particularly in [5] the outcomes of the analysis of a vibrational system shown at Fig.2 are adduced. This system corresponds to production machine installed on elastic members. It was considered that the machine consists of fixed and moving part. The last ones are the masses  $m_1, m_2, \dots, m_m$ , the motion of which is determined by the machine structure which is considered less than the mass  $M_o$  of fixed parts. The model is placed in the systems rectangular coordinates. One of them XYZ is connected to mass  $M_o$ , origin of the system O is combined with the center of mass  $G_o$ . Other  $\xi_o, \eta_o, \xi_o$ , with the origin in the same point O, is independent, fixed in space. The axes of the system XYZ coincide with principal axes of inertia of the mass  $M_o$ . In the balanced state both of these systems coincide. The connection of systems at the arbitrary moment is determined, the coordinates  $\xi_o, \eta_o, \xi_o$ , the point  $G_o$  and angles  $\varphi, \psi, \theta$ , which are selected to be small for small oscillations of the mass  $M_o$ . The mass of the  $i^{\text{th}}$  traveling part is  $m_i$ , coordinates of its center of gravity are  $x_i, y_i, z_i$ . The sum of parts  $m$ , is equal  $m$ , its coordinates are X, Y, Z.

\* Corresponding author. m\_nawafleh@hotmail.com

From the expressions for a kinetic energy after transformations we got the left parts of the Lagrange equations of the second kind:

$$\left. \begin{aligned} (M_o + m) \ddot{\xi}_o + m \ddot{X} \\ (M_o + m) \ddot{\eta}_o + m \ddot{Y} \\ (M_o + m) \ddot{\zeta}_o + m \ddot{Z} \\ (A + a) \ddot{\phi} + \sum m_i (\ddot{y}_i x_i - \ddot{x}_i y_i) \\ (B + b) \ddot{\psi} + \sum m_i (\ddot{x}_i z_i - \ddot{z}_i x_i) \\ (C + c) \ddot{\theta} + \sum m_i (\ddot{z}_i y_i - \ddot{y}_i z_i) \end{aligned} \right\} \quad (1)$$

In which:

$m\ddot{X}$ ,  $m\ddot{Y}$  and  $m\ddot{Z}$  - Inertia forces of the linearly moving parts,

$$P = \frac{1}{2} \left( \sum_{i=1}^n C_{\xi_i} u_i^2 + \sum_{i=1}^n C_{\eta_i} v_i^2 + \sum_{i=1}^n C_{\zeta_i} w_i^2 + \sum_{i=1}^n K_{\xi_i} \phi^2 + \sum_{i=1}^n K_{\eta_i} \psi^2 + \sum_{i=1}^n K_{\zeta_i} \theta^2 \right) \quad (3)$$

Where:

$u, v$  and  $w$  - Deformation of the elastic members,

$C$  - Linear stiffness of elastic members,

$K$  - Torsional stiffness of elastic members.

The deformation of the elastic members can be expressed as follows:

Substitute (4) in (3) we get:

$$P = \frac{1}{2} \left[ \sum_{i=1}^n C_{\xi_i} (\xi_o + \eta_i \phi - \zeta_i \psi)^2 + \sum_{i=1}^n C_{\eta_i} (\eta_o + \zeta_i \theta - \xi_i \phi)^2 + \sum_{i=1}^n C_{\zeta_i} (\zeta_o + \xi_i \psi - \eta_i \theta)^2 + \sum_{i=1}^n k_{\xi_i} \theta^2 + \sum_{i=1}^n K_{\eta_i} \psi^2 + \sum_{i=1}^n K_{\zeta_i} \phi^2 \right] \quad (5)$$

Finding of partial derivatives from potential energy on generalized coordinates gives right hand members of the system of differential equations depicting oscillations of

$$\left. \begin{aligned} (M_o + m) \ddot{\xi}_o + (\xi_o C_{\xi} + \phi u_{\eta} - u_{\zeta} \psi) &= -m \ddot{X} \\ (M_o + m) \ddot{\eta}_o + (\eta_o C_{\eta} + \theta v_{\zeta} - v_{\xi} \phi) &= -m \ddot{Y} \\ (M_o + m) \ddot{\zeta}_o + (\zeta_o C_{\zeta} + \psi \omega_{\xi} - \omega_{\eta} \theta) &= -m \ddot{Z} \\ (A + a) \ddot{\phi} + (\phi C_{\xi\xi} + \xi_o u_{\eta} - \eta_o v_{\xi} - \psi C_{\eta\xi} - \theta C_{\zeta\xi}) &= -\sum m_i (\ddot{y}_i x_i - \ddot{x}_i y_i) \\ (B + b) \ddot{\psi} + (\psi C_{\eta\eta} - \xi_o u_{\zeta} + \zeta_o \omega_{\xi} - \theta C_{\xi\eta} - \phi C_{\eta\zeta}) &= -\sum m_i (\ddot{x}_i z_i - \ddot{z}_i x_i) \\ (C + c) \ddot{\theta} + (\theta C_{\zeta\zeta} + \eta_o v_{\zeta} - \zeta_o \omega_{\eta}) &= -\sum m_i (\ddot{z}_i y_i - \ddot{y}_i z_i) \end{aligned} \right\} \quad (6)$$

$$\sum m_i (\ddot{y}_i x_i - \ddot{x}_i y_i), \quad \sum m_i (\ddot{x}_i z_i - \ddot{z}_i x_i) \text{ and } \sum m_i (\ddot{z}_i y_i - \ddot{y}_i z_i) \text{ - disturbing moments,}$$

A, B, C - principal moments of inertia of the mass  $M_o$  concerning fixed axes,

a, b, c - total moments of traveling masses concerning axes XYZ, and they will be expressed as follows:

$$\left. \begin{aligned} a &= I_{1z} + I_{2z} + \dots + I_{iz} \\ b &= I_{1y} + I_{2y} + \dots + I_{iy} \\ c &= I_{1x} + I_{2x} + \dots + I_{ix} \end{aligned} \right\} \quad (2)$$

where  $I_{ix}$ ,  $I_{iy}$  and  $I_{iz}$  - moments of inertia of  $i^{\text{th}}$  mass concerning axes X, Y, Z.

The right hand members of Lagrange differential equations are composed by means of the expressions for the potential energy of the system. The potential energy for n elastic members is given by the following expression:

$$\left. \begin{aligned} u_i &= \xi_o + \eta_i \phi - \zeta_i \psi \\ v_i &= \eta_o + \zeta_i \theta - \xi_i \phi \\ \omega_i &= \zeta_o + \xi_i \psi - \eta_i \theta \end{aligned} \right\} \quad (4)$$

the model of the machine installed on the elastic shock-absorbers [6](Fig.2):

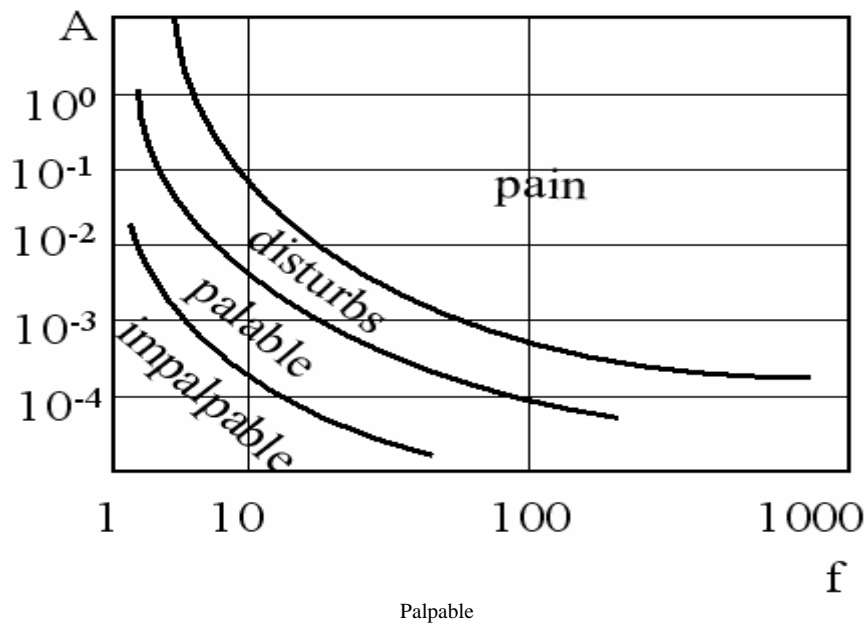


Fig. 1. Effect nature of vibrations on human organism, A-amplitude , mm, f- frequency, Hz

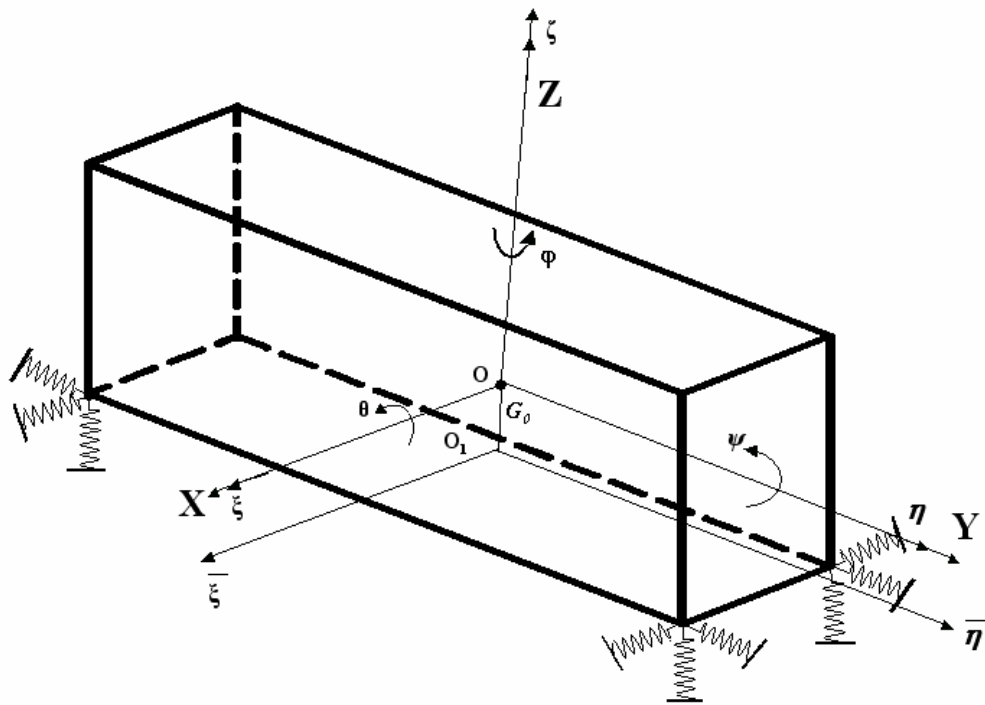


Fig.2. Model of the production machine installed on elastic members

In these equations:

\*The linear stiffnesses are:

$$\left. \begin{aligned} C_{\xi} &= \sum_{i=1}^n C_{\xi i} \\ C_{\eta} &= \sum_{i=1}^n C_{\eta i} \\ C_{\zeta} &= \sum_{i=1}^n C_{\zeta i} \end{aligned} \right\} \quad (7)$$

\* Linear – rotary stiffnesses are:

$$\left. \begin{aligned} u_{\eta} &= \sum_{i=1}^N C_{\bar{\zeta}} \eta_i & u_{\zeta} &= \sum_{i=1}^N C_{\bar{\xi}} \xi_i \\ v_{\xi} &= \sum_{i=1}^n C_{\bar{\eta}} \xi_i & v_{\zeta} &= \sum_{i=1}^n C_{\bar{\eta}} \zeta_i \\ w_{\xi} &= \sum_{i=1}^n C_{\bar{\zeta}} \xi_i & w_{\eta} &= \sum_{i=1}^n C_{\bar{\zeta}} \eta_i \end{aligned} \right\} \quad (8)$$

\*The torsional stiffnesses are:

$$\left. \begin{aligned} C_{\xi\xi} &= \sum_{n=1}^n (K_{\xi i} + C_{\eta i} \xi_i^2 + C_{\zeta i} \eta_i^2) \\ C_{\eta\eta} &= \sum_{n=1}^n (K_{\eta i} + C_{\zeta i} \xi_i^2 + C_{\bar{\zeta}} \zeta_i^2) \\ C_{\zeta\zeta} &= \sum_{n=1}^n (K_{\zeta i} + C_{\bar{\zeta}} \eta_i^2 + C_{\eta i} \xi_i^2) \end{aligned} \right\} \quad (9)$$

\* Gyroscopic stiffnesses are:

$$\left. \begin{aligned} C_{\xi\eta} &= C_{\eta\xi} = \sum_{i=1}^n C_{\zeta i} \xi_i \eta_i \\ C_{\eta\zeta} &= C_{\zeta\eta} = \sum_{i=1}^n C_{\xi i} \eta_i \zeta_i \\ C_{\zeta\xi} &= C_{\xi\zeta} = \sum_{i=1}^n C_{\eta i} \xi_i \zeta_i \end{aligned} \right\} \quad (10)$$

The given system includes in its right hand members the disturbing forces caused by the unbalanced moving masses. Equations (6) can be used at the designing of vibration dampers (absorber) in order to avoid loads transmitted by the machine onto the floor.

In many cases not all the motions of the machine are interdependent, and then the system (6) is simplified. If two principal central axes of stiffness are only principal axes of inertia, but not the central ones, the principal central axis of inertia will be the third principal central

axis of stiffness then all gyroscopic (10) and four of six linear – rotary (8) stiffnesses are equal zero. In this case the system (6) is essentially simplified and becomes:

$$\left. \begin{aligned} (M_o + m)\ddot{\xi}_o + \xi_o C_{\xi} &= -m\ddot{X} \\ (M_o + m)\ddot{\eta}_o + \eta_o C_{\eta} &= -m\ddot{Y} \\ (M_o + m)\ddot{\zeta}_o + \zeta_o C_{\zeta} &= -m\ddot{Z} \\ (A + a)\ddot{\varphi} + \varphi C_{\zeta\zeta} &= -\sum m_i (\ddot{y}_i \chi - \dot{\chi}_i y_i) \\ (B + b)\ddot{\psi} + \psi C_{\eta\eta} &= -\sum m_i (\ddot{\chi}_i z_i - \dot{z}_i \chi_i) \\ (C + c)\ddot{\theta} + \theta C_{\zeta\zeta} &= -\sum m_i (\ddot{z}_i y_i - \dot{y}_i z_i) \end{aligned} \right\} \quad (11)$$

And describe independent oscillations along each axis of coordinates and around it.

### 3. Developing of the model of the machine installed on the elastic-dissipative vibration dampers

The systems (6) and (11) are not taking into account for the dissipation of the energy of oscillations in the vibration dampers. To take into consideration this dissipation we shall add a damping to the vibration dampers and simplify the scheme a little, having shown only vertical components of each of four hearings [7]. In this case the machine is presented by the model shown at Fig.3.

The origin of the coordinated system is placed in the point of the static equilibrium of the center of masses of the machine, as the axes of coordinates the central axes of inertia of the machine are considered. The model has six degrees of freedom by the way of linear displacement along axes and angular displacements around the last. As a result of an unbalance of mobile masses there is a disturbing force [8, and 9], which can be accepted equal  $Q = \sin \omega t$ , as well as in the already reviewed model.

The restoring force of each vibration damper is proportional to its deformation. The force of a viscous strength of vibration damper absent in the model at Fig.2 is proportional to the speed of deformation.

The vibrations of the model (Fig, 3) are described by the following equations: (Equ No.12)

$$\left. \begin{aligned} m\ddot{x} &= \sum_{i=1}^4 F_{xi} + Q \sin \omega t \\ m\ddot{y} &= \sum_{i=1}^4 F_{yi} \\ m\ddot{z} &= \sum_{i=1}^4 F_{zi} - P \\ I_x \ddot{\psi} &= -F_{z1} l_{y1} + F_{z2} l_{y2} - F_{z3} l_{y1} + F_{z4} l_{y2} + \sum_{i=1}^4 F_{yi} z_{bi} \\ I_y \ddot{\varphi} &= F_{z1} l_{x2} + F_{z2} l_{x2} - F_{z3} l_{x1} - F_{z4} l_{x1} + \sum_{i=1}^4 F_{xi} z_{bi} - Q \sin \omega t z_o \\ I_z \ddot{\theta} &= F_{x1} l_{y1} - F_{x2} l_{y2} + F_{x3} l_{y1} - F_{x4} l_{y2} + F_{y2} l_{x2} - F_{y3} l_{x1} - F_{y4} l_{x1} \end{aligned} \right\}$$

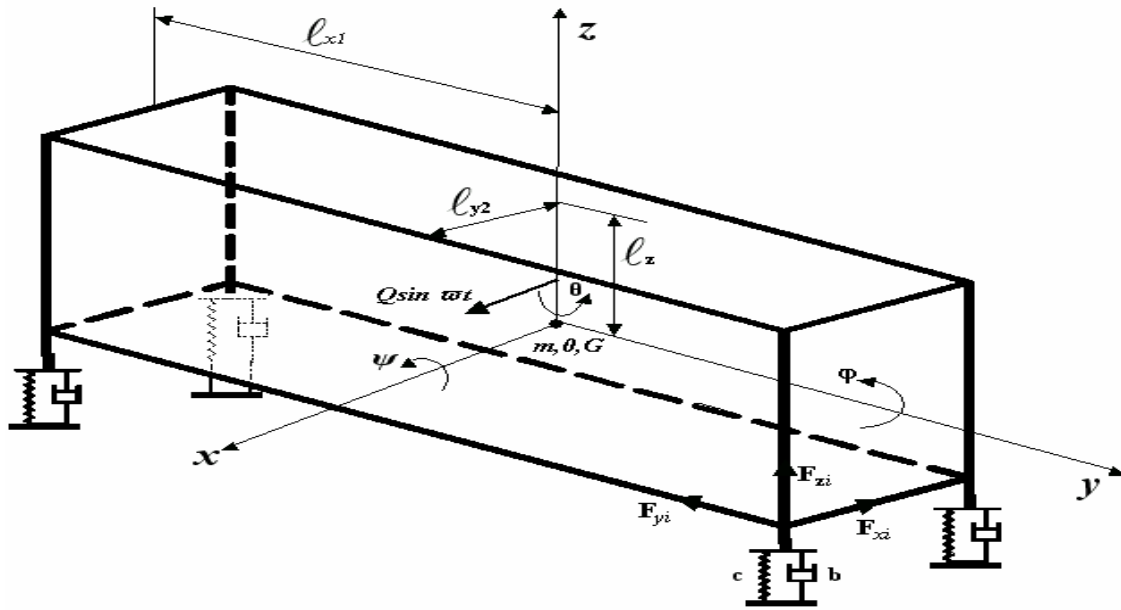


Fig.3. Model of the production machine installed on elastic-damping supports.

Where

$$\left. \begin{aligned}
 F_{x1} = F_{x3} &= -C_x(x + z_b\varphi + l_{y1}\theta) - b_x(\dot{x} + z_b\dot{\varphi} + l_{y1}\dot{\theta}) \\
 F_{x2} = F_{x4} &= -C_x(x + z_b\varphi + l_{y2}\theta) - b_x(\dot{x} + z_b\dot{\varphi} + l_{y2}\dot{\theta}) \\
 F_{y1} = F_{y2} &= -C_y(y + z_b\psi + l_{x2}\theta) - b_y(\dot{y} + z_b\dot{\psi} + l_{x2}\dot{\theta}) \\
 F_{y3} = F_{y4} &= -C_y(y + z_b\psi + l_{x1}\theta) - b_y(\dot{y} + z_b\dot{\psi} + l_{x1}\dot{\theta}) \\
 F_{z1} &= -C_z(z + l_{x2}\varphi + l_{y1}\psi) - b_z(\dot{z} + l_{x2}\dot{\varphi} - l_{y1}\dot{\psi}) \\
 F_{z2} &= -C_z(z + l_{x2}\varphi + l_{y2}\psi) - b_z(\dot{z} + l_{x2}\dot{\varphi} - l_{y2}\dot{\psi}) \\
 F_{z3} &= -C_z(z + l_{x1}\varphi + l_{y1}\psi) - b_z(\dot{z} - l_{x1}\dot{\varphi} - l_{y1}\dot{\psi}) \\
 F_{z4} &= -C_z(z + l_{x1}\varphi + l_{y2}\psi) - b_z(\dot{z} - l_{x1}\dot{\varphi} + l_{y2}\dot{\psi})
 \end{aligned} \right\} \tag{13}$$

The substitution (13) in (12) and the transformations lead to the system of linear differential equations of the second order.

$$\left. \begin{aligned}
 M\ddot{x} + b_{11}\dot{x} + b_{15}\dot{\varphi} + b_{16}\dot{\theta} + c_{11}x + c_{15}\varphi + c_{16}\theta &= Q\sin\omega t \\
 M\ddot{y} + b_{22}\dot{y} + b_{24}\dot{\psi} + b_{26}\dot{\theta} + c_{22}y + c_{24}\psi + c_{26}\theta &= 0 \\
 M\ddot{z} + b_{33}\dot{z} + b_{34}\dot{\psi} + b_{35}\dot{\varphi} + c_{33}z + c_{34}\psi + c_{35}\varphi &= -p \\
 I_x\ddot{\psi} + b_{42}\dot{y} + b_{43}\dot{z} + b_{44}\dot{\psi} + b_{45}\dot{\varphi} + b_{46}\dot{\theta} + c_{42}y + c_{43}z + c_{44}\psi + c_{45}\varphi + c_{46}\theta &= 0 \\
 I_y\ddot{\varphi} + b_{51}\dot{x} + b_{53}\dot{z} + b_{54}\dot{\psi} + b_{55}\dot{\varphi} + b_{56}\dot{\theta} + c_{51}x + c_{55}\varphi + c_{56}\theta &= -Qz_b\sin\omega t \\
 I_z\ddot{\theta} + b_{61}\dot{x} + b_{62}\dot{y} + b_{64}\dot{\psi} + b_{65}\dot{\varphi} + b_{66}\dot{\theta} + c_{61}x + c_{62}y + c_{64}\psi + c_{65}\varphi + c_{66}\theta &= 0
 \end{aligned} \right\} \tag{14}$$

in which stiffnesses  $C_{ij}$  are described by the following relations:

$$\left. \begin{aligned}
 c_{11} &= 4c_x; c_{15} = c_{51} = 4c_x z_b; c_{16} = c_{61} = 2c_x(l_{y1} - l_{y2}) \\
 c_{22} &= 4c_y; c_{24} = c_{42} = 4c_y z_b; c_{26} = c_{62} = 2c_y(l_{x2} - l_{x1}) \\
 c_{33} &= 4c_z; c_{34} = c_{43} = 4c_z(l_{y2} - l_{y1}); c_{35} = c_{53} = 2c_z(l_{x2} - l_{x1}) \\
 c_{44} &= 2c_z(l_{y1}^2 + l_{y2}^2) + 4c_y z_b^2; \\
 c_{45} &= c_{54} = c_z(l_{x2}l_{y2} + l_{x1}l_{y1} - l_{x1}l_{y2} - l_{x2}l_{y1}); \\
 c_{46} &= c_{64} = 2c_y z_b(l_{x2} - l_{x1}) \\
 c_{55} &= 2c_z(l_{x1}^2 + l_{x2}^2) + 4c_x z_b^2; c_{56} = c_{65} = 2c_x z_b(l_{y1} - l_{y2}) \\
 c_{66} &= 2c_x(l_{y1}^2 + l_{y2}^2) + 2c_y(l_{x1}^2 + l_{x2}^2) \\
 c_{12} &= c_{13} = c_{14} = 0; c_{23} = c_{25} = 0; c_{36} = 0
 \end{aligned} \right\} \quad (15)$$

The coefficients of strength are described quite similarly.

#### 4. Solution of the composed set of equations

The natural frequencies are found by means of the determinant (16) of the equation system (13) under the condition that for the zero instant at the linear and angular displacements and the speeds at all coordinates are considered equal zero and that the right side members of the equation system (13) also equal zero.

$$\begin{vmatrix}
 c_{11} - M_w^2 & 0 & 0 & 0 & c_{15} & c_{16} \\
 0 & c_{22} - M_w^2 & 0 & c_{24} & 0 & c_{26} \\
 0 & 0 & c_{33} - M_w^2 & c_{34} & c_{35} & 0 \\
 0 & c_{42} & c_{43} & c_{44} - I_x w^2 & c_{45} & 0 \\
 c_{51} & 0 & c_{53} & c_{54} & c_{55} - I_y w^2 & c_{56} \\
 c_{61} & c_{62} & 0 & c_{64} & c_{65} & c_{66} - I_z w^2
 \end{vmatrix} = 0 \quad (16)$$

As an example let us consider the production machine [5] of the mass  $m=1500$  kg. Moments of inertia concerning principal axes are  $I_x=300$  Nms<sup>2</sup>,  $I_z=630$  Nms<sup>2</sup>. Frequency of rotation speed of the main shaft  $n=230$  rpm, frequency of the disturbing force  $\omega=24$  s<sup>-1</sup>, its amplitude  $Q=5$

$$\begin{aligned}
 c_x &= c_y = 1011 \text{ Nm}^{-1}, \\
 c_z &= 3 \cdot 10^6 \text{ Nm}^{-1}.
 \end{aligned}$$

Damping factors:

$$\begin{aligned}
 b_x &= b_y = 2.5 \cdot 10^6 \text{ Nsm}^{-1}, \\
 b_z &= 4.3 \cdot 10^3 \text{ Nsm}^{-1}.
 \end{aligned}$$

Coordinates of supports:

$$\begin{aligned}
 Z_b &= 0.5 \text{ m}, \\
 \ell_{x1} &= 1.0 \text{ m}, \\
 \ell_{x2} &= 0.54 \text{ m}, \\
 \ell_{y1} &= 1.8 \text{ m}, \\
 \ell_{y2} &= 0.83 \text{ m},
 \end{aligned}$$

The solution of the set of equations for the case of natural vibrations of the machine in a vertical direction found by means of MATLAB, demonstrates, that this natural frequency makes  $71$  s<sup>-1</sup>, whereas the disturbing

frequency, as was mentioned, equal  $24$  s<sup>-1</sup>. Hence the machine runs in under resonance mode, in which natural frequency is far enough from a resonance.

The calculation, also by means of MATLAB, of the enforced vertical vibrations has shown, that their amplitude  $X_0 = 1.2 \cdot 10^{-4}$  m. Then the dimensionless dynamic factor is

$$K_d = cx_o / Q = 0.2.$$

Comparing its value with a unit, we are convinced, that the first one is much less, and we come to the conclusion, that the vibration insulation of the given machine meets the lead requirements [7].

#### 5. Conclusion

1. The model offered herein of the production machine is installed on the vibration dampers and the developed with the account of elastic and dissipative properties of the vibration dampers. The system of equation is permitted to evaluate the reduction of the machine vibrations caused by the unbalance movements of its members and, thereby transmitting it onto the floor.
2. By means of the developed system of equations, it is proven that, taken as an example the production

machine that runs far from a resonance and its vibration dampers effectively meet the requirements of the working environment.

## References

- [1] W. E. Woodson, D. W. Conover, 1966, Human engineering guide for equipment designers. Univ. of California press. Berkeley, Los Angeles.
- [2] Ya. I. korityssky.1974, Vibrations and noise in textile and light industries. M, light industries.
- [3] Ewins, D. J: Modal Testing-Theory, Practice and Application. Research Studies Press LTD. Baldock, 2000.
- [4] Huang, X., Elliott, S. J., Brennan, M. J.: Active isolation of a flexible structure from base vibration, Journal of Sound and Vibration, Vol.263, 2003, 357-376.
- [5] O. N. Nizhibitsky, I. V. Ulyanov, A.S. churilin, 1997, Studies of the antivibration properties of structure materials made of waste in textile and light industries. In: Days of science, 97. Papers of technical sciences conf.- SPB, SPGUTD.
- [6] M. A. Alnawafleh, "Oscillation Analysis in Winding Mechanisms Actuated by Rotating Frictional Drum", proceeding of the 13th European Simulation Symposium, Simulation in Industry. Society for Computer Simulation International, Marseille, France, 2001, 20-24.
- [7] V. A. Inovich, V. Ya. Onishchenko, 1990, Protection from vibrations in machinery construction, - m, Machinery construction.
- [8] M. A. Alnawafleh and Faisal M. Al-Ghathian, Dynamical Properties Analysis of Frictional Winding Mechanism with Bobbin Elastic Support. American Journal of Applied Sciences, Scientific Publication, Vol.2, No.4, 2005, 827-830.
- [9] Shilin, X.,Siu, W., and Helen, Lai Wan Chan.: Design optimization isolation system through minimization of vibration power flow. Journal of Structural Engineering and Mechanics, Vol. 28, No. 6, 2008, 677-694.



# Property Estimation with Automated Ball Indentation Using Artificial Neural Network and Finite Element Simulation

Kamal Sharma\*, Vivek Bhasin, A. K. Ghosh

Reactor Safety Division, BARC, Trombay, Mumbai, 400 085, India

## Abstract

A combined mechanical property evaluation methodology with ABI (Automated Ball Indentation) simulation and Artificial Neural Network (ANN) analysis is evolved to evaluate the mechanical properties for material. The experimental load deflection data is converted into meaningful mechanical properties for this material. An ANN database is generated with the help of contact type finite element analysis by numerically simulating the ABI process for various magnitudes of yield strength ( $\sigma_{yp}$ ) (200 MPa – 500 MPa) with a range of strain hardening exponent ( $n$ ) (0.1- 0.5) and strength coefficient ( $K$ ) (500 MPa – 1500 MPa). For the present problem, a ball indenter of 1.57 mm diameter having Young's Modulus approximately 100 times more than the test piece is used to minimize the error due to indenter deformation. Test piece dimension is kept large enough in comparison to the indenter configuration in the simulation to minimize the deflection at the outer edge of the test piece. Further, this database after the neural network training; is used to analyze measured material properties of different test pieces. The ANN predictions are reconfirmed with contact type finite element analysis for an arbitrary selected test sample. The methodology evolved in this work can be extended to predict material properties for any irradiated nuclear material in the service.

© 2010 Jordan Journal of Mechanical and Industrial Engineering. All rights reserved

Keywords: Automated Ball Indentation; ANN; Finite Element Simulation; Irradiated Nuclear Material; Miniature Specimen Testing.

## 1. Introduction

Nuclear reactor components and power piping are generally subjected to various forms of thermal cycling. As a result, the mechanical properties of the materials of the components get degraded. It is therefore of prime importance, that the altered mechanical properties of the degraded materials be known for life assessment of the components of the nuclear and thermal power plants. So determination of mechanical properties of materials by using non-conventional techniques has been an active area of research for a long time. Among some nondestructive methods for determining mechanical properties of materials, a semi-destructive type of testing, called *Automated Ball Indentation* (ABI) has been developed. The *Automated Ball Indentation* technique is capable of extracting degraded mechanical behavior and properties of thermally aged or irradiated materials from very small specimens. The significance of this technology is obvious to the nuclear industry where neutron irradiation space is limited and irradiation cost scales up with specimen volume.

For this evaluation the specimen undergoes multiple indentations by a spherical ball indenter. Furthermore, this method can be used to characterize weldments and associated Heat Affected Zone (HAZ), it also avoids the need to fabricate test specimen, and it is relatively rapid.

## 2. Review of Earlier Work

A few research groups have published a series of investigations on ball indentation technique to evaluate mechanical properties. It was *Mayer* [1] who first developed a relationship between the mean pressure and indentation diameter to evaluate the yield strength of materials. *Tabor* [2] gave an empirical relationship to find the representative strain of materials while indentation is done through a hard spherical ball. However, Tabor's relation holds very close to the test observation when the indentation process become fully plastic

*Haggag et.al.* [3] did extensive work and developed an automated ball indentation test set up for determining flow properties directly from the test around a small volume of material. The location dependence of the mechanical properties was successfully measured by *Murthy et.al.* [4]. Gradients in mechanical and fracture properties of SA 533B steel welds were studied using ball indentation technique. The local stress-strain behaviors of different microstructure zones of the weld were observed at different temperatures. *Haggag and Nansted* [5] also described a simple technique for estimating the fracture toughness by coupling the measured flow properties with a modified but empirically correlated critical fracture strain model. *Mathew et.al.* [6] studied the effects of low temperature aging (673K) up to 18 months on the mechanical and fracture properties of cast CF-8 stainless

\* Corresponding author. hello\_kamal@yahoo.com

steel in the range of 173-423K. A theoretical model is proposed to estimate fracture toughness of ferritic steel in the transition region from ball indentation test data by *Byun, kin, Hang* [7]. The key concept of the model is that the indentation energy to a critical load is related to fracture energy of material. Using this set-up many research groups [8-11] studied flow properties of different materials through the thickness variation/gradient in mechanical and fracture properties and found good agreement with the conventional test results.

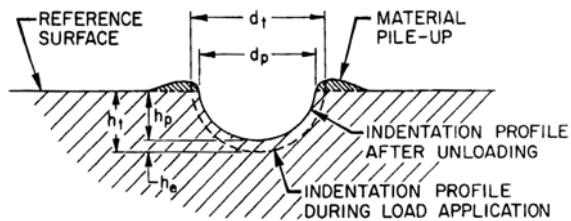


Figure 1 Automatic Ball Indentation Process.

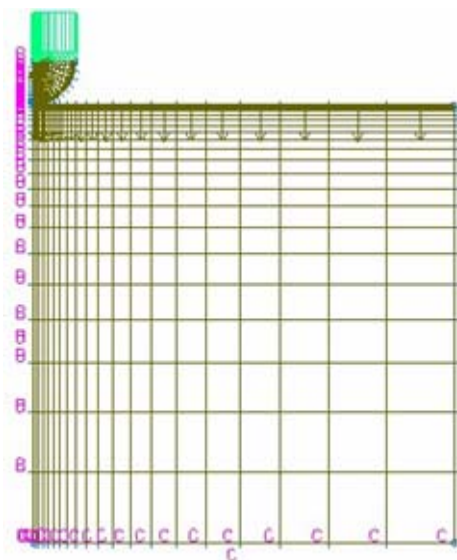


Figure 2 FE model of Indenter and Test Specimen

### 3. Numerical Model and Analysis Procedure

In the present work due to spherical nature of indenter and circular test specimen, fully axisymmetric 2D model is created. The finite element model of the ball indenter and specimen is shown in the fig 2 and the deformed model enlarged at contact area due to the loading is shown in fig 3. For the present analysis, SA 333 material properties are used. The indenter has been simulated with Young's modulus 100 times them the test specimen. This helps in simulating the hardened ball stiffness. The test specimen is modeled with 10 mm × 10 mm dimensions. The indenter in this analysis has 1.57mm diameter. The indenter and specimen have been modeled in two sections (areas) respectively. Indenter is defined as contactor surface and the specimen is defined as target surface for the contact pair. Large strain and large displacement option is applied for the analysis and constrained function contact algorithm is used for the solution. Very finer mesh has been generated at the contact element location.

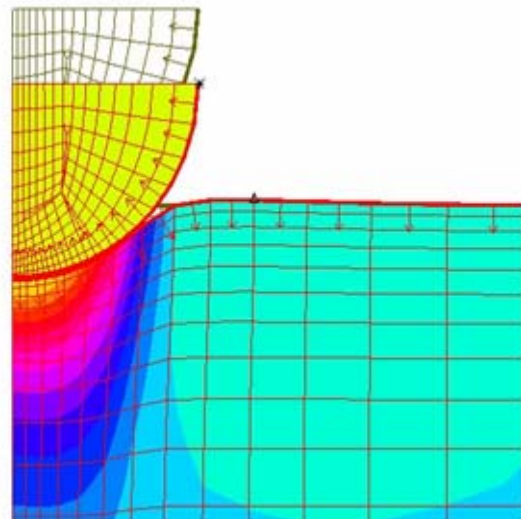


Figure 3. Deformed FE model enlarge at the contact area

#### 3.1. Material data

Material data for specimen

$\sigma_{yp} = 200$  to 500 MPa with increment of 20 MPa

$K = 500$  to 1500 MPa with increment of 100 MPa

$n = 0.1$  to 0.5 with increment of 0.1

Ultimate limit ( $\sigma_{uts}$ ) = 600 MPa

Young's modulus ( $E$ ) = 200 GPa

$\nu$  (Poisson Ratio) = 0.25

Material data for stiff indenter

Young's modulus ( $E$ ) = 20000 GPa (~ 100 times of specimen stiffness)

$\nu$  (Poisson Ratio) = 0.0.

#### 3.2. Analysis

Analysis of indenter and specimen FE model has been carried out for different values of  $\sigma_{yp}$ ,  $K$  and  $n$  and for each case the input material data is varied and load is incremented to simulate the indentation process. For the analysis purpose the power law is taken into consideration to generate the stress strain data for the different

combinations of  $\sigma_{yp}$ ,  $K$  and  $n$  and the generated database is used as material property input for the analysis. The nonlinear analysis is carried out for the case with varying steps of pressure from 5 MPa to 1000 MPa. After each analysis load-deflection curves are obtained and this generated database is used for the ANN toolbox.

### 4. Artificial Neural Network

Artificial neural network are composed of simple elements operating in parallel. This is basically a network or interconnections of artificial neurons. These elements are inspired by biological nervous system. As in nature, the network function is determined largely by the connections between elements. We can train a neural network to perform a particular function by adjusting the values of the connections (weights) between elements. Generalized line diagram of artificial neural network is shown in figure 4. In the present work the artificial neural network (ANN) is used for performing logical function on

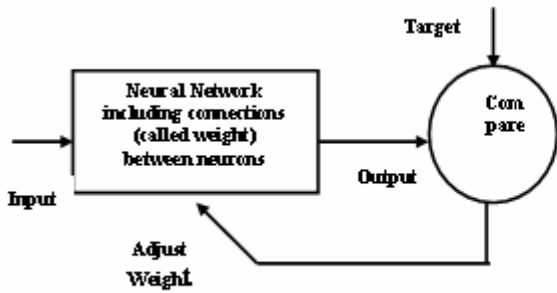


Figure 4. Line Diagram for Artificial Neural Network

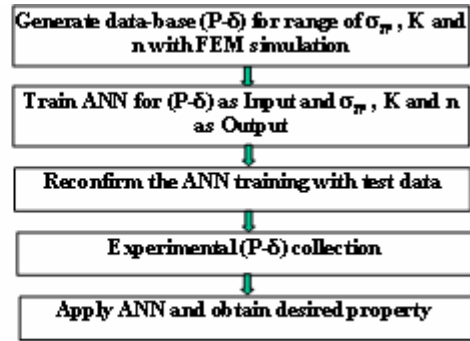


Figure 5. Methodology for the property evaluation Evaluation

its input such as load-deflection. The load-deflection input is provided to the ANN for the range of K, n, and  $\sigma_{yp}$  values. This data has been used to train the ANN. The Neural Network used in this case for the purpose of data inversion is an example of Multi layer Perceptron (MLP) network with back propagation algorithm. It consists of 6 layers before the output stage, 5 layers consisting of the intermediate neurons also known as hidden layers. The first layer is an input stage.

The command TRAINLM is used for training the network while the command PURELIN is the transfer function used to activate the neurons. Arbitrarily some load-deflection plots are chosen from the database and are input to the trained network for cross checking the network accuracy. In the subsequent step experimental data collection is carried out. After that from the ANN the respective properties for the given input will be obtained.

Table I shows the comparison of YS, n, K and UTS value of base, weld and heat affected zone obtained through BIT and conventional test. BI results for base and weld metals compared favorably with the result from conventional tensile test. Error in all the property estimation is less than 2%. Fig 6 shows the comparison of BI test results with that of conventional test results, 2<sup>nd</sup> bars show the conventional test results. Table II shows the comparison of YS, n, K and UTS value of SA 333 with conventional method, BIT method and finite element approach. Percentage error estimation is conventional vs BIT approach and FEM+ANN approach respectively. Table II shows maximum error is 5.8 % for UTS and 6.8% for strain hardening exponent estimation for Stainless Steel. Table III shows maximum error is 9.7% for UTS and 3.8% for strain hardening exponent estimation for Carbon Steel.

6. Results And Discussions

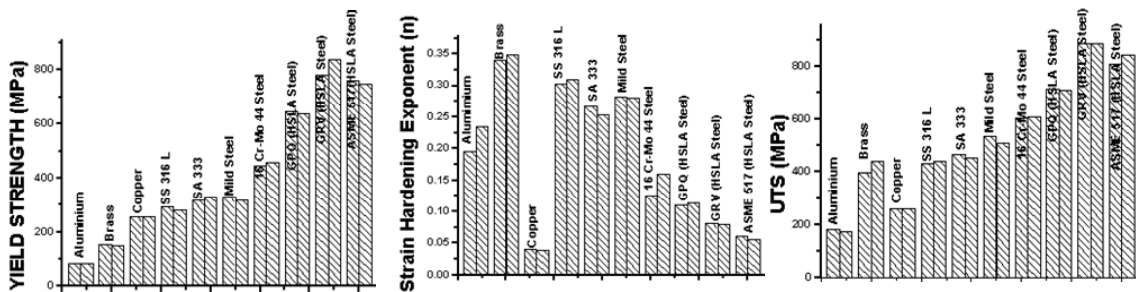


Figure 6 Comparison of BI test results with that of conventional test results, 2<sup>nd</sup> bars show the conventional test results

Table I. Comparison of mechanical properties for welded HSL steel

Welded HSLA steel	Conventional Test Results				Ball Indentation Test Results			
	YS (MPa)	UTS (MPa)	K (MPa)	n	YS (MPa)	UTS (MPa)	K (MPa)	n
Base	773	816	1030	0.062	762	808	1018	0.06
HAZ	---	---	---	---	750	727	970	0.083
Weld	565	669	999	0.098	502	672	926	0.095

Table II: Comparison of SA-333 material property with conventional, BIT and FE approach.

	UTS(MPa)	YS (MPa)	K (MPa)	n
<b>Conventional</b>	455	328	866	0.25
<b>BIT</b>	465	316	867	0.267
<b>FE approach</b>	482	313	878	0.251
<b>% Error (BIT)</b>	2.1 %	3.6 %	0.11%	6.8 %
<b>% Error (FEM+ANN)</b>	5.8%	4.7 %	1.38%	0.37%

Table III: Comparison of Mild Steel material property with conventional, BIT and FE approach.

	UTS(MPa)	YS (MPa)	K (MPa)	n
<b>Conventional</b>	508	317	1041	0.28
<b>BIT</b>	535	330	1015	0.283
<b>FE approach</b>	560	326	1074	0.291
<b>% Error (BIT)</b>	5.3%	4.1%	2.49%	1.07%
<b>% Error (FEM+ANN)</b>	9.7%	2.7%	3.25%	3.88%

## 5. Conclusion

The flow properties obtained through BIT were validated by conventional test results, which prove the effectiveness of the present BI system in which a small amount of test material will be sufficient for the entire test. In most of the nuclear industry cases extracting specimen from components, for conducting conventional tests for evaluation of properties of the material, is neither possible nor permissible.

## References

- [1] E. Meyer and Z. Ver, Dtsch. Ing., Vol. 52, 1908, 740–835.
- [2] Tabor D. The Hardness of Metals, Clarendon press, Oxford, 1951.
- [3] F.M. Haggag, "In-Situ Measurements of Mechanical Properties Using Novel Automated Ball Indentation System", American Society for Testing and Materials, Philadelphia, 1993, 27-44.
- [4] K.L. Murthy, P.Q. Mirgania, and M. D. Mathew, "Characterization of gradients in Mechanical Properties of SA-533B Steel Welds Using Ball Indentation", International journal of Pressure Vessel and Piping, Vol. 76, 1999, 361-369.
- [5] F.M. Haggag and R.K. Nanstad, "Estimating Fracture Toughness Using Tension or Ball Indentation Tests and a Modified Critical Strain Model", ASME PVP, Vol. 170, 1989, 41-46.
- [6] M.D. Mathew, K.L. Murthy, L.M. Lietzan and V.N. Shah, "Low Temperature Aging Embrittlement of CF-8 Stainless Steel," Material Science and Engineering A, Vol. 269, 1999, 186-196.
- [7] T.S. Byan, J.W. Kim, J.H. Hong, "A Theoretical Model for Determination of Fracture Toughness of Reactor Pressure Vessel Steels in the Transition Region from Automated ball Indentation Test," Journal of Nuclear Materials, Vol. 252, 1998, 187-194.
- [8] Y.H. Lee, W.J. Ji and D. Kwon, "Stress Measurement of SS400 steel Beam Using the Continuous Indentation Technique," Experimental Mechanics, Vol. 44, 2004, 55-61.
- [9] S. Ghosh, S. Yadav and G. Das, "Study of Standard Heat Treatment on Mechanical Properties of Inconel 718 using Ball Indentation Technique," Materials Letters, Vol. 62, 2008, 2619-2622.
- [10] H. Lee, J.H. Lee and G.M. Pharr, "A Numerical Approach to Spherical Indentation Techniques for Material Property Evaluation," Vol. 53, 2005, 2037-2069.
- [11] S. Ghosh, S. Yadav and G Das, "Causes of Deviation of the Ball Indentation Test Results and its Corrective Measures" International Symposium of Research Students on Materials and Engineering, Chennai, India, 2004.

# Exergoeconomic Analysis for Unit Gt14 of South Tripoli Gas Turbine Power Plant

Giuma M. Fellah\*, Fathi A. Mgherbi, Saleh M. Aboghres

Department of Mechanical and Industrial Engineering, Faculty of Engineering, Al-Fateh University, Libya

## Abstract

Exergoeconomic (thermoeconomic) analysis is performed for the unit GT14 of South Tripoli (Libya) gas turbine power plant. The designed electrical power of the unit is 100MW (based on ISO conditions). The full operating load (electrical) is 85MW. The analysis is based on real time data and performed for three different loads; those are 85% (full operating load) 60%, and 40% of design load.

A systematic and general methodology for defining and calculating exergetic efficiencies, exergy destruction and exergy related costs in thermal systems is presented. The methodology is based on the Specific Exergy Costing approach. Results of exergy analysis show the exergetic efficiency increases from 20.54% at 40% design load to 29.12% at full operating load, and hence, the ratio of the total exergy destruction to fuel input exergy decreases from 61.03% at 40% design load to 48.63% at full operating load, and the ratio of exergy loss with the exhaust gases to the input fuel exergy slightly increases from 18.43% to 22.25%. Results of exergoeconomic analysis show the average cost per unit exergy net power equal to 7.1\$/GJ at 40% design load, and equal to 5.5\$/GJ at 60% design load, and equal to 4\$/GJ at full operating load. It is found that the cost of exergy destruction in the combustion chamber presents the main contribution to the total cost of exergy loss; its value varies in the combustion chamber from 1474\$/h at 40% design load to 1123\$/h at the full operating load. The contribution and the variation of cost of exergy destruction with load are lower for the other two main components.

© 2010 Jordan Journal of Mechanical and Industrial Engineering. All rights reserved

Keywords: Exergy; Irreversibility; Exergoeconomic; Cost Formation; F-principle; P-principle.

<b>Nomenclature</b>		I	capital
c	average cost per unit exergy (\$/kJ)	CH	chemical
s	entropy (kJ/kg.K)	k	component "k"
$\dot{Z}$	equipment cost rate (\$/h)	D	destruction
y	exergy destruction ratio	F	fuel
f	exergy economic factor	L	loss
$\dot{I}$	irreversibility rate (kW)	PH	physical
x	mole fraction	P	product
PEC	purchase cost (\$)	j	stream "j"
$\dot{C}$	stream cost rate (\$/h)	tot	total
T	tempearure (K)	<b>Superscripts</b>	
<b>Symbols</b>		Cl	capital
$\epsilon$	effectiveness	OM	operating and maintenance
$\dot{\Psi}$	exergy rate (kW)		
$\Psi$	specific exergy (kJ/kg)		
<b>Subscripts</b>			
O	ambient		

## 1. Introduction

Exergoeconomic (thermoeconomic) combines a detailed exergy analysis with appropriate cost balances to study and optimize the performance of energy systems from the cost viewpoint [1]. Essentially, there are two exergoeconomic techniques proposed in literature: the Exergoeconomic Functional Analysis (T.F.A.) and the Exergetic Cost Theory [2].

\* Corresponding author. gfellah2008@yahoo.com

The history of exergy analysis of thermodynamics and thermoeconomics, the performance evaluation of an energy system from the viewpoint of the second law of thermodynamics and thermoeconomics as well as applications of thermoeconomic optimization techniques is reported [3].

A conventional vapor-compression desalting system is analyzed thermodynamically and economically by the concept of essergy and internal energy, where economic analysis using the concept of internal economy shows that the decomposition of the system into zones is not totally arbitrary [4].

The application of exergoeconomic analysis has found wide range of applications, for instance for designing and optimizing thermal energy storage units [5, 6], to evaluate the performance of multi stage flash thermal vapor compression desalination process [7], and for modeling of geothermal district heating

systems for building applications [8].

Thermoeconomic Analysis of electricity production via SOFC with integrated allothermal biomass gasification is presented [9]. Among the different approaches in literature, Specific Exergy Costing (SPECOC) [10] method is used in this work.

SPECOC method for calculating exergy-related costs in thermal systems is presented [11], where general rules are

formulated for defining fuel and product and for calculating the auxiliary costing equations (based on the F and P rules).

## 2. GT14 of South Tripoli Power Plant

Exergoeconomic analysis by using the Specific Exergy Costing method (SPECOC) [11] is performed to illustrate the power of using this kind of analysis in evaluating the performance of gas turbine power plants. Gas turbine unit GT14 of South Tripoli gas turbine power plant is selected to perform the analysis. The power plant was constructed by ABB a German-Swiss company in 1994 at Alswani city. The plant has a design total capacity of 500 MW distributed evenly among five units. This capacity constitutes more than one eighth of the total installed capacity in Libya. The aim of the analysis is to investigate the cost formation process, and to evaluate the performance of unit GT14 from exergoeconomic point of view. Gas turbine unit GT14 consists mainly of three components; a combustion chamber, a compressor, and a turbine, as shown in Fig. 1.

The thermodynamic data, the exergy balance, the cost balance and auxiliary equations for the unit GT14 are found in tables 1, 2, and 3 respectively in the appendix.

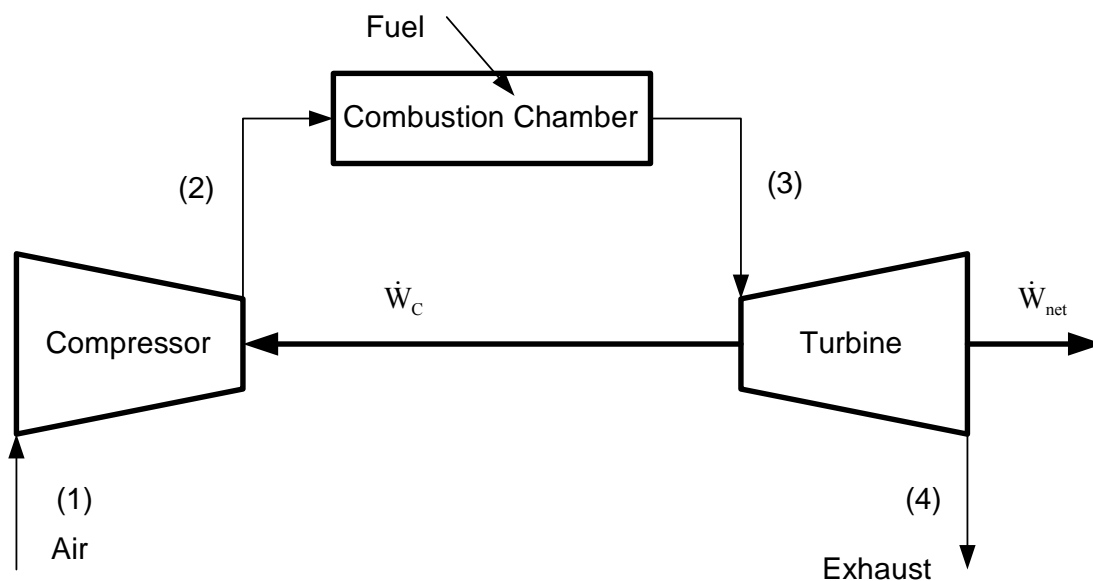


Figure 1. Schematic of the Unit GT14 of South Tripoli power station.

## 3. Assumptions

Fuel price (in Libyan dinar) is fixed and supported by the Libyan authorities; the current Libyan dinar is equal to 0.78 dollars at which the analysis is made. For the analysis the following assumptions are adopted:

- 1- Steady state and steady flow processes.
- 2- Ideal gas behavior for air and combustion products.
- 3- The fuel (light diesel) is modeled as n-Dodecane. The fuel is provided to the combustion chamber at the required pressure by a throttling process from a high-pressure source.

- 4- The combustion is complete, and  $N_2$  is inert.
- 5- All components operate without heat loss (adiabatic).
- 6- The generator efficiency is 97%.

Power plant productivity is controlled according to the demand of electrical energy by controlling of the amount of fuel, which enters to the combustion chamber.

## 4. Exergoeconomic Analysis

Exergy can be found as [12]:

Physical Exergy:

$$\psi_{PH} = (h - h_0) - T_0(s - s_0) \quad (1)$$

Chemical Exergy:

$$\psi_{CH} = RT_0 \sum x_i \ln \left( \frac{x_i}{x_{i0}} \right) \quad (2)$$

Exergy Balance:

$$\sum \dot{\Psi}_{in,k} = \sum \dot{\Psi}_{out,k} + \dot{\Psi}_{L,k} + \dot{I}_{D,k} \quad (3)$$

Effectiveness:

$$\varepsilon = \frac{\text{outlet exergies}}{\text{inlet exergies}} \quad (4)$$

### 5. The Auxiliary Equation Rules

The following two rules for formulating the auxiliary equations are valid, when finding the specific costs of exergy associated with flows is desired [11]:

#### 5.1. F-Principle:

The total cost associated with the removal of exergy must be equal to the cost at which the removed exergy was supplied to the same stream in upstream components.

#### 5.2. P-Principle:

Each exergy unit is supplied to any stream associated with the product at the same average cost.

### 6. Cost Balance

Exergy costing usually involves cost balances formulated for each system component separately. A cost balance applied to the  $k$ -th component shows that the sum of cost rates associated with all exiting exergy streams equals the sum of cost rates of all entering exergy streams plus the appropriate charges due to capital investment ( $\dot{Z}_k^{Cl}$ ) and operating and maintenance expenses ( $\dot{Z}_k^{OM}$ ). The sum of the last two terms is denoted by  $\dot{Z}_k$  [11]:

$$\dot{Z}_k = \dot{Z}_k^{Cl} + \dot{Z}_k^{OM} \quad (5)$$

The steady-state form of control volume cost balance is

$$\sum_{j=1}^{m} \dot{C}_{j,k,out} = \sum_{j=1}^{m} \dot{C}_{j,k,in} + \dot{Z}_k \quad (6)$$

Some auxiliary equations expressed explicitly or implicitly. These auxiliary equations depend on the purpose of the component within the overall system, which is expressed by the exergetic efficiency:

$$\varepsilon_k = \frac{\dot{\Psi}_{P,k}}{\dot{\Psi}_{F,k}} \quad (7)$$

An important characteristic of exergoeconomic is the definition of exergy related specific costs.

$$c = \frac{\dot{C}}{\dot{\Psi}} \quad (8)$$

### 7. Exergoeconomic Variables

The exergoeconomic evaluation is conducted at the component level with the aid of a series of exergoeconomic variables. The rate of exergy destruction is calculated with the aid of an exergy balance, which,

after introduction of fuel and product, may be written as [12]:

$$\dot{I}_{D,k} = \dot{\Psi}_{F,k} - \dot{\Psi}_{P,k} - \dot{\Psi}_{L,k} \quad (9)$$

The exergy destruction ratio relates the exergy destruction in the  $k$ -th component to the input fuel of the overall plant [11]:

$$Y_{D,k} = \frac{\dot{I}_{D,k}}{\dot{\Psi}_{Fuel}} \quad (10)$$

The cost rates  $\dot{C}_{F,k}$  and  $\dot{C}_{P,k}$  associated with the fuel and product, respectively, are formed in the same way as the exergy rates  $\dot{\Psi}_{F,k}$  and  $\dot{\Psi}_{P,k}$  associated with fuel and product. Then the average costs per unit of fuel exergy ( $c_{F,k}$ ) and product exergy ( $c_{P,k}$ ) are calculated from [10]:

$$c_{F,k} = \frac{\dot{C}_{F,k}}{\dot{\Psi}_{F,k}} \quad (11-$$

a)

$$c_{P,k} = \frac{\dot{C}_{P,k}}{\dot{\Psi}_{P,k}} \quad (11-b)$$

The cost rate associated with exergy destruction is estimated as follows:

$$\dot{C}_{D,k} = c_{F,k} \dot{I}_{D,k} \quad (12)$$

The cost balance can now be written as:

$$\sum c_{P,k} \dot{\Psi}_{P,k} = \sum c_{F,k} \dot{\Psi}_{F,k} + \dot{Z}_k \quad (13)$$

One indicator of exergoeconomic performance is the exergoeconomic factor,  $f$ . The exergoeconomic factor is defined as [11]:

$$f_k = \left( \frac{\dot{Z}_k}{c_{F,k} \dot{I}_{D,k} + \dot{Z}_k} \right) \quad (14-a)$$

Or,

$$f_k = \left( \frac{1}{\frac{c_{F,k} \dot{I}_{D,k}}{\dot{Z}_k} + 1} \right) \quad (14-b)$$

The exergoeconomic factor for a component indicates the ratio between the price of the component and the cost of exergy destruction by the component. A low value of  $f$  indicates a component with low initial cost and high exergy destruction cost. More money could be spent on a component with low  $f$  to improve the overall cost effectiveness of the system. On the other hand, a component with high  $f$  has very high component costs and low exergy destruction costs. Less money should be spent up front on a low- $f$  component to improve cost effectiveness of the system. The exergoeconomic factor can be calculated for each of the components in the system. The range of this indicator is between 0 and 1: If  $f$  is close to 0, the cost of irreversibilities is predominant (high value of 1, which is the sum of the irreversibilities and the exergy losses related to residue flows); when  $f$  is close to 1, the capital cost has greater influence. Generally,

in plants running on fossil fuels, a good compromise is reached when intermediate values occur [11] with the product for the overall system is given by:

$$\dot{C}_{P,tot} = \dot{C}_{net} + \dot{C}_4 \tag{15-a}$$

$$\dot{C}_{P,tot} = \dot{C}_1 + \dot{C}_f + \sum_k \dot{Z}_k \tag{15-b}$$

**8. Economic data**

Taking the operating cost equals to fuel and maintenance costs per year, and are given as 8418256\$ and 421230\$ respectively. Total number of hours of system operation per year is 8449 hours. The cost rate of fuel is 786\$/h, 926\$/h and 1153\$/h at 40%, 60% and 85% design load respectively. Table (1) shows the economic data for the unit GT14 (values labeled with \* are not available for the unit and typical values are taken from the literature, and are very close to real values).

**9. Results and Discussion**

The Excel Software is utilized to perform exergy and exergoeconomic analysis. The rate of exergy flow together with the input fuel exergy, compressor work, turbine work, and net power equal to 41 MW (40% design load), 62 MW (60% design load), and at 85MW (full operating load) are shown in Fig. 2. Better performance is obtained as the full operating load being approached, the analysis shows that the fuel exergy increases from 200.75MW at 40% design load to 301.06MW at full operating load, accordingly the exergy of the product of combustion at turbine inlet increases from 231MW to 305MW, and hence, turbine output increases from 37MW to 67MW. Since the unit runs more efficient at the full operating load, the compressor work decreases from 142.4MW at 40% design load to 140.15MW at full operating load, where the exergy of air leaving the compressor is kept a constant.

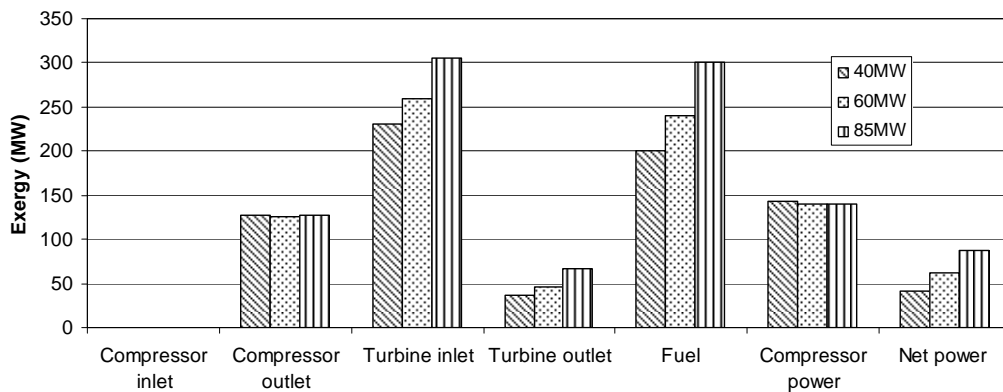


Fig. 2. Exergy flow rate at different loads.

Essentially, gas turbine power plants suffer from their low efficiency when compared with steam power plants. Fig. 3 shows that the exergetic efficiency increases from 20.54% at 40% design load to 29.12% at full operating load, and hence, the ratio of the total exergy destruction to fuel input exergy decreases from 61.03% at 40% design load to 48.63% at full operating load. Although Fig. 2 shows that exergy of the exhaust at the turbine outlet

increases from 39.4MW at 40% design load to 61.8MW at full operating load, it is found, as shown in Fig. 3, that the ratio of exergy loss with the exhaust gases to the input fuel exergy slightly increases from 18.43% to 22.25%, that mean, the performance of gas turbine power plants can be further enhanced by recovering the exergy of the exhaust gases.

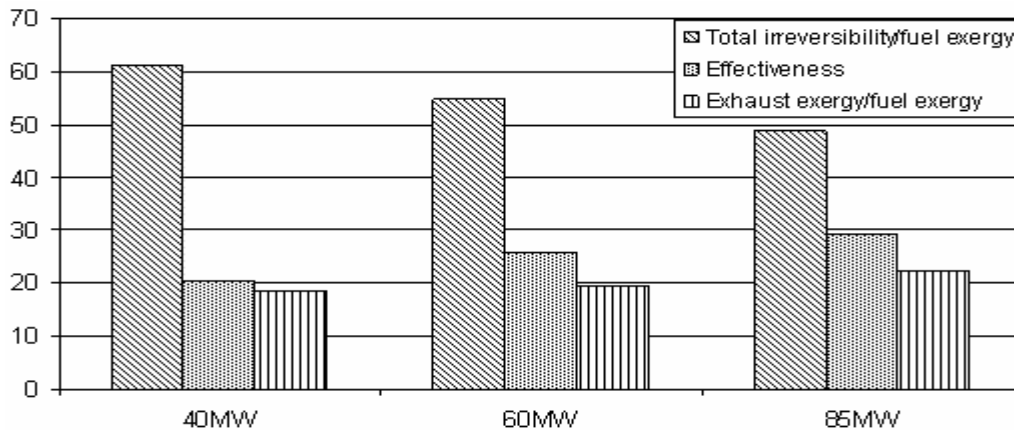


Figure 3. The Exergetic efficiency, the ratio of total Exergy destruction and the ratio of turbine outlet exergy relates the exergy fuel for the unit GT14, at different loads.

The rate of exergy destruction for the three main components is shown in Fig. 4. As expected, the exergy destruction in the combustion chamber presents the main contribution to the total exergy destruction; its value varies

from 97.28MW at 40% design load to 122.64MW at the full operating load. The contribution and the variation of exergy destruction with load are minor for the other two main components.

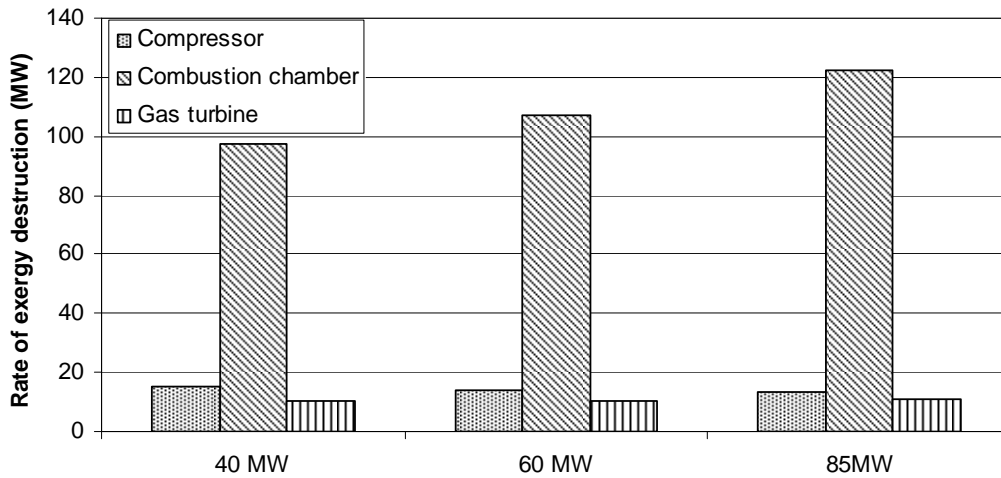


Figure 4. The rate of exergy destruction, at different loads.

Although, the rate of exergy destruction in the combustion chamber increases with the increase in the plant load and reaches great values, still the plant efficiency attains its largest value at the full operating load. The reason can be explained by take a look to Fig. 5, where the ratio of exergy destruction for the three main

components to input fuel exergy is shown. The analysis shows this ratio for the combustion chamber decreases from 48.46% at 40% design load to 40.73% for the full operating load, the same behavior is found for the other two components.

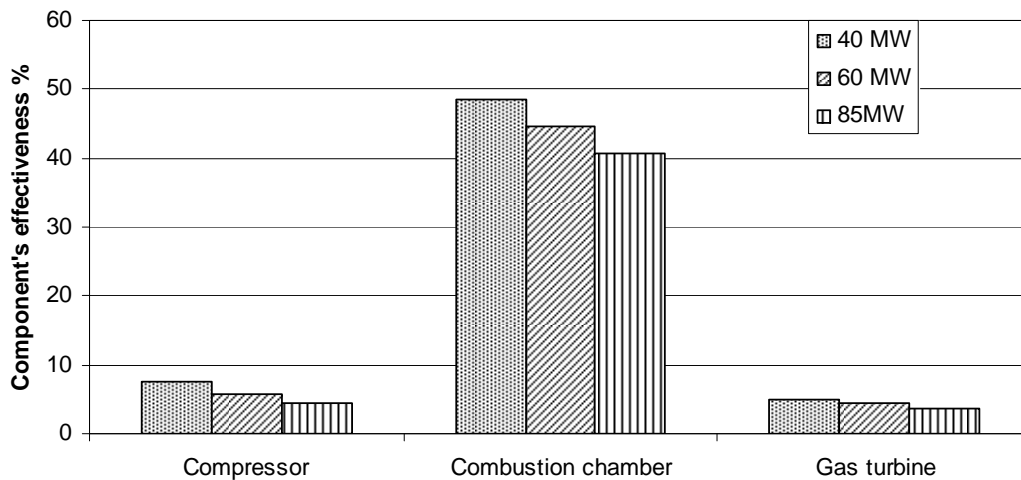


Figure 5. The Exergy destruction ratio, at different loads.

Exergoeconomic variables are evaluated for the plant components. The evaluation is based on the cost rates of the exergy streams. The average costs of the fuel per exergy unit of the fuel " $c_{F,k}$ ", the average costs of the product over exergy unit " $c_{P,k}$ ", the cost rate  $C_{D,k}$  associated with the exergy destruction, and the exergoeconomic factor  $f_k$  are illustrated. Those variables can be obtained only through a exergoeconomic analysis, while the cost rate associated with the capital investment and the operation and maintenance cost for each plant component  $\dot{Z}_k$  is obtained from the economic analysis.

The cost rate formation within the unit GT14 is shown in Fig. 6. It is obvious that the cost rate for the net power increases with the increase in the power output, it is found the cost rate for net power output increases from 1051\$/h at operating condition of 40% design load to 1383\$/h at full operating load. The analysis shows that the cost rate of fuel exergy increases from 804\$/h at 40% design load to 1205\$/h at full operating load, because the rate of fuel consumption increases with the load. Since the unit operates more efficient as the full operating load being approached, it is found the cost rate of exergy of the

product of combustion at turbine inlet decreases from 4979\$/h at 40% design load to 3961\$/h at full operating load, since the cost of the compressor work decreases from 3630\$/h at 40% design load to 2211\$/h at full operating load, and the cost rate of exergy of air leaving the

compressor decreases from 4130\$/h at 40% design load to 2710\$/h with the full operating load. The cost rate of total exergy loss decreases from 798\$/h at 40% design load to 868\$/h at full operating load.

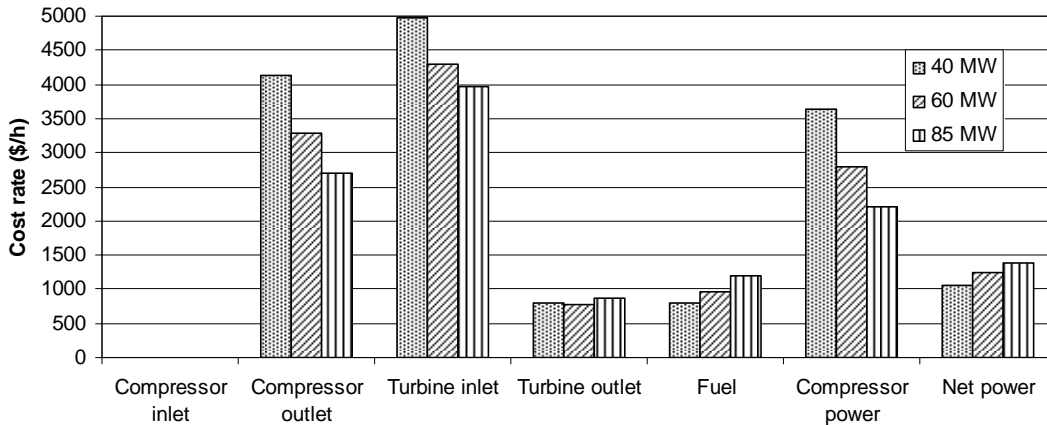


Figure 6. The cost rate formation within the unit GT14, at different load.

In Fig. 7, it can be seen that the average cost per unit exergy of the net power output and the average cost per unit compressor work input are equal (Product rule), and equals to 7.1\$/GJ at operating conditions of 40% design load, 5.5\$/GJ (60% design load), and at 4.4\$/GJ (full

operating load). The analysis shows that the cost per unit exergy of the total input fuel is constant for different loads and equals to 1.1\$/GH, since the specific fuel exergy (kJ/kmol) is constant and equals to 8061030 kJ/kmole.

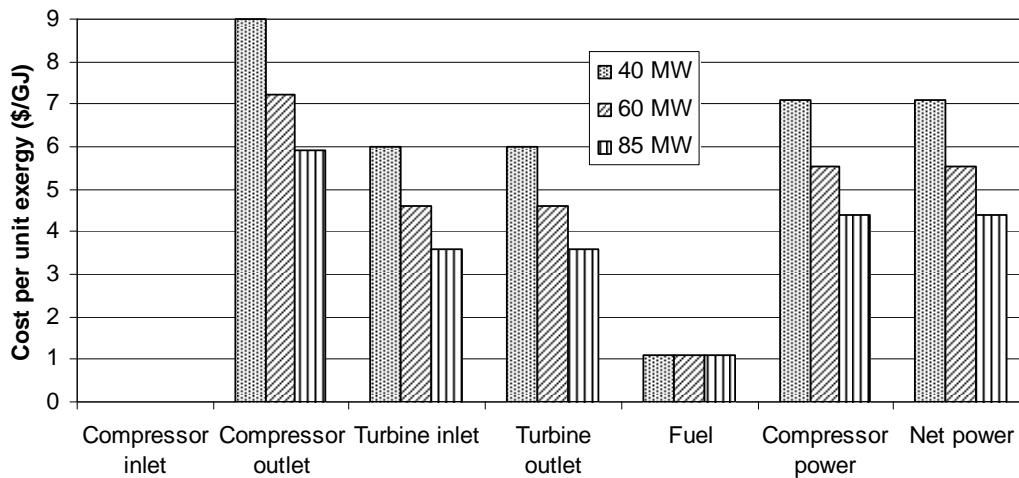


Figure 7. The specific costs per exergy unit for the streams the unit GT14, at different loads.

The cost associated with the removal of exergy for gas turbine is changing from 6 to 3.6\$/GJ (Fuel rule). Also the cost per unit exergy of air leaving the compressor decreases from 9\$/GJ at 40% design load to 6\$/GJ at full operating load. The cost per unit exergy for all streams in the system is a function of the plant efficiency, where the cost per unit exergy for all streams is decreasing with the increase of the second low efficiency of the plant.

The cost of exergy destruction for the three main components is shown in Fig. 8. As expected, the cost of exergy destruction in the combustion chamber presents the main contribution to the total cost of exergy loss; because the rate of exergy destruction in the combustion chamber

is much higher than that of the gas turbine and air compressor as shown in Fig. 4, its value varies in the combustion chamber from 1474\$/h at 40% design load to 1123\$/h at the full operating load. The contribution and the variation of cost of exergy destruction with load are lower for the other two main components. The cost of exergy destruction for each component decreases with the increase in load as a result of the decrease of the ratio of exergy flow rate with the load as shown in Fig. 5, and also because of the decrease of the cost per unit exergy of fuel with the load.

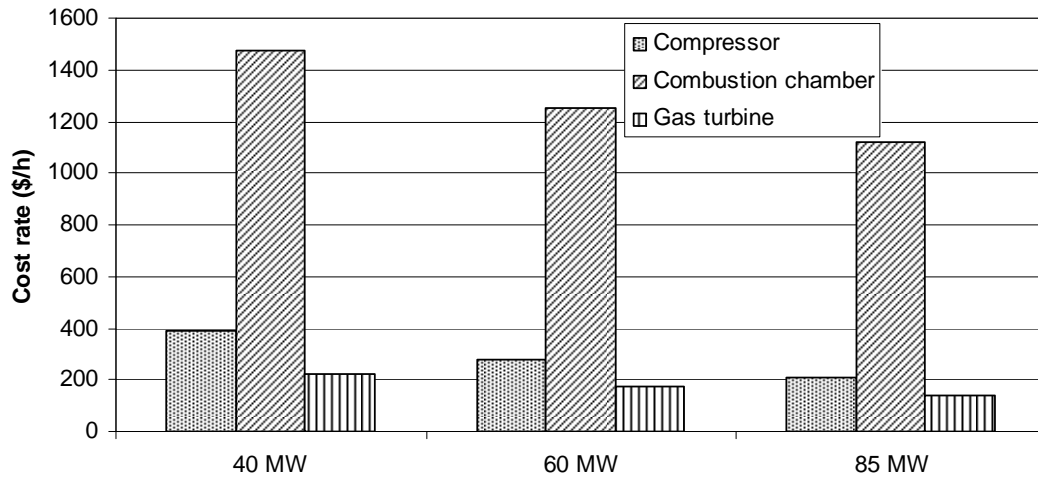


Figure 8. The Cost rate associated with Exergy destruction for the components the unit GT14, at different loads.

The exergoeconomic factor ( $f$ ) is used to identify the major cost source (capital investment or cost of exergy destruction). Fig. 9 shows the values of the exergoeconomic factor for the three main components. The lowest value of the exergoeconomic factor is found for the combustion chamber due to the high rate of exergy destruction compared to other components which as shown on the Fig. 3, its value varies from 3% at 40% design load to 3.9% at the full operating load. For air compressor, the value of the exergoeconomic factor varies

from 56.18% at 40% design load to 70.7% at the full operating load. The gas turbine has the highest value of exergoeconomic factor among all components; its value varies from 69.53% at 40% design load to 78.33% at the full operating load (the capital cost has the greater influence). Since the unit operates more efficient at the full operating load, the exergoeconomic factor increases as the full operating load being approached, since the cost of exergy destruction decreases with increasing load as shown in Fig. 8.

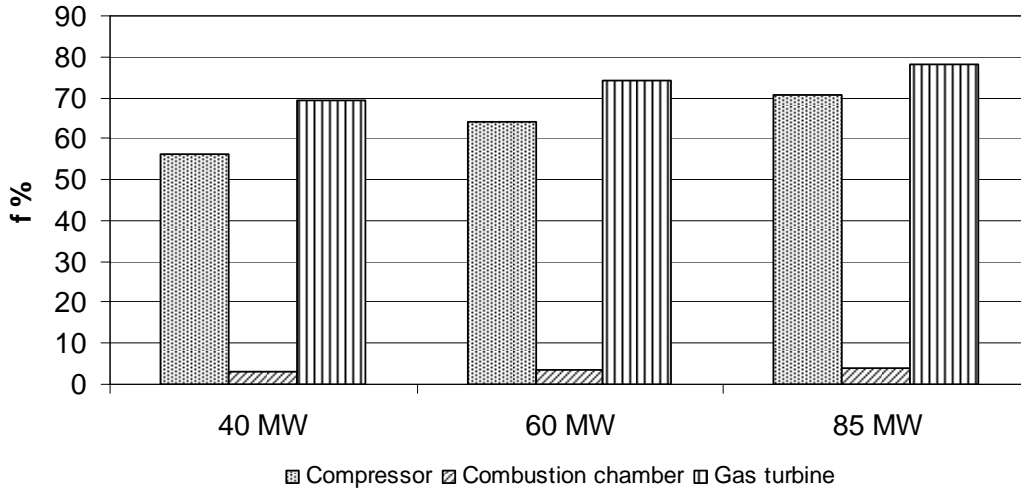


Figure 9. The Exergoeconomic factor  $f_k$  for the components the unit GT14, at different loads.

**10. Conclusions**

Exergoeconomic analysis is an effective tool used to evaluate the cost effectiveness of thermal systems, with the intent of evaluating and enhance the system performance from both economic and thermodynamics point of view. The analysis assists in the understanding of the cost value associated with exergy destroyed in a thermal system, and hence provides energy system's designers and operators

with the information, necessary for operating, maintaining, and evaluating the performance of energy systems.

Exergoeconomic analysis is performed for the unit GT14 of south Tripoli gas turbine power plant. The following conclusions are drawn:

1. The cost of each product generated by unit GT14 is calculated, and the cost formation process and the flow of costs in the system are analyzed.
2. The average cost per unit exergy for final products of the plant is identified (net power).

3. The combustion chamber has the highest cost value of exergy destruction among all components and has the lowest value of the exergoeconomic factor  $f$ .
4. Exergoeconomic analysis shows that unit GT14 attains its maximum performance at the full operating load.
5. As  $f$  factor decreases with the increasing load, part load operation must be minimized as much as possible.
6. Exergoeconomic analysis is a powerful tool that can be adopted for the performance evaluation of different thermal systems in Libya.

## References

- [1] G. Tsatsaronis, L. Lin, and J. Pisa, "Exergy Costing in Exergoeconomics". *Journal of Energy Resources Technology*, vol. 115, 1993, 9-16.
- [2] A. Agazzani, A. F. Massardo, "A Tool for Thermoeconomic Analysis and Optimization of Gas, Steam, and Combined Plants". *Journal of Engineering for Gas Turbines and Power*, Vol. 21, 1990.
- [3] G. Tsatsaronis, "Thermoeconomic Analysis and Optimization of Energy Systems". *Prog. Energy Combust. Ser.*, Vol. 19, 1993, 227-257.
- [4] Y. M. EL-Sayed, A. J. Applenc, "Application of the Thermoeconomic and Optimization of a Vapor Compression Desalting System". *Journal of Engineering Power*, 1970, 17-26.
- [5] M. A. Badar, S. M. Zubair, and A. A. AL-Farayedhi, "Second Law Based Thermoeconomic Optimization of a Sensible Heat Thermal Energy Storage System". *Energy*, Vol.18, 1993, 641-649.
- [6] M. A. Badar, S. M. Zubair, "On Thermoeconomics of a Sensible Heat, Thermal Energy Storage System". *Journal of Solar Energy Engineering*, Vol. 117, 1995, 255-259.
- [7] A. S. Nafey, H. E. S. Fath, and A. A. Mabrouk, "Thermoeconomic Analysis of Multi Stage Flashthermal Vapor Compression (Msf-Tvc) Desalination Process". Tenth International Water Technology Conference, IWTC10, Alexandria, Egypt, 2006.
- [8] L. Ozgener, A. Hepbasli, I. Dincer, M. A. Rosen, "Exergoeconomic Modeling of Geothermal District Heating Systems for Building Applications". Ninth International IBPSA Conference, Montréal, Canada, 2005.
- [9] J. Buchgeister, R. Castillo, "Thermoeconomic Analysis of electricity production via SOFC with integrated allothermal biomass gasification". Life Cycle Management Conference- Energy Efficiency, Zürich, 2007.
- [10] G. Tsatsaronis, L. Lin. "On Exergy Costing in Exergoeconomics", In: *Computer-Aided Energy Systems Analysis*, American Society of Mechanical Engineers, New York, AES-Vol.21, 1990.
- [11] A Lazzaretto, G. Tsatsaronis, "On the Calculation of Efficiencies and Costs in Thermal Systems". In: *Proceedings of the ASME Advanced Energy Systems Division*, AES-Vol.39, 1999.
- [12] Kenneth Jr W, *Advanced Thermodynamics for Engineers*, International addition. New York: McGraw-Hill, Inc.; 1995.

### Appendix

Table A-1: The thermodynamic data of the plant.

State	40%			60%			Full operating load		
	m <sup>·</sup>	P	T	m <sup>·</sup>	P	T	m <sup>·</sup>	P	T
	Kg/s	bar	K	Kg/s	bar	K	Kg/s	bar	K
1	422.32	1.023	299.75	404.31	1.023	301.3	394.48	1.023	303
2	422.32	9.8	635.45	404.31	10.4	644.10	394.48	11.0	655.90
3	426.554	9.8	1029.15	409.371	10.4	1129.0	400.829	11.0	1263.0
4	426.554	1.023	621	409.371	1.023	681.0	400.829	1.023	762.0
Fuel	4.234	12	298	5.061	12	298	6.349	12	298

Table A-2: The exergy balance of the unit GT14 components.

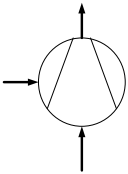
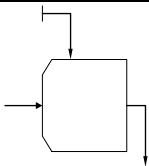
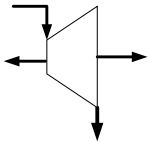
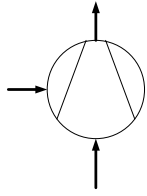
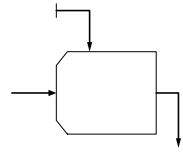
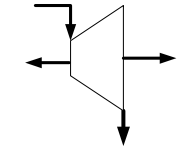
component	Schematic	Exergy balance	Additional information
Air Compressor (AC)		$\Psi_1 + W_C = \Psi_2 + I_{D,AC}$	Air supplied at zero exergy $\Psi_1 = 0$ $\Psi_P = \Psi_2 - \Psi_1$ $\Psi_F = W_{AC}$
Combustion chamber (CC)		$\Psi_{fuel} + \Psi_2 = I_{D,CC} + \Psi_3$ $\frac{W_{fuel}}{LHV} \cong 1.033 + 0.0169 \frac{b}{a} - \frac{0.0698}{a}$	$\Psi_P = \Psi_3$ $\Psi_F = \Psi_3 + \Psi_2$
Gas turbine (GT)		$I_{D,GT} = \Psi_3 - \Psi_4 - W_{GT}$	$\Psi_P = W_{GT}$ $\Psi_F = \Psi_3 - \Psi_4$

Table A-3: The cost balance and auxiliary equation of the plant components

component	Schematic	Cost balance	Additional information
Air Compressor (AC)		$C_1 + C_{AC} - C_2 + Z_{AC} = 0$	Air supplied at zero cost $C_1 = 0$ $C_F = \left( \frac{C_{AC}}{W_{AC}} \right)$ $C_P = \left( \frac{C_2}{\Psi_2} \right)$
Combustion chamber (CC)		$C_2 + C_{Fuel} - C_3 + Z_{CC} = 0$	Combustion process in the chamber is complete, auxiliary equations are not required $C_P = C_3$ $C_F = \left( \frac{C_{Fuel} + C_2}{\Psi_{Fuel} + \Psi_2} \right)$
Gas turbine (GT)		$C_3 - C_{net} - C_{AC} + Z_{GT} = 0$	One auxiliary equation required $C_P = \left( \frac{C_{AC} + C_{net}}{W_{AC} + W_{net}} \right)$ $C_F = \left( \frac{C_3 - C_4}{\Psi_2 - \Psi_4} \right)$

1

Table 1: Economic Data for the unit GT14.

Component	PEC* (10 <sup>3</sup> \$)	Z <sup>OM</sup>	Z <sup>CI</sup>	Z
Combustion Chamber	264	43	$C_f$ 2.17	48
Gas Turbine	2916	477 2	24	501
Air Compressor	2913	476	24	500 3

# Total Productive Maintenance Review and Overall Equipment Effectiveness Measurement

Osama Taisir R.Almeanazel

*Department Of Industrial Engineering, Hashemite University, Zarqa, 13115 Jordan*

## Abstract

This paper will review the goals and benefits of implementing Total Productive Maintenance, and it will also focusing on calculating the overall equipment effectiveness in one of Steel Company in Jordan, and it also discuss what called the big six losses in any industry (the quality, availability and speed). A case study taken from Steel Company in Jordan, the data taken along fifteen working days and teams formed in period of two months to find out the benefit of formation a multidiscipline team from different department to eliminate any boundaries between the departments and make the maintenance process more effectively, labors on the production line also included in way to adopt the autonomous maintenance operations (daily maintenance). As a result the company achieved 99% in quality factor of overall equipment effectiveness equation and 76% in availability where in performance it got 72%. Set of techniques like Single minute exchange die, computer maintenance management system, and production planning were suggested to the industry after calculating the OEE to improve their maintenance procedures and improve the productivity.

© 2010 Jordan Journal of Mechanical and Industrial Engineering. All rights reserved

Keywords: TPM; Total Productive Maintenance; Overall Equipment Effectiveness

## 1. Introduction

In the last few years the maintenance was traditional activities where all companies applying it without knowing its importance, but after the improving in production strategies and improve the flexibility of production line to produce a wide range of different products, the need for good maintenance strategy becomes bigger, and in the present times especially, because of automation and large-scale mechanization, higher plant availability, better product quality and long equipment life had assumed considerable significance [1]. Now many companies have shifted their focus to optimize their assets, and use equipments more effectively, and one of the main parts of the company which has a strong influence on the assets is the maintenance department or the employees responsible for maintenance [2]. The main idea behind the maintenance is to make the parts and machine ready to do what are required within the time and sizes allocated and do it with fewer amounts of resources.

Total productive maintenance (TPM) is new maintenance strategy developed to meet the new maintenance needs, TPM is an American style of productive maintenance which has been modified and improved to fit in the Japanese industrial environment. Now it is popular in Japanese industry and in other western

countries [3]. It is closely tied to JIT (Just in Time) and TQM (Total Quality Management) and it is extension of PM (preventive maintenance), where the machines work at high productivity and efficiency, and where the maintenance is all employee responsibility, and focus to prevent the problem before it may occurs [4].

Bamber (1998) presents the definitions of TPM in his review about the literature of TPM he present two definitions the first one depend on the Japanese approach and the other depend on western approach. The Japanese approach to TPM is considered to be that a full definition which contains five main points:

1. To use the equipment more efficiently.
2. It establishes a total preventive maintenance system.
3. It requires a full participation from all department operator (equipment operator, designer, and departments workers)
4. It involves everyone in the company shop floor to the top management.
5. It promotes and implements preventive maintenance based on autonomous, small group activities.

Nakajima (1988) summarized these five points in briefly defining TPM as "Productive maintenance involving total participation in addition to maximizing equipment effectiveness and establishing a through system of PM" where PM is a comprehensive planned maintenance system.

In the UK TPM has been pioneered by Edward Willmott (1997), the managing director of willmott

\* Corresponding author. bd59pv@student.sunderland.ac.uk

Consulting Group, acknowledges the five point of the which being considered definition the Japanese approach to TPM and consequently accepts this as being an accurate and true reflection of the main principles; however he provides a definition that is more suited to Western manufacturing and which is:

*"TPM seeks to engender a company-wide approach towards achieving a standard of performance in manufacturing, in terms of the overall effectiveness of equipment, machines and processes, which is truly world class"*

Another US advocate of TPM, Wireman (1991) suggests that TPM is maintenance that involves all employees in the organization and accordingly includes everyone from top management to the line employee and indicates:

*". . . it encompasses all departments including, maintenance, operations, facilities, design engineering, project engineering, instruction engineering, inventory and stores, purchasing, accounting finances, plant /site management"*

There are many different definitions for TPM and the reason behind this diversity in definition is found in the way of adoption this strategy, some industries focus on the group working more than equipment management, and other focus on equipment effectiveness, this diversity shows how important implementing TPM in company that it is covers all factors may affect the production process [5].

## 2. TPM Goals

TPM seeks to minimize all the potential losses in the production and to operate equipment with full design capability. TPM also take the quality in consideration by making a zero product defect rate, which means no production scrap or defect, no breakdown, no accident, no waste in the process running or changeover [6]. TPM can be defined by considering the following goals:

1. **Improving equipment effectiveness.** This mean looking into the six big losses which divided from three main losses:
  - a. Down time losses: classified as Equipment breakdowns and, Setup and adjustment slowdowns.
  - b. Speed losses: which can be found as Idling and short-term stoppages and Startup/restart losses.
  - c. Defects or Quality losses: every thing about Scrap and rework and Startup losses.

And finding what causes these losses and starts the improvements process. The idea is to make the equipment work as it should be working always and produce as much as it supposed to produce, you cannot accept that you producing less than any one else has the same equipment and you should always seek for the best performance at all [2].

- d. Involving operators in daily maintenance, this means to achieve autonomous maintenance where the workers who operate the equipment are allowed to take responsibility for some of maintenance activities [7] such as:
  - Repair level: Here the operators take the action to repair the machine according to given structure paper.

- Preventive level: the operator will take a corrective action to prevent the problems.
- Improvement level: the operator will be uncharged in any improvement strategy; moreover he will take the corrective action too on the problems when occurred.
  - e. Improving maintenance efficiency and effectiveness, this mean having a systematic approach to all maintenance activities. This involves the identification of the nature and level of preventive maintenance required for each piece of equipment, the creation of standards for condition-based maintenance, and the setting of respective responsibilities for operating and maintenance staff. The respective roles of "operating" and "maintenance" staff are seen as being distinct. Maintenance staff are seen as developing preventive actions and general breakdown services, whereas operating staff take on the "ownership" of the facilities and their general care. Maintenance staffs typically move for more facilitating and supporting role where they are responsible for the training of operators, problem diagnosis, and devising and assessing maintenance practice [2].
  - f. Educating and training personnel, this task is one of the most important in the TPM approach; it involves everyone in the company: Operators are taught how to work on their machines and how to maintain them properly. Because operators will be performing some of the inspections, routine machine adjustments, and other preventive tasks, training involves teaching operators how to do those inspections and how to work with maintenance in a partnership. Also involved is training supervisors on how to supervise in a TPM type team environment.
  - g. Designing and managing equipment for maintenance prevention. Equipment is costly and should be viewed as a productive asset for its entire life. Designing equipment that is easier to operate and maintain than previous designs is a fundamental part of TPM. Suggestions from operators and maintenance technicians help engineers design, specify, and procure more effective equipment. By evaluating the costs of operating and maintaining the new equipment throughout its life cycle, long-term costs will be minimized. Low purchase prices do not necessarily mean low life-cycle costs [2].

## 3. Six Big Losses

One of the major goals of TPM and OEE is to reduce or eliminate what are called the six big losses which they are the most common causes of efficiency loss in manufacturing. The link of the losses and the effectiveness in TPM is defined in terms of both the quality of the product and the equipment availability. Any operation time may face losses and these losses can be visible like scrap, changeovers and breakdowns or invisibles such as the slow running, the frequent adjustment to maintain the production within tolerance, Nakajima summarised the loss in a six big losses as following:

- Downtime Losses:

It found if the output is zero and the system produces nothing, where the unused segments of time, during the examined period are downtime losses, and mainly it can be one of two:

2. Breakdown losses this loss is due to parts failure where they cannot work any more and they need either repair or replace. These losses are measured by how long it takes from labor or parts for fixing the problem.
3. Setup and adjustment time, These losses are due to the changes in the operating conditions, like the start of the production or the start of the different shifts, changes in products and condition of the operation. The main examples of this kind of losses are equipments changeovers, exchange of dies, jigs and tools. These losses consist of setup, start-up and adjustment down times.

- Speed Losses:

When the output is smaller than the output at references speed these are called speed losses. When considering speed losses, one dose not check if the output conforms to quality specifications. This can be found in two forms:

Minor stoppage losses these losses are due to the reason of machine halting, jamming, and idling. Many companies are considering these minor stoppages as the breakdowns in order to give importance to this problem [8].

1. Speed losses these losses are due to the reduction in speed of the equipment. In other words the machine is not working at the original or theoretical speed. If the quality defect and minor stoppages occurs regularly then the machine is run at low speed to cover the problems. It is measure by comparing the theoretical to actual working load.

- Defect or quality losses:

The produced output either dose or dose not confirm to quality specifications. If it dose not comply, this is consider a quality loss.

1. Rework and quality defects; these losses are due to the defective products during the routine production. These products are not according to the specifications. So that rework is done to remove the defects or make a scrap of these products. Labor is required to make a rework which is the cost for the company and material become a scrap is also another loss for the company. The amount of these losses is calculated by the ratio of the quality products to the total production.
2. Yield losses these losses; are due to wasted raw materials .The yield losses are split into two groups. The first one is the raw materials losses which are due to the product design, manufacturing method etc. The other group is the adjustment losses due to the quality defects of the products which are produced at the start of the production process, changeovers etc.

#### 4. Overall Equipment Effectiveness

OEE is a result can be expressed as the ration of the actual output of the equipment divided by the maximum output of the equipment under the best performance condition. The Overall Equipment Effectiveness was originated from the Total Productive Maintenance practices, developed by S.Nakajima at the Japan Institute of Plant Maintenance, the aims of TPM is to achieve the ideal performance and achieve the Zero loss [8] which means no production scrap or defect, no breakdown, no accident, no waste in the process running or changeover. The quantification of these accumulations of waste in time and its comparison to the total available time can give the production and the maintenance management a general view of the actual performance of the plant. And it can help them to focus the improvement on the bigger loss.

##### 4.1. OEE Calculation

OEE is equal to the multiplication of the three main bases for the main six big losses:

1. Availability indicates the problem which caused by downtime losses.
2. Performance indicates the losses caused by speed losses and
3. Quality indicates the scrap and rework losses.

$$OEE = \text{Availability} \times \text{Performance rate} \times \text{Quality rate} \quad (1)$$

##### 4.1.1. Availability

The availability is calculated as the required availability minus the downtime and then divided by the required availability. This can be written in the form of formula as

$$\text{Availability} = ((\text{Required availability} - \text{Downtime}) / \text{Required availability}) * 100 \quad (2)$$

The required availability can be defined as the time of production to operate the equipment minus the other planned downtime like breaks, meetings etc. The down time can be defined as the actual time for which the equipment is down for repairs or changeovers. This time is also some times known as the breakdown time. The output of this formula gives the true availability of the equipment. This value is used also in the overall equipment effectiveness formula to measure the effectiveness of the equipment.

##### 4.1.2. Performance

The performance rate can be defined as the ideal or design cycle time to produce the item multiplied by the output of the equipment and then divided by the operating time. This will give the performance rate of the equipment. The formula to calculate the performance rate can be expressed as

$$\text{Performance rate} = ((\text{design cycle time} * \text{output}) / \text{Operating time}) * 100 \quad (3)$$

The design cycle time or the production output will be in the unit of production, like parts per hour and the output will be the total output in the given time period interval.

The operating time will be the availability value of the availability formula. The result of this formula will be in the percentage of the performance of the equipment.

#### 4.1.3. Quality

The quality rate can be expressed as the production input into the process or equipment minus the volume or number of quality defects then divided by the production input. The quality rate can be expressed in a formula as

$$\text{Quality rate} = ((\text{production input} - \text{quality defects}) / \text{Production input}) * 100 \quad (4)$$

The production input mean that the unit of product being feed into the production process. The quality defects mean the amount of products which are below the quality standards i.e. the rejected items after the production process. This formula is very helpful to calculate the quality problems in the production process [9].

### 5. Case Study

Steel company has been taken as case study this company is applying restricted quality inspection system in addition it has ISO 9001:2000 in 2005. The study conducted along 15 days, the company produces different type of steel and used different types of plate. In the industry the production is continues there is only three main workstation the oven and the failure in this workstation is very low and the maintenance is applied regularly, the second workstation is the dies and cutting station this is form one single workstation, and the third workstation is the cooling bed. In second workstation most failure probably occurred. The company has an old record for the previous maintenance work on the production line, and the time loses that are observed in the production process in the first 15 working days in September 2007 will be recorded. There are some standard from the industry:

- ✓ Establishing time (starting of production until stabilization), this time vary between 15 – 40 minute for the chosen operation.
- ✓ Setup time (alteration of product in the production line and enhancement until smooth flow of operation), the setup time is depend on how many dies or machine will installed on the line, and this time is mostly calculated in the second shift (Shift B), in general it is between 1 – 2 hour.

- ✓ The product time process, the production line can operate at speed of 60 plates per hour, this speed is theoretical speed.
- The downtime caused by failure, all downtime for 15 operating days have been recorded, the industry work two shifts each shift ten hours ( shift A from 7:00 to 17:00, Shift B 20:00 to 6:00).
- The production line speed (real) that will be matched up to that given by the producer (nominal), the nominal speed for the production is 60 tons per hour, and the real speed will calculated for each day.
- The number of products that need revising and the worthless products (scrap), the rework product is almost negligible because there is no rejected product happened during the study period, and according to record there is very low amount of rework operation happened. The scrap is happened in big number each operation there is 0.7 m of the extracted plate goes to scrap and any malfunction machine or breakdown there is scrap recorded.
- Time lost from the small blockages of machines (i.e. blocking pans) that are simply fixed. The previous points are documented with the cooperation of the operator's equipment.
- The operators are Knowledgeable and skilled for the expressions that is used and the significance of accuracy of measurements.

In table 1 and 2 the data taken direct from the production line for shift A and shift B, the batch size is the amount of tons the company starts the production with, the amount of scrap is the amount of defective steel caused by breakdown or malfunction failure. The speed is taken for the period of operating. For example lets take shift A in day number 10 the batch size is 51 tons and the maximum speed of production is 1 ton per min, so the expected time to produce the batch is 51 min, but there is some amount of time waste for several reason and that time was 104 min, so the real time required to produce the 51 tons of steel in that day was 155 min and the speed was (51 tons/ 155 min = 0.3 tons/min). The shift time is 10 hour (600 min) in day number 10, the operation was only for 2.58 hours and the rest was off, this time (the rested time) is not considered in the study because they are not operating time and there is nothing about the maintenance.

Table 1. the downtime and amount of scrap for the First 15 operating days in September 2007 for shift A.

Days	1	2	3	4	5	6	7	8	9	10	11	12	13	14	15
Downtime (min)	62	226	80	92	66	28	121	257	202	104	184	278	280	91	111
Scrap (ton)	0	2	1	0.5	1.25	0	1	3.75	1	2	0	4.3	4.5	3	3.5
Batch size (ton)	402	393	281	402	464	335	447	475	505	51	452	285	425	486	254

Table 2. the downtime and amount of scrap for the First 15 operating days in September 2007 for shift

Days	1	2	3	4	5	6	7	8	9	10	11	12	13	14	15
Downtime (min)	36	85	172	39	160	33	28	58	44	108	102	219	68	100	163
Scrap (ton)	0	0	2.3	1	0	0	0	0	1	3	0.5	0	0.3	1.25	3.5
Batch size (ton)	393	281	402	464	335	447	475	505	51	452	285	425	486	254	391

Table 3. the total downtime and amount of scrap for the First 15 operating days in September 2007

Days	1	2	3	4	5	6	7	8	9	10	11	12	13	14	15	total
Downtime (min)	98	311	252	131	226	61	149	315	246	212	286	497	348	191	274	3597
Scrap (ton)	0	2	3.3	1.5	1.3	0	1	3.8	2	5	0.5	4.3	4.8	4.3	7	40.8
Batch size (ton)	795	683	799	922	556	737	911	645	646	662	552	135	438	555	450	9486
Production (ton)	795	681	795.7	920.5	554.7	737	910	641.2	644	657	551.5	131	433.2	550.7	443	9445.2

### 5.1. Calculating OEE

The next step after collecting the data is to measure the OEE which will give an indication of where we may find the error or the weakness point, the calculation of OEE will depend on 4 main equations the first one used to calculate the availability and from the table 2 and 3 we can find out how much time the line was down and how much is the operating time and then we can use the equation (2) to find out the availability of the production line. The study was taking during 15 days in September 2007, all the days were normal working days and the holidays and weekends are not considered in the study; but if we want to calculate them there were 4 weekend days only which extend the study period to 19 days, so the theoretical operating time will be 19 days \* 24 hours/days = 456 hours, and the available operating time will be 19 days - 4 days = 15 days. And there are two shifts only with 10 working hours per shift which make the available operating time equal to 15 days \* 2 shift/day \* 10 hours/shift = 300 hours. And there is stoppage/pause one hour per day for 1 hour, which gives in total 15 hours 300 - 15 = 285 hours available operating time.

#### 5.1.1. The Availability Factor

Total downtime is equal to 59.95 hours as shown in table 4, for the 1<sup>st</sup> 15 operating days, the valuable operating time for the 15 days will be calculated by adding the amount of theoretical time needed to produce the batch size to the amount of down time. We know that the time needed to produce one ton is one minute, so the total time needed to produce the whole batch for 15 days is equal to 158 hours (9486 tons \* 1 hour/ 60 tons = 158.1 hours), and with addition

To the amount of downtime equal 59.95 hours that gives 158.1 hours + 59.95 hours = 218.05 hours valuable operating time.

Availability = valuable operating time / available operating time  
Availability = 218 hours / 285 hours = 0.76 = 76%

#### 5.1.2. The Performance Factor

To calculate the performance we need two main factors, the first one is the designed cycle time and we know that design cycle time is 60 ton/hour, and the total

output is 9445.2 ton by applying the performance equation we will get the following results

$$\text{Performance rate} = ((\text{design cycle time} * \text{output}) / \text{Operating time}) = (1\text{min/ton} * 9445.2 \text{ ton}) / (218 * 60) = 0.72 = 72\%$$

#### 5.1.3. The Quality Factor

To calculate the quality factor we need the total amount of defect and scrap for the 15 operating days and we find it from the table 4, total scrap or defect amount is 40.8 tons and the total batch size is 9486 tons, and the quality factor is

$$\text{Quality rate} = ((\text{production input} - \text{quality defects}) / \text{Production input}) * 10 = (9486 \text{ tons} - 40.8 \text{ tons}) / 9486 \text{ tons} = 0.996 = 99.6\%$$

#### 5.1.4. The Overall Equipment Effectiveness

After we got the three main factors we can now calculate the overall equipment by using the following equation

$$\text{OEE} = \text{Availability} * \text{performance} * \text{Quality} = 0.76 * 0.72 * 0.996 = 0.55 = 55\%$$

The world class manufacturing OEE is 85%, and the best OEE score in the company was calculated by the machines designer and it was 72%, the equipment effectiveness is reduced by 17%.

### 5.2. Implementation TPM Strategy

The company was motivated to implement TPM to cope with the new market need and to increase their production performance to the international level, and the willing to eliminate the waste which don't add value to the production like waste of time and waste of material. The first initiative was towards to increase the quality, by implementing good quality inspection system and monitoring, and that was through the creation of the quality improvement team also train employees to identify the problems related to the quality and causes, and use the data for a continuous improvement. As the result the steel company reach ISO 9001:2000 by 2005.

Launch autonomous maintenance tasks in the aim to setup and adjust the equipments, inspecting the equipments while cleaning it and checking the machine bolt tightness. The creation of multidisciplinary teams involving all the departments, even the supplier is invited to the meeting to discuss the quality of the raw material supplied. There was

a creation of three teams, the first team called SBU solve problem unit its job is to identify and resolve a problem if it occurs in the plant, and record in the 'Gap list' if it is not solved means the gap not closed. The second team which is the focus team take the problem in charge; this team solve it at a systematic level. This team is responsible as well for the evaluation of the equipments and the processes and set up an optimum practice to eliminate any losses and ensure the continuous improvement. The third team involve all the managers and the heads of department in the objective is to plan a safe and profitable strategy for the entire productivity journey.

## 6. Discussion

In Jordan Steel Company they never thought to have system which calculates their performance while they have a standard OEE since the installation of the line. But without calculated it we can not improve it, we saw the performance of the company as overall equipment effectiveness is 55%, where the availability of the line was 76% of the production time and the performance was 72% while the quality factor is 99.6%. Table 5 shows the comparison between world class measurement and the company measurement.

Table 4. the comparison between WCM and company

	OEE company	OEE world class
Availability	76%	90%
Performance	72%	95%
Quality	99%	99%

As we see from the table 4 the company achieved the world class quality factor, and as presented above the company had ISO 9001:2000 certificate in 2005, and they are applied a strong quality measurement and inspection system start from the raw materials inventory to the work in process finished with finish goods inventory. But the company needs to work hard to improve their system machines and reduce the waste time.

## 7. Conclusion

By implementing the TPM strategy they can eliminate most of the waste happened like the time waste while changeover or the downtime losses, with this maintenance strategy the responsibility of maintain the equipment is all operator and engineering responsibility, there will be no more "his or my" fault the break down will be solved as fast as possible. The operator in the shop floor should involve in each maintenance operation because he is the one close to the machine and he know what are the abnormality of the machine.

There are three main techniques will have a very good impact to improve the production line and make the

maintenance process more effectively, CMMS, production planned, and SMED, those techniques will help the company to operate at high rate of performance without losses.

The project gives new huge step to the company in calculation the performance and how they can focus on the problems, when we formed a group from each department the company got a chance to see how the team work is important in solving the problem. Another benefit of the project is to give them the chance to know what the best techniques that they can apply which will improve their performance. Calculating the OEE also give the company where they are and where is the weakness point and how to improve.

## References

- [1] Rajiv Kumar Sharma, Dinesh Kumar and Pradeep Kumar, "Manufacturing excellence through TPM implementation: a practical analysis", *Industrial Management & Data System*, Vol. 106 No. 2, 2006, 256-280.
- [2] Terry Wireman, *Total Productive Maintenance*, 2<sup>nd</sup> edition, 2004.
- [3] Muhammad Shahid Tufail, *Investigation of the ways to improve the performance of a plant*, Växjö University School of Technology and Design, 2007, <http://www.vxu.se/td>.
- [4] Heinz P. Loch, "Improving machinery reliability", 1998.
- [5] C.J. Bamber, P. Castka, J.M. Sharp, Y. Motara, "Cross-functional team working for overall equipment effectiveness (OEE)" *Journal of Quality in Maintenance Engineering*, Volume 9 Number 3, 2003, 223-238.
- [6] Nich, Rich 'total productive maintenance: lean approach', 1999, Tudor Business limited.
- [7] E. Nadarajah, M. Sambasivan, S. Yahya, "Autonomous Maintenance – An Effective Shop-Floor Tool to Improve Productivity, Institute of Technology Management and Entrepreneurship Kolej Universiti Teknikal Kebangsaan Malaysia, 2006.
- [8] Nakajima S., *Introduction to TPM*, productivity press, Portland, 1988.
- [9] Mobley R. K, *An introduction to maintenance*, 2nd ed, USA, 2002.
- [10] Bamber, "Factors affecting successful implementation of total productive maintenance", MSc Research Dissertation, University of Salford, 1998.
- [11] C.J. Bamber, J.M. Sharp and M.T. Hides, "Factors affecting successful implementation of total productive maintenance A UK manufacturing case study perspective", *Journal of Quality in Maintenance engineering*, Vol. 5 No. 3, 1999, 162-181.
- [12] Wireman T, *computerized maintenance management systems*, 1994, 2nd ed, New York, USA.
- [13] Willmott, P, *TPM: Total Productive Maintenance: The Western Way*, Butterworth-Heinemann, 1997, Oxford.

# Effect of EGR on Performance and Emission Characteristics of Natural Gas Fueled Diesel Engine

S.K. Mahla <sup>a,\*</sup>, L.M. Das <sup>b</sup>, M.K.G. Babu <sup>b</sup>

<sup>a</sup> Department of Mechanical Engineering, KC College of Engineering & Information Technology, Nawanshahr-144514, Punjab, India

<sup>b</sup> Centre for Energy Studies, Indian Institute of Technology Delhi, Hauz Khas, New Delhi-110016, India

## Abstract

In diesel engines, it is difficult to reduce both smoke and NO<sub>x</sub> simultaneously. An experimental study was conducted to determine the performance and exhaust emission characteristics of a commercial single cylinder, natural aspirated, air cooled DI diesel engine. The system was modified to work on either dual fuel or diesel alone. The objective of this work is to investigate the possibility of decreasing the exhaust emissions and to determine the performance parameters. At part loads, the dual fuelled operation suffers from higher CO and unburnt hydrocarbon emissions. This is mainly due to overall lean mixture and incomplete combustion because of small quantity of pilot fuel. To resolve these problems, the effects of cooled EGR were investigated. The experimental results show that the application of EGR reduces substantially NO<sub>x</sub>, CO and smoke. Results indicate that performance parameters are comparable with baseline diesel operation.

© 2010 Jordan Journal of Mechanical and Industrial Engineering. All rights reserved

Keywords: NO<sub>x</sub> ; CNG; Dual Fuelled; EGR; Flame Speed.

## Abbreviations

CNG	Compressed Natural Gas
BMEP	Brake Mean Effective Pressure
LPM	Litre per minute
EGR	Exhaust Gas Recirculation
U.B.H.C.	Unburned Hydrocarbon
CO	Carbon Monoxide
NO <sub>x</sub>	Oxides of Nitrogen
BTDC	Before Top Dead Centre
DI	Direct Injection
CO <sub>2</sub>	Carbon Dioxide
O <sub>2</sub>	Oxygen
MINTAKE	Mass of intake Charge
MEGR	Mass of EGR

## 1. Introduction

The concept of using alternative gaseous fuel in diesel engines has gained worldwide attention. Increasing petroleum fuel prices and their deterioration to environment led to the search for alternative fuels from past several years. CNG is one such fuel available in large quantities in many parts of world at attractive prices. It is a clean burning fuel as compared to the conventional liquid fuels like diesel or gasoline.

The use of CNG in diesel engine has both economic and environmental advantages [1]. Further CNG give higher resistance to knock which makes it possible to utilize in engine having higher compression ratio. Its self ignition temperature is 730<sup>0</sup>C and it requires intense source of energy to enable combustion i.e. glow plug, spark plug or pilot liquid fuel. It mixes rapidly with air to form homogenous air fuel mixture for efficient combustion inside engine cylinder and substantial reduction in harmful emissions [2]. In dual fuel engines gaseous fuel is mixed with intake air outside the engine cylinder and pilot liquid

\* Corresponding author. mahlas@rediffmail.com

fuel is injected at the end of compression stroke to initiate combustion.

Then, flame propagation occurs through the premixed gas-air mixture. Thus, dual fuel operation with gaseous fuel can yield higher thermal efficiency, almost comparable to diesel engines at higher loads. However, a dual fuel engine suffers poor efficiency and increased emissions at light loads. This is mainly due to the resulting very lean mixtures at low loads. The lean mixtures are hard to ignite and difficult to burn [3]. The use of exhaust gas recirculation is suggested method to improve part load performance and emissions characteristics. When considering a gaseous fuel for use in existing diesel engines, a number of issues which include, the effects of engine operating and design parameters, and type of gaseous fuel, on the performance of the dual-fuel engines, are important [4]. At lower loads the use of hot EGR promotes improvement in combustion due to increase in intake temperature. This also brings down smoke levels because of unburned in the exhaust are reburned with this method. Hence, it has been concluded that the use of EGR can effectively bring down the emission levels in the exhaust. The use of cooled EGR decreases the emission of  $\text{NO}_x$  with little sacrifice in performance and other exhaust emissions. In the present study, the main focus is to investigate the effects of cooled EGR on performance and emission characteristics of CNG-dual fuel engine.

## 2. 2. Description of The Experimental Procedure

The engine typically used for this study was a single cylinder DI commercial diesel engine. It is an air cooled, naturally aspirated constant speed compression ignition engine as per the IS: 10000 [P: 5]:1980 whose major specifications are shown in Table 1. The engine was coupled to a 5 kVA electric generator through which load was applied by increasing the field voltage shown in Annexure 1. The engine was tested at 20, 40, 60, 80 and 100 percent brake load conditions. The engine has capability to run either on pure diesel or dual fuel mode. The engine is modified to run on CNG by introducing it in the intake manifold pipe at a pressure of 1  $\text{kg}/\text{cm}^2$  and flow rate was determined by a calibrated rotameter. The CNG flow rate was kept fixed at 15 LPM for a given speed and loads, and a variable pilot injection is controlled by a governor. The entire test was performed at constant speed of 1500 r.p.m. (rated speed).

The EGR circuit consists of a water cooled heat exchanger for cooling of exhaust gas, orifice meter connected to a U-tube water manometer for measurement of flow rate of exhaust gas, surge tank, and valves fitted to control the quantity of exhaust gas being recycled. The pilot liquid fuel is measured by a calibrated glass tube by measuring the time required for the consumption of 50ml of fuel. During the experiments, engine speed, fuel consumption, air consumption rate and exhaust gas temperature were recorded. Exhaust gases were analyzed on line by an AVL DiGas analyzer, Model 4000 in which  $\text{UBHC}$ ,  $\text{CO}$ ,  $\text{O}_2$ ,  $\text{CO}_2$ , and  $\text{NO}_x$  were measured and AVL make Smoke Meter, Model 437 was used to measure the smoke opacity of exhaust gas. A piezoelectric pressure transducer, Kistler make, model 701A was used for

measuring the cylinder gas pressure and magnetic pickup, Electro make, model 3010 AMA was used to measure crank angle.

### 2.1. Fuel Properties

The fuel properties of CNG and diesel are given in Table 2.

*CNG composition:* 96.113% methane, 2.571% ethane, 0.359% propane, 0.05% I-butane, 0.09% N-butane, 0.01% I-pentane, 0.598% nitrogen, 0.149% carbon dioxide, 0.06% hexanes (CNG fractional analysis given by Gas Authority of India Ltd.)

Table 1 Engine specifications

Make	Kirloskar
Model	DAF 8
Rated Brake Power (BHP/KW)	8 / 5.9
Rated Speed (rpm)	1500
Number of Cylinder	One
Bore X Stroke (mm)	95 x 110
Displacement volume (cc)	779.704
Compression Ratio	17.5:1
Fuel Injection Timing (Degree)	26 BTDC
Injector opening pressure (bar)	200

Table 2 Fuel properties of Diesel, CNG

Fuel Properties	Diesel	CNG
Chemical Formula	$\text{C}_{10.8}\text{H}_{18.7}$	
Carbon	84-87	75
Hydrogen	33-16	25
Oxygen	0	0
Mole weight (g)	200	16-18
Density ( $\text{Kg}/\text{m}^3$ )	823 -844	0.79
Flame Speed (cm/s)	2.0-8.0	34
Flammability limits (% vol.)	0.6-7.5	5.3-15.0
Gross Heat of Combustion (MJ/kg)	42.5 – 46.5	50
Cetane Number	45 - 50	6
Auto Ignition Temperature ( $^{\circ}\text{C}$ )	230-280	730
Research Octane Number	--	130
Latent Heat of Vaporization @ 1 bar(kJ/kg)	233-251	509
Stoichiometric A/F Ratio	14.7	17.3

## 3. Exhaust Gas Recirculation

Generally EGR is an effective method for reducing  $\text{NO}_x$  formation due to lowering cylinder gas temperature resulting from the increased inert gas in the charge [5]. So, it was expected that dual fueling and use of cooled EGR could considerably reduce both smoke and  $\text{NO}_x$  especially at higher loads. Additionally the unburnt hydrocarbons are reburned in the mixture resulting in reduced unburned fuel and improve thermal efficiency at lower loads [6]. In this

work cooled EGR has been used at all load conditions. By definition, the amount of EGR is the ratio of mass of recirculated gas to the fresh charge inducted in the cylinder.

$$\% \text{ EGR} = \frac{M_{\text{EGR}}}{M_{\text{INTAKE}}}$$

$$\text{Where } M_{\text{INTAKE}} = M_{\text{AIR}} + M_{\text{EGR}} + M_{\text{CNG}}$$

#### 4. Results and Discussion

##### 4.1. Combustion Characteristics

Figs. 1 and 2 provide the experimental results of in-cylinder pressure and heat release rate at 100% load under normal diesel and dual fuel operation. For dual fuel operation with EGR result are given for cooled EGR 15% ratio. It is clear from the Fig. 2 and 3 that the maximum cylinder gas pressure decreased with the induction of EGR in the dual fuel operation. This is observed during compression and the initial stages of combustion. The reduction in peak cylinder pressure is due to high specific heat of the charge mixture and its slower burning rate. The combustion of CNG becomes visible deteriorating the heat release rate during the expansion stroke as shown in Fig. 3. It is also observed that the peak heat release can reach very high value when the quantity of CNG inducted is high. The high rate of heat release will also lead to increased NO<sub>x</sub> formation and also lead to engine knocking condition [7]. The second peak of heat release diagram observed in Fig. 3 is due to the combustion of CNG, in the expansion stroke.

The ignition delay period and combustion duration is generally prolonged in dual fuel mode than normal diesel operation. Addition of EGR further increased the delay time mainly because of reduction of charge temperature close to point of fuel injection, due to its high overall heat capacity compared to the normal single fuel operation [8]. The retardation in flame speed with EGR addition also increased the duration of combustion.

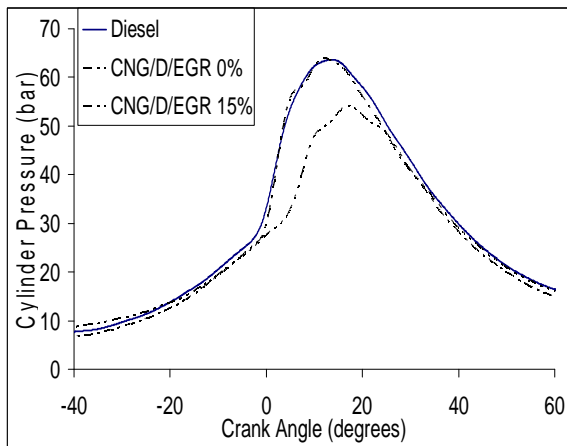


Figure 1. Cylinder pressure versus crank angle diagram at full load condition

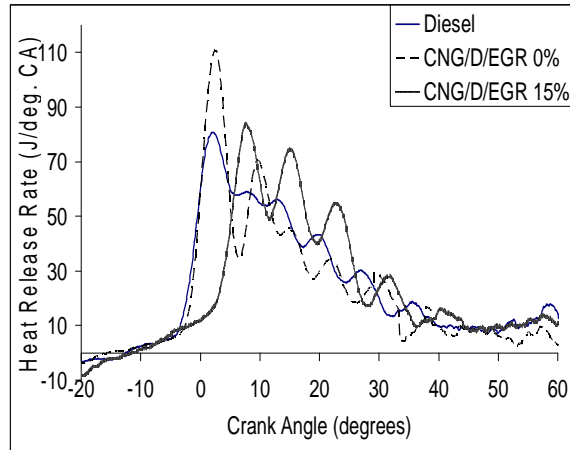


Figure 2. Heat release rate at full load condition

##### 4.2. Engine Performance

In a dual operation with EGR, it is not possible to go for higher substitution of CNG or EGR as both displace inlet air required for combustion. So, CNG flow rate was adjusted for smooth engine operation without the onset of knock while EGR was varied from 0-15% on volumetric basis.

Figure 3 represents brake thermal efficiency versus brake mean effective pressure for diesel and CNG-diesel dual fuel operation with different EGR ratio. It shows a great improvement with EGR 5% ratio, than normal diesel and dual fuel operation. The effect of using EGR in a diesel engine has three effects, dilution effect, chemical effect and thermal effect [9].

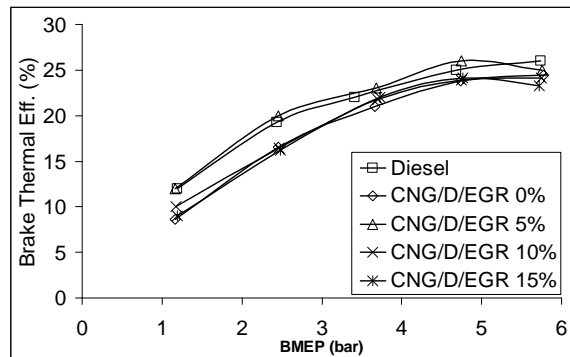


Figure 3. Brake thermal efficiency variations with BMEP

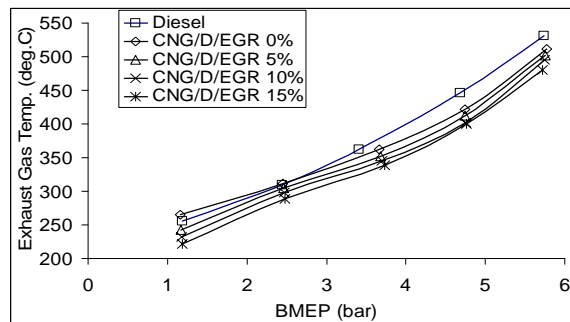


Figure 4. Exhaust gas temperature variations with BMEP

The chemical effect is associated with the participation of active free radicals present in exhaust gas to enhance combustion by taking part in pre-ignition reactions. However, this effect causes an increase in thermal efficiency. With more EGR substitution the thermal efficiency falls. This is due to the dilution effect of the EGR used, as it depleted the oxygen present in the combustion chamber [7].

Figure 4 represents exhaust gas temperature versus brake mean effective pressure for diesel and CNG-diesel operation for different EGR percentages. With EGR substitutions the exhaust temperature decreased at all loading conditions. In research work, cooled EGR has been used which acts as a thermal sink. The higher specific heat capacity of exhaust gases absorb heat during combustion and lower the exhaust temperature.

Figure 5 shows volumetric efficiency versus brake mean effective pressure for diesel and CNG-diesel with different EGR ratio. It is clear from the Fig. 6 that, with increasing EGR ratio in dual fuel operation, the volumetric efficiency is reduced. This is due to the fresh air is replaced by EGR substitutions.

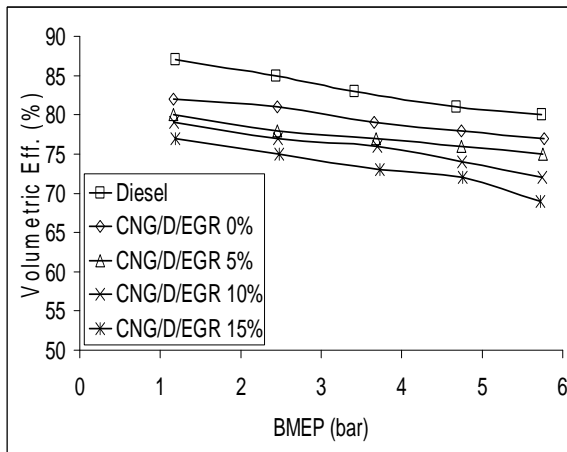


Figure 5. Volumetric efficiency variations with BMEP.

4.3. 4.3 Emission Characteristics

Figure 6 shows the relationship between the smoke opacity versus brake mean effective pressure at different EGR ratio for diesel and CNG-diesel dual fuel operation. It is well known that dual fuel operation remarkably reduced smoke emission. Moreover, combustion of CNG produces no particulates the only smoke associated are mainly due to pilot injection of diesel. With EGR substitution there is trade-off of NO<sub>x</sub> and smoke emission. Examining this figure it is clear that dual fuel operation is the potential method to reduce smoke emission. With increasing EGR ratio, smoke opacity is increased. This is because of decrease the amount of oxygen present in the combustion chamber with the substitution of EGR. It also decreases the cylinder temperature by absorbing heat during combustion

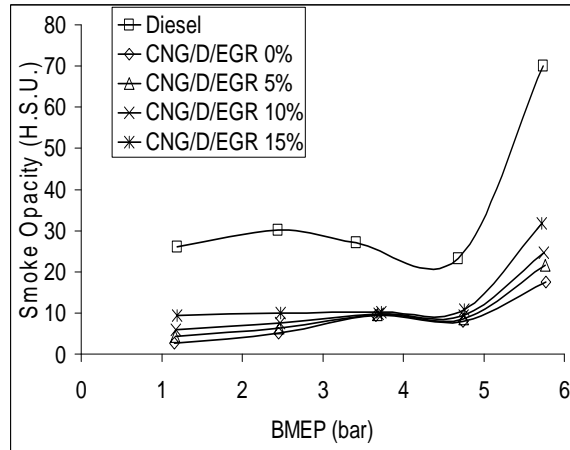


Figure 6. Smoke Opacity variations with BMEP

Both the factor increases the smoke. At light loads less smoke is produced since pilot injection of diesel is small. With increase in load the smoke formation is increased mainly due to increase in pilot fuel. Figure 8 illustrated NO<sub>x</sub> emission for diesel and CNG-diesel for different EGR percentages. In dual fuel operation NO<sub>x</sub> emission is generally low but with higher substitution of CNG high heat release rates resulting higher emission of NO<sub>x</sub>. The figure shows, that with EGR substitutions, NO<sub>x</sub> emission is reduced. A possible reason is the reduction of oxygen available for combustion, and reduction of peak combustion temperature due to high specific heat capacity.

Figure 8 shows the unburned hydrocarbon emission for diesel and CNG-diesel at different EGR ratio. Normally dual fuel operation exhibits higher emission of unburned hydrocarbon at light loads. At light loads the pilot quantity being small so flame cannot propagate fast and far enough to ignite the entire mixture. As the result it causes higher HC emissions but with increase in load the hydrocarbon emission decreases. As load progresses the pilot

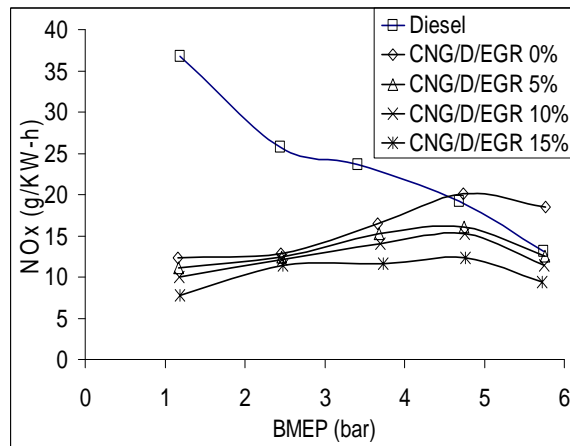


Figure 7. NO<sub>x</sub> emissions variations with BMEP

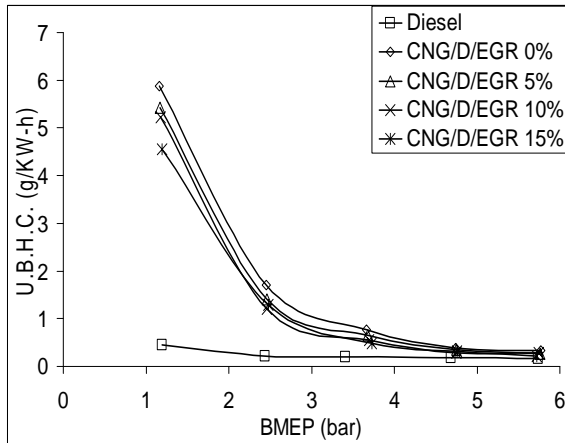


Figure 8 HC emissions variations with BMEP.

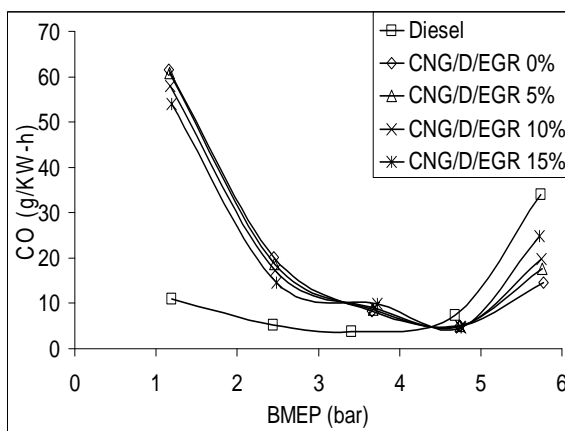


Figure 9. CO emissions variations with BMEP

quantity increases and burns the surrounding fuel-air mixture sufficiently.

From the Fig. 8 it can be seen that the unburnt hydrocarbon emissions decrease as the EGR ratio increases. This is so because a portion of the unburned gases in the exhaust from the previous cycle is recirculated and burned in the succeeding cycle. Also the presence of radicals can help to initiate combustion process especially with the increase of intake temperature due to mixing with exhaust gases [9]. Thus, the unburned hydrocarbon decreases with increasing EGR ratio. Figure 9 shows CO emissions for diesel and CNG-diesel dual fuel operation for different EGR ratio. As shown in Fig 9 the dual fuel operation yield higher CO emissions at light load conditions. At low loads, most of the fuel left unburnt as explained earlier leads to poor combustion and ignition results in higher CO emissions. At higher loads the CO emission is lower than normal diesel operation because of better utilization of fuel. This is mainly due to high gas temperature and faster combustion rates. With EGR substitutions the CO formation is higher at full load condition as shown in Fig. 10 than the dual fuel operation without EGR. At full load condition the availability of oxygen required for complete combustion decreases with increase in EGR ratio. Hence, the CO emission is higher with EGR addition in dual fuel operation at higher load than at the light load condition.

## 5. Conclusions

An experimental study was conducted to determine the performance and emission characteristics on a single cylinder direct injection diesel engine fueled with CNG. The main focus of the work was to reduce the harmful emissions and improving the performance. To achieve these goals the effect of cooled EGR were investigated. The following results were obtained from this study:

- The use of EGR up to 5% is useful in improving the brake thermal efficiency. Increasing the EGR substitution decreases the air required for combustion. However, with increasing EGR ratio decreases the thermal efficiency.
- A higher substitution of EGR was effective in reducing the emissions of  $\text{NO}_x$ . EGR is one of the potential methods in reducing the  $\text{NO}_x$  emission.
- Smoke opacity increases with increase in EGR substitution rates. This is mainly due to depletion of oxygen inside the combustion chamber.
- Peak cylinder pressure reduced and ignition delay prolonged with 15% EGR substitution. Addition of gaseous fuel makes the prolonged combustion and increases combustion duration.
- CO emission increases at higher loads with increase in EGR ratio mainly due to incomplete combustion.

## Acknowledgement

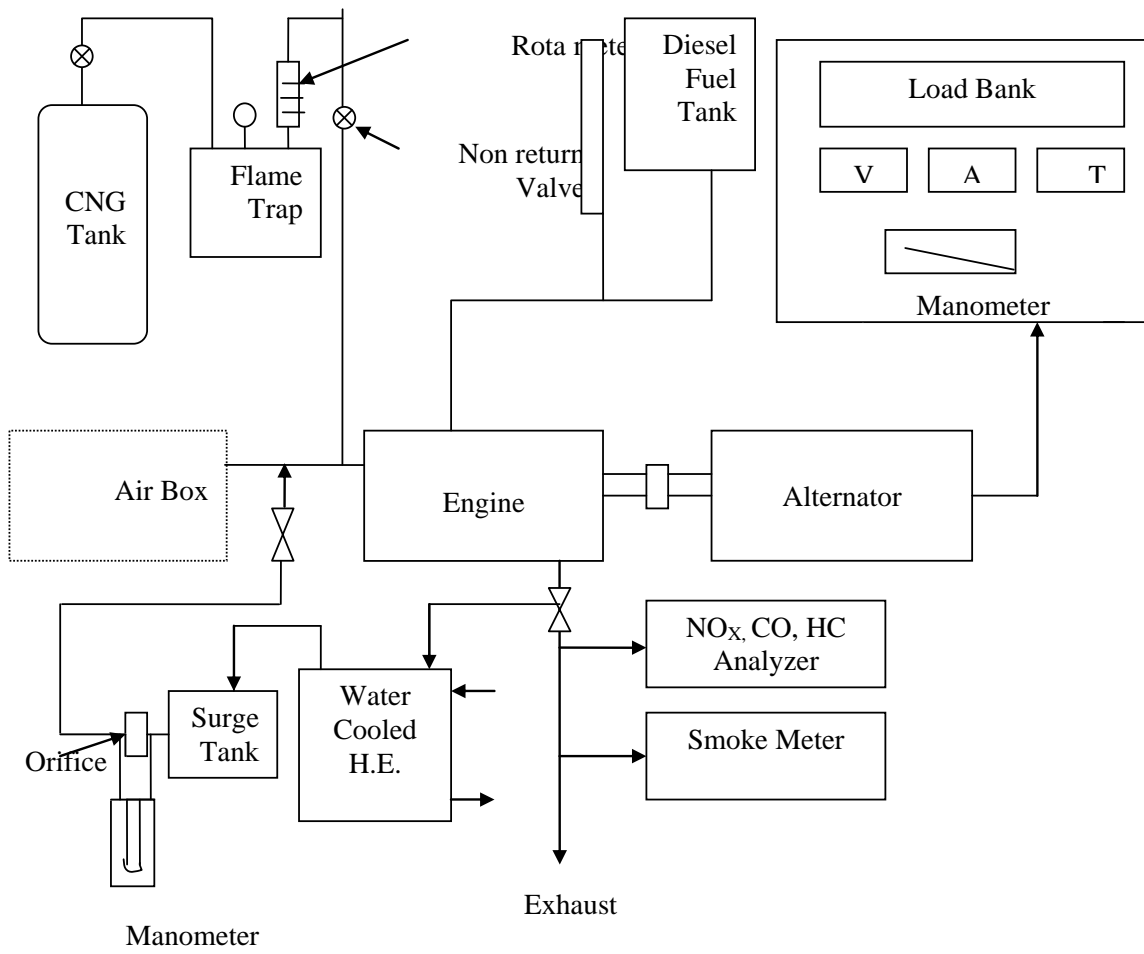
The authors would also like to thank the Staff Members of Engines and Unconventional Fuels Laboratory of Centre for Energy Studies, IIT Delhi for their help in conducting the experiments.

## References

- [1] O. Badr, G.A. Karim, B. Liu, "An examination of the flame spread limits in a dual fuel engine", *Applied Thermal Engineering*, Vol. 19, 1999, 1071-1080.
- [2] J. Kuaska, T. Okamoto, Y. Diasho, R. Kihara, T. Saito, "Combustion and exhaust gas emission characteristics of a diesel engine dual fueled with natural gas", *JSAE Review*, Vol. 21, 2000, 489-496.
- [3] G.H. Abd Alla, H.A. Soliman, O.A. Badr, M.F. Abd Rabbo, "Effect of injection timing on the performance of a dual fuel engine", *Energy Conversion and Management*, Vol. 43, 2002, 269-277.
- [4] B.B. Sahoo, N. Sahoo, U.K. Saha, "Effect of engine parameters and type of gaseous fuel on the performance of dual-fuel gas diesel engines-A Critical Review, *Renewable and Sustainable Energy Reviews*, Vol. 13, 2009, 1151-1184
- [5] G.H. Abd Alla, "Using exhaust gas recirculation in internal combustion engines: a review", *Energy Conversion and Management*, Vol. 43, 2002, 1027-1042.
- [6] M. Senthil Kumar, A. Ramesh, B. Nagalingam, "Use of hydrogen to enhance the performance of a vegetable oil fuelled compression ignition engine", *International Journal of Hydrogen Energy*, Vol. 28, 2003, 1143-1154.
- [7] R.G. Papagiannakis, D.T. Hountalas, "Experimental investigations concerning the effect of natural gas percentage on performance and emission of a DI dual fuel diesel engine", *Applied Thermal Engineering*, Vol. 23, 2003, 353-365.

- [8] M.Y.E. Selim, "Effect of exhaust gas recirculation on some combustion characteristics of dual fuel engine", Energy Conversion and Management, Vol. 44, 2003, 707-721
- [9] V. Pirouzpanah, R. K. Sarai, "Reduction of emissions in an automotive direct injection diesel engine dual-fuelled with natural gas by using variable exhaust gas recirculation", Proc. Instn. Mech. Engrs. Vol. 217 Part D: J. Automobile Engineering.

Appendix









الجامعة الهاشمية



المملكة الأردنية الهاشمية

المجلة الأردنية  
للمهندسة الميكانيكية والصناعية

JJIMIE

مجلة علمية عالمية محكمة

<http://jjmie.hu.edu.jo/>

ISSN 1995-6665

# المجلة الأردنية للهندسة الميكانيكية والصناعية

## مجلة علمية عالمية محكمة

المجلة الأردنية للهندسة الميكانيكية والصناعية: مجلة علمية عالمية محكمة أسستها اللجنة العليا للبحث العلمي، وزارة التعليم العالي والبحث العلمي، الأردن، وتصدر عن عمادة البحث العلمي والدراسات العليا، الجامعة الهاشمية، الزرقاء، الأردن.  
**هيئة التحرير**

### رئيس التحرير:

الأستاذ الدكتور موسى محسن

قسم الهندسة الميكانيكية، الجامعة الهاشمية، الزرقاء، الأردن .

### الأعضاء:

الأستاذ الدكتور عدنان الكيلاني  
الجامعة الأردنية

الأستاذ الدكتور أيمن المعاينة  
جامعة مؤتة

الأستاذ الدكتور محمد النمر  
جامعة العلوم والتكنولوجيا

الأستاذ الدكتور بلال العكش  
الجامعة الهاشمية

الأستاذ الدكتور علي بدران  
الجامعة الأردنية

الأستاذ الدكتور نسيم سواق  
جامعة مؤتة

### مساعد رئيس هيئة التحرير:

الدكتور أحمد الغندور

### فريق الدعم:

#### تنفيذ وإخراج

م. أسامة الشريط

#### المحرر اللغوي

الدكتور عبدالله جرادات

### ترسل البحوث إلى العنوان التالي :

رئيس تحرير المجلة الأردنية للهندسة الميكانيكية والصناعية  
عمادة البحث العلمي والدراسات العليا  
الجامعة الهاشمية  
الزرقاء - الأردن

هاتف: 0962-05-3903333 فرعي 4147

Email: jjmie@hu.edu.jo

Website: www.jjmie.hu.edu.jo